

*Assessment of systemic toxicity in vitro using the  
Adverse Outcome Pathway (AOP) concept: nephrotoxicity due  
to receptor-mediated endocytosis and lysosomal overload and in-  
hibition of mtDNA polymerase- $\gamma$  as case studies*



Doctoral Dissertation (Thesis)

to obtain the degree of  
“Doktor der Naturwissenschaften”  
(Dr. rer. nat.)

awarded by the  
Julius-Maximilians-Universität Würzburg

submitted by

*Sebastian Oskar Jarzina*

*From Saarbrücken / Germany*

*Würzburg 2021*





Submitted to the Faculty of Chemistry and Pharmacy on

---

Evaluators of the written Dissertation (Thesis)

1. Evaluator: \_\_\_\_\_

Supervisor - 2. Evaluator: \_\_\_\_\_

Examiners of the Public Defense

1. Examiner: \_\_\_\_\_

2. Examiner: \_\_\_\_\_

3. Examiner: \_\_\_\_\_

Date of the Public Defense

---

Doctoral Certificate awarded on

---



“

To know that we know what we know, and to know that we do not know what we do not know, that is true knowledge.

*Mikołaj Kopernik*



## Zusammenfassung

Der Bericht des US National Research Council (NRC) „Toxicity Testing in the 21st Century: A Vision and a strategy (Tox21)“, der 2007 veröffentlicht wurde, sieht einen vollständigen Paradigmenwechsel in der Toxizitätsprüfung vor. Ein zentraler Aspekt des Berichts beinhaltet den Übergang von apikal ermittelten Endpunkten für Toxizität in *in vivo* Studien, zu mehr mechanistisch basierten *in vitro* Tests. Um den Übergang zu erleichtern und den Paradigmenwechsel in der Prüfung auf Toxizität zu unterstützen, wird das Adverse Outcome Pathway (AOP) Konzept als pragmatisches Instrument weithin anerkannt. In dieser Arbeit wurde das AOP Konzept angewandt, um neue Ansätze zur Prüfung auf systemische Toxizität zu untersuchen. Dazu wurden AOPs für proximale Tubulusschäden, die durch lysosomale Überladung und Inhibition der mtDNA Polymerase- $\gamma$  initiiert werden, entwickelt. Diese AOPs wurden als mechanistische Grundlage für die Entwicklung von mechanistisch relevanten *in vitro* Tests für jedes Schlüsselereignis (KE) verwendet. Um die entwickelten *in vitro* Tests experimentell zu unterstützen, wurden proximale Tubuluszellen aus der Ratte (NRK-52E) und aus dem Menschen (RPTEC/TERT1) mit Hilfe von Modellsubstanzen behandelt. Zur Messung der Störung der lysosomalen Funktion im AOP – *Rezeptor-vermittelte Endozytose und lysosomale Überladung* wurden Polymyxin-Antibiotika (Polymyxin B, Colistin, Polymyxin B Nonapeptid) als Modellsubstanzen verwendet. Die gestörte Expression des lysosomal assoziierten Membranproteins 1/2 (LAMP 1/2) (KE1) und die Cathepsin D Freisetzung (KE2) wurden mittels Immunfluoreszenztechnik bestimmt und die Zytotoxizität (KE3) mittels CellTiter-Glo<sup>®</sup> Zellviabilitätstest gemessen. Zwischen den Zelllinien wurden signifikante Unterschiede in der Aufnahme von Polymyxinen und der Empfindlichkeit beobachtet, was die Bedeutung der *in vitro* Biokinetik zur Definition eines geeigneten Ausgangspunktes für die Risikobewertung unterstreicht.

Im Vergleich zur *in vivo* Situation, konnte eine eindeutige Expression von relevanten Transportern wie Megalin und Cubilin auf mRNA und Proteinebene in den verwendeten Zelllinien (RPTEC/TERT1 und NRK-52E) nicht gezeigt werden, was eine zusätzliche Integration von quantitativen *in vitro* zu *in vivo* Extrapolationen (QIVIVE) unabdingbar macht. Die Integration von QIVIVE durch Projektpartner der Universität Utrecht zeigte eine Verbesserung der modellierten biokinetischen Werte für Polymyxin B. Zur Bestimmung des ersten Schlüsselereignisse, (KE1) *Depletion von mitochondrialer DNA*, im AOP – *Hemmung der mitochondrialen DNA Polymerase- $\gamma$* , wurde nach Behandlung mit Modellsubstanzen (Adefovir, Cidofovir, Tenofovir, Adefovirdipivoxil, Tenofovirdisoproxil Fumarat) eine RT-qPCR Methode verwendet, um die mtDNA Kopienzahl zu bestimmen. Die mitochondriale Toxizität (KE2) wurde mittels eines hochauflösenden Bildgebungsverfahrens und MitoTracker<sup>®</sup> vom Projektpartner des Fraunhofer Institut in Hamburg gemessen, während die Zytotoxizität (KE3) mittels CellTiter-Glo<sup>®</sup> Zellviabilitätstest ermittelt wurde. Entgegen der mechanistischen Hypothese des AOPs – *Hemmung der mitochondrialen DNA Polymerase- $\gamma$* , führte eine 24 h Behandlung mit den Modellsubstanzen eher zu einer Erhöhung als zu einer Verringerung der mtDNA-Kopienzahl (KE1). Auch wurden nur geringe Auswirkungen auf die mitochondriale Toxizität (KE2) und Zytotoxizität (KE3) beobachtet. Die Behandlung von RPTEC/TERT1 Zellen über einen Zeitraum von 14 Tagen zeigte eine leichte Abnahme der mtDNA Kopienzahl nach Behandlung mit Adefovirdipivoxil und Tenofovirdisoproxil Fumarat, was den Bedarf an zeitaufgelösten Daten und Einschränkungen von kurzfristigen *in vitro* Systemen unterstreicht. Um eine erste Einschätzung für die Risikobewertung basierend auf *in vitro* Daten zu erhalten, wurden aus den erhaltenen *in vitro* Daten für jedes KE mögliche Ausgangspunkte (Points of Departure (PoD)) berechnet. Dazu wurden gängige *in vitro* PoDs berechnet, wie die Effektkonzentration, bei der 10 % bzw.



20 % Effekt gemessen wurden ( $EC_{10}$ ,  $EC_{20}$ ), die höchste Konzentration ohne Wirkung (no observed effect Konzentration (NOEC)), die niedrigste Konzentration mit beobachteter Wirkung (lowest observed effect Konzentration (LOEC)), die Benchmark 10 % (unterer / obere) Konzentrationen ( $BMC_{10}$ ,  $BMCL_{10}$ ,  $BMCU_{10}$ ) und eine modellierte nicht-toxische Konzentration (NtC). Diese wurden dann mit Serum- bzw. Gewebkonzentrationen aus *in vivo* Studien verglichen, die nach Gabe therapeutischer / supratherapeutischer Dosen gemessen wurden. Zusätzlich wurde überprüft, ob es mit Hilfe von quantitativen Beziehungen zwischen Schlüsselereignissen möglich ist, basierend auf der Bestimmung früher Schlüsselereignisse nachfolgende Effekte vorherzusagen. Diese Untersuchungen zeigten eine gute Korrelation der aus den mathematischen Beziehungen modellierten Daten mit den tatsächlich gemessenen Werten der Zytotoxizität der Modellsubstanzen Colistin und Polymyxin B-Nonapeptid. Im Rahmen der Arbeit wurden auch Unsicherheiten und Limitationen der Strategie deutlich, die maßgebliche Auswirkungen auf die Vorhersage und auf die Risikobewertung basierend auf *in vitro* Resultaten haben.



## Abstract

The US National Research Council (NRC) report "Toxicity Testing in the 21st Century: A Vision and a strategy (Tox21)", published in 2007, calls for a complete paradigm shift in toxicity testing. A central aspect of the proposed strategy includes the transition from apical endpoints in *in vivo* studies to more mechanistically based *in vitro* tests. To support and facilitate the transition and paradigm shift in toxicity testing, the Adverse Outcome Pathway (AOP) concept is widely recognized as a pragmatic tool. As case studies, the AOP concept was applied in this work to develop AOPs for proximal tubule injuries initiated by *Receptor-mediated endocytosis and lysosomal overload* and *Inhibition of mtDNA polymerase- $\gamma$* . These AOPs were used as a mechanistic basis for the development of *in vitro* assays for each key event (KE). To experimentally support the developed *in vitro* assays, proximal tubule cells from rat (NRK-52E) and human (RPTEC/TERT1) were treated with model compounds. To measure the disturbance of lysosomal function in the AOP – *Receptor-mediated endocytosis and lysosomal overload*, polymyxin antibiotics (polymyxin B, colistin, polymyxin B nonapeptide) were used as model compounds. Altered expression of lysosomal associated membrane protein 1/2 (LAMP-1/2) (KE1) and cathepsin D release from lysosomes (KE2) were determined by immunofluorescence, while cytotoxicity (KE3) was measured using the CellTiter-Glo<sup>®</sup> cell viability assay. Importantly, significant differences in polymyxin uptake and susceptibility between cell lines were observed, underlining the importance of *in vitro* biokinetics to determine an appropriate *in vitro* point of departure (PoD) for risk assessment. Compared to the *in vivo* situation, distinct expression of relevant transporters such as megalin and cubilin on mRNA and protein level in the used cell lines (RPTEC/TERT1 and NRK-52E) could not be confirmed, making integration of quantitative *in vitro* to *in vivo* extrapolations (QIVIVE) necessary. Integration of QIVIVE by project

partners of the University of Utrecht showed an improvement in the modelled biokinetic data for polymyxin B. To assess the first key event, (KE1) *Depletion of mitochondrial DNA*, in the AOP – *Inhibition of mtDNA polymerase- $\gamma$* , a RT-qPCR method was used to determine the mtDNA copy number in cells treated with model compounds (adefovir, cidofovir, tenofovir, adefovir dipivoxil, tenofovir disoproxil fumarate). Mitochondrial toxicity (KE2) was measured by project partners using the high-content imaging technique and MitoTracker<sup>®</sup> whereas cytotoxicity (KE3) was determined by CellTiter-Glo<sup>®</sup> cell viability assay. In contrast to the mechanistic hypothesis underlying the AOP – *Inhibition of mtDNA polymerase- $\gamma$* , treatment with model compounds for 24 h resulted in an increase rather than a decrease in mtDNA copy number (KE1). Only minor effects on mitochondrial toxicity (KE2) and cytotoxicity (KE3) were observed. Treatment of RPTEC/TERT1 cells for 14 days showed only a slight decrease in mtDNA copy number after treatment with adefovir dipivoxil and tenofovir disoproxil fumarate, underscoring some of the limitations of short-term *in vitro* systems. To obtain a first estimation for risk assessment based on *in vitro* data, potential points of departure (PoD) for each KE were calculated from the obtained *in vitro* data. The most common PoDs were calculated such as the effect concentration at which 10 % or 20 % effect was measured (EC<sub>10</sub>, EC<sub>20</sub>), the highest no observed effect concentration (NOEC), the lowest observed effect concentration (LOEC), the benchmark 10 % (lower / upper) concentrations (BMC<sub>10</sub>, BMCL<sub>10</sub>, BMCU<sub>10</sub>) and a modelled non-toxic concentration (NtC). These PoDs were then compared with serum and tissue concentrations determined from *in vivo* studies after treatment with therapeutic / suprathreshold doses of the respective drugs in order to obtain a first estimate of risk based on *in vitro* data. In addition, AOPs were used to test whether the quantitative key event relationships between key events allow prediction of downstream effects and effects on the adverse outcome (AO) based

on measurements of an early key event. Predictions of cytotoxicity from the mathematical relationships showed good concordance with measured cytotoxicity after treatment with colistin and polymyxin b nonapeptide. The work also revealed uncertainties and limitations of the applied strategy, which have a significant impact on the prediction and on a risk assessment based on *in vitro* results.



## Table of contents

Zusammenfassung .....	III
Abstract .....	VI
List of figures .....	XIV
List of tables .....	XVII
List of abbreviation .....	XX
<b>1 Introduction .....</b>	<b>1</b>
1.1 A paradigm shift in toxicology testing: Tox21 .....	4
1.2 The adverse outcome pathway (AOP) concept.....	6
1.3 Kidney as a target organ for toxicity.....	8
1.3.1 <i>Mechanism of drug-induced kidney injury via Receptor-mediated endocytosis and lysosomal overload and establishment of an AOP as a basis for development of in vitro assays covering key events within this AOP .....</i>	<i>13</i>
1.3.2 <i>Mechanism of drug-induced kidney injury via inhibition of mitochondrial DNA polymerase-<math>\gamma</math> and establishment of AOPs as a platform for development of in vitro assays.....</i>	<i>15</i>
1.4 Cell lines used for <i>in vitro</i> assays .....	18
1.4.1 <i>RPTEC/TERT1 cell line .....</i>	<i>19</i>
1.4.2 <i>NRK-52E cell line .....</i>	<i>20</i>
1.5 Polymyxins as model stressors for the AOP – <i>Receptor-mediated endocytosis and lysosomal overload .....</i>	<i>21</i>
1.5.1 <i>Polymyxin B and colistin.....</i>	<i>21</i>
1.5.2 <i>Polymyxin B nonapeptide.....</i>	<i>22</i>
1.6 Cadmium chloride as a model stressor for the AOP – <i>Receptor-mediated endocytosis and lysosomal overload.....</i>	<i>23</i>
1.7 Antivirals as model stressors for the AOP – <i>Inhibition of mtDNA polymerase-<math>\gamma</math>.....</i>	<i>24</i>
1.7.1 <i>Adefovir and its prodrug adefovir dipivoxil.....</i>	<i>24</i>
1.7.2 <i>Cidofovir .....</i>	<i>26</i>
1.7.3 <i>Tenofovir and its prodrug tenofovir disoproxil fumarate .....</i>	<i>27</i>
1.7.4 <i>Zalcitabine (ddC).....</i>	<i>27</i>
1.8 Identification of suitable <i>in vitro</i> endpoints covering key events within the developed AOPs.....	29
1.8.1 <i>Suitable in vitro endpoints for the AOP – Receptor-mediated endocytosis and lysosomal overload.....</i>	<i>29</i>

---

1.8.2	<i>Suitable in vitro endpoints for the AOP – Inhibition of mtDNA polymerase-<math>\gamma</math></i> .....	32
1.8.3	<i>Suitable in vitro endpoints for the AOP – Receptor-mediated endocytosis and lysosomal overload and the AOP – Inhibition of mtDNA polymerase-<math>\gamma</math></i> .....	33
1.9	<i>In vitro points of departures for risk assessment</i> .....	34
<b>2</b>	<b>Objective</b> .....	<b>36</b>
<b>3</b>	<b>Material and Methods</b> .....	<b>38</b>
3.1	Technical Equipment .....	38
3.2	Software .....	40
3.3	Chemicals, compounds, kits.....	40
3.4	Antibodies, primer, TaqMan™ probes.....	43
3.5	Cell culture conditions .....	44
3.5.1	<i>Thawing procedure</i> .....	44
3.5.2	<i>Freezing procedure</i> .....	45
3.5.3	<i>NRK-52E culture, splitting procedure and growth medium supplements</i> .....	45
3.5.4	<i>RPTEC/TERT1 culture, splitting procedure and growth medium supplements</i> .....	46
3.5.5	<i>HK-2 culture, splitting procedure and growth medium supplements</i> .....	48
3.5.6	<i>CaCo-2 culture, splitting procedure and growth medium supplements</i> .....	49
3.6	<i>In vitro assays relevant for the AOP – Receptor-mediated endocytosis and lysosomal overload</i> .....	50
3.6.1	<i>Immunocytochemistry staining (ICC) of LAMP-1/2 protein – assay for KE1 – Disturbance of lysosomal function</i> .....	50
3.6.2	<i>Immunocytochemistry staining (ICC) of cathepsin D – a putative endpoint for KE2 (disruption of lysosomes)</i> .....	53
3.7	<i>In vitro assays relevant for the AOP – Inhibition of mt-DNA polymerase-<math>\gamma</math></i> .....	55
3.7.1	<i>Determination of mtDNA copy number via qPCR – assay for KE1 – Depletion of mtDNA</i> .....	55
3.7.2	<i>Determination of mitochondrial toxicity via MitoTracker™ - a putative in vitro endpoint for KE2 (dysfunction of mitochondrial)</i> .....	60
3.8	<i>In vitro cytotoxicity assay relevant for the AOP – Receptor-mediated endocytosis and lysosomal overload &amp; for the AOP – Inhibition of mt-DNA polymerase-<math>\gamma</math></i> .....	62

---



---

3.8.1	<i>CellTiter-Glo<sup>®</sup> cell viability assay – assay for KE3 Cytotoxicity of renal tubule cells</i> .....	62
3.9	Determination of intracellular compound accumulation of polymyxin B and colistin via LC-MS/MS.....	63
3.9.1	<i>Treatment, preparation of cell sample and samples to measure plastic adsorption</i> .....	63
3.9.2	<i>Solid phase extraction (SPE) purification</i> .....	64
3.9.3	<i>Analysis of intracellular polymyxin concentrations by mass spectrometry coupled with liquid chromatography</i> .....	65
3.9.4	<i>Total cell volume calculation</i> .....	66
3.10	Determination of aprotinin uptake to assess endocytic activity.....	67
3.11	Immunocytochemistry of megalin receptor in NRK-52E and RPTEC/TERT1 cells.....	68
3.12	Megalyn and cubilin mRNA expression using TaqMan <sup>™</sup> probes.....	69
3.12.1	<i>RNA isolation</i> .....	69
3.12.2	<i>cDNA synthesis</i> .....	70
3.12.3	<i>qRT-PCR using TaqMan<sup>™</sup> probes</i> .....	70
3.13	Preparation of cell and tissue lysates and Western blot analysis of megalin.....	71
3.13.1	<i>Protein extraction from cells</i> .....	71
3.13.2	<i>Protein extraction from tissue</i> .....	72
3.13.3	<i>Protein determination by DC assay</i> .....	72
3.13.4	<i>Gradient SDS polyacrylamide gel electrophoresis and Western blot</i> .....	73
3.14	Calculation methods to determine different <i>in vitro</i> points of departure.....	74
3.14.1	<i>Effective concentration 10 % and 20 % (EC<sub>10</sub> and EC<sub>20</sub>)</i> .....	74
3.14.2	<i>Lowest / no observed effect concentration (LOEC / NOEC)</i> .....	75
3.14.3	<i>Benchmark Concentration (BMC)</i> .....	75
3.14.4	<i>Non-toxic concentration (NtC)</i> .....	75
3.14.5	<i>Visualization of different PoDs</i> .....	76
3.14.6	<i>Margin of exposure (MOE)</i> .....	76
<b>4</b>	<b>Results</b> .....	<b>77</b>
4.1	<i>AOP – Receptor-mediated endocytosis and lysosomal overload</i> .....	77
4.1.1	<i>Using the Comparative Toxicogenomic Database (CTD) to identify suitable in vitro endpoints for the AOP – Receptor-mediated endocytosis and lysosomal overload</i> .....	77
4.1.2	<i>Establishment of suitable in vitro assays linked to the AOP – Receptor-mediated endocytosis and lysosomal overload</i> .....	79

---

---

4.1.3	<i>Dose-response in vitro results across all KEs in the AOP – Receptor mediated endocytosis and lysosomal overload</i> .....	86
4.1.4	<i>Investigation of intracellular polymyxin accumulation, endocytotic activity and relevant transporter expression in RPTEC/TERT1 and NRK-52E cells to gain an understanding of differences in sensitivity between both cell lines</i> .....	88
4.1.5	<i>Prediction of colistin, polymyxin B nonapeptide and cadmium chloride downstream key events based on polymyxin B in vitro data</i> .....	104
4.2	<i>AOP – Inhibition of mtDNA polymerase-<math>\gamma</math></i> .....	118
4.2.1	<i>Using the Comparative Toxicogenomic Database (CTD) to identify suitable in vitro endpoints for the AOP – Inhibition of mtDNA polymerase-<math>\gamma</math></i> .....	118
4.2.2	<i>Establishment of suitable in vitro assays linked to the AOP – Inhibition of mtDNA polymerase-<math>\gamma</math></i> .....	119
4.2.3	<i>Dose-response in vitro results across all KEs in the AOP – Inhibition of mtDNA polymerase-<math>\gamma</math></i> .....	125
4.2.4	<i>Prediction of tenofovir disoproxil fumarate downstream key events based on adefovir dipivoxil in vitro data</i> .....	128
4.3	<i>Risk assessment based on in vitro results</i> .....	140
4.3.1	<i>In vitro points of departure related to the AOP – Receptor-mediated endocytosis and lysosomal overload</i> .....	140
4.3.2	<i>In vitro points of departure related to the AOP –Inhibition of mtDNA polymerase-<math>\gamma</math></i> .....	147
4.4	<i>Integration of physiologically based pharmacokinetic modeling (PBPK) and quantitative in vitro-to-in vivo extrapolation (QIVIVE)</i> .....	152
<b>5</b>	<b>Discussion</b> .....	<b>156</b>
5.1	<i>AOP development for kidney injury due to Receptor-mediated endocytosis and lysosomal overload – a basis for an improved mechanistic in vitro approach</i> .....	157
5.1.1	<i>Differences in cell line susceptibility due to different transporter expressions</i> .....	158
5.1.2	<i>Predicting downstream key events by using key event relationships from the AOP – Receptor-mediated endocytosis and lysosomal overload</i> .....	169
5.1.3	<i>Estimation of risk using in vitro data obtained from the AOP – Receptor-mediated endocytosis and lysosomal overload</i> .....	173
5.2	<i>AOP development for kidney injury due to Inhibition of mtDNA polymerase-<math>\gamma</math> – a basis for an improved mechanistic in vitro approach</i> .....	176

---

5.2.1	<i>Predicting downstream key events by using key event relationships from the AOP – Inhibition of mtDNA polymerase-<math>\gamma</math></i> .....	183
5.2.2	<i>Estimation of risk using in vitro data obtained from the AOP – Inhibition of mtDNA polymerase-<math>\gamma</math></i> .....	185
5.3	Adverse Outcome Pathway concept – a feasible approach for toxicity testing? ...	188
5.4	<i>In vitro</i> PoDs for <i>in vitro</i> risk assessment – fit for purpose? .....	190
<b>6</b>	<b>Summary and conclusion</b> .....	<b>194</b>
<b>7</b>	<b>References</b> .....	<b>198</b>
<b>8</b>	<b>Appendix</b> .....	<b>225</b>
	<b>Acknowledgements</b> .....	<b>272</b>
	<b>Eidesstattliche Erklärung</b> .....	<b>274</b>



## List of figures

Figure 1 Schematic description of a multi-stage strategy for toxicity testing .....	5
Figure 2 Schematic description of an AOP .....	6
Figure 3 The human kidney with its functional subunits, the nephrons.....	9
Figure 4 Schematic representation of proximal tubule cells and their transporters .....	12
Figure 5 Cellular uptake of polymyxin antibiotics via receptor-mediated endocytosis and mechanisms leading to cytotoxicity of proximal tubule cells through necrosis and the mitochondrial pathway of apoptosis (modified from (Quiros <i>et al.</i> , 2010)).....	14
Figure 6 AOP – <i>Receptor-mediated endocytosis and lysosomal overload</i> .....	15
Figure 7 Mechanism of drug induced kidney injury via <i>Inhibition of mtDNA polymerase-<math>\gamma</math></i> (modified from (Fernandez-Fernandez <i>et al.</i> , 2011)).....	16
Figure 8 AOP – <i>Inhibition of mtDNA polymerase-<math>\gamma</math></i> .....	17
Figure 9 Venn diagram with the data sets of polymyxin B, colistin and polymyxin B nonapeptide .....	77
Figure 10 Venn diagram with the data sets of gentamicin, cadmium chloride and vancomycin .....	78
Figure 11 Immunofluorescence images of LAMP-2 in RPTEC/TERT1 cells treated with polymyxin B for 24 h.....	81
Figure 12 Immunofluorescence images of LAMP-1 in NRK-52E cells treated with polymyxin B for 24 h.....	81
Figure 13 Immunofluorescence images of cathepsin D in RPTEC/TERT1 cells treated with polymyxin B for 24 h.....	82
Figure 14 Immunofluorescence images of cathepsin D in NRK-52E cells treated with polymyxin B for 24 h.....	83
Figure 15 Cytotoxicity of RPTEC/TERT1 and NRK-52E cells after treatment with polymyxins and CdCl <sub>2</sub> .....	84
Figure 16 <i>In vitro</i> results for individual KEs from the AOP – <i>Receptor-mediated endocytosis and lysosomal overload</i> .....	86
Figure 17 Standard curves for polymyxin B and colistin with the resulting straight-line equation and coefficient of determination .....	90
Figure 18 Example chromatograms of intracellular polymyxin B <sub>2</sub> / B <sub>1</sub> and colistin A / B concentrations after 24 h treatment with polymyxin B respectively colistin in RPTEC/TERT1 cells.....	92
Figure 19 Example chromatograms of intracellular polymyxin B <sub>2</sub> / B <sub>1</sub> and colistin A / B concentrations after 24 h treatment with polymyxin B respectively colistin in NRK-52E cells .....	93

Figure 20 Example chromatograms of intracellular polymyxin B <sub>1</sub> concentration after 24 h treatment with polymyxin B in RPTEC/TERT1 and NRK-52E cells .....	94
Figure 21 Time dependent increase in polymyxin B and colistin levels in RPTEC/TERT1 and NRK-52E cells.....	95
Figure 22 Time dependent increase in polymyxin B levels in RPTEC/TERT1 and NRK-52E cells.....	96
Figure 23 Fluorescence images of both cell lines after 4 h incubation with Alexa-488 labeled aprotinin.....	97
Figure 24 Fluorescence intensity of Alexa-488 labelled aprotinin per number of nuclei in both cell lines .....	98
Figure 25 Immunocytochemical localization of megalin in both cell lines .....	99
Figure 26 mRNA expression results of megalin and cubilin in NRK-52E, RPTEC/TERT1, CaCo-2, HK-2, and rat kidney using TaqMan™ probes .....	101
Figure 27 Western blot analysis of megalin in NRK-52E and rat kidney lysates .....	103
Figure 28 Calculation of additional data points from the experimentally obtained <i>in vitro</i> data after polymyxin B treatment in RPTEC/TERT1 cells .....	105
Figure 29 Calculation of additional data points from the experimentally obtained <i>in vitro</i> data after polymyxin B treatment in NRK-52E cells .....	106
Figure 30 Response-response plots obtained from polymyxin B KE data in RPTEC/TERT1 cells.....	109
Figure 31 Response-response plots obtained from polymyxin B KE data in NRK-52E cells .....	110
Figure 32 Prediction of colistin, polymyxin B nonapeptide and CdCl <sub>2</sub> cytotoxicity using response-response relationships based on polymyxin B data in RPTEC/TERT1 .....	114
Figure 33 Prediction of colistin, polymyxin B nonapeptide and CdCl <sub>2</sub> cytotoxicity using response-response relationships based on polymyxin B data in NRK-52E.....	116
Figure 34 Venn diagram with the data sets of adefovir, ADF, cidofovir, tenofovir .....	118
Figure 35 Fluorescence images of MitoTracker® dye in RPTEC/TERT1 cells treated with antivirals for 14 d.....	122
Figure 36 Cytotoxicity of RPTEC/TERT1 and NRK-52E cells after treatment with antivirals.....	124
Figure 37 <i>In vitro</i> results after 24 h for the individual KEs from the AOP – <i>Inhibition of mtDNA polymerase-γ</i> .....	126
Figure 38 <i>In vitro</i> results after 14 d for the individual KEs from the AOP – <i>Inhibition of mtDNA polymerase-γ</i> .....	127
Figure 39 Calculation of additional data points from the experimentally obtained <i>in vitro</i> data after ADV treatment in RPTEC/TERT1 cells .....	130

---

Figure 40 Response-response plots obtained from ADV KE data in RPTEC/TERT1 cells .....	133
Figure 41 Response-response plots obtained from ADV KE data in RPTEC/TERT1 cells without KE2.....	134
Figure 42 Comparison of <i>in vitro</i> results for KE2 ( <i>Mitochondrial toxicity</i> ) and KE3 ( <i>Cell viability</i> ) after 14 d treatment with ADV in RPTEC/TERT1 cells from the AOP – <i>Inhibition of mtDNA polymerase-γ</i> Blue graph represents dysfunction in mitochondria and describe the change in KE2 ( <i>Mitochondrial toxicity</i> ). Green graph represents cell viability and describes the change in KE3 ( <i>Cytotoxicity in renal tubular cells</i> ). The response for KE2 and KE3 was plotted in percent of control against the logarithmic concentration in $\mu\text{M}$ . All experiments were repeated in three technical replicates and three biological replicates. Data are presented as mean $\pm$ SD fold change (n = 3).....	136
Figure 43 Prediction of TDF cytotoxicity using response-response relationships based on ADV data in RPTEC/TERT1.....	137
Figure 44 Prediction of TDF cytotoxicity using response-response relationship based on ADV data in RPTEC/TERT1 cells excluding KE2 data .....	138
Figure 45 Visualization of different points of departure determined from <i>in vitro</i> assays after polymyxin treatment in RPTEC/TERT1 and NRK-52E cells after 24 h and comparison with serum / kidney concentrations .....	144
Figure 46 Visualization of different points of departure determined from <i>in vitro</i> assays after ADV and TDF treatment in RPTEC/TERT1 and NRK-52E cells after 24 h and 14 d and comparison with serum concentrations from human and rats .....	149
Figure 47 Physiologically based pharmacokinetic modeling of 1.0 mg/kg body weight ( <i>i.v.</i> ) polymyxin B Polymyxin B administered per <i>i.v.</i> infusion over 1 h in humans. Polymyxin B plasma concentration without transporter kinetics assuming only glomerular filtration is presented in blue. Modeled polymyxin B plasma concentration including active transporter kinetics into proximal tubule cells are presented in red. Separated points represents <i>in vivo</i> data from published human study .....	152
Figure 48 Quantitative <i>in vitro</i> -to- <i>in vivo</i> extrapolation based on nominal and intracellular <i>in vitro</i> polymyxin B concentrations QIVIVE of polymyxin B concentrations obtained from KE1 ( <i>Disturbance of lysosomal functions</i> ) (solid red graph) and KE3 ( <i>Cell toxicity</i> ) (solid blue graph) from nominal <i>in vitro</i> polymyxin B concentrations used in <i>in vitro</i> assays. QIVIVE of polymyxin B concentrations obtained from KE1 ( <i>Disturbance of lysosomal functions</i> ) (dashed red graph) and KE3 ( <i>Cell toxicity</i> ) (dashed blue graph) from intracellular <i>in vitro</i> polymyxin B concentrations.....	153
Figure 49 Integration of <i>in vitro</i> biokinetic data, <i>in vitro</i> KE data and QIVIVE modeling for prediction of <i>in vivo</i> nephrotoxicity of polymyxin B (A) Predicted exposure for polymyxin B <i>in vivo</i> doses after integration of (B) <i>in vitro</i> biokinetic data and (C) <i>in vitro</i> KEs data resulted in more accurate extrapolated <i>in vivo</i> doses consistent with doses used in clinical practice .....	154

---





---

**List of tables**

Table 1	Transporter of proximal tubule cells .....	10
Table 2	Model compounds related to the AOP – Receptor-mediated endocytosis and lysosomal overload .....	22
Table 3	Model compounds related to the AOP – <i>Inhibition of mtDNA polymerase-<math>\gamma</math></i> .....	25
Table 4	Technical equipment with supplier .....	38
Table 5	Software with supplier.....	40
Table 6	Chemicals, compounds, and kits with supplier .....	40
Table 7	Antibodies with supplier.....	43
Table 8	Primer with gene name and sequence .....	43
Table 9	TaqMan™ probes with supplier .....	44
Table 10	Growth medium supplements for NRK-52E cells.....	46
Table 11	Growth and splitting medium supplements for RPTEC/TERT1 cells .....	47
Table 12	Growth medium supplements for HK-2 cells.....	48
Table 13	Growth medium supplements for CaCo-2 cells .....	49
Table 14	Fluorochromes with maximal excitation ( $\lambda_{ex}$ ) and emission ( $\lambda_{em}$ ) wavelength used for immunocytochemistry staining .....	52
Table 15	Treatment concentrations for mtDNA copy number experiments in NRK-52E (24 h).....	56
Table 16	Treatment concentrations for mtDNA copy number experiments in RPTEC/TERT1 (24 h) .....	56
Table 17	Treatment concentrations for mtDNA copy number experiments in RPTEC/TERT1 (14 d) .....	56
Table 18	Master mix per well for one PCR reaction with components and reaction mix volume.....	58
Table 19	Quantitative real-time RT-PCR run program used for quantification of mtDNA copy number.....	58
Table 20	Opera® System settings used for the measurement of the MitoTracker® Red CMXRos uptake.....	61
Table 21	LC-MS/MS parameters for MRM detection of polymyxin B1, polymyxin B2, colistin A, and colistin B.....	66
Table 22	Quantitative real-time RT-PCR run program used for TaqMan™ assay .....	71
Table 23	BSA dilution series for standard curve.....	73
Table 24	Standard curve parameters for polymyxin B.....	90

---

Table 25 Standard curve parameters for colistin .....	91
Table 26 Mathematical equation obtained from <i>in vitro</i> experiments in RPTEC/TERT1 cells for the computation of additional data points .....	107
Table 27 Mathematical equation obtained from <i>in vitro</i> experiments in NRK-52E cells for the computation of additional data points .....	107
Table 28 Mathematical equation obtained from response-response plots describing quantitative relationship between KEs in RPTEC/TERT1 cells after polymyxin B treatment .....	111
Table 29 Mathematical equation obtained from response-response plots describing quantitative relationship between KEs in NRK-52E cells after polymyxin B treatment .....	111
Table 30 Mathematical equation obtained from <i>in vitro</i> experiment for KE1 in RPTEC/TERT1 for the computation of additional data points.....	113
Table 31 Mathematical equation obtained from <i>in vitro</i> experiment for KE1 in NRK-52E cells for the computation of additional data points.....	117
Table 32 Mathematical equation obtained from <i>in vitro</i> experiments for the calculation of additional data points .....	129
Table 33 Mathematical equations obtained from response-response plots describing quantitative relationships between KE1, KE2 and KE3 .....	132
Table 34 Serum and kidney concentrations of polymyxin antibiotics in humans and rats Serum and mean serum concentrations of polymyxin antibiotics in humans after administration of therapeutic doses of polymyxin B (0.45 - 3.38 mg/kg/d by <i>i.v.</i> injection), colistin (2.5 - 5 mg/kg/d by <i>i.v.</i> injection), and serum as well as kidney concentrations of polymyxins in rats after administration of polymyxin B (3 - 4 mg/kg/d by <i>i.v.</i> injection, resp. 5 - 25 mg/kg/d per <i>s.c.</i> injection), colistin (25 mg/kg/d per <i>s.c.</i> injection), and PBNP (40 mg/kg/d per <i>s.c.</i> injection) based on therapeutically relevant exposure levels to induce renal damages.....	142
Table 35 Calculated <i>in vitro</i> PoDs (NOEC, LOEC, BMC <sub>10</sub> ) from <i>in vitro</i> assays for the AOP – <i>Receptor-mediated endocytosis and lysosomal overload</i> PoDs are given in $\mu\text{M}$ for each key event (KE1 – 3) in both cell lines (RPTEC/TERT1 and NRK-52E) after treatment with polymyxin B (PB), colistin (Col) and polymyxin B nonapeptide (PBNP), n.a. not available <i>in vitro</i> data.....	143
Table 36 Calculated margin of exposure (MOE) based on obtained <i>in vitro</i> PoDs (NOEC, LOEC, BMC <sub>10</sub> ) for all key events (KE1 - KE3) from both cell lines (RPTEC/TERT1 & NRK-52E) and from published <i>in vivo</i> human serum, rat serum & rat kidney concentrations. Calculated MOE (< 10) considered with a high risk are marked in red, MOE between 10 – 100 considered with a moderate risk are marked in yellow and MOE considered with low (> 100) are marked in green, n.a. not available <i>in vitro</i> or <i>in vivo</i> data.....	145
Table 37 Serum concentrations of adefovir and tenofovir in humans and rats Serum and mean serum concentrations of adefovir in humans after administration of	

---

therapeutic doses of ADV (10 mg, resp. 20 mg; <i>p.o.</i> ) and serum concentrations in rats after <i>i.v.</i> administration (4 mg/kg) resp. after <i>p.o.</i> administration (10 mg/kg). Serum and mean serum concentrations of tenofovir in humans after single dose of 300 mg TDF ( <i>p.o.</i> ) and rats after <i>p.o.</i> administration of TDF (10 mg/kg, 15 mg/kg, 30 mg/kg) .....	147
Table 38 Calculated <i>in vitro</i> PoDs (NOEC, LOEC, BMC <sub>10</sub> ) from <i>in vitro</i> assays for the AOP – <i>Inhibition of mtDNA polymerase-γ</i> PODs are given in μM for each key event (KE 1 – 3) from RPTEC/TERT1 cells after 14 d treatment with adefovir, tenofovir, adefovir dipivoxil (ADV) and tenofovir disoproxil fumarate (TDF), n.a. not available <i>in vitro</i> data.....	148
Table 39 Calculated margin of exposure (MOE) based on <i>in vitro</i> PoDs (NOEC, LOEC, BMC <sub>10</sub> ) for all key events (KE1 – 3) from RPTEC/TERT1 cells and from published <i>in vivo</i> human & rat serum concentrations Calculated MOE (< 10) considered with a high risk are marked in red, MOE between 10 – 100 considered with a moderate risk are marked in yellow and MOE considered with low or even no risk (> 100; > 1000) are marked in green, n.a. not available <i>in vitro</i> or <i>in vivo</i> data .....	151
Table 40 Raw data LAMP-1/2 assay .....	225
Table 41 Raw data cathepsin assay .....	227
Table 42 Raw data cytotoxicity AOP1 .....	229
Table 43 Raw data LC-MS/MS .....	231
Table 44 Raw data cell volume .....	256
Table 45 Raw data aprotinin assay .....	258
Table 46 Raw data mtDNA copy number assay.....	259
Table 47 Raw data MitoTracker <sup>®</sup> assay .....	262
Table 48 Raw data cytotoxicity AOP2 .....	266



## **List of abbreviation**

### **A**

Å	Angstrom
ACTB / Actb	Actin beta
Ade	Adefovir
ADME	Adsorption, distribution, metabolism, excretion
ADV	Adefovir dipivoxil
AG	Aminoglycoside
AO	Adverse outcome
(q)AOP	(quantitative) Adverse outcome pathway
ATP	Adenosine triphosphate

### **B**

B2M	Beta-2-microglobulin
BCRP	Breast cancer resistance protein
BMC	Benchmark concentration
BMCL	Benchmark concentration lower confidence limit
BMCU	Benchmark concentration upper confidence limit
BMD	Benchmark dose
BMDL	Benchmark dose lower confidence limit
BMDU	Benchmark dose upper confidence limit
BP	Binding protein
BSA	Bovine serum albumin
BW	Body weight

### **C**

Cat#	Catalog number
CaCo-2	Caucasian colon adenocarcinoma 2 cells
cDNA	Complementary DNA
CE	Collision energy
CEP	Collision entrance potential
CES	Carboxylesterase
CFL	CruzFluor™

Cido	Cidofovir
Col	Colistin
C <sub>T</sub>	Cycle threshold
CUBN / Cubn	Cubilin
CV	Coefficient of variation
CXP	Cell exit potential
CYP	Cytochrome P450
<b>D</b>	
d	Diameter
DAPI	4',6-Diamidin-2-phenylindol
DC	Detergent compatible
ddC	Zalcitabine
ddH <sub>2</sub> O	Double distilled water
DMEM	Dulbecco's modified eagle medium
DNA	Deoxyribonucleic acid
dNTP	Nucleoside triphosphate
DP	Declustering potential
<b>E</b>	
EC <sub>x</sub>	Effective concentration x
EDTA	Ethylenediaminetetraacetic acid
EGF	Epidermal growth factor
Em	Maximal emission
ENT	Equilibrative nucleoside transporter
EP	Entrance potential
ER	Endoplasmic reticulum
Ex	Maximal excitation
<b>F</b>	
F	Forward primer
FAM	6-carboxyfluorescein
FBS	Fetal bovine serum
FCS	Fetal calf serum
FMO	Flavin-containing monooxygenase

**G**

g	Gravitation
GAPDH / Gapdh	Glyceraldehyde 3-phosphate dehydrogenase
GST	Glutathione-S-transferase

**H**

h	Hour
HIV	Human immunodeficiency viruses
HK-2	Human kidney 2 cells
HPLC	High-performance liquid chromatography
HRP	Horseradish peroxidase

**I**

<i>i.v.</i>	Intravenous
ICC	Immunocytochemistry
ID	Identification
IgG	Immunoglobulin G
ITS	Insulin, transferrin, sodium selenite
IU	International units

**K**

KE	Key event
(q)KER	(quantitative) Key event relationship
KO	Knockout

**L**

LAMP-1 / 2	Lysosome-associated membrane protein 1 / 2
LC	Liquid chromatography
LMP	Lysosomal membrane permeabilization
LOD	Limit of detection
LOQ	Limit of quantification
LRP2 / Lrp2	Low-density lipoprotein receptor-related protein 2

**M**

MATE	Multidrug and toxic compound extrusion
MCTF	Megalin carboxyl-terminal fragment
MDR	Multi drug resistance protein

MEM	Minimum essential media
MGB	Minor groove binder
MIE	Molecular initiating event
min	Minute
MOE	Margin of exposure
MOPS	3-(N-Morpholino) propane sulfonic acid
MOS	Margin of safety
MRP	Multidrug resistance-related protein
MS	Mass spectrometry
MTD	Maximum tolerated dose
mtDNA	Mitochondrial DNA
MT-TL1	Mitochondrially encoded tRNA leucine 1
MW	Molecular weight
<b>N</b>	
n/a	Not available
NEAA	Non-essential amino acids
NRC	National Research Council
NRK-52E	Normal rat kidney cells 52E
nRT	Non-reverse transcriptase
NRTI	Nucleoside reverse transcriptase inhibitor
NtC	Non-toxic concentration
nucDNA	Nuclear DNA
<b>O</b>	
OAT	Organic anion transporter
OCT	Organic cation transporter
OCTN	Organic cation / carnitine transporter
OECD	Organization for economic co-operation and development
<b>P</b>	
<i>p.o.</i>	Per os
PAGE	Polyacrylamide gel electrophoresis
PB	Polymyxin B
PBNP	Polymyxin B nonapeptide



PBS	Phosphate-buffered saline
PCR	Polymerase chain reaction
PDE	Phosphodiesterase
Pen	Penicillin
PEPT	Peptide transporter
PIC	Protease inhibitor cocktail
PoD	Point of departure
PVDF	Polyvinylidene fluoride
<b>Q</b>	
QID	<i>Quater in die</i>
QIVIVE	Quantitative <i>in vitro</i> to <i>in vivo</i> extrapolation
QSAR	Quantitative structure-activity relationship
<b>R</b>	
R	Reverse primer
R <sup>2</sup>	Correlation coefficient
RE	Relative error
REACH	Registration, evaluation, authorization, and restriction of chemicals
RIP	Regulated intramembrane proteolysis
RNA	Ribonucleic acid
RNS	Reactive nitrogen species
ROS	Reactive oxygen species
RPTEC/TERT1	Renal proximal tubule epithelial cells / telomerase reverse transcriptase 1
RT	Retention time
<b>S</b>	
<i>s.c.</i>	Subcutaneous
S/N	Signal-to-noise ratio
SDS	Sodium dodecyl sulfate
sec	Second
Strep	Streptomycin
SULT	Sulfotransferase

**T**

TBST	Tris-buffered saline with Tween20
TC <sub>x</sub>	Toxic concentration
TDF	Tenofovir disoproxil fumarate
Teno	Tenofovir
TRITC	Tetramethylrhodamine B isothiocyanate
TRIS	Tris(hydroxymethyl)aminomethane
<b>U</b>	
UGT	Glucuronosyltransferase
UNG	Uracil-N-glycosylase
URAT	Urate transporter
UV-Vis	Ultraviolet-visible spectroscopy
<b>V</b>	
V	Volt



## **1 Introduction**

Nowadays life without chemicals is hard to imagine. All the designed chemicals, such as pharmaceuticals, pesticides, or chemical compounds from our daily life, also pose potential risks to health and the environment. The potential risk posed by these drugs and chemicals must be investigated and evaluated before they are placed on the market. For the safety assessment of the individual substances, testing is largely based on animal experiments which are often considered as the ‘gold standard’ (Prior *et al.*, 2019). This test strategy was developed by the Organization for Economic Co-operation and Development (OECD) to identify potential adverse effects caused by chemicals using standardized and internationally agreed animal test methods. Nevertheless, these test models were developed in the early 1930s out of necessity in order to provide an acceptable level of health protection (Abbott, 2005). Ethical criticism of the use of laboratory animals for safety assessment of chemicals is understandably becoming louder.

As the demand for testing of new and existing chemicals (REACH) is growing, and legal restrictions on the use of laboratory animals have been enacted such as the 7th EU Directive on Cosmetics (76/768/EEC), a fundamental reconsideration of testing and safety assessment is required. Apart from the fact that animal experiments provide a low throughput, they are still associated with very high costs and their predictivity is very limited. An article published in Nature in 2005 expresses it in numbers: the safety testing of a single chemical requires 5,000 animals (12,000 if it is a pesticide). To comply with REACH requirements, the cost of the approximately 30,000 unregistered chemicals is estimated at 5 to 10 billion euro. To test the carcinogenic potential of a single chemical takes about 5 years and 400 rats. The finding that

more than 50 % of the chemicals are tested positive for carcinogenicity, with 90 % of them being false positive (Abbott, 2005), highlights the limited predictivity of animal tests.

Even from a scientific point of view, risk assessment based on animal experimental data is to be viewed critically (Gubbels-van Hal *et al.*, 2005). One of these challenges, which is associated with many uncertainties, is the quantitative risk assessment based on *in vivo* data. Toxicity studies in animals are carried out at relatively high doses of the test substances and are then extrapolated to low human doses, using empirically derived uncertainty factors (*e.g.*, dose to dose, route to route, species to species) (Piegorsch, 2014, National Research Council, 1994, Clewell I and Andersen, 1987, Brown, 1984). Carcinogenicity studies are often mentioned as examples, where the highest tolerable doses are used in animal experiments and then extrapolated to human doses that are several orders of magnitude lower (Abbott, 2005, Kodell and Gaylor, 1997). This leads to considerable uncertainties in the assessment. A further disadvantage of the previous test strategy in animals is the determination of apical endpoints, which provide no or at best limited information on mechanisms of toxicity (Rovida *et al.*, 2015b, Krewski *et al.*, 2009). This gap in mechanistic information contradicts the recognition that mechanistic data can make a decisive contribution to a scientifically based risk assessment.

The increasing number of chemicals requiring toxicological testing and estimates of the number of animals required have led to the awareness that comprehensive toxicological testing of all chemicals is neither practicable nor ethically justifiable. Against this background, the development of alternative test methods, which involve the replacement, reduction or refinement of laboratory animals (principles of the 3Rs) (Russell and Burch, 1959) is legally required by the European Union (Directive 2010/63/EU, 2010).

Previous initiatives to reduce the amount of laboratory animals used for toxicity testing aimed at replacing individual guideline studies with animal-free or less animal-tested methods. For some local toxic effects such as irritation and corrosion of skin and eyes, alternative test methods have already been successfully established and validated (European Commission, 2017, European Commission, 2015). However, there are no useful alternative test methods for testing for systemic organ toxicity or chronic effects.

### **1.1 A paradigm shift in toxicology testing: Tox21**

The US National Research Council (NRC) published a report in 2007 entitled: Toxicity Testing in the 21<sup>st</sup> Century: A Vision and A Strategy (Tox21) (National Research Council, 2007), which calls for a complete paradigm shift in toxicological testing and risk assessment (Worth *et al.*, 2014). A central aspect of this vision is a shift from apical endpoints in animals to *in vitro* high-throughput approaches in predominantly human cells. This should make it possible to better detect disturbances of the cellular signaling pathways caused by toxic compounds and thereby to predict toxic effects. However, a consensus suggests that it is currently not possible to completely dispense with safety testing on animals without compromising drug or chemical safety (Araújo *et al.*, 2014). Rather, a first pragmatic step towards animal-free methods is seen in the development of multi-stage test strategies (Rovida *et al.*, 2015a). Such strategies include modern *in silico* methods, *in vitro* bioactivity assays and quantitative *in vitro* – *in vivo* extrapolation in the first stage, followed by the second stage with studies on alternative model organisms like zebrafish embryos (*Danio rerio*), nematodes (*Caenorhabditis elegans*), or fruit flies (*Drosophila melanogaster*), and, if necessary, a third stage with conventional guideline studies (Hunt, 2017, Rand *et al.*, 2014, Thomas *et al.*, 2013, Dai *et al.*, 2014) (Figure 1).

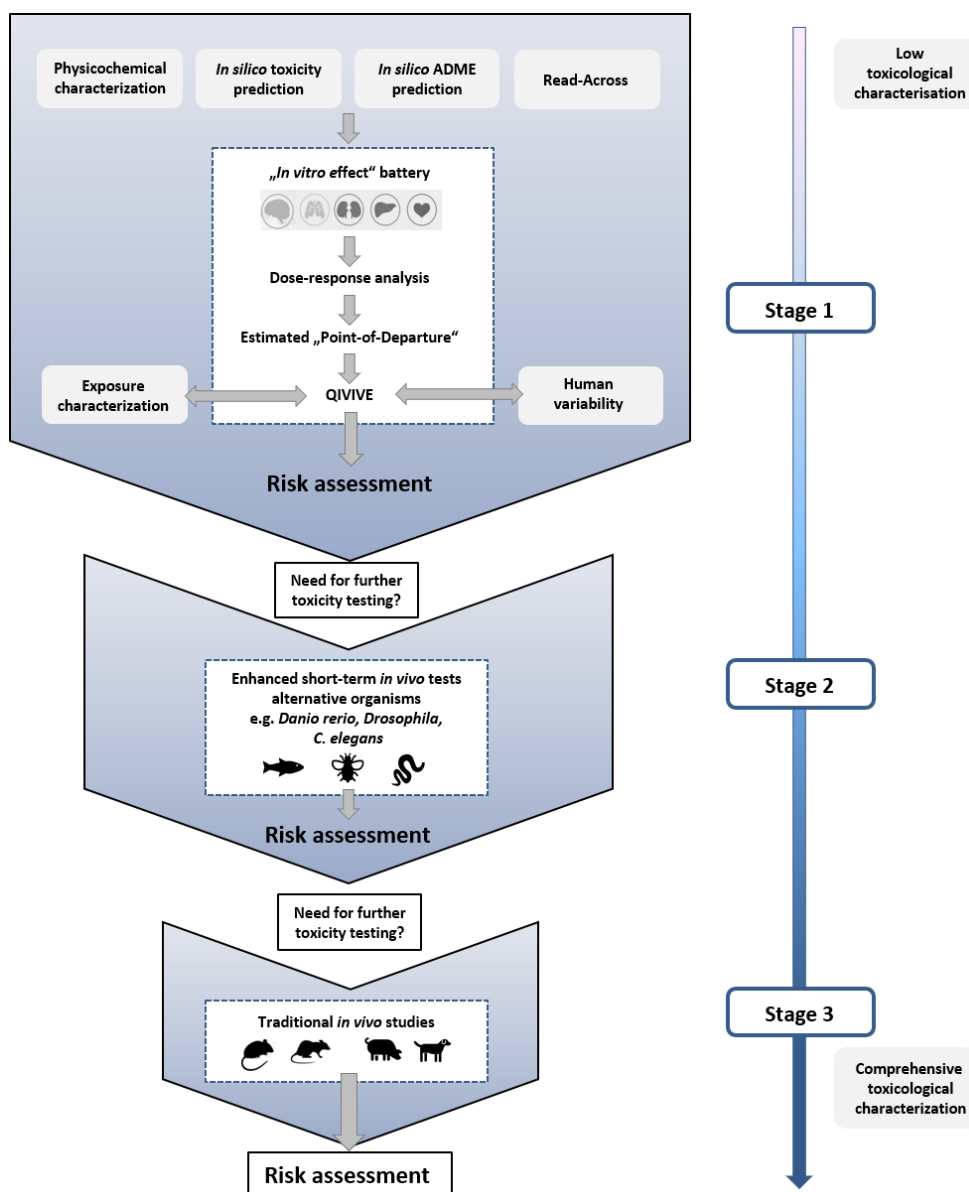


Figure 1

**Schematic description of a multi-stage strategy for toxicity testing**

Stage 1 includes *in silico* methods, *in vitro* bioactivity assays in combination with QIVIVE. Stage 2 includes improved *in vivo* tests on alternative model organisms, followed by the third stage with conventional guideline studies.



## 1.2 The adverse outcome pathway (AOP) concept

To accelerate the development of suitable alternative test methods, the OECD has adapted the Adverse Outcome Pathway (AOP) concept. An AOP is described as a “causally related sequence of key events (KE), beginning with the molecular initiating event (MIE) which describes an interaction of a chemical with a cellular target, and leading to an adverse outcome (AO) at the organ, organism, or population level at the end of the sequence” (Bal-Price and Meek, 2017, Villeneuve *et al.*, 2014, Vinken *et al.*, 2017), or simply described as a ‘biological domino effect’ (Liu *et al.*, 2019). An AOP is therefore a formal description of the mechanistic relationships between a MIE and a defined toxicity endpoint (Figure 2) (Vinken, 2013).



**Figure 2**

### Schematic description of an AOP

MIE (molecular initiating event), KE (key event), KER (key event relationship), and AO (adverse outcome).

There is broad consensus among many scientists that systematic identification of KEs and mapping of AOPs provides a solid mechanistic basis for the development of suitable alternative test batteries (Spinu *et al.*, 2019, Bal-Price and Meek, 2017, Ankley *et al.*, 2010). Using this mechanistic framework in combination with modern *in silico* methods such as quantitative structure-activity relationship models (QSAR) and quantitative *in vitro* to *in vivo* extrapolation (QIVIVE) (Benfenati *et al.*, 2019, Escher *et al.*, 2019) as well as *in vitro*, *ex vivo* models and tests in lower organism (*e.g.*, zebrafish embryos, nematodes, fruit flies) may enhance the prediction of toxicity assays while at the same time reducing the use of conventional *in vivo* studies (Figure 1)

(Bal-Price and Meek, 2017, Edwards *et al.*, 2016). To develop and implement such a test strategy, which should meet regulatory requirements, several aspects have to be considered. Basic requirements for the establishment of *in vitro* assays were already highlighted in the National Research Council's publication 'Toxicity Testing for the 21<sup>st</sup> Century: a Vision and a Strategy' (National Research Council, 2007). The most important requirement for the *in vitro* assays is to internalize the basic idea of the AOP concept and therefore to cover the anchored mechanistic framework that leads to an adverse outcome (Halappanavar *et al.*, 2020, Coady *et al.*, 2019). In order to determine safe human exposure levels for quantitative risk assessment, the data obtained from the *in vitro* assays must be translated into *in vivo* dosimetry data (Zhang *et al.*, 2018b). The degree of confidence in risk assessment based on *in vitro* data must then be evaluated and compared with the *in vivo* observations, which is of major interest for regulatory decision making (Bale *et al.*, 2014).

Animal experiments required by regulatory authorities and carried out in industry to predict systemic toxicity, especially kidney toxicity in humans, quickly reach their limits in part due to interspecies differences (Knight *et al.*, 2006, Hartung, 2017). Alternative methods that have a better predictivity are therefore more and more in demand. However, so far no *in vitro* nephrotoxicity assays have been used or applied in regulatory toxicology. Reasons for this are limitations of previous *in vitro* models such as altered metabolic activities (cancer cells), donor-to-donor variability (primary cells), and artificial non-physiological conditions in which cells are maintained (Hartung and Daston, 2009, Roggen, 2011).

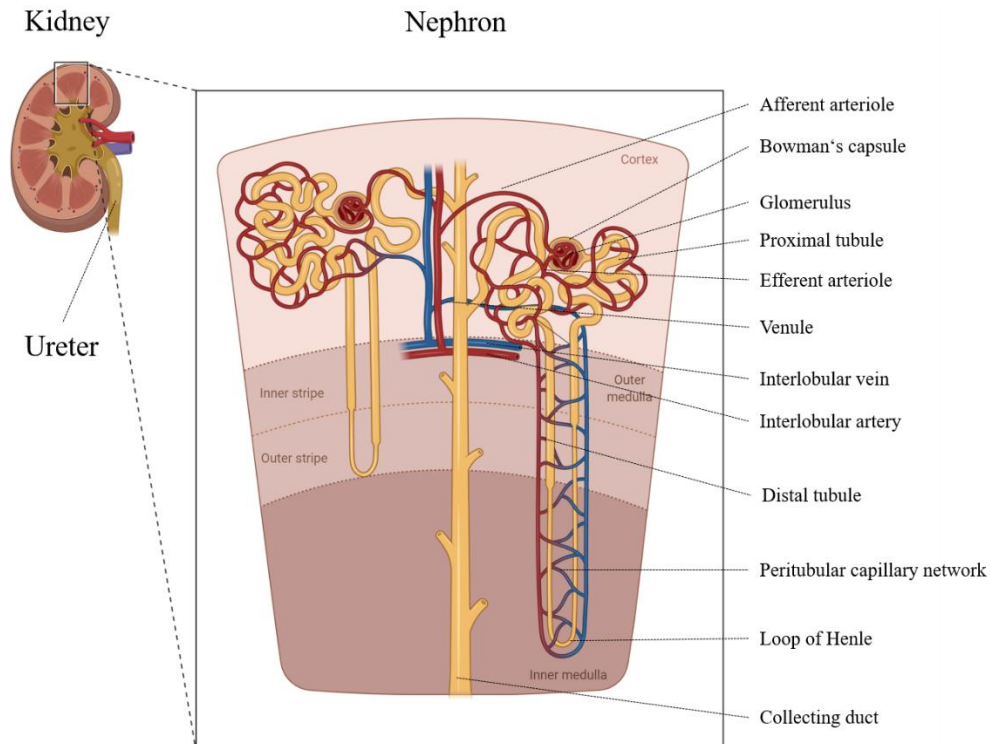
Besides the liver, the kidneys play a central role in toxicology and risk assessment. The kidneys are a target organ for many (environmental) chemicals, drugs and heavy metals as they act as an excretion organ for endogenous and exogenous substances, with a high blood flow rate in

relation to their mass (Haschek *et al.*, 2013a, Nelson *et al.*, 2018, Rall and Pope, 1995). Besides urine, these foreign substances are also concentrated in the kidneys, thus exposing the kidneys to increased exposure to xenobiotics. Especially because of the increased transport activity, accumulation and metabolism, the kidneys are particularly susceptible to various injuries (Schnellmann, 2008). One of the primary drug-induced adverse effects and consequently an exclusion criterion for further drug development in the pharmaceutical industry is kidney damage observed in experimental animals (Jang *et al.*, 2013, Giffin *et al.*, 2009). Because of this central toxicological importance and the lack of alternative methods for predicting systemic toxicity in humans, the present work focuses on the mechanisms leading to kidney toxicity.

### **1.3 Kidney as a target organ for toxicity**

Each healthy human kidney consists of approximately 0.8 – 1.5 million nephrons, which form the functional subunits of the kidney. The nephrons are composed of the glomerulus and the tubule with its segments: proximal tubule, loop of Henle, distal tubule (Figure 3) (Preuss, 1993). The Bowman's capsule, a spherical and double-walled capsule formed by parietal epithelial cells, encloses the glomerulus in which the filtration of the blood takes place. The filtration barrier consists of endothelial cells, podocytes, and the glomerular basement membrane (Miner, 2011). About 300 times a day, the entire blood volume of a person flows through his two kidneys, a total of about 1500 L. This filtration capacity of about 125 mL / min produces about 180 L of primary urine (Carroll and Abdel-Rahman, 2014). The composition of this primary urine is similar to that of blood plasma, with the exception of macromolecules with over ~ 60 kDa which are retained in the glomerulus (Christensen *et al.*, 2012). The primary urine is then concentrated in the tubule sections by absorption and secretion. Essential electrolytes, amino acids and 99 % of water are reabsorbed, while substances such as urea, uric acid, creatinine,

toxic metabolites and exogenic substances are secreted and finally excreted in the urine (Smith, 1951).



**Figure 3**

**The human kidney with its functional subunits, the nephrons**

The schematic structure of the nephron shows the individual sections, starting with the glomerulus and its filter function, through the proximal tubule, the loop of Henle, the distal tubule and the connecting collecting duct. (Adapted from “*Nephron in kidney section (labelled)*”, by BioRender.com (2020). Retrieved from <https://app.biorender.com/illustrations/edit/5cd1916b6977ac003346bd35>)

Along with the brain and lungs, the kidney is one of the organs with the best blood supply in the human body. This high blood flow rate allows many metabolites and membrane permeable xenobiotics such as drugs, fungal toxins, heavy metals and organic solvents to accumulate in high concentrations in the kidneys, resulting in different types of renal damage, especially in the proximal tubule. Proximal tubule cells possess a high number of transporters, located on the

luminal and basolateral side, that mediate influx, efflux or both (Figure 4, Table 1) (Chu *et al.*, 2016, Zennaro *et al.*, 2014, Lash *et al.*, 2006).

**Table 1**  
**Transporter of proximal tubule cells**

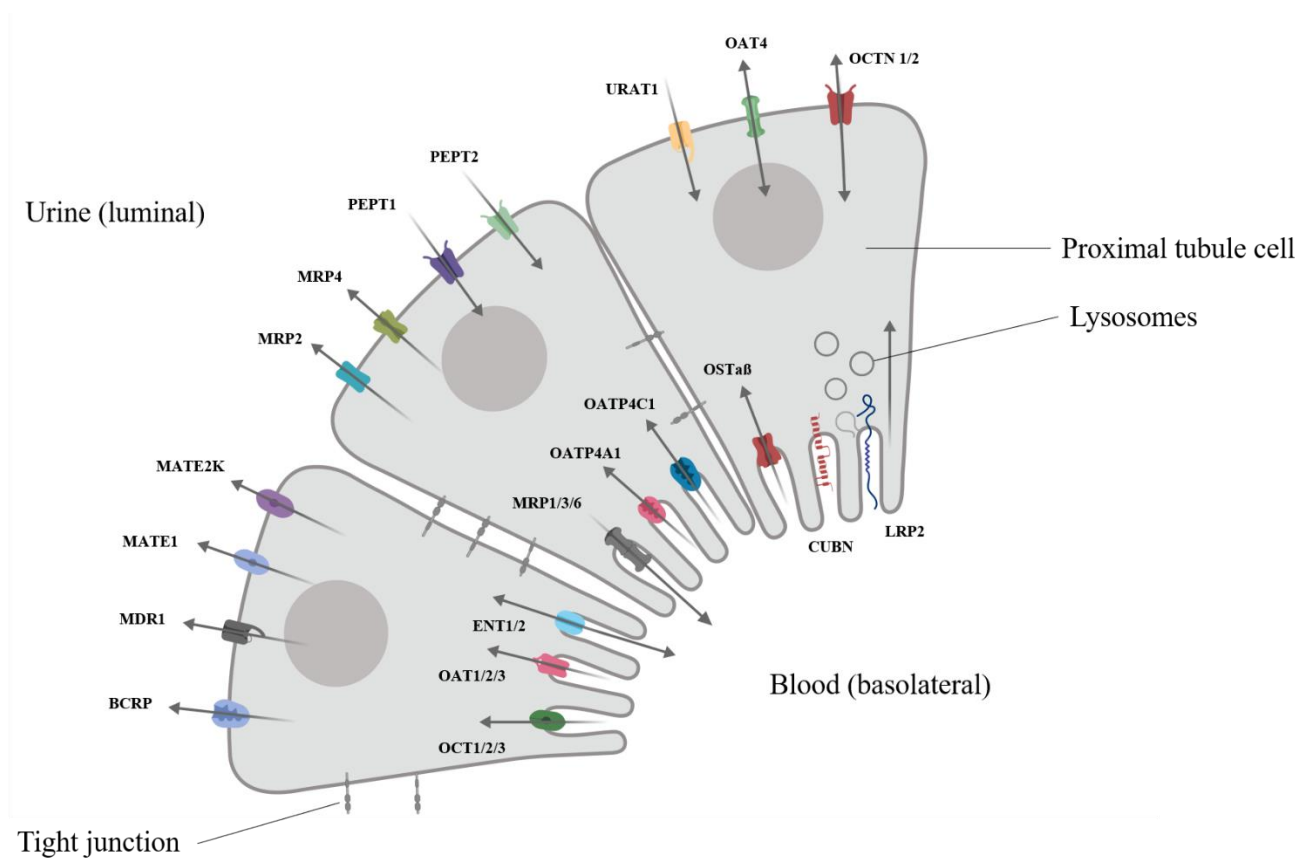
Transporters are located on the luminal and basolateral side of the proximal tubule cells responsible for influx, efflux, or both

<b>Function</b>	<b>Symbol</b>	<b>Name</b>	<b>Localization / Side</b>
<b>Influx</b>	CUBN	Cubilin	Basolateral
	LRP2	Low-density lipoprotein receptor-related protein 2	Basolateral
	OAT1-3	Organic anion transporter 1-4	Basolateral
	OATP4A1/C1	Organic anion transporter 4A1/C1	Basolateral
	OCT1-3	Organic cation transporter 1-3	Basolateral
	OST $\alpha/\beta$	Organic solute transporter $\alpha/\beta$	Basolateral
	PEPT1/2	Peptide transporter 1/2	Luminal
	URAT1	Urate transporter 1	Luminal
<b>Efflux</b>	BCRP	Breast cancer resistance protein	Luminal
	MATE1/2K	Multidrug and toxic compound extrusion 1/2K	Luminal
	MDR1	Multi drug resistance protein 1	Luminal
	MRP1-4/6	Multidrug resistance-related protein 1-4/6	Basolateral / luminal
<b>Influx and efflux</b>	ENT1/2	Equilibrative nucleoside transporter 1/2	Basolateral
	OAT4	Organic anion transporter 4	Luminal
	OCTN1/2	Organic cation / carnitine transporter 1/2	Luminal

At the ultra-structural level, the proximal tubule can be divided into three additional segments termed S1, S2 and S3 (Zhuo and Li, 2013, Cristofori *et al.*, 2007). The differences between these three segments are mainly characterized by the expression of transporters of the proximal tubule in different ratios and hence different endocytotic functions and transport (Polesel and Hall, 2019, Schuh *et al.*, 2018, Cristofori *et al.*, 2007). The megalin receptor (LRP2), which is mainly responsible for the reuptake of proteins but also for the uptake of protein structure-like antibiotics like polymyxins, is mainly expressed in the first two sections (S1 and S2) of the proximal tubule (Schuh *et al.*, 2018, Eshbach and Weisz, 2017, Christensen *et al.*, 2012). The expression pattern in the individual segments differs for the organic anion transporters 1 / 3 (OAT1/3). While OAT1 is expressed more in the S2 segment and less in S1 and S3 of the proximal tubule, OAT3 activity is strongest in the first segment (S1) and decreases in the remaining two segments (S2 >> S3) (Lungkaphin *et al.*, 2006). Thus, uptake via OAT1 and OAT3 occurs predominantly in the second section (S2) of the proximal tubule (Breljak *et al.*, 2016).

Proximal tubule cells also express a wide range of phase I and II metabolizing enzymes *e.g.*, cytochrome P450 (CYP), flavin-containing monooxygenase (FMO), glutathione S-transferase (GST), sulfotransferase (SULT), glucuronosyltransferase (UGT) (Cashman and Zhang, 2006, Krause *et al.*, 2003, Amet *et al.*, 1997, Cummings and Lash, 2000, Cummings *et al.*, 2000a, Nishimura and Naito, 2006). Due to the high metabolic activity of proximal tubule cells, these cells are a sensitive target for toxic metabolites that are responsible for a number of kidney damages like tubular necrosis, crystal nephropathy or Fanconi syndrome (Shahrbaf and Assadi, 2015). Several mechanisms that can lead to kidney injury are fairly well established. A classic example that also plays an important role in liver toxicity is the covalent binding of metabolites to cellular proteins produced by bioactivation of *e.g.*, acetaminophen or tetrachloroethene

(Mudge *et al.*, 1978, Lash and Parker, 2001, Lock and Reed, 2006). In addition to high metabolic activity, proximal tubule cells are also exposed to a higher risk of accumulation of foreign substances such as heavy metals (*e.g.*, cadmium, mercury, lead) or antibiotics of the aminoglycoside or polymyxin group due to their high capacity for endocytosis (Figure 4) (Barbier *et al.*, 2005, Nagai and Takano, 2014, Azad *et al.*, 2015).



**Figure 4**

**Schematic representation of proximal tubule cells and their transporters**

Transporters expressed on the luminal and basolateral side of the proximal tubule cells responsible for influx, efflux, or both (Created with BioRender.com (2020). Retrieved from <https://app.biorender.com/illustrations/edit/5cd2cb8ecc53ba0033a8ce43>)

Preferential uptake of antivirals such as cidofovir and adefovir via OAT1/3 also plays an important role in the development of kidney damage in response to these drugs (Izzedine *et al.*, 2005). These mechanisms, which are described in more detail in the following chapters, were selected for the development of AOPs.

### **1.3.1 Mechanism of drug-induced kidney injury via *Receptor-mediated endocytosis and lysosomal overload* and establishment of an AOP as a basis for development of *in vitro* assays covering key events within this AOP**

Substances such as aminoglycoside or polymyxin antibiotics can pass through the glomerular filter due to their low molecular weight and thus reach the proximal tubule from the luminal side. On the cellular surface of the proximal tubule cells, a variety of transporters are expressed, such as the cubilin:megalin-complex (Figure 4). The main function of this 917 kDa complex is the reabsorption of endogenous substances that have passed the glomerular filter such as vitamins, carrier proteins, lipoproteins and hormones (Eshbach and Weisz, 2017). However, due to their peptide structure, antibiotics of the polymyxin group (Table 2) or aminoglycoside group also have an affinity to the cubilin:megalin-complex and act as ligands, which leads to uptake into the proximal tubule cells via receptor-mediated endocytosis (Nielsen *et al.*, 2016). This uptake path represents the starting point and is defined in the AOP as the MIE. After uptake, the antibiotics can accumulate in high concentrations in the lysosomes and disrupt lysosomal functions (KE1). Disturbance of lysosomal functions leads to lysosomal swelling and, as a result, to bursting of lysosomes. This on the one hand leads to the release of the accumulated polymyxin antibiotics but also to the release of reactive oxygen species (ROS) and lysosomal proteases such as cathepsins into the cytosol (KE2) (Oberle *et al.*, 2010). Release of lysosomal compartments can induce activation of the mitochondrial pathway of apoptosis. Furthermore,



oxidative stress can be induced, as well as a reduction of ATP reserves, which is associated with cytotoxicity of renal tubule cells. (KE3) (Figure 5) (Quiros *et al.*, 2010).

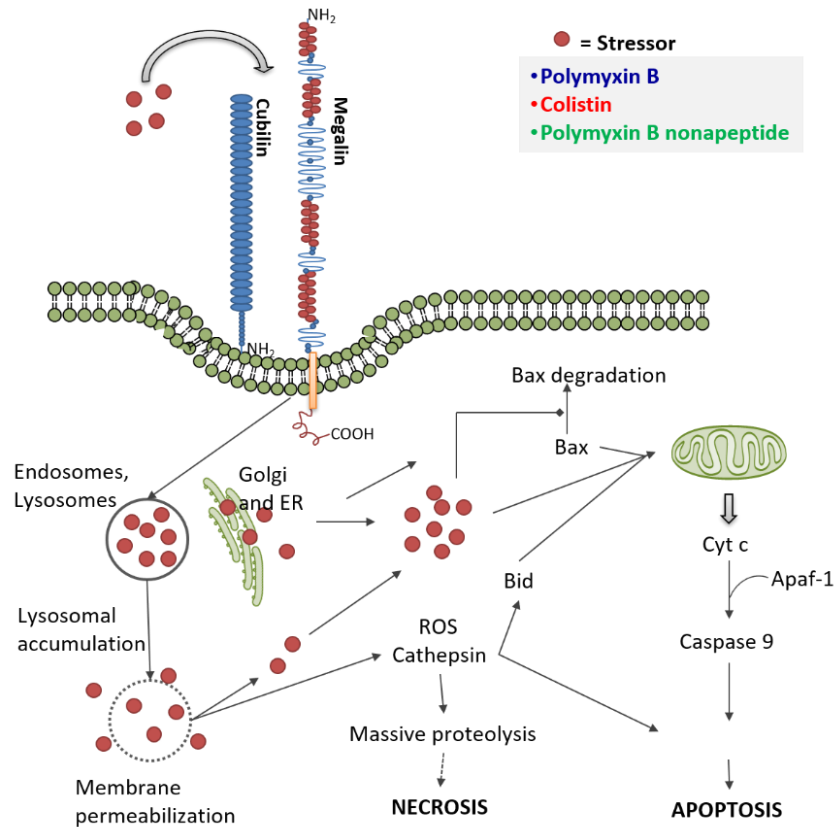
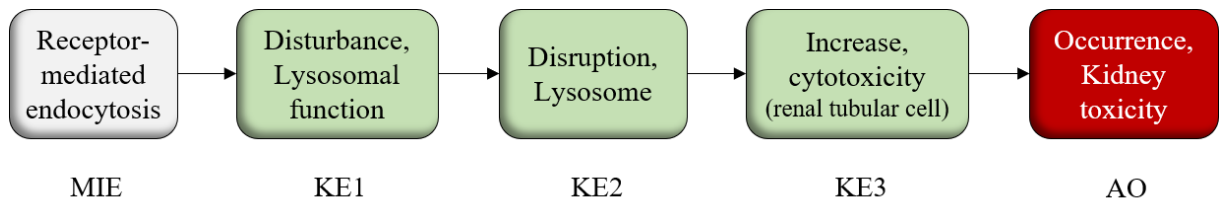


Figure 5

Cellular uptake of polymyxin antibiotics via receptor-mediated endocytosis and mechanisms leading to cytotoxicity of proximal tubule cells through necrosis and the mitochondrial pathway of apoptosis (modified from (Quiros *et al.*, 2010))

Based on the existing and published information on the mechanism, the AOP – *Receptor-mediated endocytosis and lysosomal overload* was developed in accordance with the harmonized terminology provided by AOPWiki and the following MIE and KEs leading to renal toxicity were defined:



**Figure 6**

***AOP – Receptor-mediated endocytosis and lysosomal overload***

The AOP describes the subsequent sequence of key events leading to kidney injury as an AO and can be described as *Receptor-mediated endocytosis* (MIE), leading to *Disturbance of lysosomal function* (KE1), *Disruption of lysosomes* (KE2) and *Proximal tubule cell toxicity* (KE3)

**1.3.2 Mechanism of drug-induced kidney injury via inhibition of mitochondrial DNA polymerase- $\gamma$  and establishment of AOPs as a platform for development of *in vitro* assays**

Despite their known side effects, which include nephrotoxicity and, in the worst case, acute kidney failure, nucleosidic antivirals remain important drugs to combat viruses such as HIV, hepatitis B and C (De Clercq, 2003, Reynaud *et al.*, 2009). The main target of toxicity of some of these antivirals, *e.g.*, those which belong to the group of acyclic nucleoside phosphonates (adefovir, cidofovir, and tenofovir), are the proximal tubule cells. Due to the abundant expression of transporters on the basolateral side of the proximal tubule cells (Figure 4), representatives of this group such as adefovir, cidofovir or tenofovir enter the proximal tubule cells via organic anion transporters (OAT1 / OAT3) (Hagos and Wolff, 2010). In the cells, these drugs incorporate into mitochondrial DNA (mtDNA) and inhibit mitochondrial DNA-polymerase- $\gamma$  (MIE) (Fernandez-Fernandez *et al.*, 2011). This inhibition leads to a reduction of the mtDNA copy number (KE1) and decreased expression of essential proteins of the respiratory chain, such as cytochrome c oxidase, ultimately resulting in mitochondrial dysfunction (KE2). The mitochondrial dysfunction can lead to a deficiency of energy in the cells, which in turn leads to

damage to the proximal tubule cells (KE3) (Tanji *et al.*, 2001, Markowitz and Perazella, 2005, Perazella, 2010) (Figure 7).

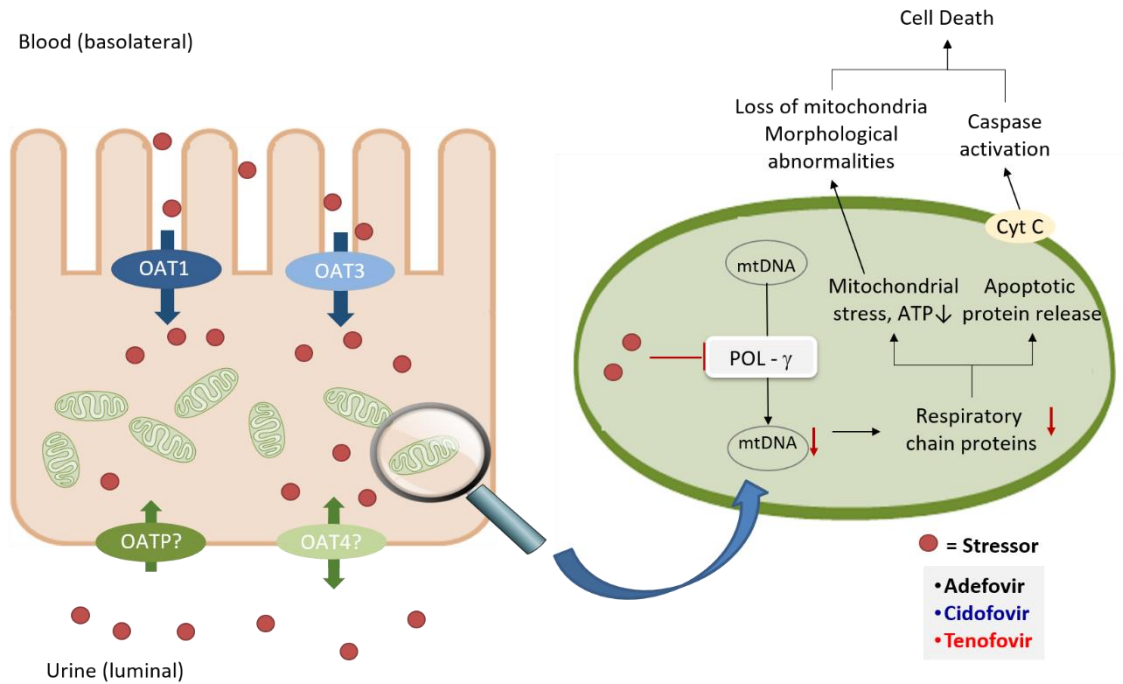
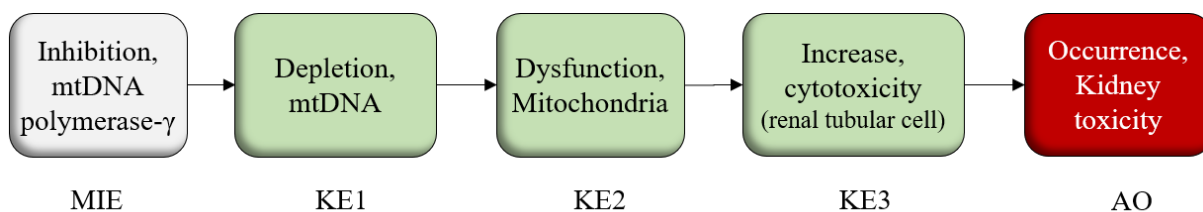


Figure 7

Mechanism of drug induced kidney injury via *Inhibition of mtDNA polymerase- $\gamma$*  (modified from (Fernandez-Fernandez *et al.*, 2011))

Based on the current understanding of the mechanism leading to cytotoxicity of proximal tubule cells by antiviral drugs, the following key events have been identified for the AOP which describes the sequential key events that link *Inhibition of mtDNA polymerase- $\gamma$*  to kidney toxicity:



**Figure 8**

***AOP – Inhibition of mtDNA polymerase- $\gamma$***

The AOP describes the subsequent sequence of key events leading to kidney injury as an AO and can be described as *Inhibition of mtDNA polymerase- $\gamma$*  (MIE), leading to *Depletion of mtDNA* (KE1), *Mitochondrial dysfunction* (KE2) and *Proximal tubule cell toxicity* (KE3)

The sequences of key events in each of the two AOPs (Figure 6, Figure 8) form the basis for developing suitable *in vitro* assays reflecting each KE across the AOPs. Mechanistic *in vitro* endpoints were assessed in human (RPTEC/TERT1) and rat renal proximal tubule epithelial cells (NRK-52E) treated with model compounds (Table 2, Table 3) relevant for each AOP in order to provide experimental support for the AOP and to establish quantitative relationships between KEs.

#### **1.4 Cell lines used for *in vitro* assays**

Since the kidneys are targets for a number of chemicals and drugs, renal damage observed in test animals is one of the primary drug-induced adverse effects and thus a potential selection criterion for further drug development (Bajaj *et al.*, 2018, Giffin *et al.*, 2009). Additionally, kidney damage is often detected late during preclinical drug development and therefore strategies are required to predict such adverse effects at an earlier stadium (Huang *et al.*, 2015, Tiong *et al.*, 2014). *In vitro* approaches that can predict these effects are lacking, but developments of improved and suitable *in vitro* systems are in progress. However, the main challenge is to imitate the complex physiological functions of the kidneys as much as possible. In addition to conventional 2D cell culture models, which are easy to handle but offer comparatively low physiological complexity, efforts are ongoing in the development of *in vitro* approaches towards 2.5D cell culture models (*e.g.*, inserts with extracellular matrix components), 3D models (*e.g.*, organoids, scaffold, fluid flow) up to complex kidney-on-chip or even human-on-chip approaches (Faria *et al.*, 2019, Lee and Kim, 2018, Kim and Takayama, 2015). Suitable renal cell lines to support these *in vitro* approaches are available, although most have some limitations (Faria *et al.*, 2019). A common rat kidney epithelial cell line (NRK-52E) and a novel immortalized human proximal tubule epithelial cell line (RPTEC/TERT1) that were utilized in this thesis are described in detail in the following sections.

#### 1.4.1 RPTEC/TERT1 cell line

The human cell line RPTEC/TERT1 is a comparatively new cell line. Immortalization of primary human RPTECs (renal proximal tubular cells) was achieved by overexpressing the catalytic subunit of human telomerase reverse transcriptase (hTERT) (Wieser *et al.*, 2008). Compared to the currently available human proximal tubule cells, this cell line is the only one that was not transformed using viral oncogenes (Wieser *et al.*, 2008, Aschauer *et al.*, 2015a). The similarity of this cell line compared to proximal tubule cells in the *in vivo* situation was demonstrated by the fact that RPTEC/TERT1 cells shows a normal and stable male diploid karyotype. They also show structural and biochemical renal proximal tubule epithelial cell characteristics without genome instability in over 90 population doublings (Wieser *et al.*, 2008). Important characteristics and functional properties include dome formation, water and cation transport (Wieser *et al.*, 2008, Wilmes *et al.*, 2014, Aschauer *et al.*, 2015a). It was also shown at the mRNA and / or protein level that RPTEC/TERT1 cells express a variety of relevant proximal tubule transporters such as megalin, cubilin, organic cation and anion transporters (OCT2, OCT3, OCTN2, OAT1, OAT3, OATP4C), multidrug and toxin extrusion protein 1/2 (MATE1/2), and ATP-binding cassette transporters (ABCB1, ABC-C2, ABC-C4, ABC-C5) (Wieser *et al.*, 2008, Aschauer *et al.*, 2015b). A relevant disadvantage of primary cells is that they undergo replicative senescence in culture and are therefore unsuitable or even useless for many toxicological applications and studies, such as chronic treatments or long-term studies (Simon *et al.*, 2014b). RPTEC/TERT1 cells do not undergo replicative senescence and thus offer advantages over primary cell lines in this aspect (Simon *et al.*, 2014b). Another advantage of RPTEC/TERT1 cells over other cell lines is the cultivation method in serum-free medium. The cells were developed for this purpose and can be cultivated and maintained in a hormonally

defined medium (Wieser *et al.*, 2008, Aschauer *et al.*, 2015b). Due to the above mentioned advantages over primary cells and other immortalized cell lines, RPTEC/TERT1 cells were used for *in vitro* nephrotoxicity studies, especially in repeated exposures, using transcriptomic, metabolic, and proteomic approaches (Wilmes *et al.*, 2013, Wilmes *et al.*, 2015, Aschauer *et al.*, 2015b).

#### 1.4.2 NRK-52E cell line

The rat cell line NRK-52E (Normal Rat Kidney-52E Epithelial Cells) is one of the most commonly used rat cell lines and is generally accepted as a suitable model for *in vitro* acute kidney injury studies and mechanistic toxicity studies *in vitro* (Vrbova *et al.*, 2016, Bessems and Vermeulen, 2001, Thomasina Barron *et al.*, 1990). This stable immortalized cell line from the renal tubules of the rat (*Rattus norvegicus*) was transformed from an epithelial subclone of the NRK cell line by transfection with the *Moloney sarcoma* virus and has similar cell properties to proximal tubules as well as typical structures of epithelial cells (Vrbova *et al.*, 2016, De Larco and Todaro, 1978, Duc-Nguyen *et al.*, 1966). The apical membrane of NRK-52E contains microvilli and kidney specific enzymes are also synthesized such as alkaline phosphatase,  $\gamma$ -glutamyl transpeptidase, N-acetyl- $\beta$ -glucosaminidase, lactate dehydrogenase and  $\beta$ -lyase (Barron 1990, Boogaard 1990, Lash 2002). The collagen-like glycoprotein laminin is expressed on the basolateral membrane as well as a number of organic anion transporters and the  $\text{Na}^+ / \text{K}^+$  -ATPase (Boogaard *et al.*, 1990, Vrbova *et al.*, 2016). However, it was shown in the NRK-52E cells that the activity of glutathione reductase and glutathione S-transferase is lower than in the *in vivo* situation (Lash *et al.*, 2002, Vrbova *et al.*, 2016). These disadvantages should be considered in toxicological and mechanistic studies.

## **1.5 Polymyxins as model stressors for the AOP – *Receptor-mediated endocytosis and lysosomal overload***

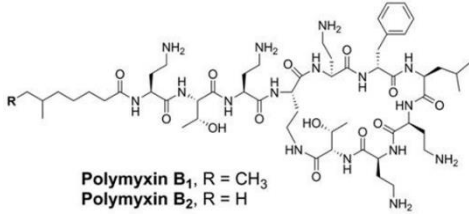

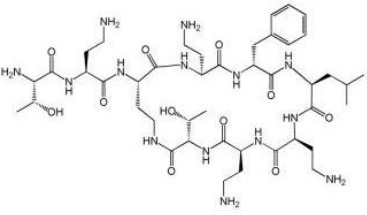
### **1.5.1 Polymyxin B and colistin**

Polymyxin B and colistin belong to the group of polypeptide antibiotics. Polymyxin B and colistin are mixtures of the polypeptides polymyxin B1 and B2 respectively colistin A and B, which are structurally differentiated by a methyl group on the fatty acid group (Table 2) (Stokniene *et al.*, 2020). Due to their similar chemical structure and antibacterial activity, both antibiotics are effective against multi-resistant Gram-negative bacteria (Heybeli *et al.*, 2019, Nation *et al.*, 2014, Gales *et al.*, 2011, Sader *et al.*, 2015). An adverse side effect after therapeutic application of polymyxin B or colistin is seen in up to 50 to 60 % of patients as acute kidney injury (AKI) (Kelesidis and Falagas, 2015, Nation *et al.*, 2014). Numerous *in vitro* and *in vivo* studies demonstrated the concentration- and time-dependent nephrotoxic potential of polymyxin B and colistin (Avedissian *et al.*, 2019, Zavascki and Nation, 2017, Vattimo *et al.*, 2016, Akajagbor *et al.*, 2013, Azad *et al.*, 2013, Abdelraouf *et al.*, 2012a, Abdelraouf *et al.*, 2012b, Kubin *et al.*, 2012, Pogue *et al.*, 2011). The primary mechanism of polymyxin-mediated renal toxicity is the damage of proximal tubule cells (Azad *et al.*, 2013). The cellular mechanisms associated with the toxicity of polymyxins in proximal tubule cells are among others oxidative stress, apoptosis, cell cycle arrest, autophagy and the accumulation of polymyxins in the cells by endocytotic uptake via the megalin receptor (Avedissian *et al.*, 2019, Abdelraouf *et al.*, 2014, Moestrup *et al.*, 1995). The high binding affinity of polymyxin B and colistin to megalin and cell accumulation have been demonstrated in several studies. An *in vivo* study with megalin-shedding rats showed that after polymyxin administration the concentration in renal tissue was 40 % lower than in control animals (Manchandani *et al.*, 2017).



Table 2

Model compounds related to the AOP – Receptor-mediated endocytosis and lysosomal overload

AOP – Receptor-mediated endocytosis and lysosomal overload		
Compound	Structural formula	Molecular weight
Polymyxin B (PB)	 <p>Polymyxin B<sub>1</sub>, R = CH<sub>3</sub> Polymyxin B<sub>2</sub>, R = H</p>	B <sub>1</sub> = 1287.5 g/mol B <sub>2</sub> = 1203.5 g/mol
Colistin (Col)	 <p>Colistin A, R = CH<sub>3</sub> Colistin B, R = H</p>	A = 1169.5 g/mol B = 1155.4 g/mol
Polymyxin B nonapeptide (PBNP)		963.15 g/mol

### 1.5.2 Polymyxin B nonapeptide

Polymyxin B nonapeptide is a polymyxin derivative that shares structural similarities with polymyxin B except for the absence of the fatty acyl tail and the N-terminal diamino butyryl (Dab) residue (Table 2) (Vaara *et al.*, 2010a, Lenhard *et al.*, 2019). Due to this structural change, polymyxin B nonapeptide lacks antibacterial activity, but still has the ability to penetrate the cell membrane, allowing secondary antibiotics to enter the cells more effectively (Lenhard *et al.*, 2019, Vaara, 2010b). In several *in vitro* and *in vivo* studies, the lower toxic potential of polymyxin B nonapeptide compared to polymyxin B and colistin was demonstrated. For instance, an acute toxicity test in mice showed that polymyxin B nonapeptide was 15 times less

toxic than polymyxin B and showed a significantly reduced nephrotoxic potential in rats compared to colistin (Vaara, 1992, Keirstead *et al.*, 2013). A 23 – day study in dogs and a 29 – day rat study confirmed the much lower toxicity of polymyxin B nonapeptide as compared to the same dose of polymyxin B (Danner *et al.*, 1989). Also, in an *in vitro* study with HK-2 cells polymyxin B nonapeptide showed a 50-fold lower cytotoxicity than polymyxin B (Keirstead *et al.*, 2013).

### **1.6 Cadmium chloride as a model stressor for the AOP – *Receptor-mediated endocytosis and lysosomal overload***

Cadmium (Cd) belongs chemically to the transition metals. Elemental cadmium is present in the earth's crust in very small amounts due to its rarity. The major use of cadmium is limited to the metal industry and as a result the concentration of cadmium in the biosphere has strongly increased (Lundholm and Andersson, 1985, Cullen and Maldonado, 2013). Furthermore, cadmium is not biodegradable and is persistent. Thus, cadmium exposure is not limited to industry; as an environmental pollutant, cadmium is also absorbed through contaminated water and food (Hristev *et al.*, 2003, Järup *et al.*, 2000). Cadmium is classified as very toxic and has been found to damage several organs such as lungs, liver and even bones (Prozialeck and Edwards, 2012, Wolff *et al.*, 2011). Chronic exposure to cadmium damages the kidneys by causing generalized and adversarial dysfunction of the proximal tubule when absorbed into the proximal tubule cells (Sabolić *et al.*, 2010, Järup *et al.*, 2000, Hong *et al.*, 2004). Absorbed cadmium is transported to the liver and induces the synthesis of metallothionein (Klaassen *et al.*, 2009, Sabolić *et al.*, 2010). Binding of Cd to metallothionein buffers the toxic effect; however, this Cd-metallothionein complex can be taken up into the proximal tubule cells via the megalin:cubilin complex and accumulation of cadmium in the kidneys occurs (Sabolić *et al.*, 2010, Prozialeck and

Edwards, 2012, Järup *et al.*, 2000, Klaassen *et al.*, 2009, Simon *et al.*, 2014b, Wolff *et al.*, 2011, Yang and Shu, 2015). Furthermore, Cd has a high affinity to thiol groups. Cadmium thereby builds conjugates with glutathione and cysteine, which can in turn be taken up into proximal tubule cells by the same mechanism (Yang and Shu, 2015). Due to the chemical similarity of Cd to essential elements such as zinc or calcium, uptake into proximal tubule cells is also promoted via calcium and zinc transporters, as well as divalent metal transporter (DMT1) and organic cation transporter (OCT1/2) (Yang and Shu, 2015, Wolff *et al.*, 2011, Sabolić *et al.*, 2010)

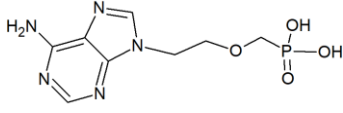
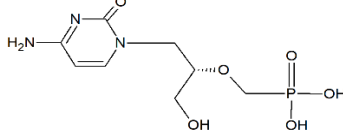
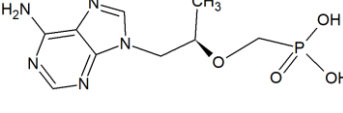
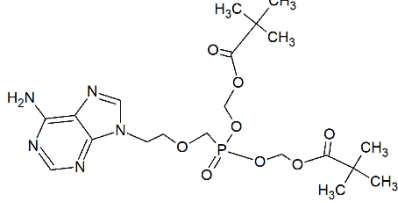
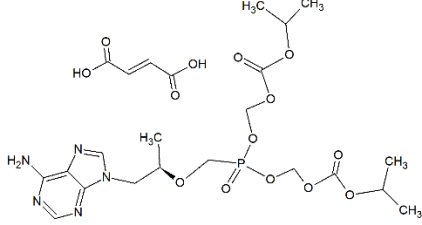
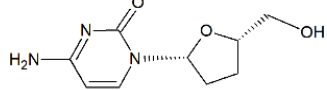
## **1.7 Antivirals as model stressors for the AOP – *Inhibition of mtDNA polymerase- $\gamma$***

### **1.7.1 Adefovir and its prodrug adefovir dipivoxil**

The nucleotide monophosphate analogue adefovir is used in the treatment of hepatitis B and human immunodeficiency virus (HIV) in the form of the acyclic phosphate compound adefovir dipivoxil as a prodrug (Table 3) (Luo *et al.*, 2016, Barditch-Crovo *et al.*, 1997, Cherrington *et al.*, 1995). Adefovir serves as a substrate for reverse transcriptase and integrates into the proviral DNA sequence, which leads to premature DNA chain termination (Barditch-Crovo *et al.*, 1997, Cherrington *et al.*, 1995). As a side effect after *in vivo* long-term treatment with adefovir renal toxicity was observed (Luo *et al.*, 2016), characterized by a decrease in glomerular filtration rate, increased serum creatinine levels, Fanconi syndrome and dose-dependent damage of renal tubules (Wang *et al.*, 2015, Ruan *et al.*, 2013, Shimohata *et al.*, 2013, Zhang *et al.*, 2013, Zheng *et al.*, 2012, Vigano *et al.*, 2011, Guishuang and Haodong, 2010, Fontana, 2009, Zeng *et al.*, 2006, Marcellin *et al.*, 2003, Kahn *et al.*, 1999, Murphy, 2017). The cellular mechanism leading to nephrotoxicity induced by adefovir is not fully understood, but structural changes in the mitochondria in the proximal tubule cells indicate possible mitochondrial toxicity (Tanji *et al.*,

2001). Due to the analogy of adefovir to the nucleotide adenosine, it is assumed that adefovir may also serve as a substrate for DNA polymerase- $\gamma$ .

**Table 3**  
Model compounds related to the AOP – Inhibition of mtDNA polymerase- $\gamma$

<b>AOP – Inhibition of mtDNA polymerase-<math>\gamma</math></b>		
<b>Compound</b>	<b>Structural formula</b>	<b>Molecular weight</b>
Adefovir (Ade)		273.19 g/mol
Cidofovir (Cido)		279.19 g/mol
Tenofovir (Teno)		305.23 g/mol
Adefovir dipivoxil (ADV)		501.47 g/mol
Tenofovir disoproxil fumarate (TDF)		635.51 g/mol
Zalcitabine (ddC)		212.22 g/mol

Replication of mitochondrial DNA (mtDNA) is regulated by the polymerase- $\gamma$  and the incorporation of the nucleoside analogue adefovir can inhibit mtDNA replication, which leads to a disruption of mitochondria (Birkus *et al.*, 2002, Brinkman *et al.*, 1998, Cherrington *et al.*, 1995, Lewis and Dalakas, 1995, Martin *et al.*, 1994).

### 1.7.2 Cidofovir

Cidofovir is a nucleotide monophosphate analogue of the DNA base cytosine which belongs to the class of antiviral drugs and is used to treat cytomegalovirus retinitis in AIDS patients (Table 3) (Lacy *et al.*, 1998, Hitchcock *et al.*, 1996). Like adefovir, the toxicity of proximal tubular epithelial cells is the dose-limiting adverse effect of cidofovir observed in *in vivo* studies and in humans (Lacy *et al.*, 1998, Lalezari *et al.*, 1997, Lalezari *et al.*, 1995). *In vitro* experiments in HK-2 cells and in primary tubule cells also showed apoptosis after cidofovir treatment (Ortiz *et al.*, 2005). However, no apoptosis was observed in human renal fibroblasts without organic anion transporter 1 (OAT1) (Will and Dykens, 2018). The toxicity is linked to rapid absorption of cidofovir into the proximal tubule cells via organic anion transporters (OAT1/3) but slow excretion (Ho *et al.*, 2000, Brown *et al.*, 2015). Mitochondrial morphological changes in the kidney, which were also observed during medication with related nucleotide analogues, were found in patients treated with cidofovir (Talmon *et al.*, 2010). It is assumed that the cytotoxicity of cidofovir is due to the same mechanism of mitochondrial toxicity as for the nucleotide analogue adefovir (Fernandez-Fernandez *et al.*, 2011, Rodríguez-Nóvoa *et al.*, 2010, Talmon *et al.*, 2010).

### **1.7.3 Tenofovir and its prodrug tenofovir disoproxil fumarate**

Tenofovir is an acyclic nucleotide analogue of adenosine monophosphate, which also belongs to the class of antiviral drugs (Table 3) (Kohler *et al.*, 2011, Izzedine *et al.*, 2005). Tenofovir has structural similarities to adefovir and cidofovir and is orally used in form of its prodrug (tenofovir disoproxil fumarate) in the treatment of HIV and chronic hepatitis B virus infections (Table 3) (Cui *et al.*, 2015, Dauchy *et al.*, 2011, Kohler *et al.*, 2011, Herlitz *et al.*, 2010, Karim *et al.*, 2010, Izzedine *et al.*, 2005). Due to its structural similarity to adefovir and cidofovir as well as its effect as a reverse transcriptase inhibitor, tenofovir is also suspected of causing damage to proximal tubule cells by the same mechanism of action via depletion of mtDNA (Lebrecht *et al.*, 2009, Gallant and Deresinski, 2003). This assumption is also supported by the finding that tenofovir is actively taken up into the proximal tubule cells via organic anion transporters (Ray *et al.*, 2006, Cihlar *et al.*, 2001). However, despite less side effects compared to adefovir and cidofovir, case reports, observational studies in humans, and *in vitro* and *in vivo* experiments showed a nephrotoxic potential of tenofovir (Herlitz *et al.*, 2010, Cooper *et al.*, 2010, Kohler *et al.*, 2009b, Lebrecht *et al.*, 2009, Cihlar *et al.*, 2009, Liborio *et al.*, 2008, Gallant *et al.*, 2004).

### **1.7.4 Zalcitabine (ddC)**

Zalcitabine (ddC) is a derivative of the nucleoside cytidine. It is pharmacologically categorized among the nucleoside reverse transcriptase inhibitors (NRTIs) (Table 3) and is used in the treatment of HIV infection (Collier *et al.*, 1996, Adkins *et al.*, 1997). Pharmaceuticals belonging to the group of NRTIs are unable to form 3'-phosphodiester bonds due to the lack of the 3'-OH group. Because of their structural similarity to deoxynucleotide triphosphates (dNTPs), NRTIs can be incorporated into a nascent DNA strand in place of dNTPs. Incorporation into DNA thus

terminates DNA elongation and inhibits reverse transcriptase as well as mitochondrial DNA polymerase, both of which are responsible for mtDNA replication (Lewis, 2003b, Lewis *et al.*, 2003a, Benbrik *et al.*, 1997). A side effect of ddC described is severe lactic acidosis leading to pH dysregulation in the kidneys, however this side effect is unrelated to a direct renal dysfunction (Loens *et al.*, 2018). As *in vivo* and *in vitro* studies have shown that mitochondrial copy number decreases after treatment with ddC (Birkus *et al.*, 2002, Stankov *et al.*, 2010), ddC is used in this work as a positive control for the *in vitro* assay to determine mtDNA copy number.

## **1.8 Identification of suitable *in vitro* endpoints covering key events within the developed AOPs**

To identify suitable *in vitro* endpoints for the individual AOPs and key events, published *in vitro* and *in vivo* findings were used to determine mechanism-based endpoints covering the individual key events of the AOPs. In addition to the published results, the publicly accessible Comparative Toxicogenomic Database (CTD) was also used. This database contains collected information from published literature analyzed by expert curators (Davis *et al.*, 2013). Information on drugs and chemicals that affect biological mechanisms and human health, as well as relationships and interactions between chemicals and diseases / proteins / genes and relationships between diseases and genes can be analyzed and filtered in this database (Davis *et al.*, 2011, Wiegers *et al.*, 2009).

### **1.8.1 Suitable *in vitro* endpoints for the AOP – *Receptor-mediated endocytosis and lysosomal overload***

#### **1.8.1.1 Key event 1 – *Disturbance of lysosomal function***

The first KE in the AOP – *Receptor-mediated endocytosis and lysosomal overload* is the disturbance of lysosomal functions (Figure 6). A promising endpoint is the measurement of the expression of lysosomal associated membrane protein 1/2 (LAMP-1/2). LAMP-1/2 are the most abundant proteins of the lysosomal membrane, which are assumed to have a protective function for lysosomes (Luzio *et al.*, 2014, Saftig and Klumperman, 2009, Luzio *et al.*, 2007, Fukuda, 1991). Due to its high occurrence, LAMP is used as a lysosomal marker and marker for lysosomal storage disorders which is characterized by a disturbed LAMP expression (Damaghi *et al.*, 2015, Appelqvist *et al.*, 2011, Ginet *et al.*, 2009, Kroemer and Jäättelä, 2005, Hua *et al.*, 1998, Meikle *et al.*, 1997). Polybasic drugs, which also include polymyxin antibiotics, are



known to accumulate in lysosomes because of their high binding affinity to megalin (Manchandani *et al.*, 2017, Moestrup *et al.*, 1995, Pavelka and Roth, 2015). The accumulation in the lysosomes leads to disturbance of lysosomal functions such as pH changes and an enlargement of the lysosomes may be associated with an increased LAMP expression, which was also observed after treatment with lysosomotropic drugs in several *in vitro* studies (Lu *et al.*, 2017, Ginet *et al.*, 2009, Puyal *et al.*, 2009, Chen *et al.*, 2001). A query of the CTD on gentamicin and cadmium chloride, which are also presumed stressors of the AOP – *Receptor-mediated endocytosis and lysosomal overload*, revealed an association of both compounds with LAMP-2, which was linked to the lysosomal pathway and kidney disease / acute kidney injury (see chapter 4.1.1). Based on published findings and analysis of the CTD, measurement of LAMP expression of lysosomes may thus offer a potential *in vitro* endpoint for the first KE (*Disturbance of lysosomal function*) in the AOP – *Receptor-mediated endocytosis and lysosomal overload*.

#### **1.8.1.2 Key event 2 – Disruption of lysosomes**

The second KE in AOP – *Receptor-mediated endocytosis and lysosomal overload* is the disruption of lysosomes (Figure 6). The rupture of lysosomes, or lysosomal membrane permeabilization (LMP) and the associated release of intralysosomal components, has been proven to be a key step in the cell death signaling cascade, which can be induced by a number of stimuli such as oxidative stress, death receptor ligation or DNA-damaging drugs (Wang *et al.*, 2018, Groth-Pedersen *et al.*, 2015, Mrschtik and Ryan, 2015, Repnik *et al.*, 2012, Appelqvist *et al.*, 2011, Johansson *et al.*, 2010, Oberle *et al.*, 2010, Kirkegaard and Jäättelä, 2009, Boya and Kroemer, 2008, Kroemer and Jäättelä, 2005, Kågedal *et al.*, 2005). Intralysosomal components that are released from the lysosomes into the cytoplasm after membrane destabilization and

which are associated with apoptosis are cathepsins, especially the aspartyl protease cathepsin D (Mrschtik and Ryan, 2015, Quiros *et al.*, 2011, Johansson *et al.*, 2010). Cathepsins are lysosomal proteolytic enzymes which are classified into three groups: cysteine proteases (cathepsin B, C, H, L, and S), aspartyl protease (cathepsin D, E) and serine proteases (cathepsin A, G) (Turk *et al.*, 2012, Reiser *et al.*, 2010). When released into the cytoplasm, cathepsins catalyze the proteolytic activation of caspase 3 and 7. Additionally, they induce the mitochondrial pathway of apoptosis by activating Bid. In the absence of ATP, a massive proteolysis induced by cathepsins occurs, resulting in necrotic cell death (Appelqvist *et al.*, 2012, Golstein and Kroemer, 2007, Chwieralski *et al.*, 2006). The most abundant lysosomal proteases include the aspartyl protease cathepsin D and the cysteine proteases cathepsin B and L (Oberle *et al.*, 2010, Turk and Stoka, 2007). It was also found that cathepsin D predominantly occurs in proximal tubule cells and the expression of cathepsin D could also be detected in RPTEC/TERT1 cells (Thul *et al.*, 2017, Uhlén *et al.*, 2017, Cocchiario *et al.*, 2016, Fox *et al.*, 2016, Uhlén *et al.*, 2015, Wilmes *et al.*, 2013, Uhlén *et al.*, 2010, Uhlén *et al.*, 2005). In particular, upregulation of cathepsin D in damaged tubule cells was demonstrated (Cocchiario *et al.*, 2016). Analysis of the CTD content on gentamicin, cadmium chloride and vancomycin showed a common match for the genes for cathepsin A, cathepsin C, cathepsin D and cathepsin S, which are also associated with the lysosomal pathway, kidney disease and acute kidney injury (see chapter 4.1.1). Since the release of cathepsins into the cytoplasm was also observed after treatment with aminoglycosides and kanamycin (Quiros *et al.*, 2011, Jiang *et al.*, 2006, Steyger *et al.*, 2003, Hashino *et al.*, 1997), the measurement of the release of cathepsin D seems to be a potential suitable *in vitro* endpoint for the second key event in the AOP – *Receptor-mediated endocytosis and lysosomal overload*.

## 1.8.2 Suitable *in vitro* endpoints for the AOP – Inhibition of mtDNA polymerase- $\gamma$

### 1.8.2.1 KE1 – Depletion of mitochondrial DNA

The first key event in the AOP – Inhibition of mtDNA polymerase- $\gamma$  is the depletion of mtDNA (Figure 8). After treatment with antiviral drugs such as adefovir, cidofovir or tenofovir, which are inhibitors of viral DNA polymerases (Barditch-Crovo *et al.*, 1997, Cherrington *et al.*, 1995), mitochondrial damages were observed in *in vivo* experiments in various species, including humans. In addition to mitochondrial ultra-structural anomalies such as a reduced number of mitochondria, changes in the shape and size of the mitochondria, as well as decrease and deformation of the cristae, disturbed expression of mitochondrial encoded proteins was also observed (Ramamoorthy *et al.*, 2014, Herlitz *et al.*, 2010, Talmon *et al.*, 2010, Côté *et al.*, 2006). Because mitochondria possess their own DNA (mtDNA), which encodes 13 essential proteins, 22 tRNAs and 2 ribosomal RNA genes in humans, mitochondria are equipped with their own polymerases that are responsible for the replication and repair of mtDNA (Krasich and Copeland, 2017, Tanji *et al.*, 2001). It is generally assumed that antivirals can also serve as a substrate for mitochondrial DNA polymerase, in particular for the subunit gamma, leading to enzyme inhibition and subsequent depletion of mtDNA in the mitochondria as observed in *in vivo* studies (Herlitz *et al.*, 2010, Kohler *et al.*, 2009a, Lebrecht *et al.*, 2009, Côté *et al.*, 2006, Lewis, 2003b, Lewis *et al.*, 2001, Tanji *et al.*, 2001, Zhao *et al.*, 2017, Hall, 2013, Biesecker *et al.*, 2003, Kohler *et al.*, 2011, Morton, 1998). Based on these *in vivo* findings, measurement of mtDNA copy number may present an appropriate *in vitro* endpoint for the second key event *Depletion of mtDNA* in the AOP – Inhibition of mtDNA polymerase- $\gamma$ .

### **1.8.2.2 KE2 – Dysfunction of mitochondrial**

The second key event in the AOP – *Inhibition of mtDNA polymerase- $\gamma$*  describes the dysfunction of mitochondria (Figure 8). As a consequence of the depletion of mtDNA from the first key event by *Inhibition of mtDNA polymerase- $\gamma$*  after treatment with antivirals, disturbed expression of essential mitochondrial proteins such as cytochrome C oxidase was observed *in vivo* (Zhao *et al.*, 2017, Herlitz *et al.*, 2010, Lebrecht *et al.*, 2009, Lewis *et al.*, 2001). Since important proteins of the mitochondrial respiratory chain are deregulated (Lebrecht *et al.*, 2009, Daugas *et al.*, 2005, Lewis *et al.*, 2001, Tanji *et al.*, 2001), mitochondrial toxicity inevitably occurs as observed in experimental animals and humans after treatment with TDF, tenofovir or cidofovir (Ramamoorthy *et al.*, 2014, Hall, 2013, Herlitz *et al.*, 2010, Talmon *et al.*, 2010, Lebrecht *et al.*, 2009, Kohler *et al.*, 2009a, Côté *et al.*, 2006, Daugas *et al.*, 2005). To determine a possible *in vitro* endpoint for the second key event, the measurement of mitochondrial toxicity seems to be a suitable endpoint in the AOP – *Inhibition of mtDNA polymerase- $\gamma$* .

### **1.8.3 Suitable *in vitro* endpoints for the AOP – Receptor-mediated endocytosis and lysosomal overload and the AOP – Inhibition of mtDNA polymerase- $\gamma$**

#### **1.8.3.1 KE3 – Proximal tubule cell toxicity**

As a result of the rupture of lysosomes and the release of cathepsins as a second key event in the AOP – *Receptor-mediated endocytosis and lysosomal overload* and the mitochondrial toxicity in the AOP – *Inhibition of mtDNA polymerase- $\gamma$* , the cytotoxicity of the proximal tubule cells results as a the third key event (Figure 6 and Figure 8). Cytotoxicity of proximal tubule cells has been demonstrated in *in vitro* as well as in *in vivo* studies in several species and seems to be a suitable *in vitro* endpoint for both AOPs (Lenhard *et al.*, 2019, Lu *et al.*, 2017, Zhao *et al.*, 2017, Nieskens *et al.*, 2016, Vattimo *et al.*, 2016, Zhang *et al.*, 2015, Hall, 2013, Keirstead

*et al.*, 2013, Repnik *et al.*, 2012, Fernandez-Fernandez *et al.*, 2011, Quiros *et al.*, 2010, Karasawa and Steyger, 2011, Kirkegaard and Jäätelä, 2009, Liborio *et al.*, 2008, Daugas *et al.*, 2005, Izzedine *et al.*, 2005, Ho *et al.*, 2000).

### **1.9 *In vitro* points of departures for risk assessment**

In order to be able to define health-related guideline values for chemicals or drugs, specific values are determined in the risk assessment. These values are modelled and determined by deriving a point of departure (PoD) from dose-response relationships. In mammalian toxicity studies, the no observed adverse effect level (NOAEL) or benchmark dose / concentration (BMD / BMC) is typically derived and used to calculate the margin of safety (MoS) or margin of exposure (MoE) (Adler *et al.*, 2011). For environmental toxicology, for example, the maximum chemical concentration with an acceptable low or no toxic effect is recommended or even required (OECD, 2006, EPA, 1991). In order to be able to determine a maximum chemical concentration at which no effects or first effects occur, there are several approaches that are being pursued. The usual concepts used in risk assessment are for example: the no observed effect or lowest observed effect concentration (NOEC / LOEC), effective concentration (EC<sub>x</sub>), or the Benchmark dose / concentration (BMD / BMC). All these approaches offer advantages but also disadvantages. The NOEC approach is a statistically determined value, which represents the highest concentration of a test compound, where no statistically significant treatment-related effect can be observed (OECD, 2006). Since the calculation of the NOEC / LOEC depends on the selected and utilized test concentrations and the inclusion of confidence intervals is lacking, this approach is often criticized (Landis and Chapman, 2011, Laskowski, 1995, Van Der Hoeven, 1997). The benchmark dose model was first described in 1984 by Crump as a method of determining a point of departure where a certain change, in most cases of 10 %,

occurs in the dose response curve, considering the 95 % confidence interval (Crump, 1984). The determination of a BMC offers advantages over the NOEC / LOEC approach because the BMC is independent of the selected test concentrations. However, a definite group size is required in order to calculate a BMC. Therefore the BMC approach is categorically excluded in studies with a small group size (Wignall *et al.*, 2014). The effective concentration (EC<sub>x</sub>) approach determines an x % - effect for the measured endpoint from the regression curve of the dose-response relationship. However, it is often critically discussed which effect concentration should be selected, because it is not entirely clear which effective concentration is the most optimal (EC<sub>1</sub>, EC<sub>10</sub>, EC<sub>20</sub>...) (Green *et al.*, 2013, Murado and Prieto, 2013, Stadnicka-Michalak *et al.*, 2018). Stadnicka-Michalak and colleagues describe a further approach for the calculation of a PoD. The algorithm developed and described there, the non-toxic concentration (NtC), combines several properties. On the one hand, the highest concentration that does not cause more than 10 % effect is determined ( $\leq EC_{10}$ ), on the other hand, the 95 % confidence intervals are additionally included, taking into account the measured biological replicas that do not differ significantly from the control (Stadnicka-Michalak *et al.*, 2018). As there is no consensus in the scientific community as to which of these approaches is the most appropriate to identify a PoD (Green *et al.*, 2013), all predictable approaches have been pursued for this work and are described in Material & Methods section.

## 2 Objective

The overall goal of this PhD thesis is to contribute to worldwide efforts to reduce, refine and replace animal tests and to address the unmet need for non-animal approaches to systemic toxicity testing. As an exemplary key target for systemic toxicity, the kidney was selected as the basis for application of the AOP concept. Using fairly well-established mechanisms of nephrotoxicity, the aim was to apply the AOP concept to identify and experimentally support key events leading to nephrotoxicity as an adverse outcome. Based on the mechanistic understanding, this work aimed to establish suitable *in vitro* assays covering the individual key events in each AOP, which might allow prediction of the outcome and may thus be fit for purpose for regulatory decision making based on *in vitro* data.

To achieve this, the specific strategic objectives of this PhD thesis were defined as follows:

- 1) To investigate whether publicly available information from publications and databases (*e.g.*, PubMed, Comparative Toxicogenomic Database) can be used to identify quantifiable key events that are consistent with the underlying AOPs
- 2) To establish *in vitro* assays for each individual key event to acquire dose-response data in two different cell lines (human & rat), using appropriate model compounds for each AOP
- 3) With the help of the obtained dose-response data from the individual key events, it was to be tested if prediction of the outcome can be made via the key event relationships
- 4) To identify potential differences in the sensitivity of the *in vitro* models that may have an influence on the generated AOPs and risk assessment

- 5) To visualize different points of departure derived from *in vitro* assays and to compare the *in vitro* results with *in vivo* findings in order to determine the reliability of *in vitro* data for risk assessment



### 3 Material and Methods

#### 3.1 Technical Equipment

**Table 4**  
**Technical equipment with supplier**

<b>Equipment</b>	<b>Supplier</b>
96- / 12-well plates	CellStar <sup>®</sup> , Greiner Bio-One, Kremsmünster; AUT
96-well multiwell plates	Roche AG, Basel, CHE
96-well OptiPlate <sup>®</sup>	PerkinElmer Inc., Waltham, MA, USA
Autosampler	Agilent Tech. Inc., Santa Clara, CA, USA
Blotting chamber	BioRad <sup>®</sup> Mini Trans-Blot <sup>®</sup> Cell, Hercules, CA, USA
Blotting paper	580 x 580, 500 mg/m <sup>3</sup> , Hartenstein, Würzburg, GER
Cell culture flasks (75 cm <sup>2</sup> , 25 cm <sup>2</sup> )	CellStar <sup>®</sup> , Greiner Bio-One, Kremsmünster, AUT
Centrifuges	Labofuge <sup>™</sup> GL, Heraeus, Hanau, GER 5415c, Eppendorf AG, Hamburg, GER Universal 320R, Hettich, Tuttlingen, GER
Chamber slides (8-well)	Ibidi GmbH, Planegg, GER
Column oven	Knauer GmbH, Berlin, GER
Confocal microscope TCS SP5 II with an HCX PL APO lambda blue 63.0 x 1.40 OIL UV objective	Leica Microsystems, Wetzlar, GER
Eppendorf LoBind <sup>™</sup> tubes	Eppendorf AG, Hamburg, GER
Fuchs-Rosenthal counting chamber	Hartenstein, Würzburg, GER
Gel documentation system	ImageQuant <sup>™</sup> LAS 400, GE Healthcare, Chicago, IL, USA
Gel electrophoresis	Hoefer Scientific Instruments SE250, Holliston, MA, USA
HPLC column Synergi <sup>™</sup> Hydro-RP (2 mm x 150 mm, 4 µm, 80 Å)	Phenomenex LTD, Torrance, CA, USA
HPLC system Agilent 1100	Agilent Tech. Inc., Santa Clara, CA, USA
Incubator	HERAcell <sup>®</sup> , Heraeus, Hanau, GER

Laminar Flow	Antair BSK 6 Mikrosysteme, Köln, GER
LightCycler® 480 sealing foil	Roche, Basel, CHE
Mastercycler®	Eppendorf AG, Hamburg, GER
Microplate reader	Mithras LB 940, Berthold, Bad Wilbad, GER
Microscope	TMS-F, Nikon, Tokyo, JPN ECLIPSE 55i, Nikon, Tokyo, JPN
Multipette	Transferpette® S-8, Brand, Wertheim, GER
Orbital shaker	KL 2, Edmund Bühler, Hechingen, GER
Pipettes	Sarstedt, Nürnberg, GER Gilson, Middleton, WI, USA Reference, Eppendorf, Hamburg, GER
Precision scale	AG245, Mettler-Toledo, Columbus, OH, USA
Precolumn SecurityGuard™ Cartridges, AQ C18 4 x 2.0 mm,	Phenomenex LTD, Torrance, CA, USA
QIAshredder® spin column	Qiagen N.V., Hilden, GER
Real-Time PCR system Light-Cycler® 480	Roche AG, Basel, CHE
SPE cartridge (Strata-X 33 µm polymeric reversed phase, 10 mg / 1 mL)	Phenomenex LTD, Torrance, CA, USA
Triple quadrupole mass spectrometer with Turbo-Ion® Spray source Qtrap API 2000	AB Sciex Instruments, Darmstadt, GER
UV-Vis spectrophotometer	NanoDrop™ 2000c, Thermo Fisher Scientific™, Waltham, MA, USA Buck Scientific M-500, Norwalk, CT, USA
Vacuum concentrator SpeedVac Plus SC110A	Thermo Fisher Scientific™, Waltham, MA, USA
Vacuum degasser	Agilent Tech. Inc., Santa Clara, CA, USA

### 3.2 Software

**Table 5**  
Software with supplier

Software	Supplier
Analyst™ 1.4.1 Software	AB SCIEX GmbH, Darmstadt, GER
BioRender® 2019 online application	BioRender®, Toronto, ON, USA
BMD Software 2.7	United States Environmental Protection Agency, Washington, WA, USA
GraphPad Prism 5.01	GraphPad Software, Inc., La Jolla, CA, USA
ImageQuant™ LAS 400 Control software	GE Healthcare, Chicago, IL, USA
Leica application suite advanced fluorescence (LAS AF)	Leica Microsystems, Wetzlar, GER
LightCycler 480 Software	Roche AG, Basel, CHE
MikroWin 2000	Mikrotek Laborsysteme GmbH, Overath, GER
NIH ImageJ Software	National Institute of Health, Bethesda, MD, USA
Non-toxic concentrations determination online application	<a href="https://utox.shinyapps.io/NtC_NtC/">https://utox.shinyapps.io/NtC_NtC/</a> (Stadnicka-Michalak <i>et al.</i> , 2018)
RIVM PROAST Web, Version 65.2	National Institute for Public Health and the Environment, Bilthoven, NE

### 3.3 Chemicals, compounds, kits

**Table 6**  
Chemicals, compounds, and kits with supplier

Chemicals, compounds, kits	Cat. # / Purity	Supplier
$\beta$ -mercaptoethanol	M6250 / $\geq 99.0\%$	Sigma-Aldrich Chemie GmbH, München, GER
Acetic acid	A6283 / $\geq 99.0\%$	Sigma-Aldrich Chemie GmbH, München, GER
Acetonitrile	34851 / $\geq 99.9\%$	Sigma-Aldrich Chemie GmbH, München, GER
Adefovir	SML0240 / $\geq 98\%$	Sigma-Aldrich Chemie GmbH, München, GER
Adefovir Dipivoxil	A9730 / $\geq 98\%$	Sigma-Aldrich Chemie GmbH, München, GER
BSA	A7030 / $\geq 98\%$	Sigma-Aldrich Chemie GmbH, München, GER

*Material and Methods*

CellTiter-Glo® Luminescent Cell Viability Assay	G9241; G9242	Promega Corp., Fitchburg, WI, USA
Cidofovir	S1516 / 99.97 %	SelleckChem®, München, GER
Clarity Western ECL Substrate	1705061	BioRad®, Hercules, CA, USA
Colistin	C4461 / ≥ 98.0 %	Sigma-Aldrich Chemie GmbH, München, GER
DC-Assay	5000112	BioRad®, Hercules, CA, USA
DMEM (high glucose)	P04-03500	PAN-Biotech, Aidenbach, GER
DMEM (no glucose)	11966-025 / D5030	Gibco®/Life Technologies, Carlsbad, CA, USA
DMSO (Dimethyl sulfoxide)	D8418 / ≥ 99.9 %	Sigma-Aldrich Chemie GmbH, München, GER
EDTA	E9884 / ≥ 99.4 %	Sigma-Aldrich Chemie GmbH, München, GER
EGF (Epidermal growth factors)	E9644	Sigma-Aldrich Chemie GmbH, München, GER
Ethanol (70 % and 99.9 %)	P075.4	Carl Roth GmbH & Co. KG, Karlsruhe, GER
FCS (fetal calf serum)	S0615	Merck KGaA Millipore, Billerica, MA, USA
First strand synthesis kit	K2562; K2563	Thermo Fisher Scientific™, Waltham, MA, USA
GlutaMAX®	M11-004	Thermo Fisher Scientific™, Waltham, MA, USA
Gradient gel	PG-S	FastGene® PAGE 4 – 12 %, 8 x 10 cm, Nippon Genetics Europe, Dueren, GER
Ham's F12 Medium	21765-029	Gibco®/Life Technologies, Carlsbad, CA, USA
Hydrocortisone	H6909	Sigma-Aldrich Chemie GmbH, München, GER
ITS (Insulin, Transferrin, sodium selenite)	I1884-1VL	Sigma-Aldrich Chemie GmbH, München, GER
LightCycler® 480 SYBR Green I Master	04707516001	Roche AG, Mannheim, GER
Methanol (≥ 99 %)	0798.3	Carl Roth GmbH & Co. KG, Karlsruhe, GER
MOPS buffer (Tris-base 6 g, MOPS 10.47 g, EDTA 0.3 g, SDS 1 g)	PG-MOPS10	Nippon Genetics Europe GmbH, Dueren, GER
Non-essential amino acids	11140035	Thermo Fisher Scientific™, Waltham, MA, USA
Nonidet P40	11754599001	Sigma-Aldrich Chemie GmbH, München, GER
Paraformaldehyde	8187150100	Sigma-Aldrich Chemie GmbH, München, GER
PBS	D8537	Sigma-Aldrich Chemie GmbH, München, GER
Penicillin / Streptomycin	P11-010	PAA Laboratories, Pasching, AUT

*Material and Methods*

Phalloidin-tetramethylrhodamine B isothiocyanate	P1951	Sigma-Aldrich Chemie GmbH, München, GER
Polymyxin B	P4932 / $\geq 98.0\%$	Sigma-Aldrich Chemie GmbH, München, GER
Polymyxin B nonapeptide	P2076 / $\geq 98.0\%$	Sigma-Aldrich Chemie GmbH, München, GER
Protease inhibitor cocktail	78430;78429	Thermo Fisher Scientific™, Waltham, MA, USA
Protein ladder	26634; 26623	Spectra™ Multicolor Broad Range, Thermo Fisher Scientific™, Waltham, MA, USA
Proteinase K	19157	Qiagen N.V., Hilden, GER
QIAamp® DNA mini-Kit	56304	Qiagen N.V., Hilden, GER
Qiagen RNeasy® mini-Kit	74104	Qiagen N.V., Hilden, GER
RNase A	19101	Qiagen N.V., Hilden, GER
Sodium chloride	S9888 / $\geq 99.0\%$	Sigma-Aldrich Chemie GmbH, München, GER
Sodium deoxycholate	30970 / $\geq 98.0\%$	Sigma-Aldrich Chemie GmbH, München, GER
Sodium fluoride	201154 / $\geq 99.0\%$	Sigma-Aldrich Chemie GmbH, München, GER
Sodium orthovanadate	450243 / $\geq 99.9\%$	Sigma-Aldrich Chemie GmbH, München, GER
Sodium pyruvate	P2256 / $\geq 99.0\%$	Sigma-Aldrich Chemie GmbH, München, GER
TaqMan™ universal PCR Master mix	4305719	Thermo Fisher Scientific™, Waltham, MA, USA
Tenofovir	PHR1592 / $\geq 98.0\%$	Sigma-Aldrich Chemie GmbH, München, GER
Tenofovir Disoproxil Fumarate	1643656 / $\geq 98.0\%$	Sigma-Aldrich Chemie GmbH, München, GER
Tris HCl	10812846001 / $\geq 99.0\%$	Sigma-Aldrich Chemie GmbH, München, GER
Triton X-100	X100	Sigma-Aldrich Chemie GmbH, München, GER
Trypan blue	T6146	Sigma-Aldrich Chemie GmbH, München, GER
Trypsin/EDTA	T3924	Sigma-Aldrich Chemie GmbH, München, GER
Tween20	P1379	Sigma-Aldrich Chemie GmbH, München, GER
Vectashield® antifade mounting medium with DAPI	H-1200-10	Vectorlab, Biozol, Eching, GER
Zalcitabine (ddC)	S1719 / 100 %	SelleckChem®, München, GER

### 3.4 Antibodies, primer, TaqMan™ probes

**Table 7**  
Antibodies with supplier

Antibody	Reactivity	Cat#	Supplier
Anti-Cathepsin D mouse monoclonal IgG <sub>2</sub> b kappa	Human ( <i>homo sapiens</i> )	NBP1-04278	Novus Biologicals, Centennial, CO, USA
Anti-LAMP-2 mouse monoclonal IgG <sub>1</sub> kappa antibody		sc-18822	
Anti-Megalyn mouse monoclonal IgG <sub>1</sub> kappa antibody	Human ( <i>homo sapiens</i> ) Rat ( <i>rattus norvegicus</i> )	sc-515772	Santa Cruz, Dallas, TX, USA
Anti-Cathepsin D mouse monoclonal IgG <sub>2</sub> kappa antibody	Rat ( <i>rattus norvegicus</i> )	sc-377124	
Anti-LAMP-1 mouse monoclonal IgG <sub>1</sub> kappa antibody		sc-20011	
Anti-mouse binding protein mIgG-BP-CFL-488	Mouse ( <i>mus musculus</i> )	sc-516176	Cell Signaling Technology, Danvers, MA, USA
Anti-mouse IgG HRP-linked AB		7076	

**Table 8**  
Primer with gene name and sequence

Gene name and symbol	Organism	Primer sequence (5'-3')	Publication
Mitochondrially encoded tRNA leucine 1 (MT-TL1)	Human ( <i>homo sapiens</i> )	F: CACCCAAGAACAGGGTTTGT R: TGGCCATGGGTATGTTGTTA	(Rooney <i>et al.</i> , 2015); (Thakar <i>et al.</i> , 2015)
Beta-2-microglobulin (B2M)		F: TGCTGTCTCCATGTTTGATGTATCT R: TCTCTGCTCCCCACCTCTAAGT	
Nucleotide position 2469 – 2542	Rat ( <i>rattus norvegicus</i> )	F: AATGTTTCGTTTGTTC AACGATT R: AGAAACCGACCTGGATTGCTC	(Lebrecht <i>et al.</i> , 2009)
Actin beta (Actb)		F: CTATGTTGCCCTAGACTTCGAGC R: TTGCCGATAGTGATGACCTGA	In house primer

**Table 9**  
**TaqMan™ probes with supplier**

Gene name and symbol	Organism	TaqMan™ probe ID	Dye label and concentration	Supplier
Glyceraldehyde 3-phosphate dehydrogenase (GAPDH)	Human ( <i>homo sapiens</i> )	Hs03929097_g1	FAM-MGB / 20 x	Thermo Fisher Scientific™, Waltham, MA, USA
Low-density lipoprotein receptor-related protein 2 (LRP2)		Hs00189742_m1		
Cubilin (CUBN)		Hs00153607_m1		
Glyceraldehyde 3-phosphate dehydrogenase (Gapdh)	Rat ( <i>rattus norvegicus</i> )	Rn01775763_g1		
Low-density lipoprotein receptor-related protein 2 (Lrp2)		Rn00578067_m1		
Cubilin (Cubn)		Rn00584200_m1		

### 3.5 Cell culture conditions

All cell culture work was performed under sterile conditions under a laminar flow hood.

#### 3.5.1 Thawing procedure

Frozen cells were thawed quickly in a 37 °C water bath and were subsequently transferred into pre-warmed medium (37 °C). To remove DMSO, cells were spun for 5 min at 170 g for 5 min. Thereafter the supernatant was removed, and the cell pellet was resuspended in 5 mL pre-warmed growth medium (37 °C) and seeded in a T25 cell culture flask. Cells were incubated at 37 °C and 5 % CO<sub>2</sub>. 24 h after thawing a medium change was performed. When the cells reached 80 – 90 % confluence, the cells were split into a T75 culture flask for routine cultivation.

### **3.5.2 Freezing procedure**

Freezing medium for RPTEC/TERT1 and NRK-52E cells was freshly prepared before each freezing procedure. DMEM high glucose medium containing 10 % FCS, 2 mM Glutamax<sup>®</sup>, 1 x Pen/Strep, and 10 % DMSO was used and cooled to approx. 4 °C. Cells were split as described in the sections below (3.5.3 - 0) and resuspended in freezing medium at approx.  $1 \times 10^6$  cells / mL in appropriately labelled cryovials. Cryovials were frozen at -20 °C for 4 hours followed by freezing at -80 °C over night and subsequently transferred to liquid nitrogen for storage.

### **3.5.3 NRK-52E culture, splitting procedure and growth medium supplements**

Cells were cultured for routine purposes in 75 cm<sup>2</sup> cell culture flasks (Greiner, CellStar, Cat#: 658175) with 12 mL medium (Table 10) at 37 °C and 5 % CO<sub>2</sub>. Confluent monolayers were washed in 5 mL Ca<sup>2+</sup> and Mg<sup>2+</sup> free PBS and cells were trypsinized with 1.5 mL Trypsin / EDTA (Sigma, Trypsin - EDTA (1 x) Cat# T3924) at 37 °C for 5 – 8 min, with regular checking for monolayer disassociation. After cells were trypsinized, 10 mL culture medium was added, and the cell suspension was centrifuged for 5 min at approx. 1200 rpm (220 x g). The supernatant was discarded, and the cell pellet was resuspended in 12 mL growth medium. For routine culture the cells were split 1:10 in 12 mL growth medium per 75 cm<sup>2</sup> flask. Cells were discarded after 20 – 25 rounds of splitting (until passage 60).



**Table 10**  
**Growth medium supplements for NRK-52E cells**

<b>NRK-52E</b>				
<b>Supplier ECACC 87012902</b>				
<b>Medium</b>	<b>DMEM with 4.5 g/L glucose (high glucose) 500 mL; 1.5 g/L sodium bicarbonate (Pan-biotech, Cat#. P04-03500)</b>			
<b>Supplements (for 500 mL)</b>	<b>Stock solution</b>	<b>Volume added</b>	<b>Final concentration</b>	<b>Supplier &amp; Cat#.</b>
FBS	100 x	25 mL	5 %	Merck Millipore; S0615; Lot#0865C
GlutaMAX®	100 x	5 mL	1 x	PAA Laboratories, Cat#. M11-004
Non-Essential Amino Acids (NEAA or MEM)	100 x	5 mL	1 x	Thermo Fisher Scientific™; Gibco; Cat#. 11140035
Pen/Strep	100 x	5 mL	1 x	PAA Laboratories, Cat#. P11-010

### 3.5.4 RPTEC/TERT1 culture, splitting procedure and growth medium supplements

Cells were cultured for routine purposes in 75 cm<sup>2</sup> cell culture flasks (Greiner, CellStar, Cat#: 658175) with 12 mL growth medium (Table 11) at 37 °C and 5 % CO<sub>2</sub>. Growth medium () was discarded, and cells were trypsinized with 1.5 mL Trypsin / EDTA (Sigma, Trypsin - EDTA (1x) Cat# T3924) at 37 °C for 8 – 10 min, with regular checking for monolayer disassociation. After cells were detached, 10 mL splitting medium (Table 11) (DMEM medium; Sigma, DMEM, Cat#. D5030) was added, and the cell suspension was centrifuged for 5 min at approx. 1200 rpm (220 x g). The supernatant was discarded, and the cell pellet was resuspended in 12 mL growth medium. For routine culture the cells were counted, and approx. 6 x 10<sup>6</sup> cells were

split in a new 75 cm<sup>2</sup> flask with 12 mL growth medium (Table 12) per flask. A medium change was performed after 4 – 5 days. Cells were discarded after 20 – 25 rounds of splitting.

**Table 11**  
**Growth and splitting medium supplements for RPTEC/TERT1 cells**

<b>RPTEC/TERT1</b>				
<b>Supplier Evercyte (CHT-003-0002)</b>				
<b>Growth medium</b>	<b>DMEM <u>no glucose</u> (Gibco, Thermo Fischer; Cat#. 11966-025) and Ham's F12 (Gibco, Thermo Fischer; Cat#. 21765-029) (mixed 1:1)</b>			
<b>Splitting medium</b>	<b>DMEM (Sigma, Cat#. D5030) with Pen/Strep (100 X) 5 ml per 500 ml, and FCS 35 ml per 500 ml.</b>			
<b>Supplements (for 500 mL)</b>	<b>Stock solution</b>	<b>Volume added</b>	<b>Final concentration</b>	<b>Supplier &amp; Cat#.</b>
EGF (Epidermal growth factor)	0.2 mg	5 µL	10 ng/mL	Sigma Aldrich Cat#. E9644
GlutaMAX®	100 x	5 mL	10 ng/mL	Thermo Fischer Cat#. 35050038
ITS (Insulin, transferrin, sodium selenite)	100 x	5 mL	5 µg/mL (insulin) 5 µg/mL (transferrin) 5 ng/mL (sodium selenite)	Sigma Aldrich Cat#. I1884-1VL
Hydrocortisone	50 µM	1 mL	36 ng/mL	Sigma Aldrich Cat#. H6909
Pen/Strep	100 x	5 mL	1 x	PAA Laboratories, Cat#. P11-010

### 3.5.5 HK-2 culture, splitting procedure and growth medium supplements

Cells were cultured for routine purposes in 75 cm<sup>2</sup> cell culture flasks (Greiner, CellStar, Cat#: 658175) with 12 mL medium (Table 12) at 37 °C and 5 % CO<sub>2</sub>. Confluent monolayers were washed in 5 mL Ca<sup>2+</sup> and Mg<sup>2+</sup> free PBS and cells were trypsinized with 1.5 mL Trypsin / EDTA (Sigma, Trypsin - EDTA (1x) Cat# T3924) at 37 °C for 5-8 min, with regular checking for monolayer disassociation. After cells were trypsinized, 10 mL culture medium was added, and the cell suspension was centrifuged for 5 min at approx. 1200 rpm (220 x g). The supernatant was discarded, and the cell pellet was resuspended in 12 mL growth medium. For routine culture the cells were split 1:4 in 12 mL growth medium (Table 12) per 75 cm<sup>2</sup> flask. Cells were discarded after 20-25 rounds of splitting (until passage 60).

**Table 12**  
Growth medium supplements for HK-2 cells

<b>HK-2</b>				
<b>Medium</b>	<b>DMEM/F12 (1:1) 500 mL; 1.2 g/L NaHCO<sub>3</sub>; Pan-biotech, Cat. No. P04-41450</b>			
<b>Supplements (for 500 mL)</b>	<b>Stock solution</b>	<b>Volume added</b>	<b>Final concentration</b>	<b>Supplier &amp; Cat#.</b>
FBS	100 x	50 mL	10 %	Merck Millipore; S0615; Lot#0865C
L-Glutamine	100 x	5 mL	2 mM	PAA Laboratories, Cat#. M11-004
Pen/Strep	100 x	5 mL	1 x	PAA Laboratories, Cat#. P11-010

### 3.5.6 CaCo-2 culture, splitting procedure and growth medium supplements

CaCo-2 cells were cultured using 12 mL culture medium in 75 cm<sup>2</sup> cell culture flasks (Greiner, CellStar, Cat#: 658175) at 37 °C and 5 % CO<sub>2</sub>. Once a week the confluent cell layer was washed with 5 mL Ca<sup>2+</sup> and Mg<sup>2+</sup> free PBS and the cells were trypsinized with 1.5 mL trypsin / EDTA (Sigma, Trypsin - EDTA (1x) Cat# T3924) at 37 °C for 5 – 8 min. After incubation with trypsin, 10 mL culture medium was added, and the cell suspension was centrifuged at 1200 rpm (220 x g) for 5 minutes. Afterwards the supernatant was aspirated, and the cell pellet was resuspended with 12 mL fresh culture medium. Cells were split for routine culture 1:10 in 12 mL growth medium per 75 cm<sup>2</sup> flask and discarded after 20 – 25 rounds of splitting (until passage 60).

**Table 13**  
**Growth medium supplements for CaCo-2 cells**

<b>CaCo-2</b>				
<b>Medium</b>	<b>DMEM with 4.5 g/L glucose (high glucose) 500 mL; 1.5 g/L sodium bicarbonate</b> <b>Pan-biotech, Cat. No. P04-03500</b>			
<b>Supplements (for 500 mL)</b>	<b>Stock solution</b>	<b>Volume added</b>	<b>Final concentration</b>	<b>Supplier &amp; Cat#.</b>
FBS	100 x	100 mL	20 %	Merck Millipore; S0615; Lot#0865C
GlutaMAX®	100 x	5 mL	10 ng/mL	Thermo Fischer Cat#. 35050038
Pen/Strep	100 x	5 mL	1 x	PAA Laboratories, Cat#. P11-010
Non-Essential Amino Acids (NEAA or MEM)	100 x	5 mL	1 x	Thermo Fischer; Gibco; Cat#. 11140035
Na-Pyruvate	100 x	5 mL	1 x	Thermo Fischer Cat#. 11360070

### **3.6 *In vitro* assays relevant for the AOP – Receptor-mediated endocytosis and lysosomal overload**

#### **3.6.1 Immunocytochemistry staining (ICC) of LAMP-1/2 protein – assay for KE1 – Disturbance of lysosomal function<sup>1</sup>**

##### **3.6.1.1 Cell seeding and treatment**

For fluorescence staining of lysosomal membrane protein 1/2 (LAMP-1/2), cells were seeded at a density of 140 cells per  $\mu\text{L}$  in 300  $\mu\text{L}$  growth medium per chamber on an 8-well chamber slide (Ibidi®) and were allowed to grow for 48 h (NRK-52E) or 10 d (RPTEC/TERT1), respectively. Before treatment, stock solutions (1000  $\mu\text{M}$ ) of test compounds dissolved in growth medium were freshly prepared and serial dilutions were made before each experiment (1000  $\mu\text{M}$ ; 500  $\mu\text{M}$ ; 250  $\mu\text{M}$ ; 62.5  $\mu\text{M}$ ; 31.25  $\mu\text{M}$ ; 15.6  $\mu\text{M}$ ; 7.8  $\mu\text{M}$ ). The supernatant was aspirated, and 300  $\mu\text{L}$  compound solution, respectively growth medium for controls, were added to the cells. Cells were treated for 24 h.

##### **3.6.1.2 LAMP-1/2 staining and measuring of lysosomal disturbance**

After exposure, cells were washed twice with 150  $\mu\text{L}$  PBS and fixed with 150  $\mu\text{L}$  4 % paraformaldehyde in 1 x PBS for 10 min at room temperature (RT). After fixation, cells were washed 10 min with 150  $\mu\text{L}$  1 x PBS on an orbital shaker followed by permeabilization with 150  $\mu\text{L}$  0.2 % Triton X-100 in 1 x PBS for 5 min at RT on an orbital shaker. The permeabilized cells were washed twice with 1 x PBS (150  $\mu\text{L}$ ) for 10 min at RT on an orbital shaker and then

---

<sup>1</sup> This experimental work was carried out in part by Pia Reiser at the University of Würzburg, Department of Toxicology, Würzburg, Germany, and images were kindly acquired for this thesis.

incubated with 150  $\mu$ L 5 % BSA dissolved in 1 x PBS for 1 h at RT to block unspecific binding sides. After blocking, the BSA solution was aspirated and 100  $\mu$ L primary antibody diluted 1:100 in 1 % BSA in 1 x PBS were directly pipetted onto the cells. Cells were incubated overnight at 4 °C (NRK-52E: Anti-LAMP-1 monoclonal mouse antibody (Santa Cruz; sc-20011); RPTEC/TERT1: Anti-LAMP-2 monoclonal mouse antibody (Santa Cruz; sc-18822)). After incubation with primary antibody, cells were washed three times for 15 min with 0.2 % Tween in 1 x PBS (150  $\mu$ L) on an orbital shaker. Tween solution was aspirated, and cells were incubated for 1 h at RT with 100  $\mu$ L fluorescent dye-conjugated mouse IgG kappa binding protein (1:50) (m-IgG $\kappa$  BP-CFL 488; Santa Cruz, sc-516176). After incubation the cells were washed three times for 15 min with 0.2 % Tween in 1 x PBS on an orbital shaker and once with 150  $\mu$ L sterile water. To stain the cytoskeleton, phalloidin-tetramethylrhodamine B isothiocyanate (phalloidin-TRITC) was diluted in 100 % methanol to a stock concentration of 0.1 mg/mL and further diluted in 1 x PBS to a working concentration of 0.095  $\mu$ M. After cells were washed once with 1 x PBS for 10 min at RT 150  $\mu$ L phalloidin-TRITC working solution was added and the cells were incubated on an orbital shaker at RT for 60-90 min. After incubation phalloidin-TRITC solution was aspirated and the cells were washed once with 1 x PBS. The chamber slides were allowed to dry for 15 min at RT. To preserve fluorescence 50 – 100  $\mu$ L DAPI mounting medium (Vectashield<sup>®</sup>) were added to the cells. The chamber slides were stored at 4 °C in the dark until image acquisition.

Images were taken with a TCS SP5 II confocal microscope with an HCX PL APO lambda blue 63.0 x 1.40 OIL UV objective (Leica Microsystems, Wetzlar, GER) (n = 10 cells/group). Maximum excitation (Ex) and emission (Em) wavelengths used for individual fluorochromes are shown in Table 14.

**Table 14**  
**Fluorochromes with maximal excitation ( $\lambda_{ex}$ ) and emission ( $\lambda_{em}$ ) wavelength used for immunocytochemistry staining**

<b>Dye</b>	<b><math>\lambda_{ex}</math></b>	<b><math>\lambda_{em}</math></b>
Vectashield <sup>®</sup> Antifade mounting medium with DAPI	360 nm	460 nm
Fluorescent dye-conjugated mouse IgG kappa binding protein (m-IgG $\kappa$ BP-CFL 488)	490 nm	525 nm
Phalloidin-tetramethylrhodamine B isothiocyanate	545 nm	573 nm

Before quantification, images were blinded and randomized. Quantification of fluorescence intensity was performed using NIH ImageJ<sup>®</sup> software. Using profile plots a two-dimensional graph of the intensity of pixels along a line was displayed. While the x-axis represents distance in pixels, the y-axis shows the pixel intensity. The mean values of the determined intensities were automatically calculated by the software and presented in a data sheet. Each assay was performed in three independent experiments carried out in triplicates.

### **3.6.2 Immunocytochemistry staining (ICC) of cathepsin D – a putative endpoint for KE2 (disruption of lysosomes)<sup>2</sup>**

#### **3.6.2.1 Cell seeding and treatment**

To measure lysosomal membrane permeabilization (LMP) and cathepsin D release into the cytosol, cells were seeded at a density of 140 cells per  $\mu\text{L}$  in 300  $\mu\text{L}$  growth medium per chamber on 8-well chamber slides (Ibidi®) and were allowed to grow for 48 h (NRK-52E) or 10 d (RPTEC/TERT1) respectively. Stock solutions (1000  $\mu\text{M}$ ) of test compounds dissolved in growth medium were freshly prepared and serial dilution were made before each experiment (1000  $\mu\text{M}$ ; 500  $\mu\text{M}$ ; 250  $\mu\text{M}$ ; 62.5  $\mu\text{M}$ ; 31.25  $\mu\text{M}$ ; 15.6  $\mu\text{M}$ ; 7.8  $\mu\text{M}$ ). Growth medium was aspirated before treatment and the cells were exposed for 24 h to the freshly prepared compound solutions (300  $\mu\text{L}$ ) for 24 h.

#### **3.6.2.2 Cathepsin D staining and analysis of lysosomal membrane permeabilization**

After treatment time, cells were washed twice with PBS (150  $\mu\text{L}$ ) and fixed with 150  $\mu\text{L}$  of a 4 % para-formaldehyde solution dissolved in 1 x PBS for 10 min at RT. Fixed cells were then washed with 150  $\mu\text{L}$  1 x PBS for 10 min followed by a 5 min permeabilization with 150  $\mu\text{L}$  of a 0.2 % Triton X-100 solution at RT. The permeabilized cells were washed twice with 1 x PBS (150  $\mu\text{L}$ ) for 10 min at RT on an orbital shaker and then incubated with 150  $\mu\text{L}$  5 % BSA dissolved in 1 x PBS for 1 h at RT to block unspecific binding sites. The BSA solution was aspirated and 100  $\mu\text{L}$  primary antibody diluted 1:100 in 1 % BSA in 1 x PBS were pipetted

---

<sup>2</sup> This experimental work was carried out in part by Pia Reiser at the University of Würzburg, Department of Toxicology, Würzburg, Germany, and images were kindly acquired for this thesis.



onto the cells and incubated at 4 °C overnight. Primary antibodies used to stain cathepsin D were anti-Cathepsin D mouse monoclonal IgG kappa antibody (Santa Cruz; sc-377124) for NRK-52E cells and anti-Cathepsin D mouse monoclonal IgG2b kappa (Novus Biologicals; NBP1-04278) for RPTEC/TERT1 cells. The solution was aspirated, and cells were incubated for 1 h at RT with 100 µL fluorescent dye-conjugated mouse IgG kappa binding protein (1:50) (m-IgGκ BP-CFL 488; Santa Cruz, sc-516176). The cells were washed three times for 15 min each with a 0.2 % Tween solution followed by a further washing step with 150 µL sterile water. To stain the cytoskeleton, phalloidin-TRITC was diluted in 100 % methanol to a stock concentration of 0.1 mg/mL and further diluted in 1 x PBS to a working concentration of 0.095 µM. Cells were incubated with 150 µL phalloidin-TRITC working solution on an orbital shaker at RT for 60 – 90 min. Phalloidin-TRITC solution was aspirated and cells were washed with 1 x PBS and the chamber slides were allowed to dry for 15 min at RT. To preserve fluorescence 50 – 100 µL DAPI mounting medium (Vectashield®) were added to the cells and chamber slides were stored at 4 °C in the dark until image acquisition.

Images were taken with a TCS SP5 II confocal microscope (Leica Microsystems) and an HCX PL APO lambda blue 63.0 x 1.40 OIL UV objective (n = 10 cells/group). Maximum excitation (Ex) and emission (Em) wavelengths used for individual fluorochromes are given in Table 14.

Before quantification, images were blinded and randomized. Quantification of fluorescence intensity was performed using NIH ImageJ® software. Using profile plots a two-dimensional graph of the intensity of pixels along a line was displayed. While the x-axis represents distance in pixels, the y-axis shows the pixel intensity and mean values of the determined intensities were automatically calculated by the software and presented in a data sheet. Each assay was performed in three independent experiments carried out in triplicates.

In untreated cells, intralysosomal localization of Cathepsin D is evident by an intense punctual staining throughout the cytoplasm. Upon lysosomal leakage or rupture, the staining of cathepsin D becomes more diffuse throughout the cytoplasm.

### **3.7 *In vitro* assays relevant for the AOP – Inhibition of mt-DNA polymerase- $\gamma$**

#### **3.7.1 Determination of mtDNA copy number via qPCR – assay for KE1 – Depletion of mtDNA**

##### **3.7.1.1 Cell treatment and isolation of DNA**

Cells were seeded in a 12 well plate at a density of 120,000 cells per well in 1000  $\mu$ L growth medium. NRK-52E cells were allowed to grow for 48h until they reached 100 % confluence. RPTEC/TERT1 cells were allowed to grow for 10 d until they reached 100 % confluence with medium change after 5 days. In initial concentration-range experiments, the followed concentration ranges were determined in NRK-52E and RPTEC/TERT1 cells after 24 h treatment and in RPTEC/TERT1 cells after 14 d treatment (Table 15, Table 16, Table 17) in order to analyse effects on mitochondria without causing overt cytotoxicity. The supernatant was aspirated, and test compounds dissolved in growth medium were added directly to the cells. For short term experiments, cells were treated for 24 h. For long term exposure experiments, compounds were freshly dissolved in growth medium and added to the cells every 24 h for 14 d.

Table 15

Treatment concentrations for mtDNA copy number experiments in NRK-52E (24 h)

<b>Compound</b>	<b>Concentration [<math>\mu</math>M]</b>					
<i>Adefovir</i>	2000	1000	250	62.5	15.6	0
<i>ADV</i>	500	250	62.5	15.6	0	-
<i>Cidofovir</i>	2000	1000	250	62.5	15.6	0
<i>ddC</i>	2000	1000	250	62.5	15.6	0
<i>TDF</i>	1000	250	62.5	15.6	0	-
<i>Tenofovir</i>	2000	1000	250	62.5	15.6	0

Table 16

Treatment concentrations for mtDNA copy number experiments in RPTEC/TERT1 (24 h)

<b>Compound</b>	<b>Concentration [<math>\mu</math>M]</b>					
<i>Adefovir</i>	2000	1000	250	62.5	15.6	0
<i>ADV</i>	500	250	62.5	15.6	0	-
<i>Cidofovir</i>	2000	1000	250	62.5	15.6	0
<i>ddC</i>	2000	1000	250	62.5	15.6	0
<i>TDF</i>	1000	250	62.5	15.6	0	-
<i>Tenofovir</i>	2000	1000	250	62.5	15.6	0

Table 17

Treatment concentrations for mtDNA copy number experiments in RPTEC/TERT1 (14 d)

<b>Compound</b>	<b>Concentration [<math>\mu</math>M]</b>					
<i>Adefovir</i>	250	62.5	15.6	3.9	0.98	0
<i>ADV</i>	15.6	3.9	0.98	0.24	0.06	0
<i>Cidofovir</i>	125	62.5	15.6	3.9	0.98	0
<i>ddC</i>	250	62.5	15.6	3.9	0.98	0
<i>TDF</i>	62.5	15.6	3.9	0.98	0.24	0
<i>Tenofovir</i>	2000	1000	250	62.5	15.6	0

After treatment the supernatant were aspirated, and the cells were washed with 1 x PBS followed by trypsination with 200  $\mu$ L trypsin at 37 °C for 5 – 10 min until the cells were detached. Detached cells were resuspended in 1000  $\mu$ L 1 x PBS and quantitatively transferred to 1.5 mL PCR-graded tubes (Eppendorf AG). For DNA isolation the QIAamp<sup>®</sup> DNA mini Kit (Qiagen N.V.) was used according to the manufacturer's instructions. Briefly, cells were centrifuged for 5 min at 330 x g. The supernatant was carefully aspirated, and the cell pellet was resuspended in 200  $\mu$ L 1 x PBS. To the cell suspension, 20  $\mu$ L proteinase K, 4  $\mu$ L RNase A and 200  $\mu$ L buffer AL (Qiagen N.V.) were added and vortexed for 15 sec. followed by 10 min incubation at 56 °C in a heat block. After incubation 200  $\mu$ L ethanol (100 %) was added and vortexed for 15 sec. The cell lysate was quantitatively transferred to a QIAamp<sup>®</sup> column and centrifuged for 1 min at RT at ~ 5000 x g. The flow-through was discarded and the column was washed with 500  $\mu$ L buffer AW1 and centrifuged for 1 min at RT at ~5000 x g followed by a second washing step with 500  $\mu$ L AW2 buffer and centrifugation at maximum speed for 3 min and discarding the flow-through. The column containing complete DNA was placed onto a new 1.5 mL PCR-graded tube (Eppendorf AG) and 100  $\mu$ L elution buffer was pipetted directly onto the filter membrane. After an incubation time of 1 min at RT the QIAamp column was centrifuged for 1 min. at ~ 5000 x g and the eluate was placed on ice. The amount of isolated DNA was quantified using a NanoDrop device (Thermo Fisher Scientific<sup>™</sup>) by measuring the absorbance at 260 nm ( $A_{260}$ ). Each assay was performed in three independent experiments carried out in triplicates.

### 3.7.1.2 Quantification of mtDNA copy number via quantitative real-time RT-PCR

To determine mtDNA copy number, quantitative real-time RT-PCR was performed using the Real-Time PCR system LightCycler® 480 (Roche), LightCycler® 480 SYBR Green I Master (Roche) and LightCycler® Multiwell Plates 96. Preliminary experiments showed a constant primer amplification efficiency at 5 µM primer concentration. For PCR reactions, 25 µL master mix per well were used (Table 18).

**Table 18**  
Master mix per well for one PCR reaction with components and reaction mix volume

Components	Volume for 1 reaction [µL]
LightCycler® 480 SYBR Green I Master	12.5
Primer forward (5 µM)	1
Primer reverse (5 µM)	1
Nuclease free water	8.5
DNA probe (3 ng/µL)	2

The 96-well PCR plate was covered with a sealing foil and centrifuged for 2 min at 4000 x g.

The cycling conditions for the LightCycler® are listed in Table 19.

**Table 19**  
Quantitative real-time RT-PCR run program used for quantification of mtDNA copy number

	Temperature	Time	Cycles
Heating	50 °C	2 min	1
Initialization	95 °C	10 min	1
Denaturation	95 °C	15 sec	40
Primer hybridization and elongation	60 °C (rat primer) 62 °C (human primer)	1 min	
Melting curve analysis			

At the end of the program, the LightCycler<sup>®</sup> software was used to generate melting curves of the PCR products to ensure the specificity of the amplicons. Quantifications were performed in duplicates and all samples were normalized to housekeeping genes (rat: Actb; human: B2M). The change in mtDNA copy number in relation to control samples were calculated using the  $\Delta\Delta C_T$  method. Mean values were calculated from cycle threshold ( $C_T$ ) mtDNA respectively nucDNA from duplicates and relative quantification (mtDNA relative to nucDNA) were calculated as described follow:

$$\Delta C_T (\text{control}) = C_T \text{ mtDNA } (\text{control}) - C_T \text{ nucDNA } (\text{control})$$

$$\Delta C_T (\text{sample}) = C_T \text{ mtDNA } (\text{sample}) - C_T \text{ nucDNA } (\text{sample})$$

$$\Delta\Delta C_T = \Delta C_T (\text{sample}) - \Delta C_T (\text{control})$$

$$\text{relative mtDNA copy number} = 2^{-\Delta\Delta C_T}$$

Calculated  $2^{-\Delta\Delta C_T}$  values correspond to the ratio of the mitochondrial DNA copy number to the copy number of nuclear DNA. Significance analysis of mtDNA copy number in treated samples was evaluated performing a one-way ANOVA followed by Dunnett's test using GraphPad Prism 5.01 software. Each assay was performed in three independent experiments carried out in triplicates.

### 3.7.2 Determination of mitochondrial toxicity via MitoTracker™ - a putative *in vitro* endpoint for KE2 (*dysfunction of mitochondrial*)<sup>3</sup>

To determine mitochondrial toxicity, the MitoTracker™ assay (Thermo) was used. This assay, in combination with the MitoTracker Red CMXRos dye (Thermo) allows to stain intact mitochondria in living cells that possess a membrane potential. Hence, a lower membrane potential in the mitochondria means less accumulation of the dye in mitochondria. Staining in mitochondria is proportional to mitochondrial toxicity and this staining can be measured by automated image analysis using an Opera® System (PerkinElmer Inc., MA, USA). A known substance that decreases the membrane potential in mitochondria is valinomycin, which was used as a positive control in this assay (Moraes *et al.*, 2019). Therefore, cells were seeded on a CellCarrier™ 384 TC plate (PerkinElmer Inc. MA, USA) at a concentration of 75,000 cells per mL and 20 µL of the cell suspension was added to each well. After seeding cells were incubated for 36 h at 37 °C and 5 % CO<sub>2</sub>. Stock solutions for each tested compound (2000 µM) were prepared in water and serial dilutions (1:1) were made before each experiment. After cells reached confluence 10 µL dissolved test compounds were added to each well, resulting in a final volume of 30 µL. Cells were incubated for 24 h. After treatment 10 µL of a 200 nM solution of MitoTracker® Red CMXRos (final concentration 50 nM) diluted in prewarmed growth medium was added to each well and the cells were incubated for additional 45 min at 37 °C and 5 % CO<sub>2</sub>. MitoTracker® Red CMXRos uptake was measured using an Opera® System (PerkinElmer Inc., MA, USA) with the settings shown in Table 20. The 561 nm laser was switched on 15 min before

---

<sup>3</sup> This experimental work was performed by Dr. Bernhard Ellinger at the Fraunhofer Institute for Molecular Biology and Applied Ecology, Division Translational Medicine, ScreeningPort, in Hamburg, Germany, and kindly provided for this thesis.

use to allow temperature equilibration. After temperature equilibration the 60xW\_UP-LAPO\_60x\_NA=1.2 objective was selected, and a reference image was taken using an Opera<sup>®</sup> Adjustment plate (PerkinElmer Inc., MA, USA).

**Table 20**  
**Opera<sup>®</sup> System settings used for the measurement of the MitoTracker<sup>®</sup> Red CMXRos uptake**

<b>Slider name</b>	<b>Filter name</b>	<b>Time [ms]</b>
Camera 1	450/50	Inactive
Camera 2	600/40	80
Camera 3	690/50	Inactive
Detect Dichroic Mirror	568	n/a
Primary Dichroic Mirror	405/561/635	n/a
UV Excitation	425	n/a
UV Emission	475	n/a
UV Bandpass	450/50	n/a

To facilitate automated image analysis, a layout containing the compound area as well as a valinomycin control (positive compound) in row 23 and the water control area in well 24 was created and stored. A sub-layout of 5 evenly dispersed fields per well was created and stored. The settings including a measurement height of 1  $\mu\text{m}$  were stored in an exposure file format. The obtained images were transferred to the file server and uploaded into Columbus<sup>™</sup> 2.4.0 (PerkinElmer Inc., MA, USA) using the build-in helper function. Analysis was performed using the ‘MT-analysis-17072014’ protocol available within Columbus<sup>™</sup> 2.4.0 (PerkinElmer Inc., MA, USA). Results were exported and analyzed in ABase (ID Business Solution Limited., Guildford, GB).



### **3.8 *In vitro* cytotoxicity assay relevant for the AOP – Receptor-mediated endocytosis and lysosomal overload & for the AOP – Inhibition of mt-DNA polymerase- $\gamma$**

#### **3.8.1 CellTiter-Glo<sup>®</sup> cell viability assay – assay for KE3 Cytotoxicity of renal tubule cells**

The CellTiter-Glo<sup>®</sup> reagent contains the benzothiazole luciferin and an enzyme called luciferase. In the case of the CellTiter-Glo<sup>®</sup> assay, the enzyme is a special recombinant luciferase that is thermostable and enables the luminescence signal to be maintained for more than five hours. The luminescence signal that can be measured with this assay is proportional to the amount of ATP present in the cells, which is directly proportional to the number of living cells. Luminescence is based on a luciferase-catalyzed reaction of the ATP with luciferin and molecular oxygen. In the presence of Mg<sup>2+</sup>, the luciferin is oxidatively decarboxylated to oxyluciferin.

For cytotoxicity assays cells were plated into 96-well tissue culture plates (10,000 cells per well) in 100  $\mu$ L medium and were allowed to grow for 48 h (NRK-52E) respectively 10 d (RPTEC/TERT1). Stock solutions for each compound (2000  $\mu$ M) were prepared in growth medium and serial dilutions (1:1) were made before each experiment. After cells reached confluence, the growth medium was aspirated and 100  $\mu$ L of treatment solution were added for 24 h. After treatment time cell viability was measured using CellTiter-Glo<sup>®</sup> assay (Promega).

CellTiter-Glo<sup>®</sup> reagents and buffer were mixed under light-protected conditions and 100  $\mu$ L CellTiter-Glo<sup>®</sup> solution was added directly to each well, followed by 2 min incubation on an orbital shaker and 10 min incubation at RT in the dark to stabilize the luminescence signal. The suspension was mixed via pipetting and 50  $\mu$ L of each well were transferred into the corre-

sponding well of a white 96-well plates (PerkinElmer Inc.). The luminescence signal was measured on a multiplate reader (Mithras LB 940; Berthold Tech.). Each assay was performed in three independent experiments carried out in triplicates.

### **3.9 Determination of intracellular compound accumulation of polymyxin B and colistin via LC-MS/MS**

#### **3.9.1 Treatment, preparation of cell sample and samples to measure plastic adsorption**

NRK-52E and RPTEC/TERT1 cells were seeded in 12-well plates (1 mL cell suspension per well contains 120,000 cells) and were allowed to grow for 48 h (NRK-52E) or 10 d (RPTEC/TERT1) until they reached 100 % confluence. After cells achieved 100 % confluence, the supernatant was aspirated, and the cells were washed twice with 1 x PBS. Due to the hydrophilic character of polymyxin B and colistin, the compounds were dissolved in cell culture medium reaching a final concentration of 34  $\mu\text{M}$ . To support kinetic modeling, both cell lines were additionally treated with 62.5  $\mu\text{M}$  and 125  $\mu\text{M}$  polymyxin B, respectively. The cells were treated with test compounds for 1 – 2 min, 1 h, 3 h, 6 h, and 24 h. In addition, recovery samples were prepared by replacing the treatment solution with growth medium after 24 h treatment with test compounds and further incubation with growth medium for 24 h. Following compound treatment respectively incubation with growth medium, the supernatant was aspirated, and cells were washed three times with 1 x PBS to remove any residual extracellular test compounds. The remaining cells were trypsinized by adding 200  $\mu\text{L}$  of trypsin and incubated for 5 – 8 min. After incubation with trypsin, detached cells were washed with 1000  $\mu\text{L}$  1 x PBS and the cells were transferred to LoBind™ tubes (Eppendorf). Cell count was determined using a Fuchs-Rosenthal counting chamber (Hartenstein). Cells were centrifuged for 5 min at 4 °C at 10.000

rpm and the supernatant was aspirated. Cells were resuspended in 1000  $\mu\text{L}$  1 x PBS and centrifuged for 5 min at 4 °C at 10.000 rpm. After centrifugation the supernatant was aspirated, and the cell pellet was resuspended in 250  $\mu\text{L}$  ammonium acetate buffer (10 mM) and 250  $\mu\text{L}$  of 30 % methanol with 1 % acetic acid containing colistin as an internal standard (for polymyxin B determination) respectively polymyxin B as an internal standard (for colistin determination). Cells were sonicated for 10 min and centrifuged for 5 min at 4 °C at 14.000 rpm. The supernatant was transferred quantitatively into new LoBind™ tubes (Eppendorf) and dried in a centrifugal vacuum concentrator for 2 – 3 h. All samples were stored at -20 °C until solid phase extraction (SPE) purification and LC-MS/MS analysis. To measure compound plastic binding, the empty 12 well plates were washed with 1.5 mL acetonitrile on an orbital shaker for 2 h, the supernatant was collected, and compound concentrations were measured via LC-MS/MS.

### **3.9.2 Solid phase extraction (SPE) purification**

For sample purification via solid phase extraction, SPE cartridges Strata-X 33  $\mu\text{m}$  polymeric reversed phase, 10 mg / 1 mL (Phenomenex) were used. In the conditioning step the cartridges were rinsed with 200  $\mu\text{L}$  methanol (100 %) and subsequently with 200  $\mu\text{L}$  ddH<sub>2</sub>O to activate the sorbent bed. The dried samples were dissolved in 200  $\mu\text{L}$  1 % acetic acid and transferred onto the SPE cartridge. The SPE cartridge was rinsed once with 200  $\mu\text{L}$  1 % acetic acid. Impurities were removed by rinsing the cartridge once with 200  $\mu\text{L}$  10 % methanol. A fresh LoBind™ tube (Eppendorf) was placed under the SPE cartridge to eluate the sample by rinsing twice with 200  $\mu\text{L}$  90 % methanol containing 1 % acetic acid. The samples were dried in a centrifugal vacuum concentrator for 2 – 3 h. All samples were stored at -20 °C until LC-MS/MS analysis.

### **3.9.3 Analysis of intracellular polymyxin concentrations by mass spectrometry coupled with liquid chromatography**

A triple quadrupole mass spectrometer coupled to a Turbo-Ion<sup>®</sup> Spray source (Qtrap<sup>®</sup> API 2000, AB Sciex Instruments, Darmstadt, GER) was used for analyses. The mass spectrometer was equipped with an Agilent 1100 HPLC system consisting a binary pump system, a vacuum degasser and an autosampler (Agilent 1100). Chromatographic separation was performed at 40 °C with a column oven (Knauer, Berlin, GER) on a Synergi Hydro-RP column (2 mm x 150 mm, 4 µm, 80 Å; Phenomenex, Aschaffenburg, GER) coupled to a precolumn (SecurityGuard<sup>™</sup> Cartridges, AQ C18 4 x 2.0 mm) using a binary step gradient at a flow rate of 0.2 mL/min with the following gradient: 0 min 100 % A, 15 min 0 % A, 20 min 0 % A, 21 min 100 % A, and 30 min 100 % A. The mobile phase consisted of 3 % acetonitrile containing 1 % acetic acid (solvent A) and 97 % acetonitrile containing 1 % acetic acid (solvent B). The injection volume was set to 10 µL and total analysis time was 30 min. Following chromatographic separation, multiple ion monitoring was used to detect the triply charged, twice charged, and single charged ions. Parameter settings for multiple reaction monitoring (MRM) detection including mass transitions for polymyxin B1 / B2 and colistin A / B (triply, twice and single charged ions), declustering potential (DP), entrance potential (EP), collision entrance potential (CEP), collision energy (CE), cell exit potential (CXP), and retention time (RT) are listed in Table 21.

Table 21

LC-MS/MS parameters for MRM detection of polymyxin B1, polymyxin B2, colistin A, and colistin B

Parameters including transition values for the triply  $[M+3H]^{3+}$ , twice  $[M+2H]^{2+}$  and single  $[M+H]^+$  charged ions; declustering potential (DP), entrance potential (EP), collision entrance potential (CEP), collision energy (CE), cell exit potential (CXP), and retention time (RT)

<i>Charge</i>	<i>Compound</i>	<i>Transition [m/z]</i>	<i>DP [V]</i>	<i>EP [V]</i>	<i>CEP [V]</i>	<i>CE [V]</i>	<i>CXP [V]</i>	<i>RT [min]</i>
$[M+3H]^{3+}$	Colistin A	386.0 → 101.1	31	7.5	16.21	27	2	11.2
	Colistin B	390.7 → 101.1	31	8	16.33	27	2	11.0
	Polymyxin B2	397.3 → 101.1	51	7	16.49	29	2	11.1
	Polymyxin B1	402.1 → 101.1	31	8	16.61	27	2	11.4
$[M+2H]^{2+}$	Colistin A	578.6 → 101.1	66	9	21.06	53	2	11.2
	Colistin B	585.6 → 101.1	66	9.5	21.24	49	2	11.0
	Polymyxin B2	595.6 → 101.1	66	12	21.49	49	2	11.1
	Polymyxin B1	602.6 → 101.1	71	9.5	21.66	47	2	11.4
$[M+H]^+$	Colistin A	1156.03 → 302.2	151	11	35.6	77	4	11.2
	Colistin B	1170.03 → 302.2	151	11	35.95	75	4	11.0
	Polymyxin B2	1190.05 → 302.3	151	12	36.46	79	4	11.1
	Polymyxin B1	1204.04 → 302.2	151	11	36.81	79	4	11.4

### 3.9.4 Total cell volume calculation

To determine the cell volume of NRK-52E and RPTEC/TERT1 cells, a cell culture flask with 70 – 80 % confluent cell layer was trypsinized with 1.5 mL trypsin / EDTA (Sigma, Trypsin - EDTA (1x) Cat# T3924) at 37 °C for 5 – 8 min until cells detached. Images were taken from rounded cells on an ECLIPSE 55i microscope (Nikon) (n = 28) and the diameter of each cell was measured using NIH ImageJ®. Single cell volume was calculated based on the method

described by Zhang et al. (2015) (Zhang *et al.*, 2015), using the mathematical formula for the volume of a sphere where  $d$  the diameter of a single cell is:

$$V_{Sphere} = \left(\frac{1}{6}\right) * \pi * d^3$$

The volume of each cell was calculated based on this equation and mean values ( $n = 28$ ) of cell volume were used to calculate total volume of viable cells in the cell samples:

$$V_{Total\ cell\ volume} = n_{cell\ number} * V_{mean\ cell}$$

Intracellular compound concentration was finally calculated by the total amount of polymyxins measured per sample divided by the total volume of viable cells per sample:

$$C_{compound\ intracellular} = \frac{C_{compound\ in\ sample}}{V_{Total\ cell\ volume}}$$

### **3.10 Determination of aprotinin uptake to assess endocytic activity**

Cells were seeded at a density of 140 cells/ $\mu$ L in 300  $\mu$ L growth medium per chamber on an 8-well chamber slide (Ibidi<sup>®</sup>) and were allowed to grow for 48 h (NRK-52E) or 10 d (RPTEC/TERT1), respectively, until cells reached confluence. A stock solution (2 mg/mL) of Alexa Fluor 488 labeled aprotinin was diluted in 1 x PBS to a working concentration of 100  $\mu$ g/mL and was added to the cells (300  $\mu$ L). Cells were incubated for 4 h at 37 °C and 5 % CO<sub>2</sub> atmosphere. After incubation the aprotinin solution was aspirated and cells were washed 3 times with 1 x PBS on an orbital shaker followed by fixation with 150  $\mu$ L 4 % paraformaldehyde in 1 x PBS for 10 min at RT. Cells were washed 10 min with 150  $\mu$ L 1 x PBS on an orbital shaker, and chamber slides were allowed to dry for 15 min at RT. To stain the cell nuclei and to preserve fluorescence 50 – 100  $\mu$ L DAPI mounting medium (Vectashield<sup>®</sup>) were added to the cells.

Chamber slides were stored at 4 °C in the dark until image acquisition. Images of intracellular Alexa Fluor 488 labeled aprotinin were taken with a TCS SP5 II confocal microscope with an HCX PL APO lambda blue 63.0 x 1.40 OIL UV objective (Leica Microsystems) (n = 4 images per group). Images were quantified using ImageJ<sup>®</sup> software using profile plots to measure Alexa-488 intensity of control and exposed cells. Fluorescence intensity of Alexa Fluor 488 labeled aprotinin was divided by the number of nuclei per image and results were plotted as mean fluorescence intensity per number of nuclei.

### **3.11 Immunocytochemistry of megalin receptor in NRK-52E and RPTEC/TERT1 cells**

NRK-52E and RPTEC/TERT1 cells were seeded on 8-well chamber slides (Ibidi<sup>®</sup>) (140 cells /  $\mu$ L in 300  $\mu$ L per chamber) and allowed to grow for 10 d (RPTEC/TERT1) or 48 h (NRK-52E), respectively. Confluent cells were washed twice with 150  $\mu$ L 1 x PBS and fixed with 150  $\mu$ L 4 % paraformaldehyde solution for 10 min at RT. Following fixation, the cells were washed with 150  $\mu$ L 1 x PBS for 10 min and permeabilized with 0.2 % Triton X-100 (150  $\mu$ L) for 5 min at RT. Primary antibody used for megalin staining (anti-megalín mouse monoclonal IgG<sub>1</sub> antibody (Santa Cruz, sc-515772)) was diluted 1:100 in 1 % BSA in 1 x PBS. Cells were incubated overnight at 4 °C with 100  $\mu$ L diluted antibody per chamber. Primary antibody solution was aspirated, and cells were incubated for 1 h with 100  $\mu$ L fluorescent dye-conjugated mouse IgG kappa binding protein (1:50) (m-IgG $\kappa$  BP-CFL 488; Santa Cruz, sc-516176) at RT. The cells were washed three times for 15 min each with a 0.2 % Tween solution followed by a further washing step with 150  $\mu$ L sterile water. Chamber slides were then allowed to dry for 15 min at RT. To preserve fluorescence and to stain cell nuclei 50 – 100  $\mu$ L DAPI mounting medium (Vectashield<sup>®</sup>) were added to the cells. Chamber slides were stored at 4 °C in the dark

until image acquisition. Images were taken with a TCS SP5 II confocal microscope with an HCX PL APO lambda blue 63.0 x 1.40 OIL UV objective (Leica Microsystems, Wetzlar, GER). Maximum excitation and emission wavelength for each dye are shown in Table 14.

### **3.12 Megalin and cubilin mRNA expression using TaqMan™ probes**

#### **3.12.1 RNA isolation**

Total RNA was isolated from NRK-52E, RPTEC/TERT1, HK-2, CaCo-2 cells (cells provided kindly by the working group of Prof. Stopper), and rat kidney tissue using Qiagen RNeasy® Mini kit according to the manufacturer's protocol.  $1 \times 10^6$  cells or  $\leq 30$  mg rat kidney were used for RNA isolation. Cells were washed with 1 x PBS and trypsinized for 5-10 min at 37 °C until cells were detached. Rat kidney was washed twice with 1 x PBS and transferred to 1.5 mL PCR-graded tubes (Eppendorf AG, Hamburg, GER). Detached cells and rat kidney were resuspended in 350  $\mu$ L RLT buffer containing 10 %  $\beta$ -mercaptoethanol. The cells were lysed by vortexing. Kidney tissue was homogenized using a pistol. The kidney lysate was then pipetted onto QIAshredder® spin columns and centrifuged for 2 min at maximum rpm. The kidney eluate and cell lysates were then mixed with 350  $\mu$ L ethanol, transferred to RNeasy® spin columns and centrifuged at 10,000 rpm for 15 sec. The eluate was discarded, and the filter was washed with 350  $\mu$ L RW1 buffer and centrifuged for 15 sec at 10,000 rpm. After centrifugation, the eluate was discarded, and 80  $\mu$ L DNase Mix were added to the filter and incubated at RT for 15 min. The samples were then washed with 350  $\mu$ L RW1 buffer, centrifuged at 10,000 rpm for 15 sec, and the eluate was discarded. Subsequently, the samples were washed twice with 500  $\mu$ L RPE buffer each and centrifuged at 10,000 rpm for 15 sec. The eluates were discarded, and the samples were centrifuged for 2 min at 10,000 rpm. The spin columns were then transferred to PCR-



graded 1.5 mL Eppendorf tubes. For RNA elution, 30  $\mu$ L nuclease-free water was pipetted onto the filter, followed by 1-minute centrifugation at 10,000 rpm. The RNA concentration was measured using a NanoDrop™ and the samples were stored at -80 °C for further experiments.

### **3.12.2 cDNA synthesis**

Total RNA was converted to cDNA using the First Strand Synthesis Kit™ (Thermo Scientific™). From each sample, 1  $\mu$ g RNA was diluted with nuclease free water in a 0.5 mL tube (Eppendorf AG, Hamburg) to a total volume of 9  $\mu$ L. A volume of 2  $\mu$ L mastermix 1 containing 1  $\mu$ L of Oligo (dT)<sub>18</sub> Primer (100  $\mu$ M) and 1  $\mu$ L of Random Hexamer Primers (100  $\mu$ M) was added to each sample and centrifuged briefly. The reaction mix was then incubated in a Mastercycler® (Eppendorf AG, Hamburg) for 5 min at 65 °C followed by a 1-minute incubation period on ice. A second master mix containing 5 x reaction buffer (4  $\mu$ L), RiboLock® RNase inhibitor (1  $\mu$ L), dNTP mix (1  $\mu$ L) and M-MuLV reverse transcriptase (2  $\mu$ L) was added to the sample, mixed and briefly centrifuged. In addition, an n-RT (non-reverse transcriptase) control was performed by adding RNase-free water instead of reverse transcriptase. The cDNA synthesis was performed using a Mastercycler® (Eppendorf AG, Hamburg) and the samples were run with a gradient of 5 min at 25 °C, 1 h at 37 °C and 5 min at 70 °C. The obtained cDNA samples were stored at -80 °C for further experiments.

### **3.12.3 qRT-PCR using TaqMan™ probes**

TaqMan™ gene expression assay was performed as described by the manufacturer (Thermo Scientific™). For PCR with TaqMan™ probes, a cDNA concentration between 1 and 100 ng is recommended by the manufacturer. Previously conducted experiments showed a recommended cDNA concentration of 10 ng which was also used for PCR with TaqMan™. The measurements

were performed in four technical and three biological replicates. Per sample 4  $\mu\text{L}$  of a 2.5 ng/ $\mu\text{L}$  cDNA solution was used and diluted with 10  $\mu\text{L}$  of TaqMan™ Gene Expression Master Mix.

**Table 22**  
**Quantitative real-time RT-PCR run program used for TaqMan™ assay**

	UNG activation	Polymerase activation	PCR (44 x)	
			Denaturation	Annealing / Extension
Temp.	50 °C	95 °C	95 °C	60 °C
Time	2 min	20 sec	3 sec	30 sec

In addition, 1  $\mu\text{L}$  TaqMan™ assay probes (20 x) were added, and the mix was brought to a total volume of 20  $\mu\text{L}$  with 5  $\mu\text{L}$  RNase free water. To determine megalin mRNA expression, quantitative real-time RT-PCR was performed using the Real-Time PCR system LightCycler® 480 (Roche) and LightCycler® Multiwell Plates 96. The 96-well PCR plate was covered with a sealing foil and centrifuged for 2 min at 4000 x g. The cycling conditions for the LightCycler® are listed in Table 22.

### **3.13 Preparation of cell and tissue lysates and Western blot analysis of megalin**

#### **3.13.1 Protein extraction from cells**

NRK-52E cells were cultured in 6-well plates ( $1 \times 10^6$  cells per well) and washed twice with ice cold 1 x PBS in order to remove culture medium. All subsequent steps were performed on ice. After washing, 100  $\mu\text{L}$  freshly prepared Ripa buffer (Tris HCl (50 mM), NaCl (150 mM), Nonidet P40 (1 %), Na-desoxycholat (0.25 %), EDTA (1 mM), NaF (100 mM),  $\text{Na}_3\text{VO}_4$  (200

mM), Protease Inhibitor Cocktail (1:50)) were added to the cells and incubated for 15 min. The cells were then removed from the bottom with a cell scraper and divided into two 1.5 mL Eppendorf tubes. By pipetting up and down, the lysate was carefully mixed and then incubated for 20 min at 4 °C on an orbital shaker. The samples were then centrifuged for 15 min at 10,000 rpm and 4 °C. The supernatant was then transferred into new Eppendorf tubes followed by protein determination.

### **3.13.2 Protein extraction from tissue**

All work steps were carried out on ice. Approximately 5 mg of a rat kidney was transferred to a sterile Eppendorf tube and shock frozen using liquid nitrogen. In the next step, the tissue was lysed with a pestle in 300 µL freshly prepared Ripa buffer. The pestle was then washed twice with 300 µL Ripa buffer each. The samples were then shaken for 2 h at 4 °C on an orbital shaker. After 2 h incubation, the samples were centrifuged for 20 min at 20,000 rpm and 4 °C and then put on ice. The supernatant was then transferred to a fresh Eppendorf tube followed by protein determination.

### **3.13.3 Protein determination by DC assay**

Protein determination was performed using the DC assay (BioRad®). A dilution series was prepared with a BSA stock solution (1 mg/mL) dissolved in lysis buffer and stored on ice (Table 23). The samples were diluted 1:4 in lysis buffer and 20 µL of the samples respectively the BSA standard were mixed with 100 µL reagent A' and vortexed. Then, 800 µL of reagent B were added to standard and samples. The samples were vortexed and incubated for 15 min at RT. Samples and standard were then transferred into UV/VIS cuvettes and the measurement was performed at 750 nm on a spectrometer (Buck Scientific M-500) in duplicates. The protein

content of the samples was then calculated using the straight-line equation of the BSA standard curve.

**Table 23**  
**BSA dilution series for standard curve**

<b>Concentration BSA [<math>\mu\text{g/mL}</math>]</b>	<b><math>\mu\text{L}</math> BSA</b>	<b><math>\mu\text{L}</math> Lysis buffer</b>
1000	80	0
800	80	20
600	60	40
400	40	60
200	20	80
0	0	80

#### **3.13.4 Gradient SDS polyacrylamide gel electrophoresis and Western blot**

Proteins extracted from NRK-52E cells and rat kidney were mixed with Laemmli buffer (6 x) and heated for 10 min at 100 °C in a heating block. The samples were then separated on a gradient gel (Nippon Genetics Europe, FastGene® PAGE 4 -12 %, 8 x 10 cm) and the gel was run in MOPS buffer (Tris-base 6.06 g, MOPS 10.47 g, EDTA 0.3 g, SDS 1 g, 1000 mL H<sub>2</sub>O) at 4 °C for 2 h and 80 V (Hoefer Scientific Instruments SE250). After separation, the proteins were transferred using the wet transfer method (3 g TRIS, 14.4 g glycine, 800 mL H<sub>2</sub>O, 200 mL methanol) to a PVDF membrane for 1 h at 100 V and 4 °C. After the transfer the membrane was shaken for 1 h in 5 % milk in TBST (Tris-buffered saline with Tween20) at RT to block non-specific binding sites. The primary antibody was diluted in 5 % milk in TBST (1:1000) and incubated overnight at 4 °C. The membrane was washed 3 times each 15 min with TBST on an orbital shaker. The secondary antibody (anti-mouse IgG HRP-linked antibody; Cell Signaling Technology) was diluted in 5 % in TBST (1:2500) and incubated with the membrane for 1 h at

RT followed by three washing steps for 15 min with TBST. In the process of ECL (enhanced chemiluminescence) detection, primary antibodies bound to specific antigens can be made detectable by chemiluminescence using secondary antibodies coupled with horseradish peroxidase (HRP). The BioRad® Clarity Western ECL substrate was mixed 1:1 (4 mL peroxide solution + 4 mL luminol solution) and incubated for 2 min with the PVDF membrane on an orbital shaker. The stained membrane was then detected using a Gel Doc (ImageQuant™ LAS 4000).

### 3.14 Calculation methods to determine different *in vitro* points of departure

To obtain a first estimation for risk assessment, several PoDs were calculated from the dose-response relationships obtained from the applied *in vitro* assays after treatment with the test substances. Therefore, the most common PoDs (EC<sub>10</sub>, EC<sub>20</sub>, NOEC, LOEC, BMC<sub>10</sub>, BMCL<sub>10</sub>, BMCU<sub>10</sub>) as well as a novel approach (NtC) were calculated and compared. The calculations of the individual PoDs are described in the following sections.

#### 3.14.1 Effective concentration 10 % and 20 % (EC<sub>10</sub> and EC<sub>20</sub>)

The EC<sub>10</sub> and EC<sub>20</sub> values were calculated using the log concentration vs. normalized response nonlinear regression curve fit in GraphPad Prism 5.01 (GraphPad Software Inc., La Jolla, CA, USA). This method of logistic regression is described by the formula below, in which the y variable describes the response, the x variable the concentration and the Hillslope parameter the steepness of the dose-response curve.

$$y = \frac{1}{1 + 10^{((\log EC_{50} - \log(x)) * Hillslope)}}$$

### 3.14.2 Lowest / no observed effect concentration (LOEC / NOEC)

The lowest observed effect concentration (LOEC) is defined as the lowest tested concentration that is significant different from control. The tested concentration below the determined LOEC is defined as the no observed effect concentration (NOEC), which in most cases is also the lowest not significantly tested concentration (Issuance, 2005). To determine significant differences between control and response, a one-way analysis of variance (ANOVA) with post hoc analysis using Dunnett's multiple comparison test was performed using GraphPad Prism 5.01 software (\*  $p < 0.05$ ; \*\*  $p < 0.01$ ; \*\*\*  $p < 0.001$ ).

### 3.14.3 Benchmark Concentration (BMC)

To calculate a suitable benchmark concentration for this study, a level of extra risk of 10 % was applied ( $BMC_{10}$ ), which is also recommended by the U.S. Environmental Protection Agency (EPA) and the European Food Safety Authority (EFSA) (EPA, 2012, EFSA *et al.*, 2017). In addition, the benchmark concentration lower confidence limit ( $BMCL_{10}$ ) and the benchmark concentration upper confidence limit ( $BMCU_{10}$ ) were determined considering the 95 % confidence interval. The Benchmark Dose Software (BMDS) Version 2.7 (U.S. EPA) was used to calculate the  $BMC_{10}$  as well as the  $BMCL_{10}$  and  $BMCU_{10}$ .

### 3.14.4 Non-toxic concentration (NtC)

A further new approach to determine a PoD is the non-toxic concentration (NtC) described by Stadnicka-Michalak and colleagues (Stadnicka-Michalak *et al.*, 2018), which combines several properties of the methods described above, like the  $EC_x$ , NOEC / LOEC, and the BMC approach. Thus, an algorithm was developed to determine the highest concentration causing no more than 10 % effect ( $\leq EC_{10}$ ), considering each measured biological replicate, including the

95 % confidence intervals, and whose effect is not significantly different from no effect. The online application provided by the authors was used to calculate the NtC under consideration of the necessary parameters such as biological replicates and concentrations ([https://utox.shinyapps.io/NtC\\_NtC/](https://utox.shinyapps.io/NtC_NtC/)).

### 3.14.5 Visualization of different PoDs

After the various potential PoDs were determined from *in vitro* KE assays, they were graphically plotted in Excel for ease of comparison, and the results of the different cell lines, KE assays and treatment times were compared for each model compound. In addition, human and rat serum concentrations from published *in vivo* studies were used and also graphically presented in order to relate the *in vitro* results to existing *in vivo* data for a first estimate of human risk based on *in vitro* KE data.

### 3.14.6 Margin of exposure (MOE)

After the PoDs were determined from the *in vitro* assays, the range of margin of exposure (MOE) from the PoDs was calculated using *in vivo* serum or kidney concentrations. The MOE (or Margin of Safety (MOS)) refers to human exposure (extent of contact with a substance) and the point of departure determined in a test. This allows the distance between the PoD and the exposure to be calculated (EFSA, 2005). Using the PoDs determined from the *in vitro* assays and the *in vivo* data collected, the MOE for the individual KE was calculated using the following formula:

$$MOE = \frac{\textit{Point of departure}}{\textit{Estimated exposure}}$$





## 4 Results

### 4.1 AOP – Receptor-mediated endocytosis and lysosomal overload

#### 4.1.1 Using the Comparative Toxicogenomic Database (CTD) to identify suitable *in vitro* endpoints for the AOP – Receptor-mediated endocytosis and lysosomal overload

In order to define suitable *in vitro* endpoints for the AOP – Receptor-mediated endocytosis and lysosomal overload and to develop appropriate *in vitro* assays the online database Comparative Toxicogenomic Database (CTD; <http://ctdbase.org>) was used as a supporting tool. The publicly available CTD contains manually collected information on drugs and chemicals that affect biological mechanisms and human health (Davis *et al.*, 2013). The curators of the CTD analyze published literature and incorporate information on relationships and interactions between chemicals and diseases / proteins / genes, and relationships between diseases and genes into the database (Davis *et al.*, 2011, Wiegers *et al.*, 2009). A helpful tool of the CTD to compare and examine related data sets for up to three different drugs or chemicals with gene interactions is the VennViewer.

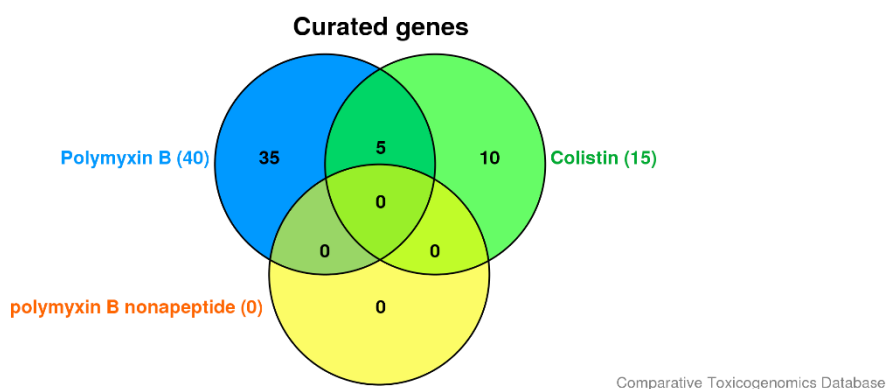


Figure 9

Venn diagram with the data sets of polymyxin B, colistin and polymyxin B nonapeptide

By using the VennViewer online function of the CTD, Venn diagrams can be generated for up to three selected drugs / chemicals to find genes which share a common association with the selected compounds. All three polymyxin antibiotics were analyzed to identify common gene interactions that may indicate appropriate endpoints associated with the AOP – *Receptor-mediated endocytosis and lysosomal overload* (Figure 9). Due to the limited available data in the database (for polymyxin B - 40 gene data; colistin - 15 gene data; polymyxin b nonapeptide - no data available), no shared genes for these three drugs were identified. The five overlapping genes for polymyxin B and colistin (interleukin-6 (IL-6); MAS-related GPR-B6 (MRGPRB2); MAS-related GPR-X2 (MRGPRX2); O-GlcNAcase (OGA); tumor necrosis factor (TNF)) showed no association with the lysosomal pathway or the AOP. A further analysis was performed with compounds that are known to be taken up into the proximal tubule cells via megalin receptor and that damage the proximal tubule cells by the same mechanism of *Receptor-mediated endocytosis and lysosomal overload*. Well-known compounds that act via this mechanism are gentamicin, cadmium chloride and vancomycin (Wallig *et al.*, 2017, Hori *et al.*, 2017, Haschek *et al.*, 2013b, Quiros *et al.*, 2010, Beauchamp *et al.*, 1992).

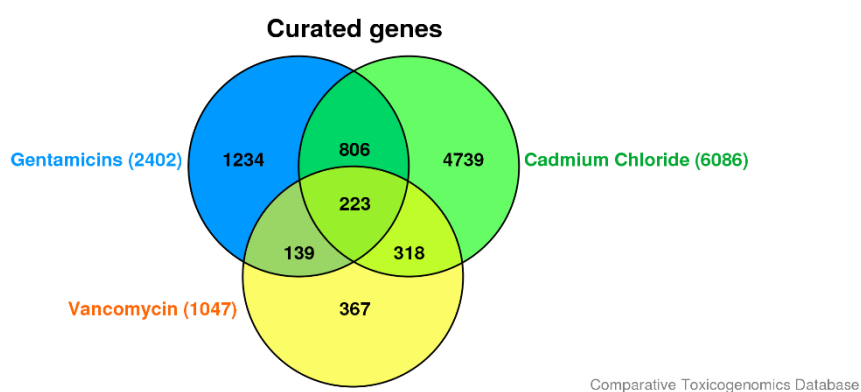


Figure 10

Venn diagram with the data sets of gentamicin, cadmium chloride and vancomycin

The CTD contains a sufficient amount of data for these three compounds to allow a detailed analysis for overlapping genes (for cadmium chloride - 6086 gene data; gentamicin - 2402 gene data; vancomycin – 1047 gene data). The analysis revealed 223 gene overlaps with all three compounds (Figure 10). These genes were filtered for relevant pathways and diseases associated with the AOP – *Receptor-mediated endocytosis and lysosomal overload*. The analysis showed a common match for the genes encoding for cathepsin A, cathepsin C, cathepsin D and cathepsin S, which are also associated with the lysosomal pathway, kidney disease and acute kidney injury in the CTD. Gentamicin and cadmium chloride, the two compounds with the biggest data sets, were separately analyzed for overlapping genes. Analysis of the 1029 genes revealed, in addition to the cathepsins mentioned above, overlaps with the lysosomal-associated membrane protein 2 (LAMP-2). This protein is also associated with the lysosomal pathway and shows associations with kidney disease and acute kidney injury in CTD. A match with LRP2 gene, which is responsible for the expression of megalin, and which is also associated with kidney disease and acute kidney injury, was filtered in the database.

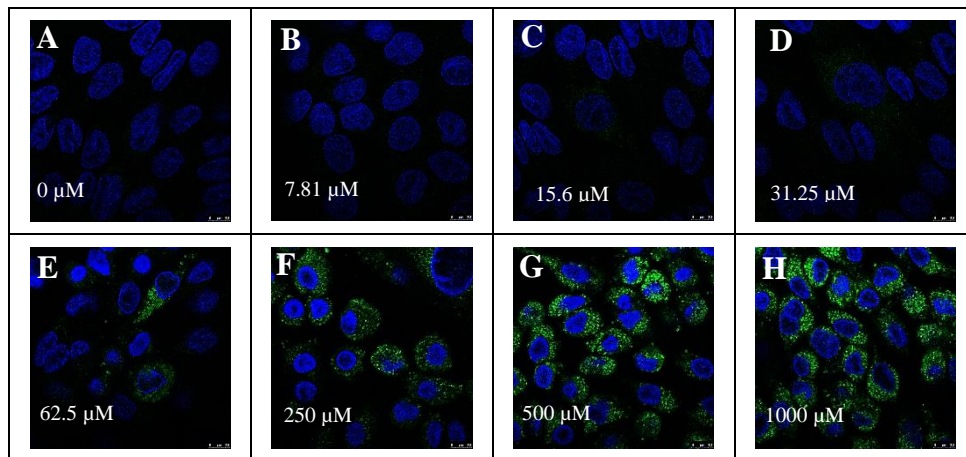
#### **4.1.2 Establishment of suitable *in vitro* assays linked to the AOP – *Receptor-mediated endocytosis and lysosomal overload***

To identify suitable *in vitro* endpoints for the individual AOPs and key events, published *in vitro* and *in vivo* findings were used to determine mechanism-based endpoints covering the individual key events of the AOPs. In addition to the published results, the publicly accessible Comparative Toxicogenomic Database (CTD) was also used. An analysis using the CTD showed an affiliation of LAMP-2 with gentamicin and cadmium chloride, which are also chemical stressors for the AOP – *Receptor-mediated endocytosis and lysosomal overload*. LAMP-2 is linked to the lysosomal pathway and kidney disease / acute kidney injury (see chapter 4.1.1).

Further analysis of CTD data on gentamicin, cadmium chloride and vancomycin revealed a common match for genes encoding for cathepsin A, cathepsin C, cathepsin D and cathepsin S, which are also associated with the lysosomal pathway, kidney disease and acute kidney injury (see chapter 4.1.1). Based on these findings, *in vitro* assays were established to address the individual key events.

**4.1.2.1 Polymyxins induced lysosomal associated membrane protein 1 / 2 (LAMP-1/2) expression in RPTEC/TERT1 and NRK-52E cells – *in vitro* assay for the key event Disturbance of lysosomal functions**

To detect the disturbance of lysosomal functions in the first key event in the AOP – *Receptor-mediated endocytosis and lysosomal overload* (Figure 6), LAMP-1/2 expression was determined as a potential *in vitro* endpoint. To detect the expression of LAMP-1/2 in untreated and treated cells, immunofluorescence of the stained LAMP-1/2 protein was measured after 24 h treatment with polymyxins in both RPTEC/TERT1 and NRK-52E cells. The results showed a significant concentration-dependent increase in LAMP-1/2 fluorescence in response to polymyxin B, colistin and polymyxin B nonapeptide treatment, with the lowest increase observed for polymyxin b nonapeptide (Figure 11 and Figure 16), consistent with its lower cytotoxicity as compared to polymyxin B and colistin (see chapter 4.1.2.3; Figure 16 (C)). The polymyxin B mediated increase of LAMP-1/2 immunofluorescence was consistently observed in both RPTEC/TERT1 (Figure 11) and NRK-52E cells (Figure 12).

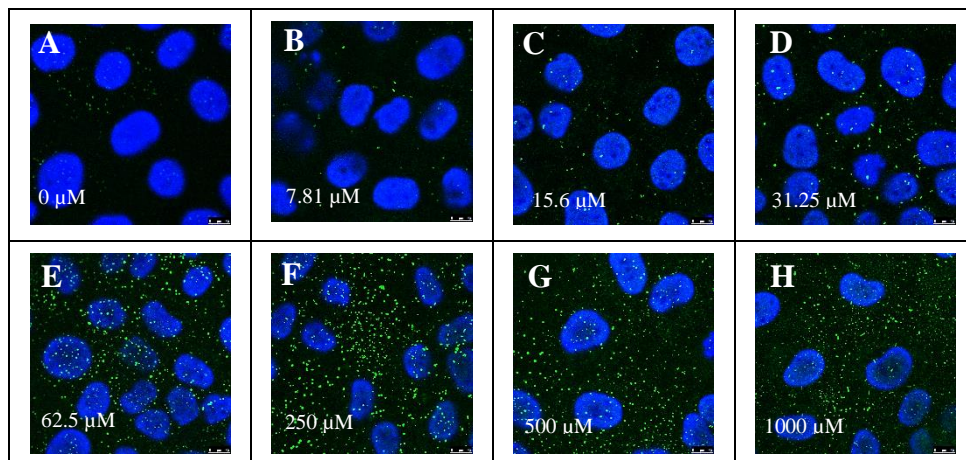


**Figure 11**

**Immunofluorescence images of LAMP-2 in RPTEC/TERT1 cells treated with polymyxin B for 24 h**

Cell nuclei were stained with DAPI (blue). Anti-LAMP-2 mouse monoclonal antibody coupled with Alexa-488 (green) was used to stain LAMP-2 in RPTEC/TERT1 cells and immunofluorescence was monitored by confocal laser microscopy. Untreated RPTEC/TERT1 cells showed poor LAMP-2 staining (A), while in treated cells a concentration-dependent increase in LAMP-2 staining in the cytosol was observed (B) – (H). Scale bar: 0.75  $\mu\text{m}$ .

Images were kindly acquired by Pia Reiser.



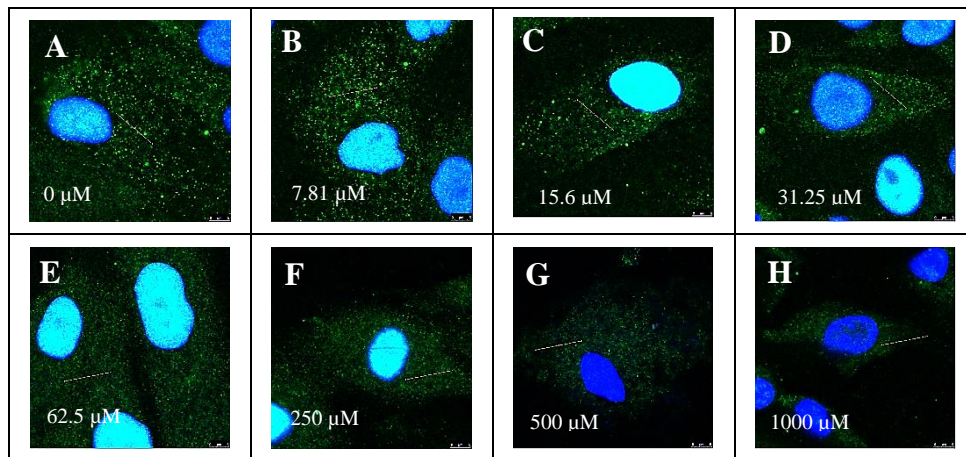
**Figure 12**

**Immunofluorescence images of LAMP-1 in NRK-52E cells treated with polymyxin B for 24 h**

Cell nuclei were stained with DAPI (blue). Anti-LAMP-1 mouse monoclonal antibody coupled with Alexa-488 (green) was used to stain LAMP-1 in NRK-52E cells and immunofluorescence was detected by confocal laser microscopy. Untreated NRK-52E cells showed poor LAMP-1 staining (A), while in treated cells a concentration-dependent increase in LAMP-1 staining was observed (B) – (H). Scale bar: 0.75  $\mu\text{m}$ . Images were kindly acquired by Pia Reiser.

**4.1.2.2 Cathepsin D release indicates ruptured lysosomes and release of lysosomal components after polymyxins treatment – in vitro assay for the key event Disruption of lysosomes**

The second key event in the AOP – *Receptor-mediated endocytosis and lysosomal overload* describes the *Disruption of the lysosomes* (Figure 6). As a potential *in vitro* endpoint, the release of cathepsin D into the cytoplasm was determined. To measure the release of cathepsin D from the lysosomes into the cytoplasm, cathepsin D was stained in both cell lines and fluorescence was measured.

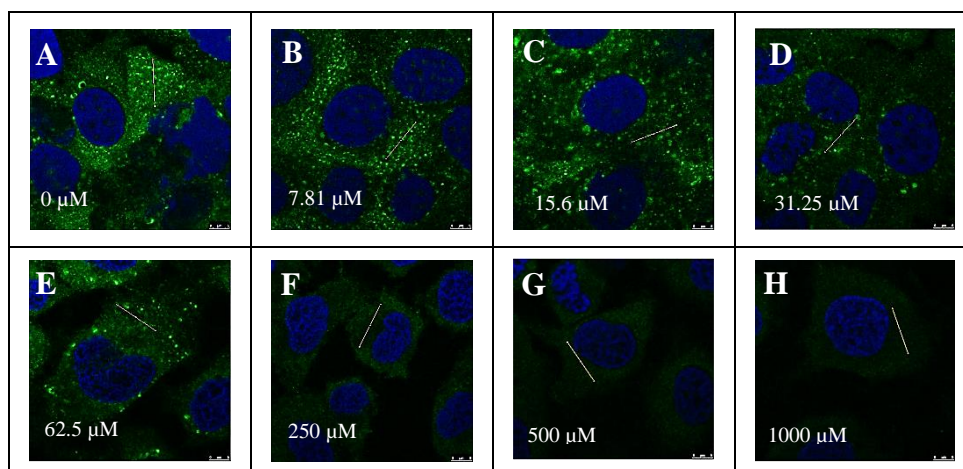


**Figure 13**

**Immunofluorescence images of cathepsin D in RPTEC/TERT1 cells treated with polymyxin B for 24 h**

Cell nuclei were stained with DAPI (blue). Anti-cathepsin D mouse monoclonal antibody coupled with Alexa-488 (green) was used to stain cathepsin D in RPTEC/TERT1 cells and immunofluorescence was detected by confocal laser microscopy. Cathepsin D staining in untreated RPTEC/TERT1 cells appeared in characteristic punctate structures throughout the cytosol, reflecting lysosomal localization (A). In contrast, RPTEC/TERT1 cells treated with polymyxin B showed a concentration-dependent re-distribution of cathepsin D staining indicative of leaky lysosomes and the release of cathepsin D into the cytosol (B) – (H). Scale bar: 0.5  $\mu$ m. Images were kindly acquired by Pia Reiser.

In intact lysosomes in healthy cells, Cathepsin D staining appeared as characteristic punctual structures within the cytoplasm, reflecting lysosomal localization (Figure 13 (A) for RPTEC/TERT1 cells and Figure 14 (A) for NRK-52E cells). In ruptured lysosomes, staining of cathepsin D appeared diffuse throughout the cytoplasm, indicating leaky and disrupted lysosomes with release of lysosomal components such as the stained cathepsin D into the cytoplasm (Figure 13 (B) – (H) for RPTEC/TERT1 cells and Figure 14 (B) – (H) for NRK-52E cells). The results showed a dose-dependent decrease of the fluorescence signal, indicating re-distribution of cathepsin D from the lysosomes into the cytoplasm in polymyxin B treated RPTEC/TERT1 and NRK-52E cells (Figure 13 and Figure 14).



**Figure 14**

**Immunofluorescence images of cathepsin D in NRK-52E cells treated with polymyxin B for 24 h**

Cell nuclei were stained with DAPI (blue). Anti-cathepsin D mouse monoclonal antibody coupled with Alexa-488 (green) was used to stain cathepsin D in NRK-52E cells and immunofluorescence was detected by confocal laser microscopy. Cathepsin D staining in untreated NRK-52E cells appeared in characteristic punctual structures throughout the cytosol, reflecting lysosomal localization (A). In contrast, NRK-52E cells treated with polymyxin B showed a concentration -dependent re-distribution of cathepsin D staining indicative of leaky lysosomes and the release of cathepsin D into the cytosol (B) – (H). Scale bar: 0.5  $\mu\text{m}$ . Images were kindly acquired by Pia Reiser.

#### 4.1.2.3 Polymyxins and CdCl<sub>2</sub> increased cytotoxicity in RPTEC/TERT1 & NRK-52E cells – *in vitro* assay for the key event Increase of cytotoxicity in renal tubule cells

Cytotoxicity of renal tubule cells was determined as the last and third key event (KE3 - *Increase in cytotoxicity in renal tubular cell*) in the AOP – *Receptor-mediated endocytosis and lysosomal overload* (Figure 6). Therefore, RPTEC/TERT1 and NRK-52E cells were treated for 24 h with polymyxins and CdCl<sub>2</sub> as model stressors for the AOP. Cytotoxic potential of stressors was measured after treatment using CellTiter-Glo® cell viability assay as a routine *in vitro* assay. Treatment for 24 h with stressors resulted in a concentration-dependent decrease in cell viability in both cell lines (Figure 15). It also revealed that the RPTEC/TERT1 cells were more sensitive against polymyxins than the NRK-52E cells, as the greatest decreases in cell viability, after treatment with polymyxin antibiotics, were observed in these cells (Figure 15).

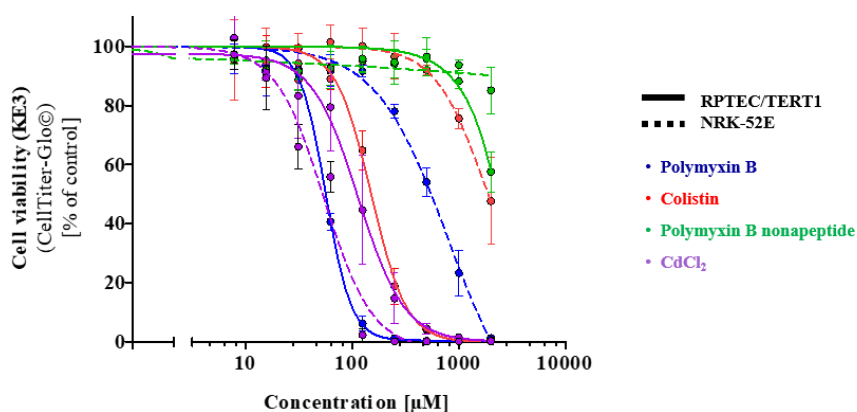


Figure 15

#### Cytotoxicity of RPTEC/TERT1 and NRK-52E cells after treatment with polymyxins and CdCl<sub>2</sub>

Results of both cell lines (RPTEC/TERT1 cells (—) and NRK-52E cells (---)) after 24 h of treatment with polymyxin antibiotics and cadmium chloride (polymyxin B, colistin, polymyxin B nonapeptide, CdCl<sub>2</sub>). The response of KE3 was plotted in percent of control against the logarithmic concentration in µM. All experiments were repeated in three technical replicates and three biological replicates. Data are presented as mean ± SD fold change (n = 3)



In addition to the difference in sensitivity between the two cell lines, a biological ranking of polymyxins among themselves was also measured, with polymyxin B showing the strongest cytotoxic potential, followed by colistin and PBNP. This biological ranking was also observed in both upstream key events ((KE1) Figure 16 (A) & (KE2) Figure 16 (B)) and is consistent with previously published studies in HK-2 cells (Keirstead *et al.*, 2013). Surprisingly, NRK-52E were slightly more sensitive to CdCl<sub>2</sub> treatment compared to RPTEC/TERT1 cells, with a strong concentration-dependent decrease in cell viability observed in both cell lines (Figure 15).

### 4.1.3 Dose-response *in vitro* results across all KEs in the AOP – Receptor mediated endocytosis and lysosomal overload

*In vitro* endpoints reflecting each KE were assessed in rat (NRK-52E (—)) and human renal proximal tubule epithelia cells (RPTEC/TERT1 (---)) and treated for 24 h with model compounds (polymyxin B, colistin, polymyxin B nonapeptide) in order to experimentally support the AOP and to establish quantitative relationships between KEs.

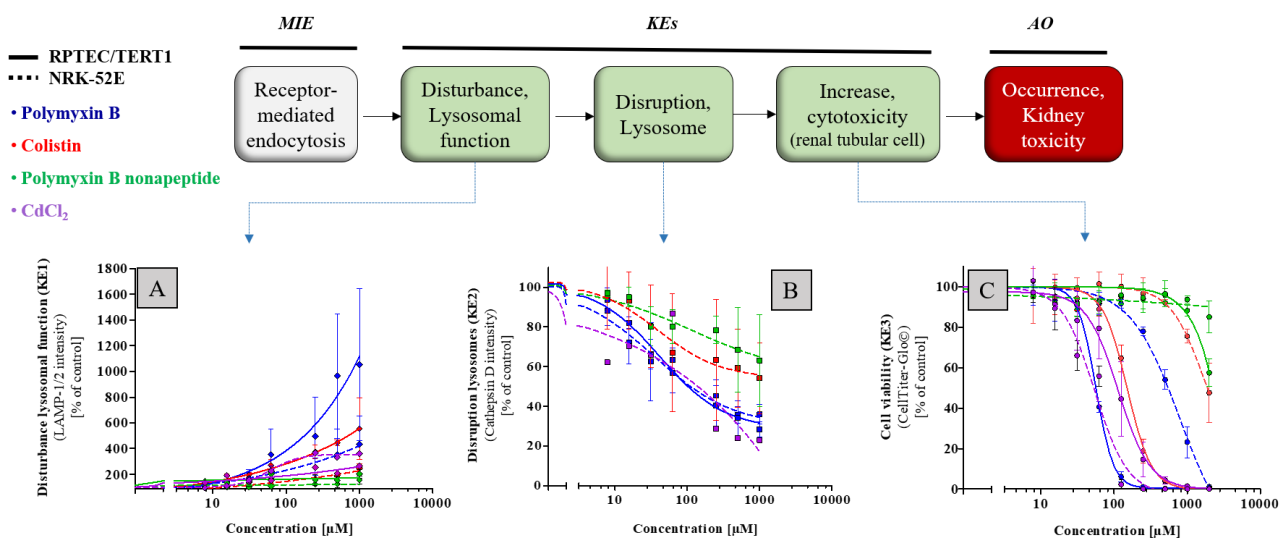


Figure 16

#### *In vitro* results for individual KEs from the AOP – Receptor-mediated endocytosis and lysosomal overload

Results of both cell lines (RPTEC/TERT1 cells (—) and NRK-52E cells (---)) after 24 h of treatment with polymyxin antibiotics and cadmium chloride (polymyxin B, colistin, polymyxin B nonapeptide, CdCl<sub>2</sub>) of individual KEs. (A) LAMP-1/2 intensity describes changes in KE1 (*Disturbance lysosomal function*). (B) cathepsin D intensity describes changes in KE2 (*Disruption of lysosomes*). (C) cell viability describes the change in KE3 (*Cytotoxicity in renal tubular cells*). The response of each KE was plotted in percent of control against the logarithmic concentration in μM. All experiments were repeated in three technical replicates and three biological replicates.

Data are presented as mean ± SD fold change (n = 3)

Data obtained for KE1 (LAMP-1/2 intensity – *Disturbance of lysosomal function*) showed a concentration-dependent increase in LAMP-1/2 intensity in both cell lines associated with an increase in LAMP-1/2 expression in treated RPTEC/TERT1 and NRK-52E cells. Compared to colistin-treated RPTEC/TERT1 cells, the polymyxin B-treated RPTEC/TERT1 cells showed a stronger increase in LAMP-2 intensity. Also, the results showed a higher increase in intensity in RPTEC/TERT1 cells compared to NRK-52E cells after polymyxin B treatment (Figure 16 (A)).

Analysis of KE2 (cathepsin D intensity - *Disruption of lysosomes*) revealed a concentration-dependent decrease in intensity in both cell lines (RPTEC/TERT1 and NRK-52E) after 24 h treatment with polymyxin B. However, no differences in the decrease in intensity between both cell lines were observed (Figure 16 (B)).

The differences between cell lines and between polymyxin antibiotics were most evident in KE3 (*Increase in cytotoxicity in renal tubular cell*). After 24 h treatment with polymyxin antibiotics, a concentration-dependent decrease in cell viability was observed in both cell lines. The strongest decrease in cell viability was observed in RPTEC/TERT1 cells after treatment with polymyxin antibiotics. Polymyxin B showed the strongest cytotoxic effect in both cell lines, followed by colistin and PBNP, which showed the lowest effect (Figure 16 (C)).

In general, RPTEC/TERT1 cells were found to be more sensitive to polymyxin antibiotics than NRK-52E cells, except for KE2 where no difference between the two cell lines was observed. Overall, the ranking of the biological response to the different polymyxin antibiotics was consistent across endpoints (polymyxin B > colistin > PBNP) (Figure 16 (A) – (C)). Interestingly, NRK-52E cells were more sensitive to treatment with CdCl<sub>2</sub> than RPTEC/TERT1 (Figure 16). Analysis of KE1 (*LAMP-1/2 intensity - Disturbance of lysosomal function*) showed a stronger

concentration-dependent increase in LAMP1/2 intensity for NRK-52E cells compared to RPTEC/TERT1 cells (Figure 16 (A)). A concentration-dependent decrease in cell viability was also evident for KE3 (*Increase in cytotoxicity in renal tubular cell*) after 24 h of treatment with CdCl<sub>2</sub>. Thereby, NRK-52E cells showed a greater decrease in cell viability than RPTEC/TERT1 cells (Figure 16 (C)).

#### **4.1.4 Investigation of intracellular polymyxin accumulation, endocytotic activity and relevant transporter expression in RPTEC/TERT1 and NRK-52E cells to gain an understanding of differences in sensitivity between both cell lines**

After treatment with the polymyxin antibiotics, differences in the sensitivity of both cell lines became evident (Figure 16). The RPTEC/TERT1 cells were found to be more sensitive in response to polymyxin antibiotics compared to NRK-52E cells, and also differences in the ranking of the biological response of the polymyxins were evident (Figure 16). This different sensitivity of the cell lines may be related to differential uptake and accumulation of polymyxins in the cells due to different endocytotic activity. To understand these differences in sensitivity between both cell lines, intracellular accumulation of test compounds was measured over time via LC-MS/MS after treatment with polymyxin B and colistin in both cells (Chapter 4.1.4.1). In addition, endocytotic activity was examined in both cell lines using an aprotinin assay (Chapter 4.1.4.2). Immunocytochemical localization of megalin was investigated in both cell lines (Chapter 4.1.4.3), and the expression of relevant transporters (megalin, cubilin) reported to be responsible for receptor-mediated endocytosis of polymyxins were examined at the mRNA respectively protein levels (Chapter 4.1.4.4 & 4.1.4.5).

#### 4.1.4.1 Intracellular compound accumulation of polymyxin B and colistin

After treatment with polymyxin antibiotics, RPTEC/TERT1 cells were found to be more sensitive to polymyxin antibiotics than NRK-52E cells (Figure 16). Furthermore, a ranking of the biological response was observed in both cell lines, especially in cytotoxicity (PB > Col. > PBNP) (Figure 16). In order to understand if the differences in polymyxin cytotoxicity between RPTEC/TERT1 and NRK-52 E cells may be due to differences in cellular uptake of the stressors, the intracellular concentrations of polymyxin B and colistin were measured in both cell lines via LC-MS/MS. The LC-MS/MS method was adapted from several methods (Jansson *et al.*, 2009, Ma *et al.*, 2008, Cheng *et al.*, 2010b) and modified and improved for chromatographic measurement for cell culture (*e.g.*, by vacuum concentration, purification and increasing the concentration of the analytes with SPE cartridges). Since both polymyxin antibiotics exhibit similar chemical structure and properties, colistin was used as the internal standard for polymyxin B, and polymyxin B was used as the internal standard for colistin. Calibration curves for polymyxin B and colistin are shown in Figure 17 and were linear across the concentration range (62.5 – 4000 nM) with a correlation coefficient  $R^2 = 0.9997$  for polymyxin B (Figure 17 (A)) and  $R^2 = 0.9992$  for colistin (Figure 17 (B)). Accuracy was expressed as the quotient of measured analyte concentration divided by nominal analyte concentration as relative error (RV in %) and precision as coefficient of variation (CV in %) (Table 24 and Table 25). The limit of detection (LOD) and limit of quantification (LOQ) was calculated by using the signal-to-noise ratio (S/N) method. A signal-to-noise ratio of three was used to estimate the LOD and a signal-to-noise ratio of ten was used to estimate the LOQ (Shrivastava and Gupta, 2011). The LOD was 15 nM and the LOQ was 50 nM for both polymyxin B and colistin.

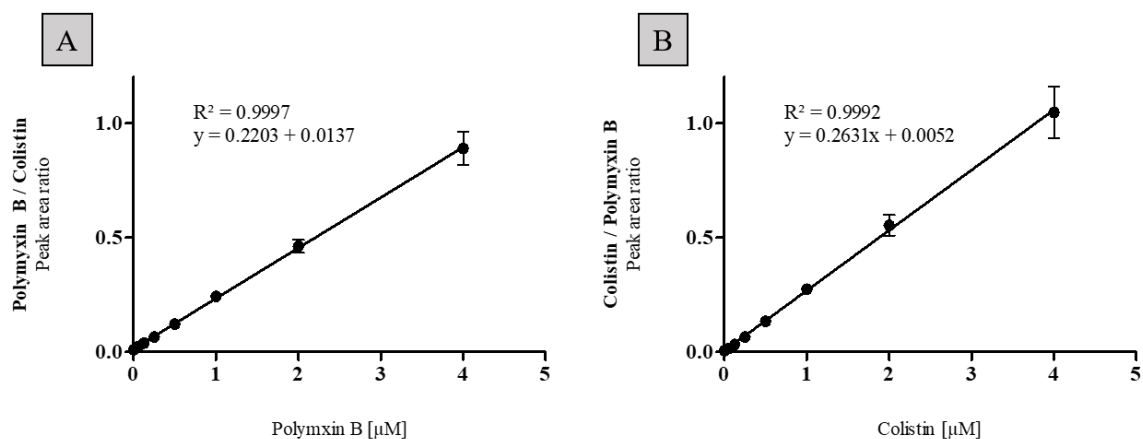


Figure 17

Standard curves for polymyxin B and colistin with the resulting straight-line equation and coefficient of determination

Table 24

Standard curve parameters for polymyxin B

Concentrations are given in µM, peak area for analyte and internal standard, calculated peak area ratio, calculated analyte concentration in µM, accuracy (relative error (RE)) and precision (coefficient of variation (CV)) in percentage

Concentration polymyxin B [µM]	Peak area polymyxin B	Peak area colistin (internal standard)	Peak area polymyxin B / colistin	Calculated polymyxin B concentration [µM]	RE [%]	CV [%]
0	6927	643450	0.01066998	-0.016	-	0.11
0.0625	22896	622625	0.038331386	0.051	81.6	2.24
0.125	35875	648900	0.058404606	0.113	90.4	3.31
0.25	67530	660425	0.107043246	0.238	95.2	0.66
0.5	135703	655575	0.212979746	0.486	97.2	1.07
1	265798	662625	0.426800797	1.032	103.2	1.18
2	250136	695275	0.348830233	2.019	100.9	2.45
4	497503	686050	0.672959306	3.943	98.6	7.58

**Table 25**  
**Standard curve parameters for colistin**

Concentrations are given in  $\mu\text{M}$ , peak area for analyte and internal standard, calculated peak area ratio, calculated analyte concentration in  $\mu\text{M}$ , accuracy (relative error (RE)) and precision (coefficient of variation (CV)) in percentage

Concentration colistin [ $\mu\text{M}$ ]	Peak area colistin	Peak area polymyxin B (internal standard)	Peak area colistin / polymyxin B	Calculated colistin concentration [ $\mu\text{M}$ ]	RE [%]	CV [%]
0	7466	1109250	0.006391589	0.023	-	0.47
0.0625	19413	1136717	0.016430338	0.061	97.6	0.09
0.125	39540	1135000	0.033228049	0.154	123.5	0.17
0.25	78152	1166717	0.066456352	0.231	92.5	0.92
0.5	152183	1115467	0.134173234	0.575	115.1	1.10
1	329533	1163800	0.274201024	1.329	133.0	0.84
2	665933	1163250	0.553404225	2.768	138.4	4.52
4	1253850	1180100	1.046116246	4.251	106.3	11.2

Example chromatograms of intracellular measured polymyxin stressors in RPTEC/TERT1 and NRK-52E cells are shown in Figure 18 & Figure 19. Each of these are chromatograms of the triply charged ions of polymyxin B2 and B1 and colistin A and B in RPTEC/TERT1 (Figure 18) and NRK-52E (Figure 19), respectively, after 24 h of treatment with 34  $\mu\text{M}$  polymyxin B and colistin, respectively. Polymyxin and colistin peaks were well separated from other peaks with  $m/z$  of 397.3/402.1 (polymyxin B) and 386.0/390.7 (colistin). Chromatograms of colistin peaks in NRK-52E cells showed more baseline noise (Figure 19 (C) and (D)) but could be well integrated in all measured samples. In Figure 20, polymyxin B1 peaks obtained from RPTEC/TERT1 and NRK-52E samples are shown to demonstrate the clear differences in peak area.

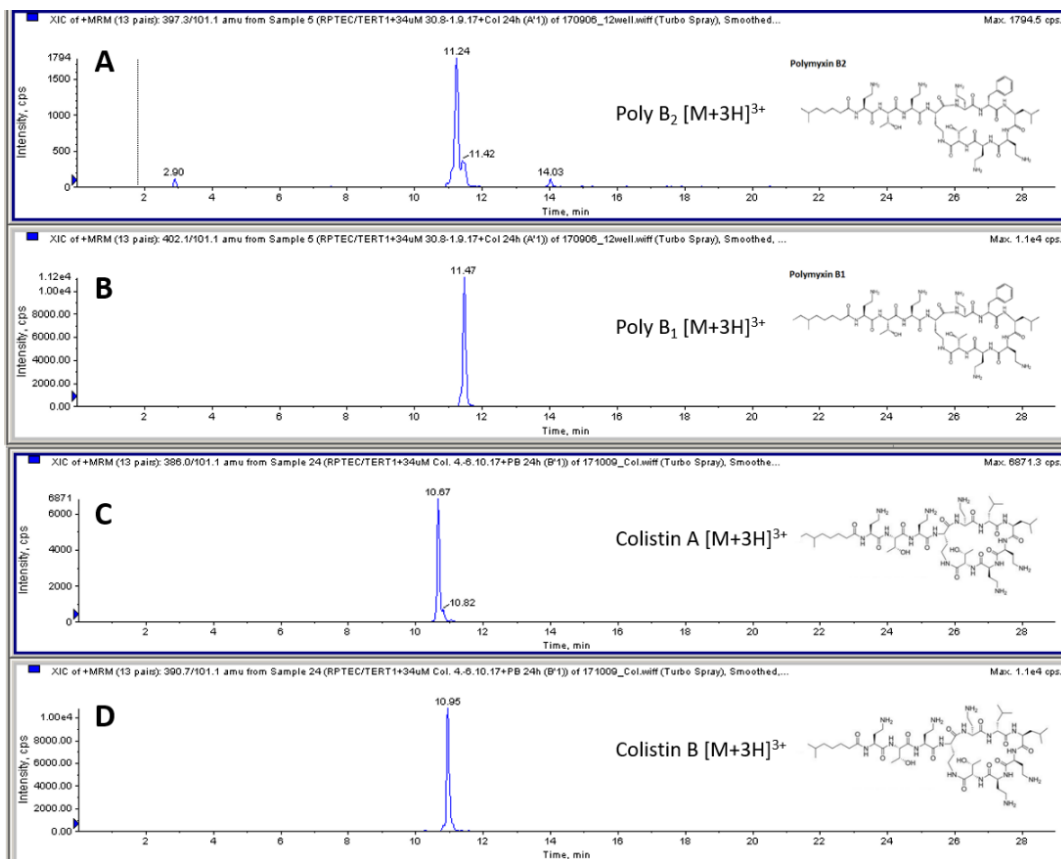


Figure 18

**Example chromatograms of intracellular polymyxin B<sub>2</sub> / B<sub>1</sub> and colistin A / B concentrations after 24 h treatment with polymyxin B respectively colistin in RPTEC/TERT1 cells**

Example chromatograms of intracellular triple charged ions [M+3H]<sup>3+</sup> of polymyxin B<sub>2</sub> (A) and B<sub>1</sub> (B) and colistin A (C) and B (D) in RPTEC/TERT1 cells after 24 h treatment with 34 μM polymyxin B respectively colistin. The X-axis shows the retention time in minutes and the Y-axis the intensity in counts per second (cps).



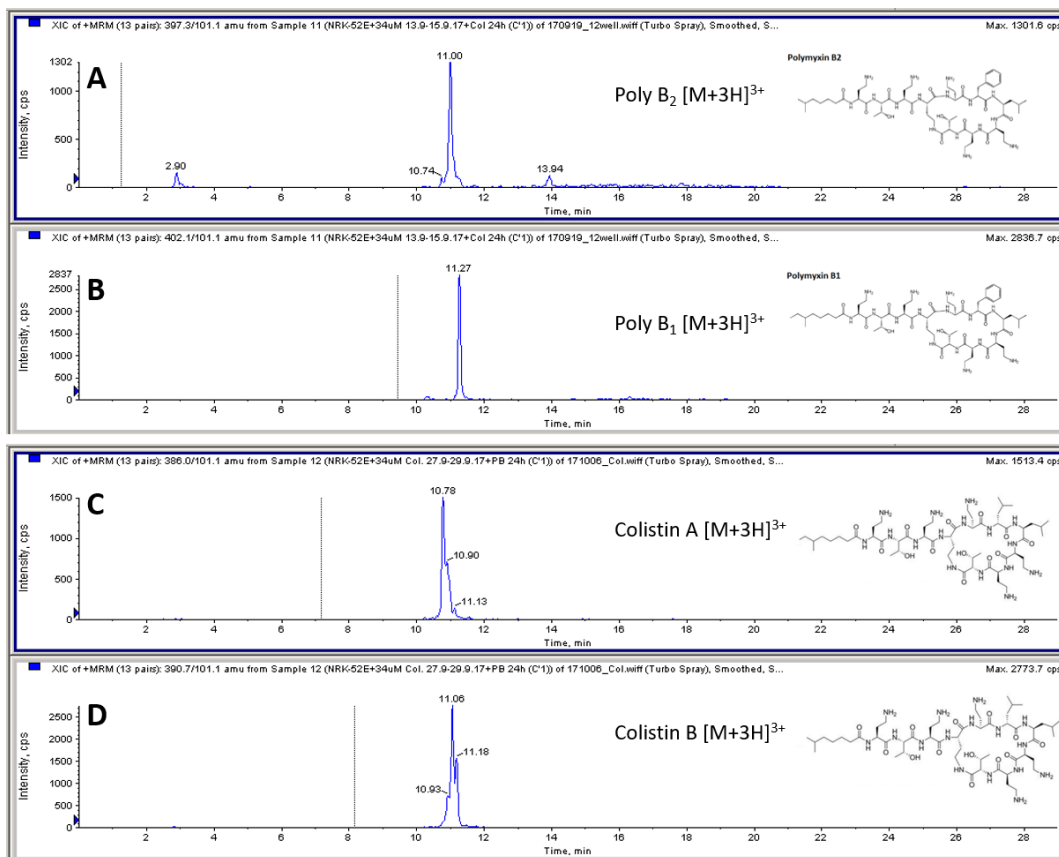
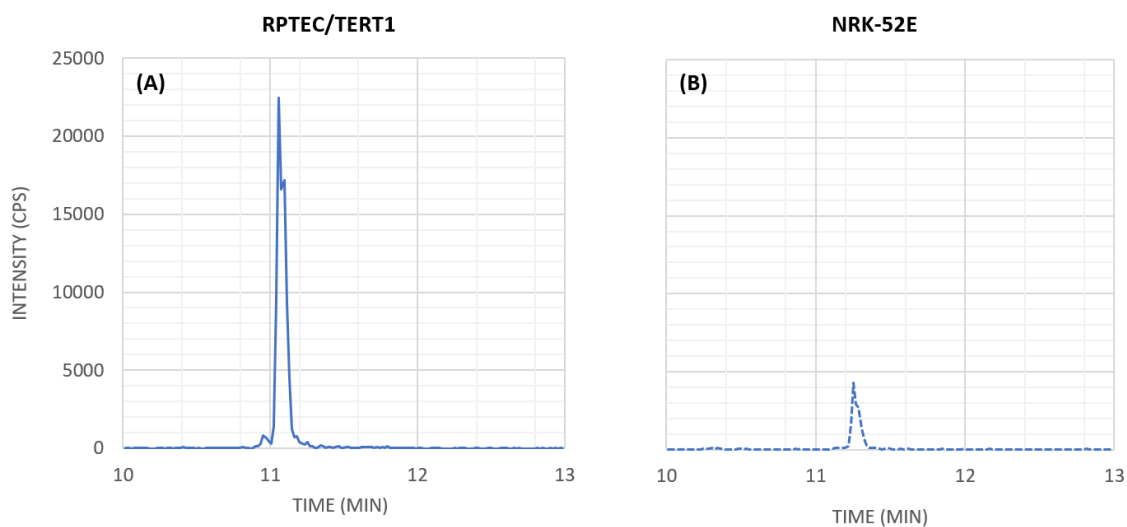


Figure 19

Example chromatograms of intracellular polymyxin B<sub>2</sub> / B<sub>1</sub> and colistin A / B concentrations after 24 h treatment with polymyxin B respectively colistin in NRK-52E cells

Example chromatograms of intracellular triple charged ions [M+3H]<sup>3+</sup> of polymyxin B<sub>2</sub> (A) and B<sub>1</sub> (B) and colistin A (C) and B (D) in NRK-52E cells after 24 h treatment with 34 μM polymyxin B respectively colistin. The X-axis shows the retention time in minutes and the Y-axis the intensity in counts per second (cps).



**Figure 20**

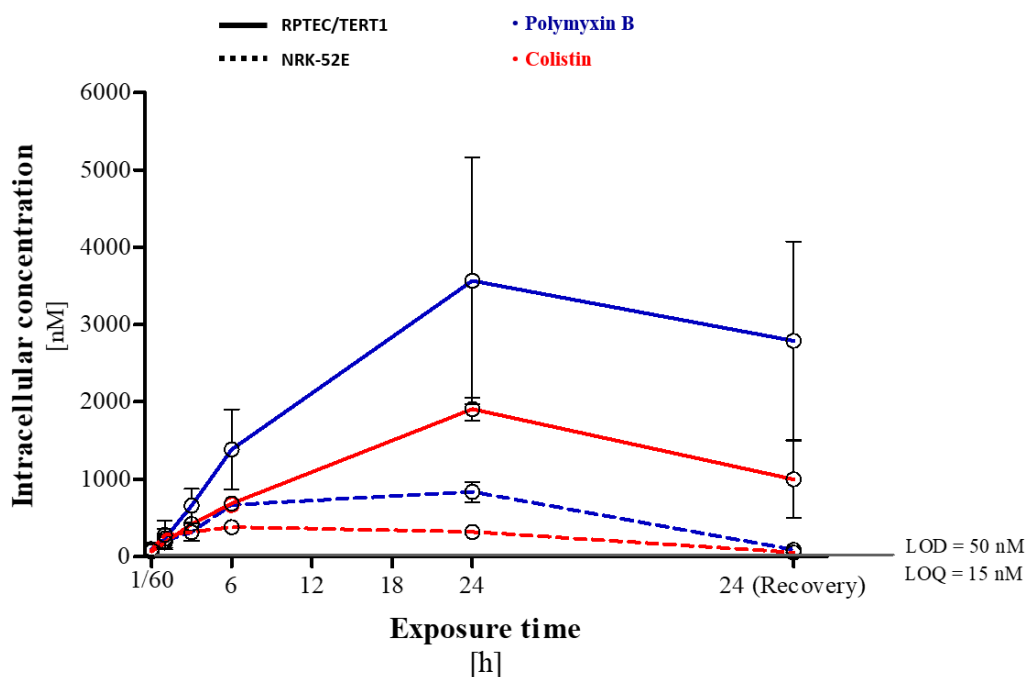
**Example chromatograms of intracellular polymyxin B<sub>1</sub> concentration after 24 h treatment with polymyxin B in RPTEC/TERT1 and NRK-52E cells**

Example chromatograms of intracellular triple charged polymyxin B<sub>1</sub> in (A) RPTEC/TERT1 (—) and (B) NRK-52E (---) after 24 h treatment with 34  $\mu$ M polymyxin B. The X-axis shows the retention time in minutes and the Y-axis the intensity in counts per second (cps).

Initial comparison of peak heights already suggested different intracellular polymyxin concentrations between both cell lines. These observations supported our suggestion of higher accumulations of polymyxins in the RPTEC/TERT1 cells as compared to NRK-52E cells.

To provide better quantitative information about the temporal accumulation in both cell lines, to investigate possible differences in accumulation of polymyxin B vs. colistin, and to support kinetic modeling, the intracellular concentration of polymyxin B and colistin was measured over time in both cell lines (Figure 21; Figure 22). Temporal measurement showed an increase in intracellular polymyxin B and colistin within 1 h in both cell lines. Significantly higher intracellular concentrations of both polymyxins were already observed after 6 hours in RPTEC/TERT1 cells compared to NRK-52E cells and were even more pronounced after 24 h

treatment (Figure 21; Figure 22). An accumulation of polymyxins after 24 h up to 3.5-fold higher than in NRK-52E was observed in the RPTEC/TERT1 cells. Following a 24-hour recovery phase, a slight decrease of both polymyxin concentrations were observed in RPTEC/TERT1 as well as in NRK-52E cells (Figure 21; Figure 22). These results support the assumption that the increased sensitivity of RPTEC/TERT1 cells is related to a higher intracellular concentration, respectively increased uptake of polymyxins in these cells as compared to NRK-52E cells.



**Figure 21**

**Time dependent increase in polymyxin B and colistin levels in RPTEC/TERT1 and NRK-52E cells**

The cells were treated for 1 min, 1 h, 3 h, 6 h, and 24 h followed by a 24 h recovery phase. Subsequently, the intracellular concentration was measured via LC-MS/MS. The intracellular concentrations of polymyxin B (blue) and colistin (red) in the RPTEC/TERT1 (—) and NRK-52E (---) cells respectively were plotted against time. All experiments were repeated in three technical replicates and three biological replicates. Data are presented as mean ± SD fold change (n = 3)

Also, differences between the intracellular concentrations of polymyxin B and colistin were notable. Polymyxin B accumulation was significantly higher in both cell lines compared with colistin. This effect was most pronounced after 24 h (Figure 21; Figure 22). The measured intracellular concentrations also correspond with the observed ranking of biological response to the different polymyxin antibiotics observed for the *in vitro* endpoints (polymyxin B > colistin) (Figure 16 (A) – (C)), as well as with published findings in HK-2 cells (Keirstead *et al.*, 2013).

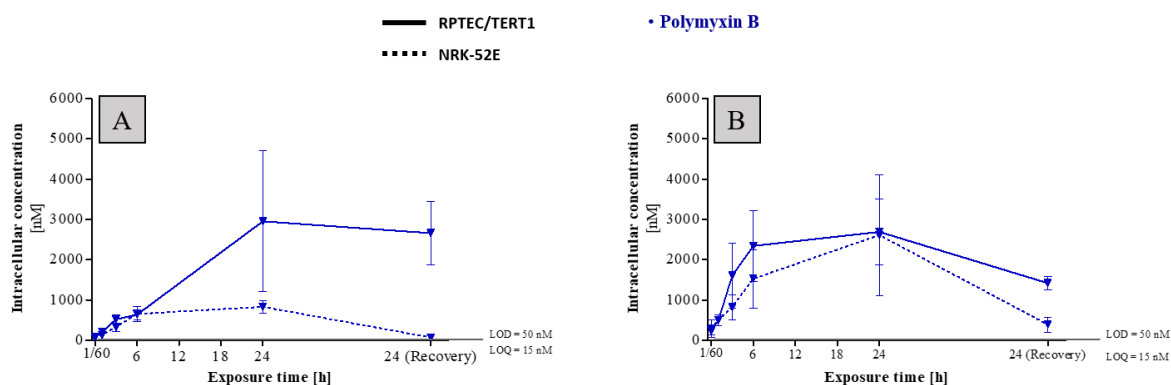


Figure 22

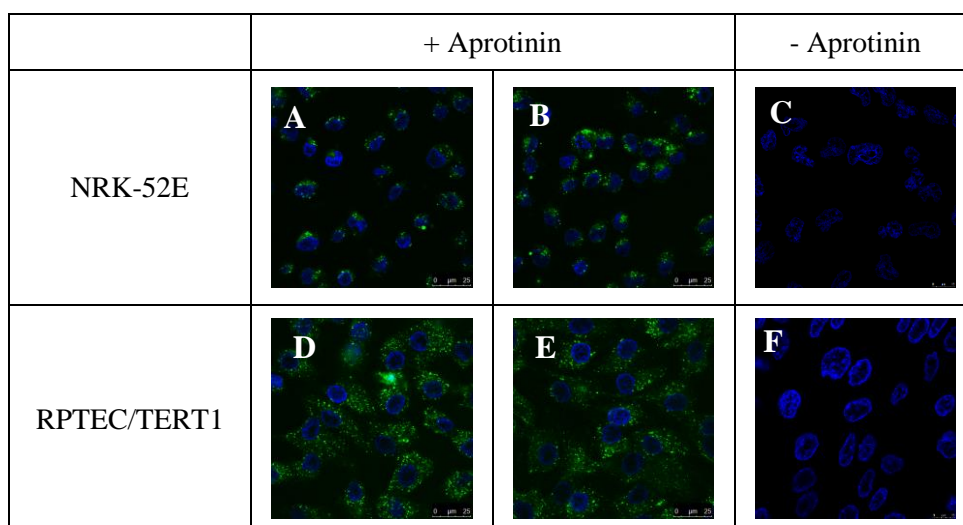
**Time dependent increase in polymyxin B levels in RPTEC/TERT1 and NRK-52E cells**

The cells were treated for 1 min, 1 h, 3 h, 6 h, and 24 h followed by a 24 h recovery phase with 62.5 μM (A) resp. 125 μM (B) polymyxin B. Subsequently, the intracellular concentration was measured via LC-MS/MS. The intracellular concentrations of polymyxin B (blue) in the RPTEC/TERT1 (—) and NRK-52E (---) cells respectively were plotted against time. All experiments were repeated in three technical replicates and three biological replicates. Data are presented as mean ± SD fold change (n = 3)

These results demonstrated a relationship between the accumulation of polymyxin antibiotics and the sensitivity of the cell lines. In order to investigate whether different endocytotic activities in the cells are responsible for the accumulation of polymyxin antibiotics, the endocytotic activity was subsequently examined using an aprotinin assay.

**4.1.4.2 Determination of aprotinin uptake to assess endocytic activity**

To understand if the marked differences in intracellular accumulation of polymyxin B and colistin between the two cell lines via LC-MS/MS may be due to differences in the endocytic activity of RPTEC-TERT1 vs. NRK-52 E cells, uptake of Alexa-488 labelled aprotinin was determined as a measure of endocytic activity.



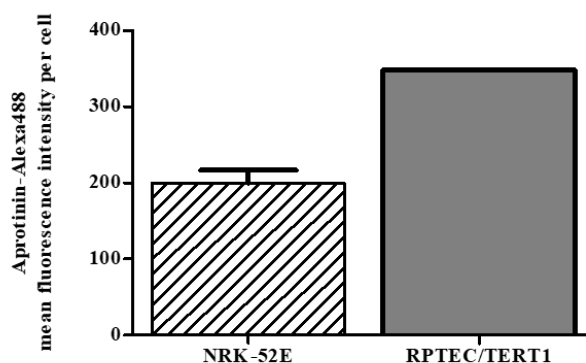
**Figure 23**

**Fluorescence images of both cell lines after 4 h incubation with Alexa-488 labeled aprotinin**

Images of NRK-52E cells (A – C) and images of RPTEC/TERT1 cells (D – F). Nuclei were stained with DAPI (blue), Alexa-488 labelled aprotinin (green) after 4 h incubation in both cell lines visible in cytoplasm (A, B, D, E). Figure C and F represent fluorescence images without treatment with Alexa-488 labeled aprotinin. Images were taken with a 63 x 1.4 oil UV objective. Scale bar: 25 µm

Aprotinin, a small bovine pancreatic trypsin inhibitor, also functions as a ligand for megalin. This natural polypeptide, which is labelled with the fluorescent dye Alexa-488, can be taken up into the cells via the megalin receptor and subsequently visualized using a confocal microscope. Both cell lines were treated with Alexa-488 labelled aprotinin for 4 h and fluorescence images were taken of the fixed cells (see chapter 3.10). After 4 hours of treatment with Alexa-488

labelled aprotinin, a fluorescence signal in the cytoplasm could be observed in both cell lines. Punctate staining reflecting lysosomal localization extended across the entire cytoplasm in both cell lines (Figure 23). To obtain quantitative data, the intensity of the fluorescence signal of the images was measured and related to the number of cells.



**Figure 24**

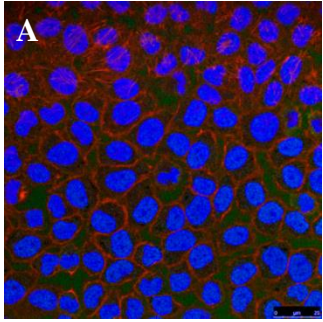
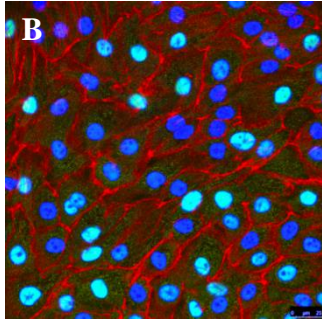
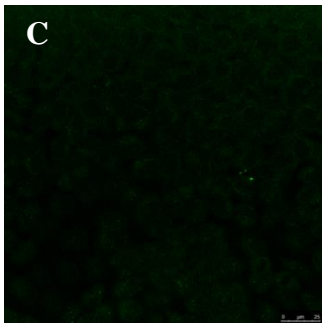
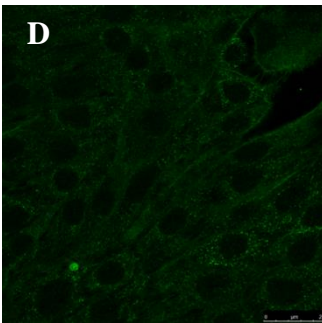
**Fluorescence intensity of Alexa-488 labelled aprotinin per number of nuclei in both cell lines**

All experiments were repeated in four technical replicates (n = 4 images per group) and three biological replicates. Data are presented as mean  $\pm$  SD fold change (n = 3)

Analysis of Alexa-488 intensity in both cell lines showed a clear distinction of intensity between NRK-52E and RPTEC/TERT1 cells. Alexa-488 intensity recorded in the RPTEC/TERT1 cells was nearly two times higher than in the NRK-52E cells after 4 hours of treatment (Figure 24). These findings are consistent with the intracellular substance accumulation determined by LC-MS (Figure 21) and the increased sensitivity of RPTEC/TERT1 cells to polymyxin antibiotics (Figure 16).

**4.1.4.3 Immunocytochemical localization of megalin in NRK-52E and RPTEC/TERT1**

In order to understand the different uptake of polymyxin antibiotics in the cell lines, we speculated that differential expression of the membrane transporter megalin in RPTEC/TERT1 vs. NRK-52E cells may play a role. Therefore, megalin was stained using immunofluorescence and images of the stained cells were taken using a confocal microscope in order to better understand the megalin expression and to study possible differences between the two cell lines. Surprisingly, a clear staining along the cell membrane was not observed (Figure 25).

Staining	NRK-52E	RPTEC/TERT1
<ul style="list-style-type: none"> <li>• DAPI (blue)</li> <li>• Megalin antibody with Alexa 488 (green)</li> <li>• Phalloidin with TRITC (red)</li> </ul>		
<ul style="list-style-type: none"> <li>• Megalin antibody with Alexa-488 (green)</li> </ul>		

**Figure 25**

**Immunocytochemical localization of megalin in both cell lines**

Cell nuclei were stained with DAPI (blue) and the cytoskeleton with TRITC (red). Anti-megalin mouse monoclonal antibody coupled with Alexa-488 (green) was used to stain megalin in both cell lines and viewed by confocal laser microscopy. (A) & (C) shows the images of the stained NRK-52E cells, (B) & (D) the images of the RPTEC/TERT1 cells. (A) & (B) are the merged images of the triple staining. (C) & (D) show the staining of megalin. Scale bar: 25  $\mu$ m

Instead, punctate staining was detected in both cell lines within the cytoplasm. This signal was more prominent and stronger in the RPTEC/TERT1 cells as compared to the NRK-52E cells (Figure 25). Considering the unexpected localization, no solid conclusion as to whether megalin expression in the RPTEC/TERT1 cells is increased could be drawn. To resolve this question, we therefore chose to investigate expression of megalin and cubilin at the mRNA level in both cell lines.

#### ***4.1.4.4 Expression levels of megalin and cubilin mRNA using TaqMan™ probes***

After localization of megalin in both cell lines, we investigate the expression of the transporters megalin and cubilin at mRNA level in order to determine possible differences between cell lines. In order to obtain further information on the mRNA expression of the transporters, in addition to the two cell lines used (RPTEC/TERT1 and NRK-52E), the mRNA expression of megalin and cubilin was also investigated in HK-2 and CaCo-2 cells as well as in kidney tissue of a control rat. Rat kidney also served as a positive control for the TaqMan™ assay. After the mRNA of the cells respectively rat kidney was isolated and transcribed into cDNA, the mRNA expression of megalin and cubilin was determined via qRT-PCR using TaqMan™ probes and the LightCycler® system.



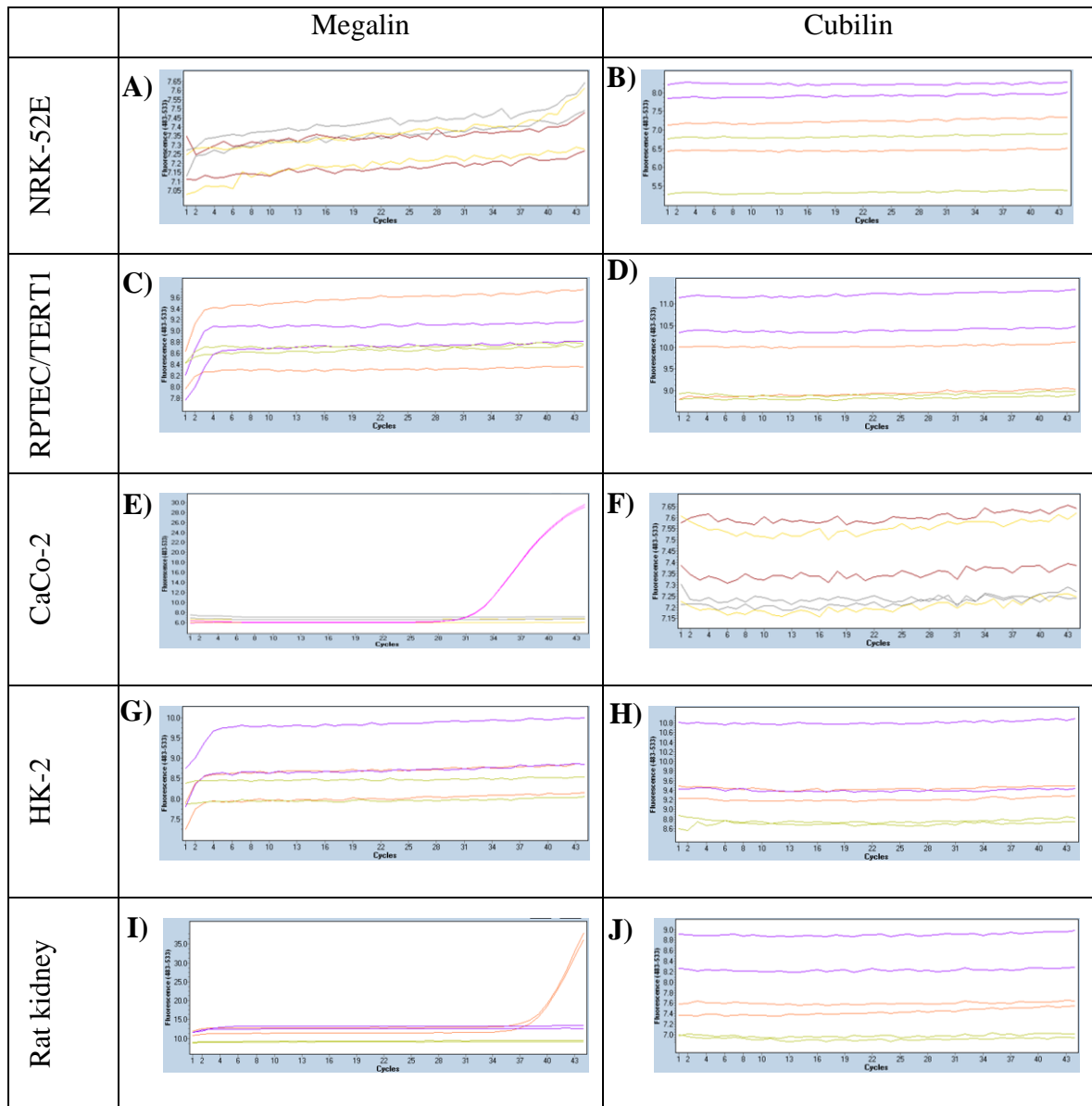


Figure 26

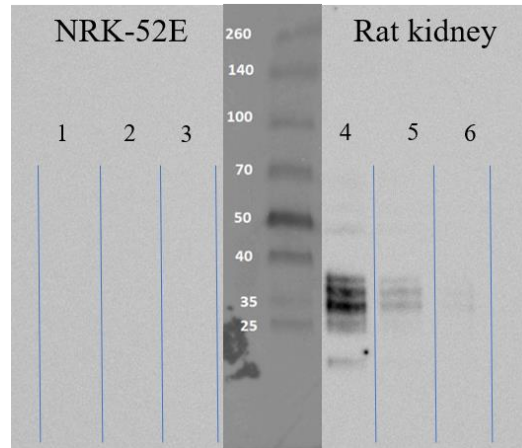
**mRNA expression results of megalin and cubilin in NRK-52E, RPTEC/TERT1, CaCo-2, HK-2, and rat kidney using TaqMan™ probes**

On the Y-axis the fluorescence intensity is plotted (483 - 533 nm) and on the X-axis the PCR cycles. The results of the CaCo-2 cells showed an increase in megalin mRNA (purple) while no increase was measured for the nRT (orange) and H<sub>2</sub>O control (green) (E). Rat kidney results also showed an increase in megalin mRNA (orange) and no increase was measured for nRT (grey) and H<sub>2</sub>O control (yellow) either (I). No increase in megalin mRNA was measured for NRK-52E (A), RPTEC/TERT1 (C), HK-2 (G) cells and no increase in cubilin mRNA was detected for all tested cell lines (B), (D), (F), (H), respectively rat kidney (J).

Analysis of megalin mRNA expression by TaqMan™ probes showed weak signals in rat kidney (Figure 26 (I)). Also, the expression of megalin in the CaCo-2 cells was detectable, but the increase was only visible after 32 cycles (Figure 26 (E)). Analysis of megalin mRNA expression in NRK-52E, RPTEC/TERT1, and HK-2 cells surprisingly showed no detectable megalin mRNA (Figure 26 (A), (C), (G)). Similarly, cubilin mRNA was not detected in any of the cell lines and in rat kidney (Figure 26 (B), (D), (F), (H), (J)).

#### ***4.1.4.5 Analysis of megalin transporter at protein level via Western Blot***

Since measurement at mRNA level failed to provide reliable results regarding the expression of megalin transporter (Figure 26), the expression was additionally examined at the protein level. A Western blot was performed with cell lysates obtained from NRK-52E cells and rat kidney. The rat kidney lysate was again used as a positive control. After the cell lysate of NRK-52E and rat kidney was isolated, the proteins were separated by SDS-PAGE and gradient gel electrophoresis, followed by protein transfer to a PVDF membrane. Megalin was detected using a mouse anti-megalin antibody (sc-515772, Santa Cruz, USA). Western blot analysis of the cell lysate of NRK-52E cells showed no bands for megalin in all three plotted protein concentrations (Figure 27 (1) - (3)). Analysis of the rat kidney lysate showed, after gradient gel separation, prominent bands in all three plotted protein concentrations between 35 and 40 kDa (Figure 27 (4) - (6)). However, no bands larger than 500 kDa were detected, which corresponds to the size of megalin.



**Figure 27**

**Western blot analysis of megalin in NRK-52E and rat kidney lysates**

Megalin were subjected to SDS-PAGE and the proteins were transferred to PVDF membrane. The left panel shows the cell lysate of NRK-52E cells (line 1: 25  $\mu$ g, line 2: 12.5  $\mu$ g, line 3: 6.15  $\mu$ g). The right panel shows the staining by the mouse anti-megalin antibody from the lysate of the rat kidney (line 4: 25  $\mu$ g, line 5: 12.5  $\mu$ g, line 6: 6.15  $\mu$ g). No bands could be detected in the NRK-52E cell lysate, while three prominent bands between 35 and 40 kDa were detected in the rat kidney lysate. Molecular weight marker is displayed in the center

After investigations at the mRNA and protein level resulted in no clear evidence of expression of megalin and cubilin in the cell lines, expression of transporters seems to be potentially down-regulated in the cells. However, since polymyxin B and colistin had been measured in the cells with increasing concentrations over time (Figure 21), alternative mechanisms might be responsible for the cellular uptake. In addition to receptor-mediated endocytosis via the megalin:cubilin complex, nonspecific fluid phase endocytosis and uptake via PEPT2 transporters could also play an important role (Ma *et al.*, 2009, Lu *et al.*, 2015, Zavascki and Nation, 2017, Schuh *et al.*, 2018). Since the megalin receptor is mainly expressed in the first two segments (S1 and S2) of the proximal tubule (Schuh *et al.*, 2018, Eshbach and Weisz, 2017, Christensen *et al.*, 2012), it might be important to consider from which segment of the proximal tubule the cells were obtained, possibly explaining different megalin expression.

#### **4.1.5 Prediction of colistin, polymyxin B nonapeptide and cadmium chloride downstream key events based on polymyxin B *in vitro* data**

After suitable *in vitro* assays were established and cells were treated with model stressors, the aim was to test whether the data obtained from the *in vitro* assays after polymyxin B treatment could be used to generate key event relationships (KERs). The next step was to verify whether these relationships could be used to predict downstream key events for other stressors associated with the same AOP. Therefore, data from KE1 after colistin, PBNP and CdCl<sub>2</sub> treatment were used.

##### **4.1.5.1 Calculation of additional data points from experimental data**

One way to establish quantitative relationship between the key events (the relationship between a KE<sub>up</sub> and a KE<sub>down</sub> event) and thus improve quantitative understanding is to generate response-response plots. This allows the key event relationships to be captured by simple mathematical equations. However, the basic prerequisite for generating response-response plots is an adequate amount of data from the experimental *in vitro* assays collected and the same chemical concentrations of the test substances used in the assays. In order to fulfill these requirements, additional data points were calculated from the obtained *in vitro* experiments after polymyxin B treatment in RPTEC/TERT1 and NRK-52E cells. Using the online tool PROAST web (<https://proastweb.rivm.nl/>), the best-fit function was determined and the regression equation with the corresponding data was displayed in GraphPad Prism 5.01. With the mathematical equations obtained (Table 26 and Table 27), 400 additional data points in a concentration range between 5 µM and 2000 µM were computed in 5 µM steps and graphically plotted using GraphPad Prism 5.01. (Figure 28 (D) – (F) and Figure 29 (D) – (F)).

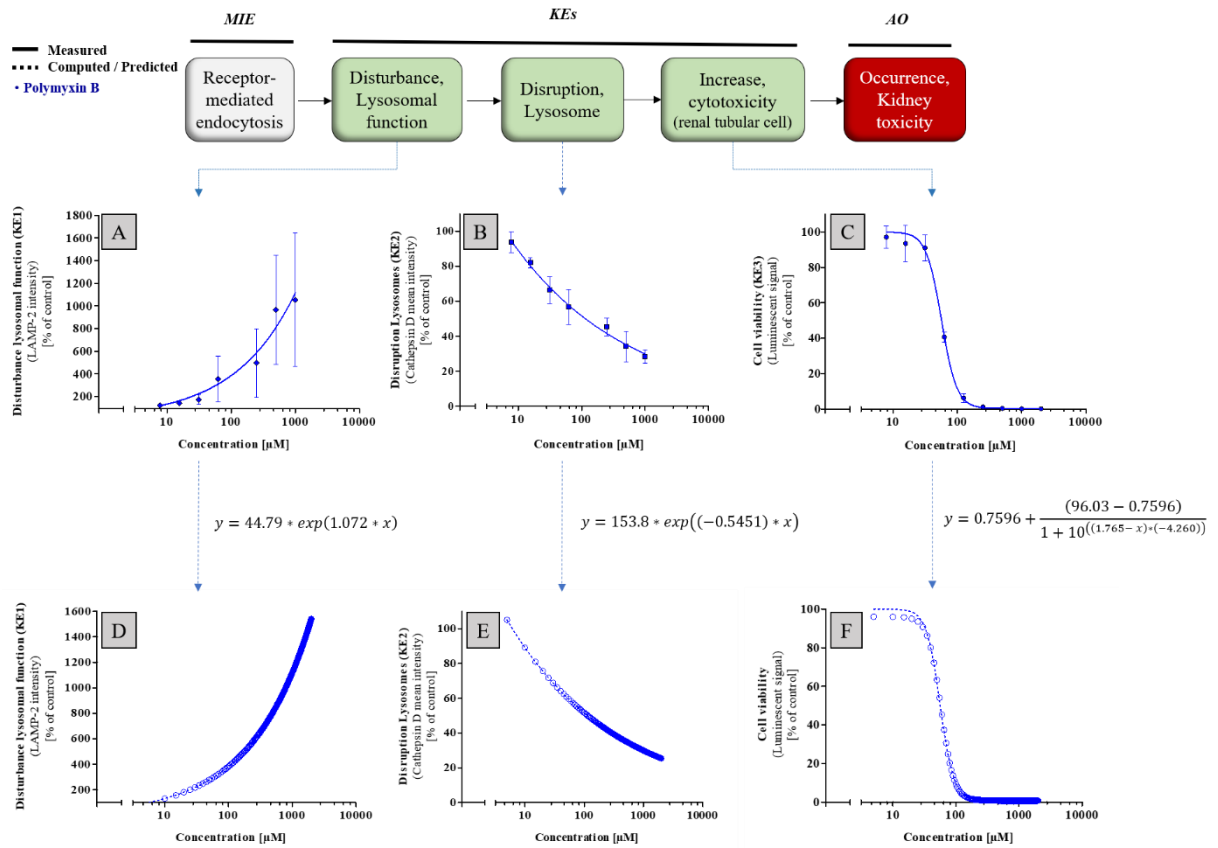


Figure 28

**Calculation of additional data points from the experimentally obtained *in vitro* data after polymyxin B treatment in RPTEC/TERT1 cells**

(A) *in vitro* results from KE1 (LAMP-2 intensity), (B) *in vitro* results from KE2 (cathepsin D intensity), (C) *in vitro* results for KE3 (cell viability), (D) computed data points from the obtained mathematical equation for KE1 (LAMP-2 intensity), (E) computed data points from the obtained mathematical equation for KE2 (cathepsin D intensity), (F) computed data points from the obtained mathematical equation for KE3 (cell viability)

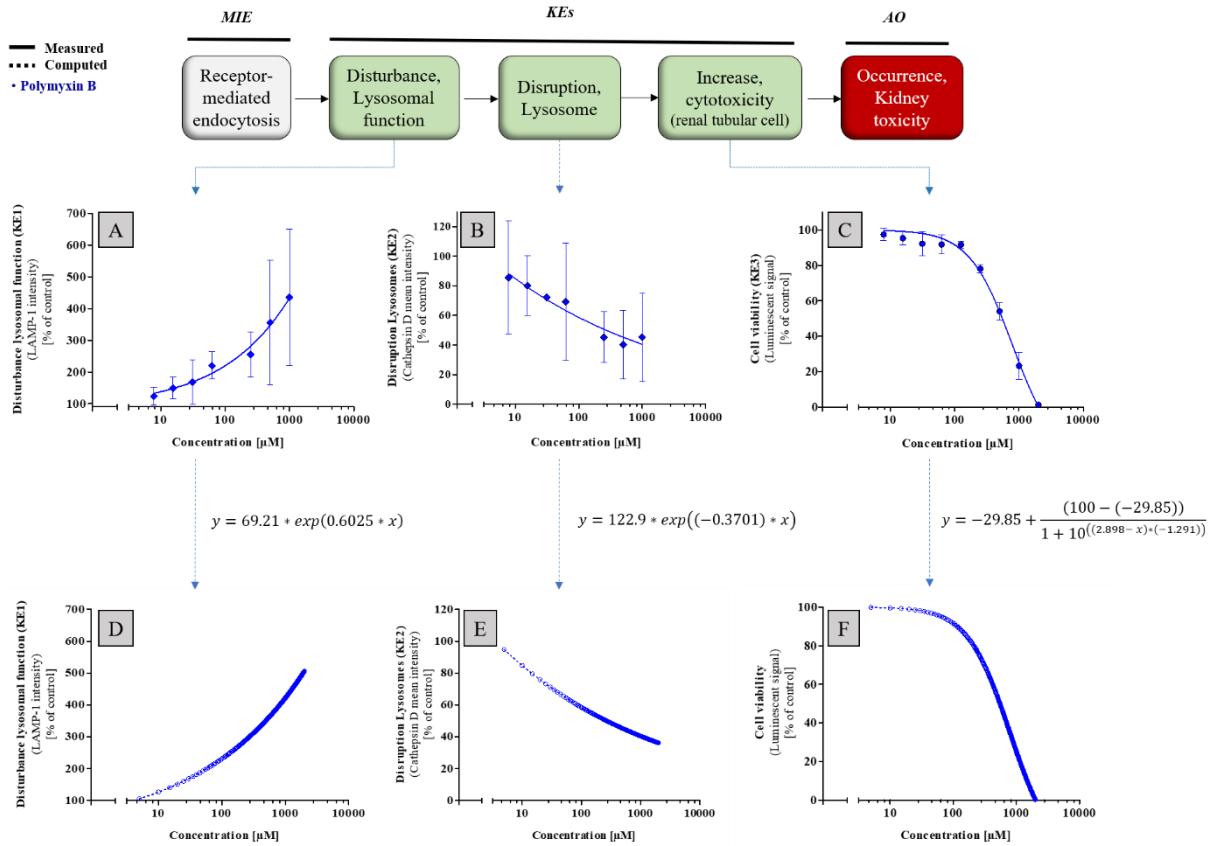


Figure 29

**Calculation of additional data points from the experimentally obtained *in vitro* data after polymyxin B treatment in NRK-52E cells**

(A) *in vitro* results from KE1 (LAMP-1 intensity), (B) *in vitro* results from KE2 (cathepsin D intensity), (C) *in vitro* results for KE3 (cell viability), (D) computed data points from the obtained mathematical equation for KE1 (LAMP-2 intensity), (E) computed data points from the obtained mathematical equation for KE2 (cathepsin D intensity), (F) computed data points from the obtained mathematical equation for KE3 (cell viability)

Table 26

Mathematical equation obtained from *in vitro* experiments in RPTEC/TERT1 cells for the computation of additional data points

Key event	Mathematical equation
KE1 (LAMP-2 intensity)	$y = 44.79 * \exp(1.072 * x)$
KE2 (cathepsin D intensity)	$y = 153.8 * \exp(-0.5451 * x)$
KE3 (cell viability)	$y = 0.7596 + \frac{95.2704}{1 + 10^{((1.765-x)*(-4.260))}}$

Table 27

Mathematical equation obtained from *in vitro* experiments in NRK-52E cells for the computation of additional data points

Key event	Mathematical equation
KE1 (LAMP-1 intensity)	$y = 69.21 * \exp(0.6025 * x)$
KE2 (cathepsin D intensity)	$y = 122.9 * \exp(-0.3701 * x)$
KE3 (cell viability)	$y = -29.85 + \frac{129.85}{1 + 10^{((2.898-x)*(-1.291))}}$

#### **4.1.5.2 Generating response-response plots from polymyxin B data to establish quantitative relationship between KEs**

As described above, a method to better understand the quantitative understanding of an AOP and the quantitative relationship between the KEs (KER), is the generation of response-response plots for each KER within the AOP. The relationship between the individual key events described using the regression equation obtained from the response-response plots can then provide information on how much change in an upstream KE ( $KE_{up}$ ) is needed to trigger a change in a downstream KE ( $KE_{down}$ ).

Using the case study of the AOP for *Receptor-mediated endocytosis and lysosomal overload*, response-response plots were generated using the additional computed data points from the individual *in vitro* assays for the respective key events. Thus, response-response plots were generated for disruption of lysosomes (KE2 - cathepsin D intensity) as a function of disturbance of lysosomal function (KE1 – LAMP-1/2 intensity) ( $qKER_1$ ) (Figure 30 (D) and Figure 31 (D)) and for cell viability (KE3 - cytotoxicity of renal tubular cell) as a function of disruption of lysosomes (KE2 - cathepsin D intensity) ( $qKER_2$ ) (Figure 30 (E) and Figure 31 (E)). After generating the individual response-response plots, the online application PROAST web was used to determine the best-fit function. The data were then plotted in GraphPad Prism 5.01 and the mathematical equation of the response-response curves description were generated (Table 28 and Table 29).



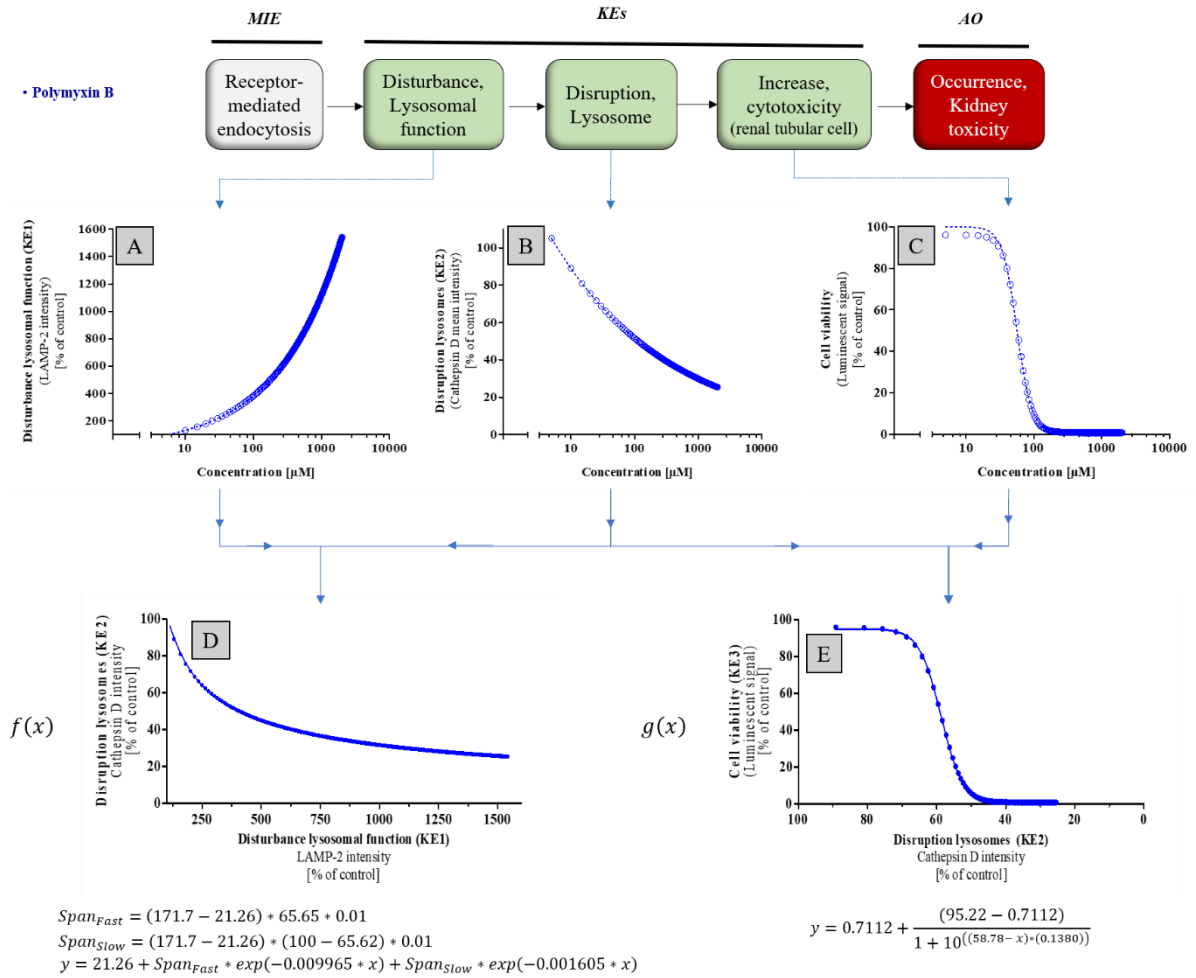


Figure 30

**Response-response plots obtained from polymyxin B KE data in RPTEC/TERT1 cells**

The KE2 – *Disruption of lysosomes* (KE2 - cathepsin D intensity) (B) was plotted as a function of KE1 – *Disturbance of lysosomal function* (KE1 – LAMP-2 intensity) (A). The resulting response-response function is described with the corresponding mathematical equation and shows the quantitative relationship between KE1 and KE2 (D). KE3 – *Cell viability* (KE3 – increase cytotoxicity of renal tubule cell) (C) was plotted as a function of KE2 – *Disruption of lysosomes* (KE2 – cathepsin D intensity) (B). The resulting response-response function with its mathematical description and the quantitative relationship between KE2 and KE3 is shown below (E)

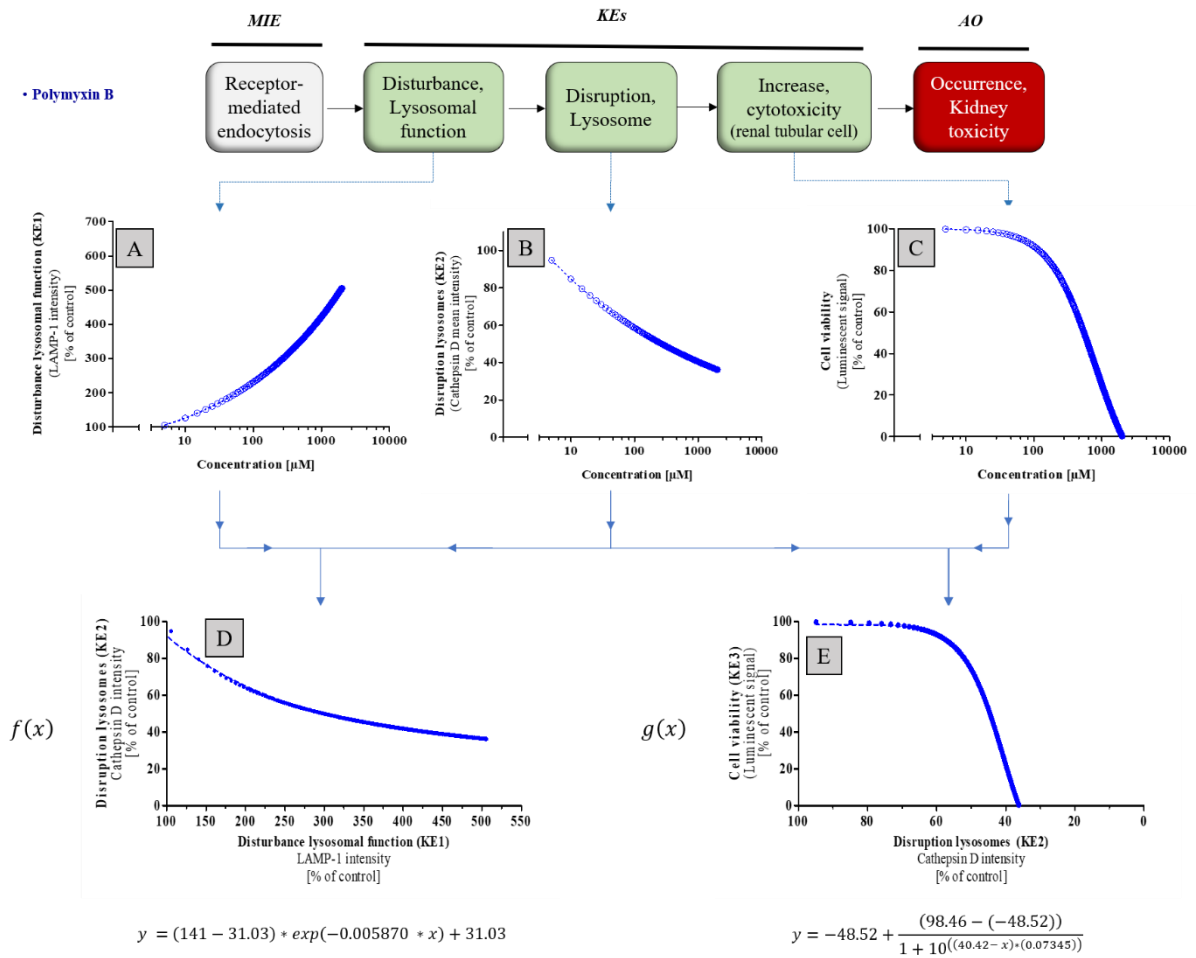


Figure 31

**Response-response plots obtained from polymyxin B KE data in NRK-52E cells**

The KE2 – *Disruption of lysosomes* (KE2 - cathepsin D intensity) (B) was plotted as a function of the KE1 – *Disturbance of lysosomal function* (KE1 – LAMP-1 intensity) (A). The resulting response-response function is described with the corresponding mathematical equation and shows the quantitative relationship between KE1 and KE2 (D). KE3 – *Cell viability* (KE3 – increase cytotoxicity of renal tubule cell) (C) was plotted as a function of the KE2 – *Disruption of lysosomes* (KE2 – cathepsin D intensity) (B). The resulting response-response function with its mathematical description and the quantitative relationship between KE2 and KE3 is shown below

(E)

**Table 28**

**Mathematical equation obtained from response-response plots describing quantitative relationship between KEs in RPTEC/TERT1 cells after polymyxin B treatment**

<b>Key event relationship</b>	<b>Mathematical equation</b>
qKER <sub>1</sub> : KE <sub>1</sub> → KE <sub>2</sub>	$y = 21.26 + 98.77 * \exp(-0.009965 * x) + 51.72 * \exp(-0.001605 * x)$
qKER <sub>2</sub> : KE <sub>2</sub> → KE <sub>3</sub>	$y = 0.7112 + \frac{94.51}{1 + 10^{((58.78 - x) * (0.1380))}}$

**Table 29**

**Mathematical equation obtained from response-response plots describing quantitative relationship between KEs in NRK-52E cells after polymyxin B treatment**

<b>Key event relationship</b>	<b>Mathematical equation</b>
qKER <sub>1</sub> : KE <sub>1</sub> → KE <sub>2</sub>	$y = 109.97 * \exp(-0.005870 * x) + 31.03$
qKER <sub>2</sub> : KE <sub>2</sub> → KE <sub>3</sub>	$y = -48.52 + \frac{146,98}{1 + 10^{((40.42 - x) * (0.07345))}}$

#### **4.1.5.3 Prediction of colistin, PBNP and CdCl<sub>2</sub> cytotoxicity in RPTEC/TERT1 and NRK-52E cells using response-response relationships obtained from polymyxin B data**

The obtained response-response relationships were then used to predict cytotoxicity as a late KE (KE<sub>down</sub>) based on measurement of an early KE. The experimentally determined upstream KE (KE<sub>up</sub>) (KE1 – *Disturbance of lysosomal function*) after treatment with colistin, PBNP and CdCl<sub>2</sub> in RPTEC/TERT1 and NRK-52E cells was used as a starting point for the prediction (Figure 32 (A) and Figure 33 (A)). In the first step, additional data points were calculated from the *in vitro* assay results as already described in the chapter above. The best-fit function was determined using the PROAST web tool and 400 additional data points in a concentration range between 5 µM and 2000 µM were computed using the mathematical formula obtained (Table 30 and Table 31). This dataset of 400 data points was then calculated with the mathematical description of the KER1 (Figure 32 (F) and Figure 33 (G)), which was previously generated based on the polymyxin B data in order to predict the response in the KE2 for colistin, PBNP and CdCl<sub>2</sub> treated cells. The predicted data obtained for KE2 (Figure 32 (D) and Figure 33 (E)) were used to predict the response in KE3 (Figure 32 (E) and Figure 33 (F)) using the mathematical description of KER2 (Figure 32 (G) and Figure 33 (H)).

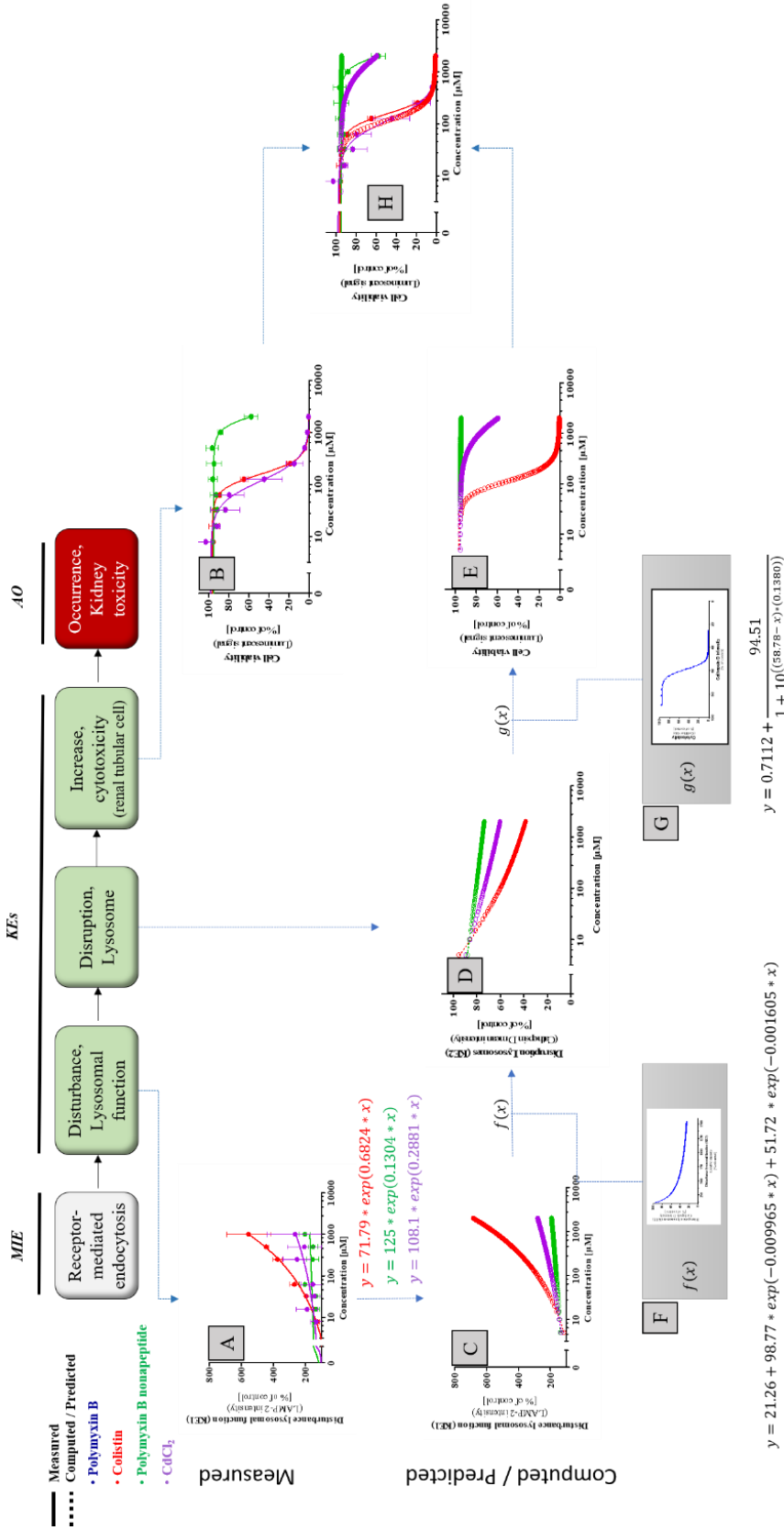
Compared to the measured cytotoxicity after colistin treatment in RPTEC/TERT1 cells, the predicted cytotoxicity of colistin was quite close and reflected the measured dose-response curve nearly identically (Figure 32 (H)). The predicted cytotoxicity after PBNP treatment in the RPTEC/TERT1 cells showed no decrease in cell viability in the concentration range between 0 µM to 1000 µM (Figure 32 (E) and (H)) and hence agreed with the lack of cytotoxicity observed in the *in vitro* assay (Figure 32 (B) and (H)). However, only for the highest tested concentration (2000 µM) a decrease in cell viability was measured in the RPTEC/TERT1 cells (Figure 32 (B)) which was not predicted via key event relationships (Figure 32 (E) and (H)). In contrast to

the nearly consistent predictions of polymyxin antibiotics, the prediction of cytotoxicity after CdCl<sub>2</sub> treatment was inconsistent with the real cytotoxicity that was observed in RPTEC/TERT1 cells (Figure 32 (H)). The *in vitro* results obtained for KE3 (*Increase cytotoxicity of renal tubule cell*) after CdCl<sub>2</sub> treatment showed a concentration-dependent decrease in cell viability beginning at a CdCl<sub>2</sub> concentration of 31.25 μM that decreased to 0 % at a CdCl<sub>2</sub> concentration of 500 μM (Figure 32 (B)). However, prediction of cell viability via key event relationships showed an increase in cytotoxicity in RPTEC/TERT1 cells only in the concentration range above approximately 500 μM (Figure 32 (E) and (H)). Thus, the overall prediction of cytotoxicity after CdCl<sub>2</sub> treatment in RPTEC/TERT1 cells was poor, suggesting lower cytotoxicity than that actually measured (Figure 32 (H)).

Table 30

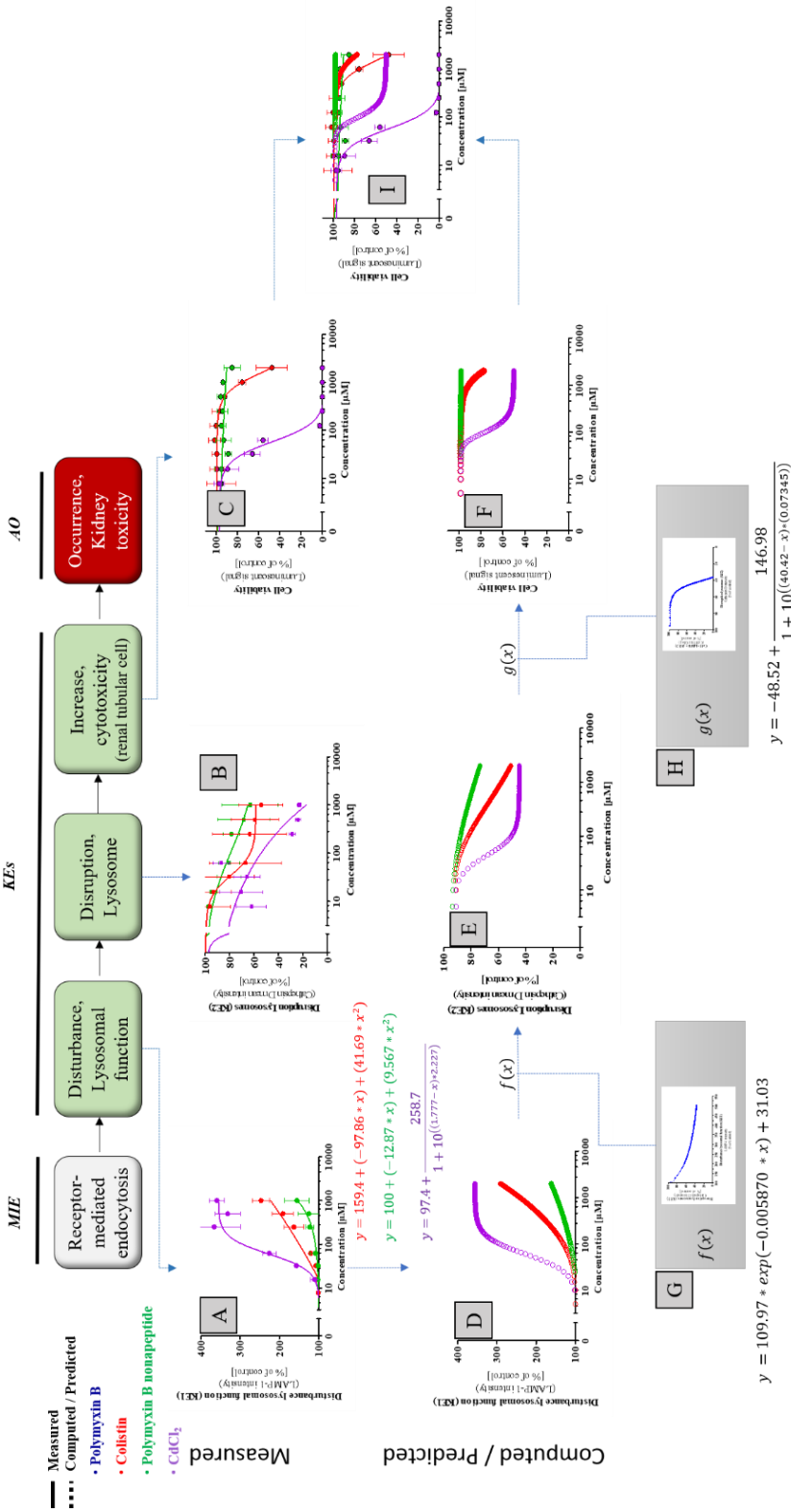
Mathematical equation obtained from *in vitro* experiment for KE1 in RPTEC/TERT1 for the computation of additional data points

Key event	Mathematical equation
KE <sub>1</sub> (LAMP-2 intensity) (colistin)	$y = 71.79 * \exp(0.6824 * x)$
KE <sub>1</sub> (LAMP-2 intensity) (PBNP)	$y = 125 * \exp(0.1304 * x)$
KE <sub>1</sub> (LAMP-2 intensity) (CdCl <sub>2</sub> )	$y = 108.1 * \exp(0.2881 * x)$



**Figure 32**  
**RPTEC/TERT1**  
**Prediction of colistin, polymyxin B nonapeptide and CdCl<sub>2</sub> cytotoxicity using response-response relationships based on polymyxin B data in**  
**RPTEC/TERT1**  
 (A) *in vitro* results from KE1 (Disturbance of lysosomal function) after colistin, PBNP and CdCl<sub>2</sub> treatment in RPTEC/TERT1 cells, (B) *in vitro* results from KE3 (Increase cytotoxicity of renal tubule cell) after colistin, PBNP and CdCl<sub>2</sub> treatment in RPTEC/TERT1 cells, (C) computed data points from the obtained mathematical equations for KE1 (Disturbance of lysosomal function), (D) predicted data for KE2 (Disturbance of lysosomes), (E) predicted data for KE3 (Increase cytotoxicity of renal tubule cell), (F) response-response plot based on polymyxin B data describing KE relationship between KE1 and KE2, (G) response-response plot based on polymyxin B data describing KE relationship between KE2 and KE3. (H) Comparison of measured *in vitro* results from KE3 (Increase cytotoxicity of renal tubule cell) and predicted data for KE3 (Increase cytotoxicity of renal tubule cells)

The prediction of cytotoxicity after colistin, PBNP and CdCl<sub>2</sub> treatment in the NRK-52E showed similar results as the prediction in RPTEC/TERT1. The predicted cytotoxicity after colistin treatment was similar to the measured cytotoxicity, with a lower toxic effect at the higher concentrations being predicted compared to the measured cytotoxicity (Figure 33 (C), (F) and (I)). After PBNP treatment in NRK-52E cells, a decrease in cell viability at the highest concentration (2000 µM) to 85 % was measured, whereas prediction of cytotoxicity showed no decrease in cell viability over the complete concentration range of PBNP (Figure 33 (C), (F) and (I)). The prediction of cytotoxicity after CdCl<sub>2</sub> treatment was – similarly to the prediction in RPTEC/TERT1 cells – quite poor and showed a lower predicted toxicity than that actually measured (Figure 33 (I)). Since NRK-52E cells proved to be more sensitive in response to CdCl<sub>2</sub> treatment than RPTEC/TERT1 cells, a decrease in cell viability was observed beginning at a treatment concentration of 15.6 µM, which decreased in a dose-dependent manner and showed 100 % cytotoxicity at 125 µM (Figure 33 (C)). Predicted cytotoxicity after CdCl<sub>2</sub> treatment showed a concentration-dependent decrease in cell viability above a concentration of 62.5 µM, which decreased to 50 % cell viability and showed no further decrease in cell viability above 500 µM (Figure 33 (F)). As shown previously for the RPTEC/TERT1 cells (Figure 32), the prediction of cytotoxicity in the NRK-52E cells after polymyxin treatment was found to be similar to the decrease in cell viability from the *in vitro* assays, while a poorer prediction was observed for CdCl<sub>2</sub> (Figure 33 (I)). Generally, prediction of CdCl<sub>2</sub> cytotoxicity in both cell lines was poor compared to measured cytotoxicity. This serves as a good example to demonstrate that stressors potentially acting by more than one AOP are difficult to predict using key event relationships generated from a single AOP.



**Figure 33**  
**NRK-52E**  
**Prediction of colistin, polymyxin B nonapeptide and CdCl<sub>2</sub> cytotoxicity using response-response relationships based on polymyxin B data in NRK-52E cells**

(A) *in vitro* results from KE1 (*Disturbance of lysosomal function*) after colistin, PBNP and CdCl<sub>2</sub> treatment in NRK-52E cells, (B) *in vitro* results from KE2 (*Disruption of lysosomes*) after colistin, PBNP and CdCl<sub>2</sub> treatment in NRK-52E cells, (C) *in vitro* results from KE3 (*Increase cytotoxicity of renal tubule cell*) after colistin, PBNP and CdCl<sub>2</sub> treatment in NRK-52E cells, (D) computed data points from the obtained mathematical equations for KE1 (*Disturbance of lysosomal function*), (E) predicted data for KE2 (*Disruption of lysosomes*), (F) predicted data for KE3 (*Increase cytotoxicity of renal tubule cell*), (G) response-response plot based on polymyxin B data describing KE relationship between KE1 and KE2, (H) response-response plot based on polymyxin B data describing KE relationship between KE2 and KE3. (I) Comparison of measured *in vitro* results from KE3 (*Increase cytotoxicity of renal tubule cell*) and predicted data for KE3 (*Increase cytotoxicity of renal tubule cell*).



Table 31

Mathematical equation obtained from *in vitro* experiment for KE1 in NRK-52E cells for the computation of additional data points

Key event	Mathematical equation
KE <sub>1</sub> (LAMP-1 intensity) (colistin)	$y = 159.4 + (-97.86 * x) + 41.69 + x^2$
KE <sub>1</sub> (LAMP-1 intensity) (PBNP)	$y = 100 + (-12.87 * x) + 9.567 * x^2$
KE <sub>1</sub> (LAMP-1 intensity) (CdCl <sub>2</sub> )	$y = 97.4 + \frac{258.7}{1 + 10^{((1.777 - x) * 2.227)}}$

## 4.2 AOP – Inhibition of mtDNA polymerase- $\gamma$

### 4.2.1 Using the Comparative Toxicogenomic Database (CTD) to identify suitable *in vitro* endpoints for the AOP – Inhibition of mtDNA polymerase- $\gamma$

For the identification of suitable *in vitro* endpoints for the AOP- *Inhibition of mtDNA polymerase- $\gamma$* , the online database Comparative Toxicogenomic Database (CTD; <http://ctdbase.org>) was used as a tool, in the same way as for the identification of *in vitro* endpoints for the AOP- *Receptor-mediated endocytosis and lysosomal overload* (Chapter 4.1.1). Venn diagrams were generated by using the VennViewer online function and all antivirals used in this work were analyzed in order to identify common gene interactions that may indicate appropriate endpoints. A VennView analysis for the prodrug tenofovir disoproxil fumarate could not be conducted because this compound was not available in the database. Low to moderate data sets were available for the remaining stressors (for adefovir - 11 gene data; tenofovir - 32 gene data; ADF - 104 gene data; cidofovir - 276 gene data) (Figure 34).

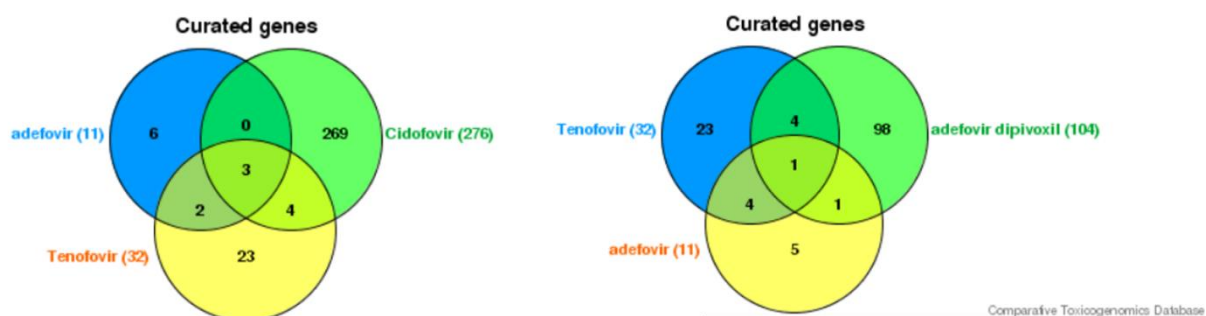


Figure 34

Venn diagram with the data sets of adefovir, ADF, cidofovir, tenofovir

However, Venn analysis revealed only a few overlaps (1 – 4) for commonly regulated genes (Figure 34). The rare gene overlaps were examined for associations related to the AOP- *Inhibition of mtDNA polymerase- $\gamma$* , mtDNA depletion, mitochondrial toxicity, mitochondrial dysfunction, renal injury, or proximal tubule damage with no results. After analyses in the Comparative Toxicogenomic Database failed to provide promising results, we restricted the identification of suitable *in vitro* endpoints to publicly available information from published literature (e.g., PubMed) for the AOP - *Inhibition of mtDNA polymerase- $\gamma$* .

#### **4.2.2 Establishment of suitable *in vitro* assays linked to the AOP – *Inhibition of mtDNA polymerase- $\gamma$***

While Venn analysis with adefovir, cidofovir, tenofovir and TDF in the Comparative Toxicogenomic Database failed to identify appropriate *in vitro* endpoints due to limited available data, we used published results from PubMed to identify appropriated *in vitro* endpoints. Since *in vitro* studies in different cells (e.g., HK-2, mouse renal proximal tubular epithelial cells) demonstrated the link between inhibition of DNA polymerase- $\gamma$  and consequent mtDNA abundance in association with NRTIs as well with adefovir and tenofovir (Lewis *et al.*, 2001, Zhao *et al.*, 2017, Vidal *et al.*, 2006) the measurement of mtDNA abundance seems to be a suitable *in vitro* endpoint for KE1 (*Depletion of mtDNA*) in the AOP – *Inhibition of mtDNA polymerase- $\gamma$* . These *in vitro* findings were also observed in *in vivo* studies in several species (e.g., rats, mice, dogs, monkeys, woodchucks) as well as in HIV infected patients medicated with NRTIs, adefovir or tenofovir, in which mitochondrial toxicity was revealed as well as reduction in mtDNA content (Lewis, 2003b, Lewis *et al.*, 2001, Lewis *et al.*, 2003a, Morton, 1998, Herlitz *et al.*, 2010, Lebrecht *et al.*, 2009, Kohler *et al.*, 2009a, Tanji *et al.*, 2001, Arnaudo *et al.*, 1991, Masanés *et al.*, 1998, Pezeshkpour *et al.*, 1991, Côté *et al.*, 2006, Hall, 2013). Measurement of mtDNA

content seems to be an appropriate *in vitro* endpoint for this AOP and can be measured relative to nuclear DNA copy number via qPCR, which has been reported as a suitable *in vitro* assay (Rooney *et al.*, 2015, Thakar *et al.*, 2015, Lebrecht *et al.*, 2009, Biesecker *et al.*, 2003). *In vitro* studies in HepG2 cells showed the strong potential of zalcitabine (ddC) to decrease mtDNA content and was selected as a positive control for this *in vitro* assay (Birkus *et al.*, 2002). Concomitant with mtDNA depletion, mitochondrial toxicity was observed in the *in vitro* and *in vivo* studies and has been integrated in this AOP as the KE2 (*Mitochondrial dysfunction*). As a suitable *in vitro* assay, the MitoTracker<sup>®</sup> Red assay was applied, which stains living, intact mitochondria and is dependent on the membrane potential of the mitochondria. The assay was performed by Dr. Bernhard Ellinger (Fraunhofer Institute for Molecular Biology and Applied Ecology, Translational Medicine Unit, Screening-Port, Hamburg, Germany) and the experimental results were provided with kind permission. Based on these findings *in vitro* assays were established to address the individual key events.

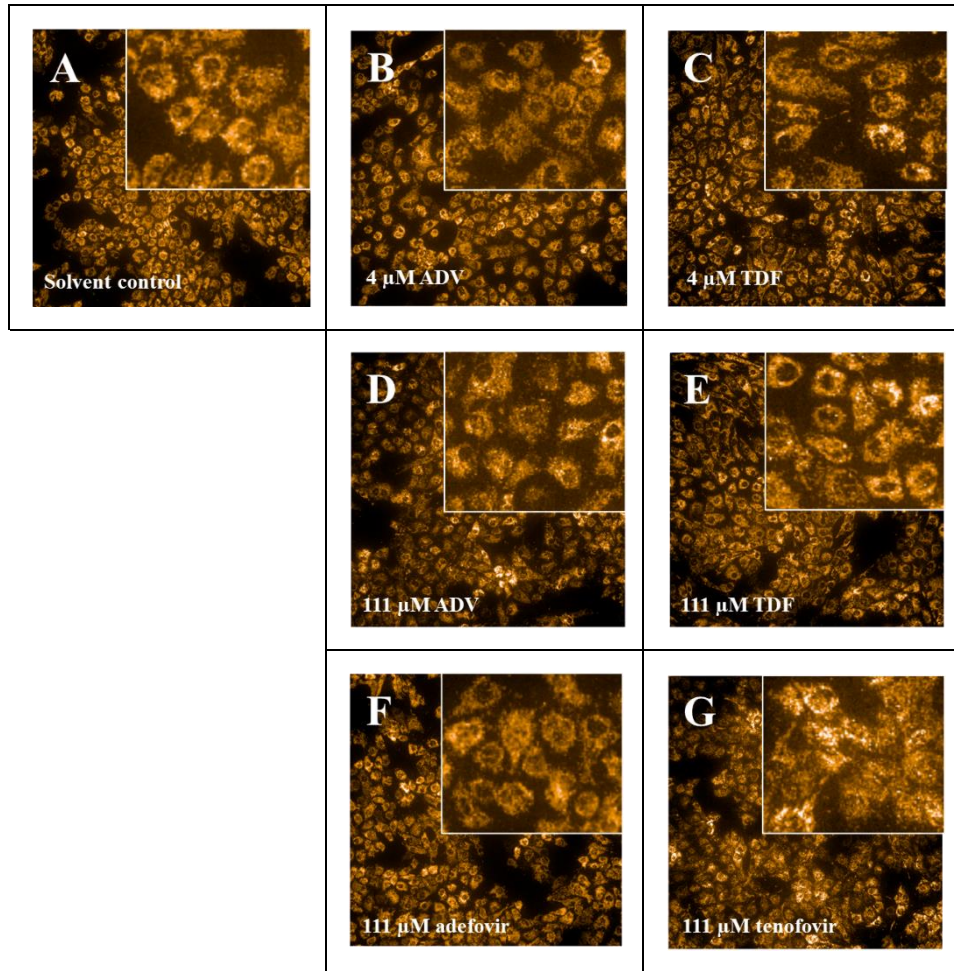
#### **4.2.2.1 Antiviral prodrugs reduced mtDNA content after long-term treatment in RPTEC/TERT1 cells – *in vitro* assay for the key event Depletion of mtDNA**

As a potential *in vitro* endpoint for KE1, mtDNA content was measured in both cell lines after 24 h of treatment with the antivirals. The mtDNA content in the RPTEC/TERT1 cells remained unchanged for all antivirals used as well as for the positive control ddC (Figure 37 (A)). After treatment with cidofovir, tenofovir and TDF, the results even showed an increase in mtDNA content in NRK-52E cells (Figure 37 (A)). Note that increase in mtDNA copy number is contrary to *in vivo* observations, which demonstrated a decrease in mtDNA content (Lewis, 2003b, Lewis *et al.*, 2001, Lewis *et al.*, 2003a, Morton, 1998, Herlitz *et al.*, 2010, Lebrecht *et al.*, 2009, Kohler *et al.*, 2009a, Tanji *et al.*, 2001, Arnaudo *et al.*, 1991, Masanés *et al.*, 1998, Pezeshkpour

*et al.*, 1991, Côté *et al.*, 2006, Hall, 2013). Considering that a 24 h treatment was probably too short to mimic a chronic *in vivo* treatment, RPTEC/TERT1 cells were treated daily with antivirals for a period of 14 days due to their advantage of prolonged cultivation time (Wieser *et al.*, 2008, Aschauer *et al.*, 2015a, Aschauer *et al.*, 2015b). Long-term treatment resulted in a concentration-dependent decrease in mtDNA content for the prodrugs ADV and TDF, as well as for the positive control ddC (Figure 38 (A)). An increase in mtDNA content was observed for cidofovir, while mtDNA content for adefovir and tenofovir remained unchanged (Figure 38 (A)).

#### **4.2.2.2 Prodrugs induced mitochondrial toxicity after long-term treatment in RPTEC/TERT1 cells – *in vitro* assay for the key event Dysfunction of mitochondria**

After the results for KE1 (*Depletion of mtDNA*) following 24 h treatment with antivirals in both cell lines revealed no decrease but rather an increase in mtDNA copy number (Figure 37 (A)), the focus in KE2 (*Dysfunction of mitochondria*) was directed to 14 days treatment with antivirals in the RPTEC/TERT1 cells. Mitochondrial toxicity was observed after daily treatment for 14 days for the prodrugs ADV and TDF (Figure 35 (D) & (E) and Figure 38 (B)). Fluorescence images of MitoTracker<sup>®</sup> Red stained RPTEC/TERT1 cells after 14 days of treatment with 111  $\mu$ M ADV (Figure 35 (D)) or TDF (Figure 35 (F)) showed more pronounced defects at the mitochondrial membranes than RPTEC/TERT1 cells treated with 4  $\mu$ L ADV (Figure 35 (B)), or 4  $\mu$ L TDF (Figure 35 (C)), respectively, as well as compared to untreated cells (Figure 35 (A)). A more distinct indication of prodrug-induced mitochondrial effects was provided by the organization of mitochondria in the cells.



**Figure 35**

**Fluorescence images of MitoTracker® dye in RPTEC/TERT1 cells treated with antivirals for 14 d**

RPTEC/TERT1 cells were treated for 14 d with antivirals and stained with MitoTracker® Red dye (orange). MitoTracker® Red uptake images were taken using an Opera® System (PerkinElmer Inc., MA, USA). Untreated RPTEC/TERT1 cells showed healthy and stained mitochondria in cells distributed over the entire cytoplasm (A). Effects of adefovir and ADV treatment on mitochondrial function and organization are presented in images (B), (D) & (F), while (B) represents treatment with 4  $\mu\text{M}$  and (D) & (F) treatment with 111  $\mu\text{M}$  ADV respectively adefovir. TDF and tenofovir induced effects on mitochondrial function and organization are shown in (C), (E) & (G), while (B) represents treatment with 4  $\mu\text{M}$  and (E) & (G) treatment with 111  $\mu\text{M}$  TDF respectively tenofovir. Images were created by Dr. Bernhard Ellinger (Fraunhofer Institute for Molecular Biology and Applied Ecology, Translational Medicine Unit, ScreeningPort, Hamburg, Germany) and provided with kind permission.

While in untreated cells mitochondria were equally distributed throughout the cytoplasm (Figure 35 (A)), mitochondria in RPTEC/TERT1 cells treated with ADV (Figure 35 (D)) and TDF (Figure 35 (E)), respectively, showed no longer homogeneous distribution. In treated cells, mitochondria were found to be more centralized around the cell nuclei (Figure 35 (D) & (E)). In contrast, such centralization of mitochondria was not evident in cells treated with adefovir or tenofovir (Figure 35 (F) & (G)). In cells treated with tenofovir lack of mitochondrial toxicity was also consistent with the lack of decrease in mtDNA copy number from KE1 (*Depletion of mtDNA*) and lack of cytotoxicity after tenofovir treatment in KE3 (*Cytotoxicity renal tubule cells*) (Figure 38). Treatment with tenofovir even showed increased mitochondrial activity in the entire cytoplasm, which was recognizable by a more pronounced MitoTracker<sup>®</sup>Red staining (Figure 35 (G)).

#### **4.2.2.3 Long-term treatment of antivirals increases cytotoxic effects in RPTEC/TERT1 & NRK-52E cells – in vitro assay for key event Increase of cytotoxicity in renal tubule cells**

Finally, to detect cytotoxic effects in the third and last key event (KE3 - *Increase of cytotoxicity in renal tubule cells*), the same method was used for the AOP - *Inhibition of mtDNA polymerase- $\gamma$*  using CellTiter-Glo<sup>®</sup> cell viability assay, as in the AOP - *Receptor-mediated endocytosis and lysosomal overload* (see chapter 4.1.2.3). Following 24 hours of treatment with antiviral stressors, the prodrugs ADV and TDF caused the greatest concentration-dependent decreases in cell viability in RPTEC/TERT1 and NRK-52E cells, although NRK-52E cells were found to be more sensitive than RPTEC/TERT1 cells (Figure 36 (A)). In contrast, 24 h treatment with adefovir, cidofovir, tenofovir, and ddC resulted in minor, non-significant decreases in cell viability across both cell lines (Figure 36 (A)). Since supposedly a short treatment time of 24 h

appeared to be insufficient to induce cytotoxic effects, a 14-day treatment in RPTEC/TERT1 cells followed in addition to the short-term treatment, since these cells are suitable for long-term treatment due to their long doubling time of approximately 96 – 120 h (Wieser *et al.*, 2008, Aschauer *et al.*, 2015a, Aschauer *et al.*, 2015b). Repeated treatment with antivirals daily for 14 d caused a further decrease in cell viability in RPTEC/TERT1 cells, which could not be confirmed for tenofovir (Figure 36 (B)). However, the most pronounced cytotoxic effects were observed for the prodrugs ADV and TDF (Figure 36 (B)), which was also reflected in the upstream key events, where the strongest effects were also observed for ADV and TDF compared with the other stressors (Figure 38 (A) & (B)).

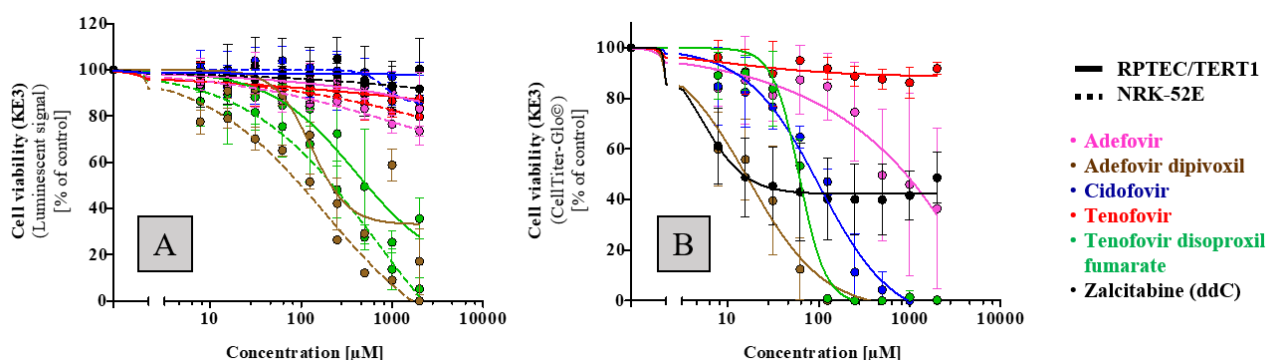


Figure 36

**Cytotoxicity of RPTEC/TERT1 and NRK-52E cells after treatment with antivirals**

Results of both cell lines (RPTEC/TERT1 cells (—) and NRK-52E cells (---)) after 24 h (A) resp. 14 d (B) of treatment with antivirals (adefovir, adefovir dipivoxil, cidofovir, tenofovir, tenofovir disoproxil fumarate, zalcitabine). The response of KE3 was plotted in percent of control against the logarithmic concentration in µM. All experiments were repeated in three technical replicates and three biological replicates. Data are presented as mean ± SD fold change (n = 3)



#### 4.2.3 Dose-response *in vitro* results across all KEs in the AOP – *Inhibition of mtDNA polymerase- $\gamma$*

*In vitro* endpoints reflecting each KE were assessed in rat (RPTEC/TERT1 (—)) and human renal proximal tubule epithelia cells (NRK-52E (---)) and treated for 24 h with model compounds (adefovir, adefovir dipivoxil, cidofovir, tenofovir, tenofovir disoproxil fumarate) and positive control (zalcitabine) in order to experimentally support the AOP and to establish quantitative relationships between KEs. After 24 h treatment with the antiviral drugs, no decrease in mitochondrial DNA copy number (KE1) was observed in either cell lines (Figure 37 (A)). In NRK-52E cells, a significant increase in the mtDNA copy number was observed after cidofovir, tenofovir and TDF treatment. RPTEC/TERT1 cells showed no significant increase or decrease in mtDNA copy number after treatment with antivirals. Also, mitochondrial toxicity (KE2) was not evident after treatment with cidofovir and tenofovir in NRK-52E cells respectively after treatment with cidofovir in RPTEC/TERT1 cells but was observed after treatment with TDF in RPTEC/TERT1 (Figure 37 (B)). However, in both cell lines a decrease in cell viability was observed after 24 h treatment with the prodrugs ADV and TDF in both cell lines, which was more pronounced in NRK-52E cells as compared to RPTEC/TERT1 cells. No significant cytotoxicity was observed after 24h treatment with adefovir, cidofovir and tenofovir (Figure 37 (C)).

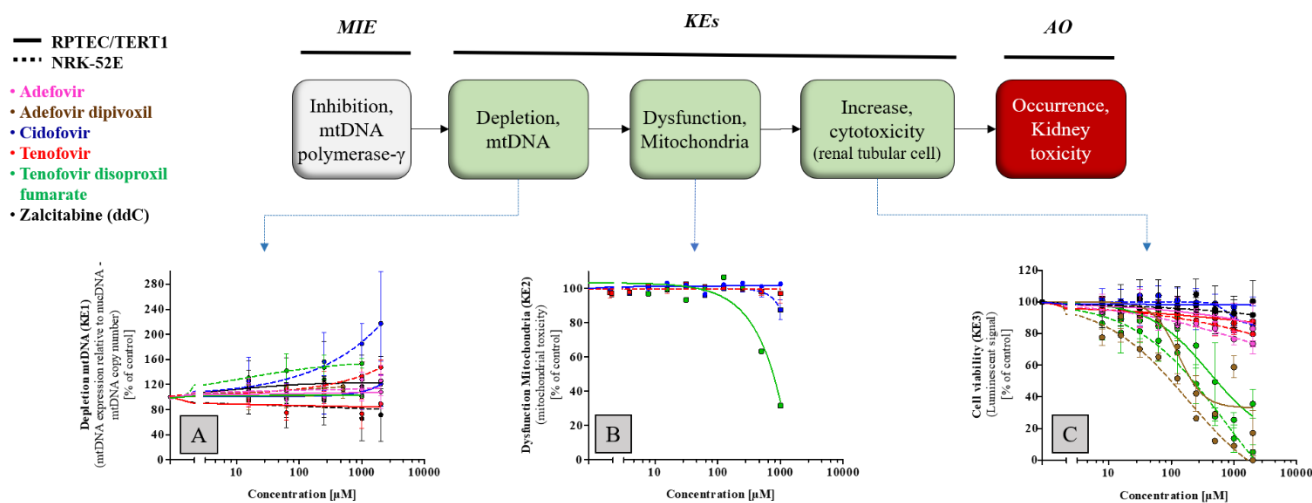


Figure 37

*In vitro* results after 24 h for the individual KEs from the AOP – Inhibition of mtDNA polymerase- $\gamma$

Results of both cell lines (RPTEC/TERT1 cells (—) and NRK-52E cells (---)) after 24 h of treatment with antivirals (adefovir, adefovir dipivoxil, cidofovir, tenofovir, tenofovir disoproxil fumarate, zalcitabine) of individual KEs. (A) mtDNA copy number describes changes in KE1 (*Depletion mtDNA*). (B) Mitochondrial toxicity describes changes in KE2 (*Dysfunction of mitochondria*). (C) Cell viability describes the change in KE3 (*Cytotoxicity in renal tubular cells*). The response of each KE was plotted in percent of control against the logarithmic concentration in  $\mu$ M. All experiments were repeated in three technical replicates and three biological replicates.

Data are presented as mean  $\pm$  SD fold change (n = 3)

Since analysis of the first key event after 24 h treatment revealed an increase rather than a decrease in mtDNA copy number as would have been expected from *in vivo* studies, a long-term exposure was simulated, which may be more relevant to the *in vivo* situation. Due to the long doubling time of RPTEC/TERT1 cells (approx. 96 - 120 h), these cells can be incubated over a time period up to 14 days (Wieser *et al.*, 2008, Aschauer *et al.*, 2015a, Aschauer *et al.*, 2015b). For this purpose, RPTEC/TERT1 cells were treated with the antivirals daily for 14

days. After 14-day treatment, the prodrugs ADV and TDF showed decrease in mtDNA copy number (KE1). A strong decrease in mtDNA copy number was also observed for ddC, which was included as a positive control. In contrast, no significant changes in mtDNA copy numbers were seen in response to adefovir and tenofovir, while 14 days treatment with cidofovir resulted in an increase in mtDNA copy number (Figure 38 (A)).

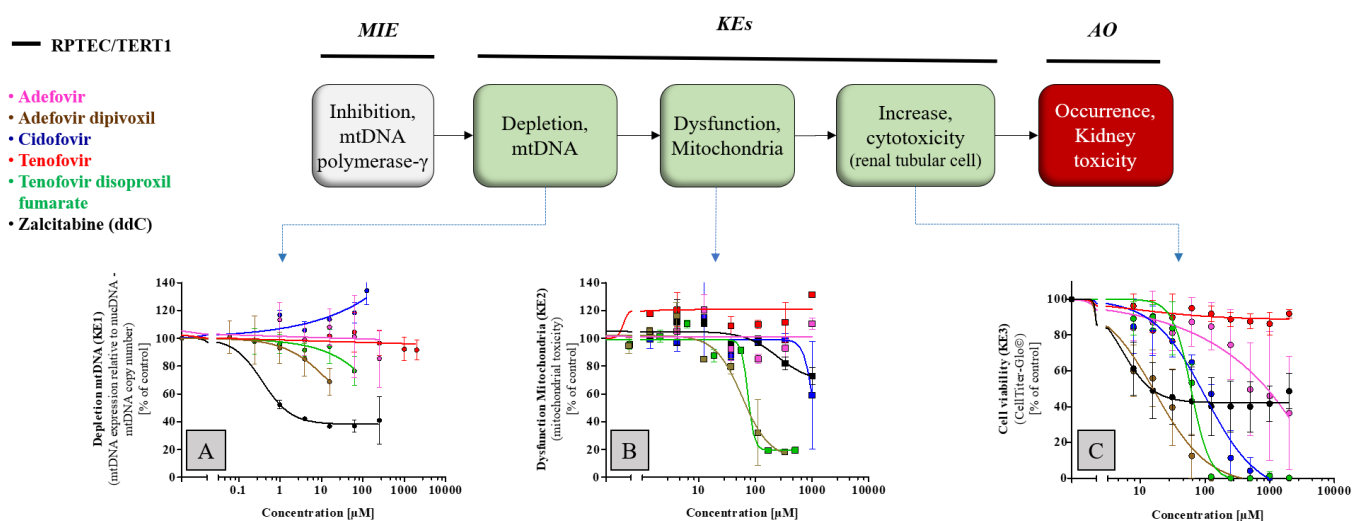


Figure 38

*In vitro* results after 14 d for the individual KEs from the AOP – Inhibition of mtDNA polymerase- $\gamma$

Results RPTEC/TERT1 cells (—) after 14 d of treatment with antivirals (adefovir, adefovir dipivoxil, cidofovir, tenofovir, tenofovir disoproxil fumarate, zalcitabine) of individual KEs. (A) mtDNA copy number describes changes in KE1 (*Depletion mtDNA*). (B) Dysfunction mitochondria describe the change in KE2 (*Mitochondrial toxicity*). (C) Cell viability describes the change in KE3 (*Cytotoxicity in renal tubular cells*). The response of each KE was plotted in percent of control against the logarithmic concentration in  $\mu\text{M}$ . All experiments were repeated in three technical replicates and three biological replicates. Data are presented as mean  $\pm$  SD fold change (n = 3)

A dose-dependent dysfunction of mitochondria (KE2) was measured for the prodrugs ADV and TDF, whereas for cidofovir and ddC only a slight decrease was observed at the highest concentration tested (Figure 38 (B)). For adefovir and tenofovir, no decrease in KE2 - *Dysfunction of mitochondria* was observed (Figure 38 (B)). With the exception of tenofovir, a decrease in cell viability (KE3) was observed following treatment with all antiviral drugs, whereby the most pronounced effects were observed in response to the prodrugs ADV and TDF (Figure 38 (C)).

#### **4.2.4 Prediction of tenofovir disoproxil fumarate downstream key events based on adefovir dipivoxil *in vitro* data**

Following the establishment of suitable *in vitro* assays and cell treatment with model compounds, we also tested in the AOP – *Inhibition of mtDNA polymerase- $\gamma$* , whether the generation of key event relationships can be utilized to predict downstream key events for other stressors associated with the same AOP. Here, we focused on the *in vitro* results obtained in RPTEC/TERT1 cells after 14 days treatment with the prodrugs ADV and TDF (Figure 38). Long-term treatment with prodrugs over 14 days was found to be more suitable for generating response-response curves and for prediction compared to 24 h treatments. Reasons for this are firstly that the *in vitro* 14 day KE1 data were consistent with *in vivo* findings (decrease in mtDNA copy number was measured), and secondly responses in mitochondrial toxicity (KE2) and cytotoxicity (KE3) were observed, which is a necessary prerequisite to establish key event relationships.

**4.2.4.1 Calculation of additional data points from experimental data**

Since after long-term treatment a decrease in mtDNA copy number in KE1 could only be observed for the prodrugs ADV and TDF, only dose-response data after 14-day treatment with ADV and TDF in RPTEC/TERT1 could be used for further computations, establishment of response-response plots and prediction.

To generate further data points from the responses received after ADV treatment, the best-fit functions were determined using the online tool PROAST web (<https://proastweb.rivm.nl>), as described above (chapter 4.1.5). Using the obtained regression equations for KE1 and KE3 (Table 32), additional data points in the concentration range between 0.06 µM and 1000 µM were computed and graphically plotted in GraphPad Prism 5.01 (Figure 39 (C) and (D)).

**Table 32**

**Mathematical equation obtained from *in vitro* experiments for the calculation of additional data points**

<b>Key event</b>	<b>Mathematical equation</b>
KE1 ( <i>mtDNA copy number</i> )	$y = 93.5 + (-12.92 * x) + (-6.057 * x^2)$
KE2 ( <i>mitochondrial toxicity</i> )	$y = 13.44 + \frac{88.56}{1 + 10^{((1.767-x)*(-1.803))}}$
KE3 ( <i>cell viability</i> )	$y = -3.823 + \frac{103.823}{1 + 10^{((1.227-x)*(-1.055))}}$

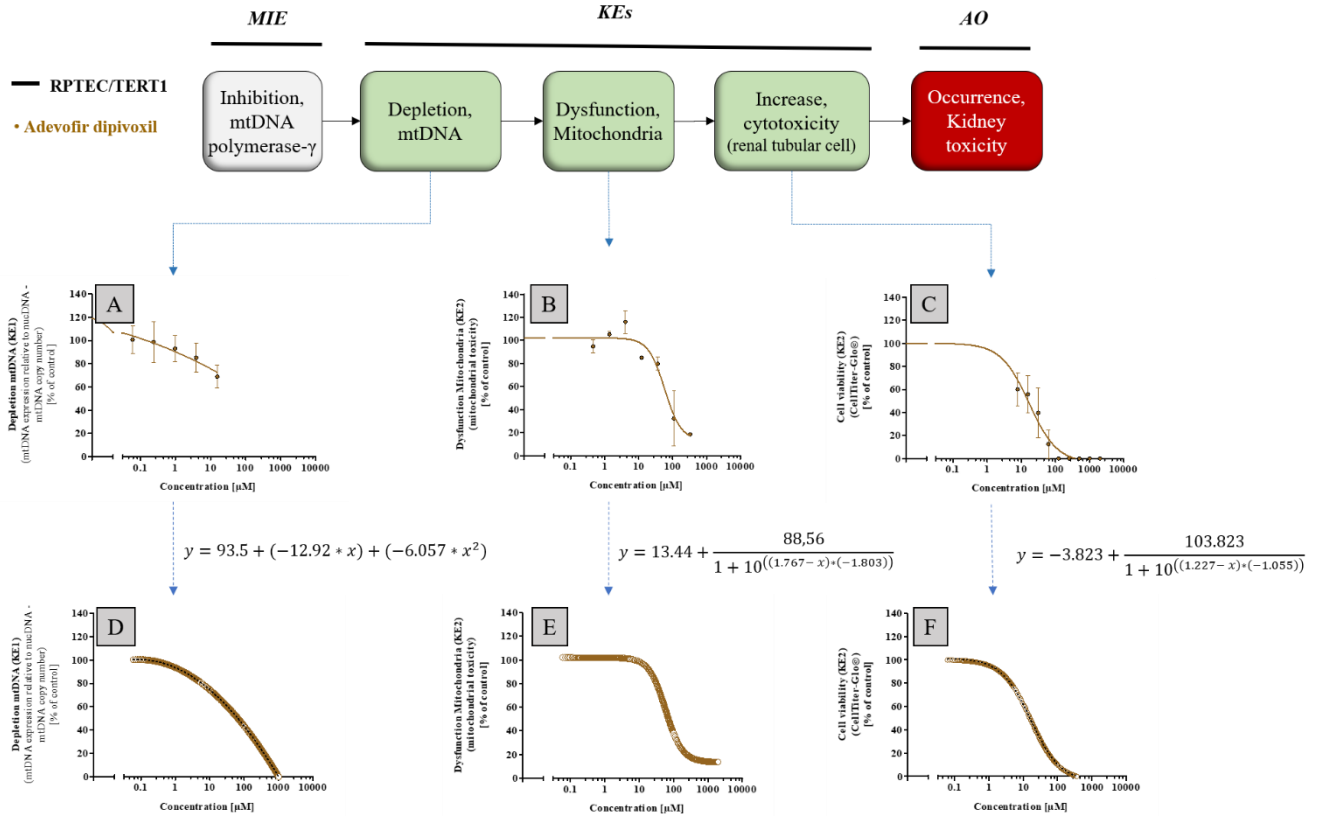


Figure 39

Calculation of additional data points from the experimentally obtained *in vitro* data after ADV treatment in RPTEC/TERT1 cells

(A) *in vitro* results from KE1 (*mtDNA copy number*), (B) *in vitro* results from KE2 (*mitochondrial toxicity*), (C) *in vitro* results from KE3 (*cell viability*), (D) computed data points from the obtained mathematical equation for KE1 (*mtDNA copy number*), (E) computed data points from the obtained mathematical equation for KE2 (*mitochondrial toxicity*), (F) computed data points from the obtained mathematical equation for KE3 (*cell viability*)

#### **4.2.4.2 *Generating response-response plots from ADV data to establish quantitative relationship between KEs***

To establish the quantitative relationship between the KEs, the same strategy was used as for the AOP – *Receptor-mediated endocytosis and lysosomal overload* (see chapter 4.1.5.2). With the computed data from KE1, KE2 and KE3 after ADV treatment in RPTEC/TERT1 cells, response-response plots were generated. The computed data of KE2 (*Dysfunction of mitochondria*) were plotted as a function of KE1 (*Depletion of mtDNA copy number*), and KE3 (*Cell viability*) as a function of KE2 (*Dysfunction of mitochondria*) (Figure 40 (D) & (E)). In addition, a response-response plot between KE1 and KE3 was also generated by plotting the computed data of KE3 (*Cell viability*) as a function of KE1 (*Depletion of mtDNA copy number*) (Figure 41 (C)). After the response-response plots were created, the best fit function for each response-response function was determined using the online tool PROAST web. The corresponding mathematical equations of the quantitative key event relationships (qKER<sub>1</sub>, qKER<sub>2</sub> and qKER<sub>1A</sub>) was determined, and the data were graphically plotted in Graph Pad Prism 5.01 (Figure 40, Figure 41 and Table 33).

**Table 33**  
**Mathematical equations obtained from response-response plots describing quantitative relationships between KE1, KE2 and KE3**

<b>Key event relationship</b>	<b>Mathematical equation</b>
qKER <sub>1</sub> : KE <sub>1</sub> → KE <sub>2</sub>	$y = 13.44 + \frac{88.56}{1 + 10^{((1.767-x)*(-1.803))}}$
qKER <sub>2</sub> : KE <sub>2</sub> → KE <sub>3</sub>	$y = 51385 + \left( \frac{-19780.96}{1 + 10^{(356.2 - x)*(-0.009705)}} \right) + \left( \frac{-31611.5}{1 + 10^{(112.2 - x)*(-0.2875)}} \right)$
qKER <sub>1A</sub> : KE <sub>1</sub> → KE <sub>3</sub>	$y = -2.685 + \frac{112.985}{1 + 10^{((70.37-x)*0.03484)}}$



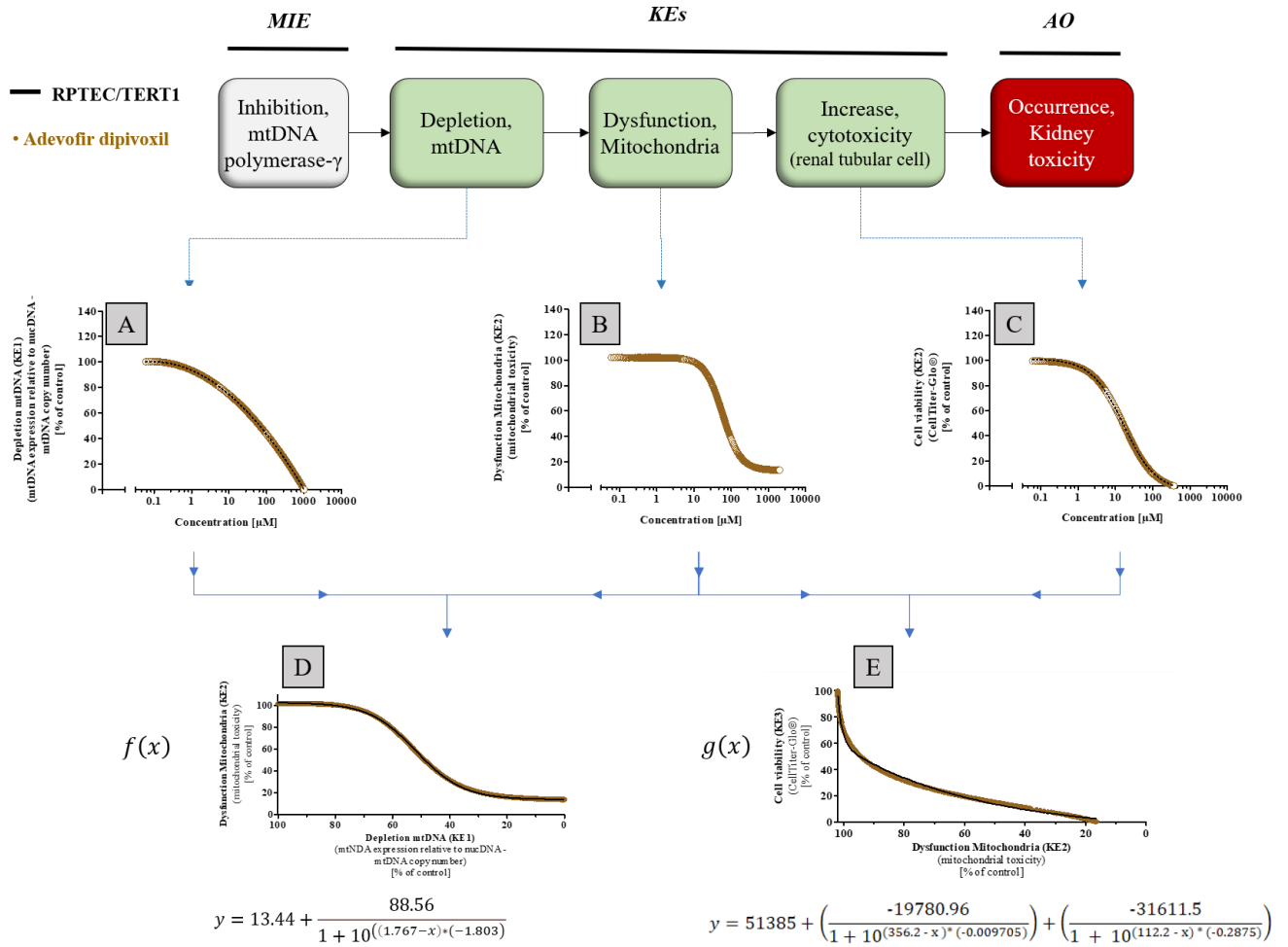
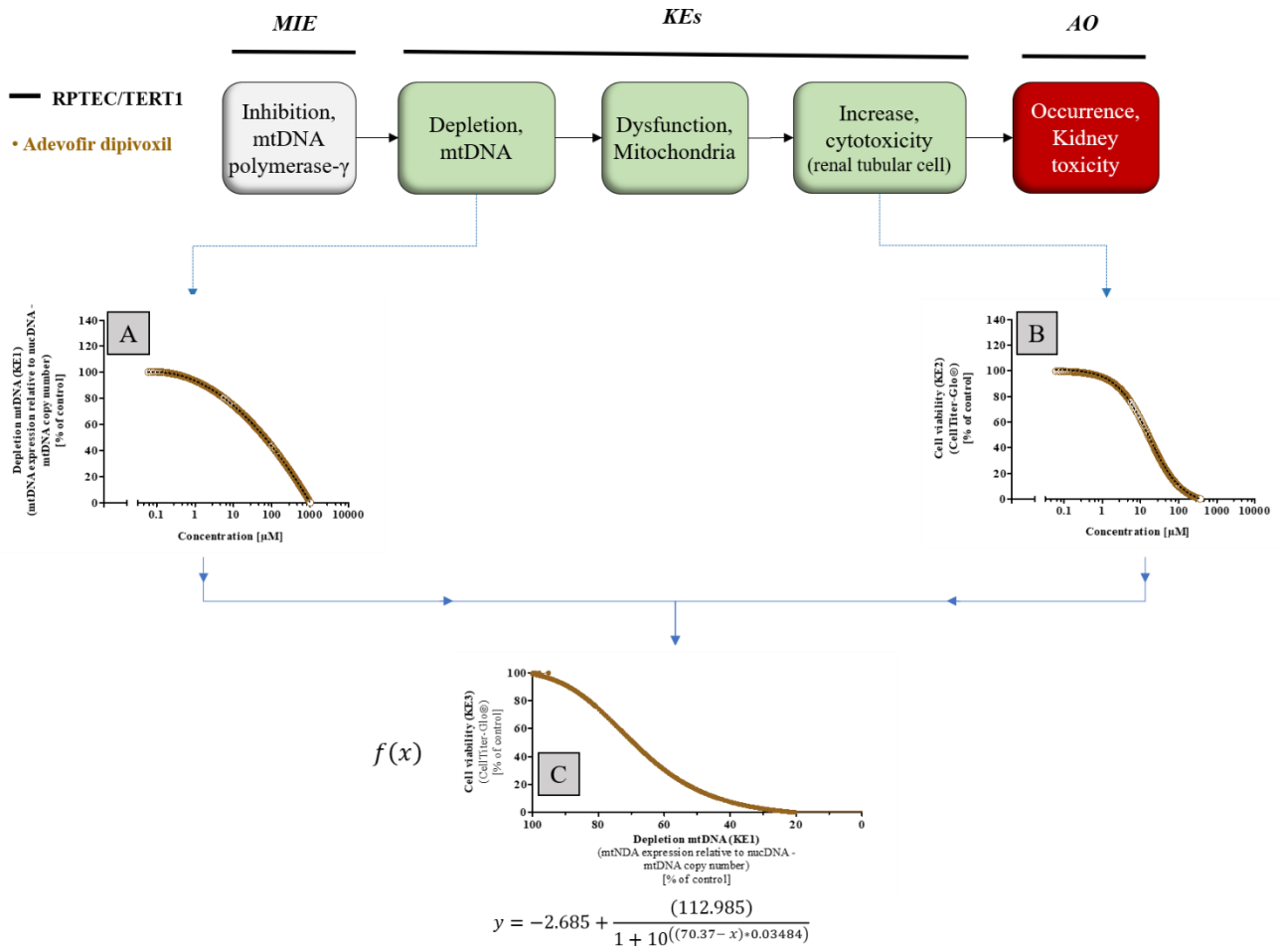


Figure 40

Response-response plots obtained from ADV KE data in RPTEC/TERT1 cells

The KE2 – *Dysfunction mitochondria* (KE2 – *mitochondrial toxicity*) (B) was plotted as a function of KE1 - *Depletion of mtDNA copy number* (KE1 – *mtDNA copy number*) (A). The resulting response-response function is described with the corresponding mathematical equation and shows the quantitative relationship between KE1 and KE2 (qKER<sub>1</sub>) (D). KE3 – *Cell viability* (KE3 – *Increase cytotoxicity of renal tubule cell*) (C) was plotted as a function of KE2 - *Dysfunction mitochondria* (KE2 – *mitochondrial toxicity*) (B). The resulting response-response function with its mathematical description and the quantitative relationship between KE2 and KE3 is shown below (E)



**Figure 41**

**Response-response plots obtained from ADV KE data in RPTEC/TERT1 cells without KE2**

The KE3 – Cell viability (KE3 – Increase cytotoxicity of renal tubule cell) (B) was plotted as a function of KE1 - Depletion of mtDNA copy number (KE1 – mtDNA copy number) (A). The resulting response-response function is described with the corresponding mathematical equation and shows the quantitative relationship between KE1 and KE3 (qKER<sub>1A</sub>) (C)

#### 4.2.4.3 Prediction of TDF cytotoxicity in RPTEC/TERT1 cells using the response-response relationship obtained from ADV data

To follow the same strategy as in the first AOP, in order to obtain an adequate amount of data from the experimental *in vitro* assays collected and the same chemical concentrations of the test substances used in the assays, additional data points were calculated from the results of the *in vitro* assay describing KE1 (*Depletion of mtDNA copy number*) (Figure 43) (A)). Since treatment with TDF in RPTEC/TERT1 cells showed a decrease of only approximately 20 % in mtDNA copy number and was hence weak, no best-fit model could be determined using the online application PROAST. To obtain additional data points for the prediction, 37 data points in a concentration range between 0.24 and 62.5  $\mu\text{M}$  were manually selected and plotted using GraphPad<sup>®</sup> Prism 5.01 (Figure 43 (D)). Using these selected data and the mathematical description of the quantitative KER<sub>1</sub> (Figure 43 (G) and Table 33), a prediction of KE2 (*Mitochondrial toxicity*) was computed (Figure 43 (E)). Prediction of KE2 (*Mitochondrial dysfunction*) showed no decrease in mitochondrial function up to the highest concentration used (62.5  $\mu\text{M}$ ) (Figure 43 (E)) which was consistent with the measured *in vitro* results (Figure 43 (B)). The predicted data from KE2 were used to predict KE3 (*Cell toxicity*) using the mathematical description of the quantitative KER<sub>2</sub> (Figure 43 (H) and Table 33). The prediction of KE3 proved to be not feasible. Closer examination of the *in vitro* results for KE2 (*Mitochondrial dysfunction*) and KE3 (*Cell toxicity*) revealed that the response in the downstream key event (KE3) was observed at lower concentrations than the response in the upstream key event (KE2) (Figure 42). Thus, a decrease in cell viability was seen in the absence of mitochondrial toxicity. Hence, the question "how much response in an upstream KE is needed to trigger a response in a downstream KE" cannot be answered and makes a prediction via the key event relationship unfeasible. To test whether prediction for cytotoxicity is feasible by using only *in vitro* KE1 data and *in vitro* KE3

data, the key event relationship between KE1 and KE3 (qKER<sub>1A</sub>) was used and KE2 was skipped for the prediction (Figure 41 (C) Figure 44).

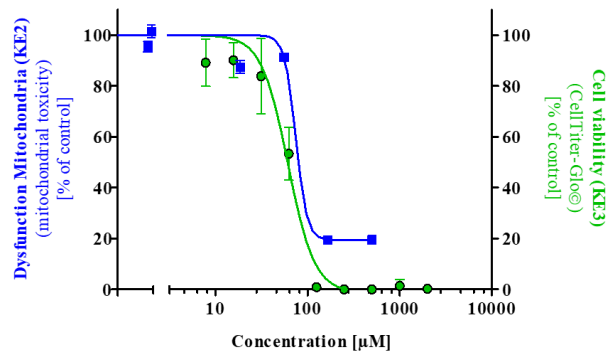


Figure 42

**Comparison of *in vitro* results for KE2 (Mitochondrial toxicity) and KE3 (Cell viability) after 14 d treatment with ADV in RPTEC/TERT1 cells from the AOP – Inhibition of mtDNA polymerase- $\gamma$**

Blue graph represents dysfunction in mitochondria and describe the change in KE2 (Mitochondrial toxicity). Green graph represents cell viability and describes the change in KE3 (Cytotoxicity in renal tubular cells). The response for KE2 and KE3 was plotted in percent of control against the logarithmic concentration in  $\mu\text{M}$ . All experiments were repeated in three technical replicates and three biological replicates. Data are presented as mean  $\pm$  SD fold change (n = 3)

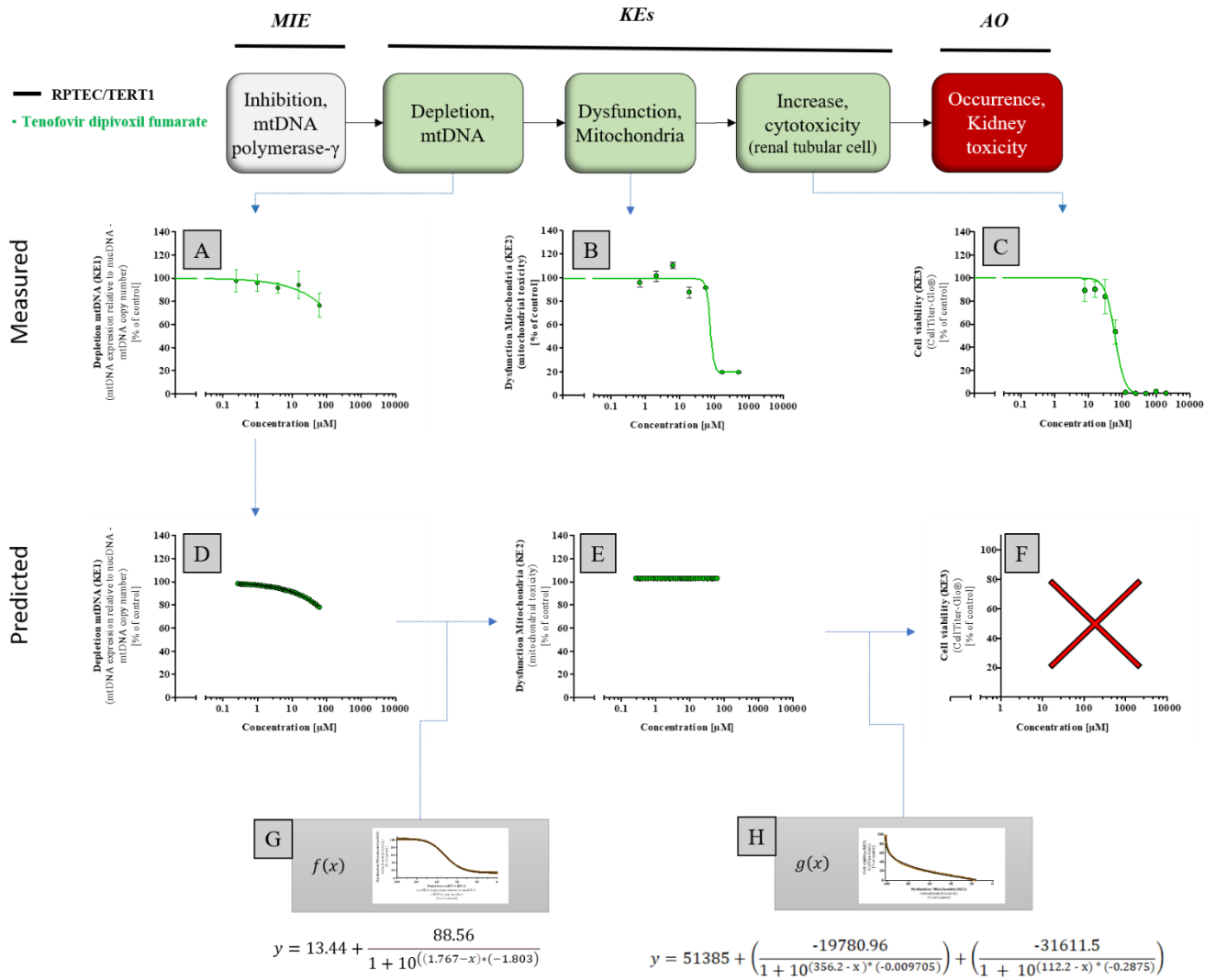


Figure 43

Prediction of TDF cytotoxicity using response-response relationships based on ADV data in RPTEC/TERT1

(A) *in vitro* results from KE1 (Depletion of mtDNA copy number) after 14 d TDF treatment in RPTEC/TERT1 cells, (B) *in vitro* results from KE2 (mitochondrial toxicity) after 14 d TDF treatment, (C) *in vitro* results from KE3 (Cell viability) after 14 d TDF treatment in RPTEC/TERT1 cells, (D) computed data points from the obtained mathematical equation for KE1 (Depletion of mtDNA copy number), (E) predicted data for KE2 (mitochondrial toxicity), (F) predicted data for KE3 (Cell viability) –data were not able to predict. (G) response-response plot based on ADV data describing KE relationship between KE1 and KE2, (H) response-response plot based on ADV data describing KE relationship between KE2 and KE3

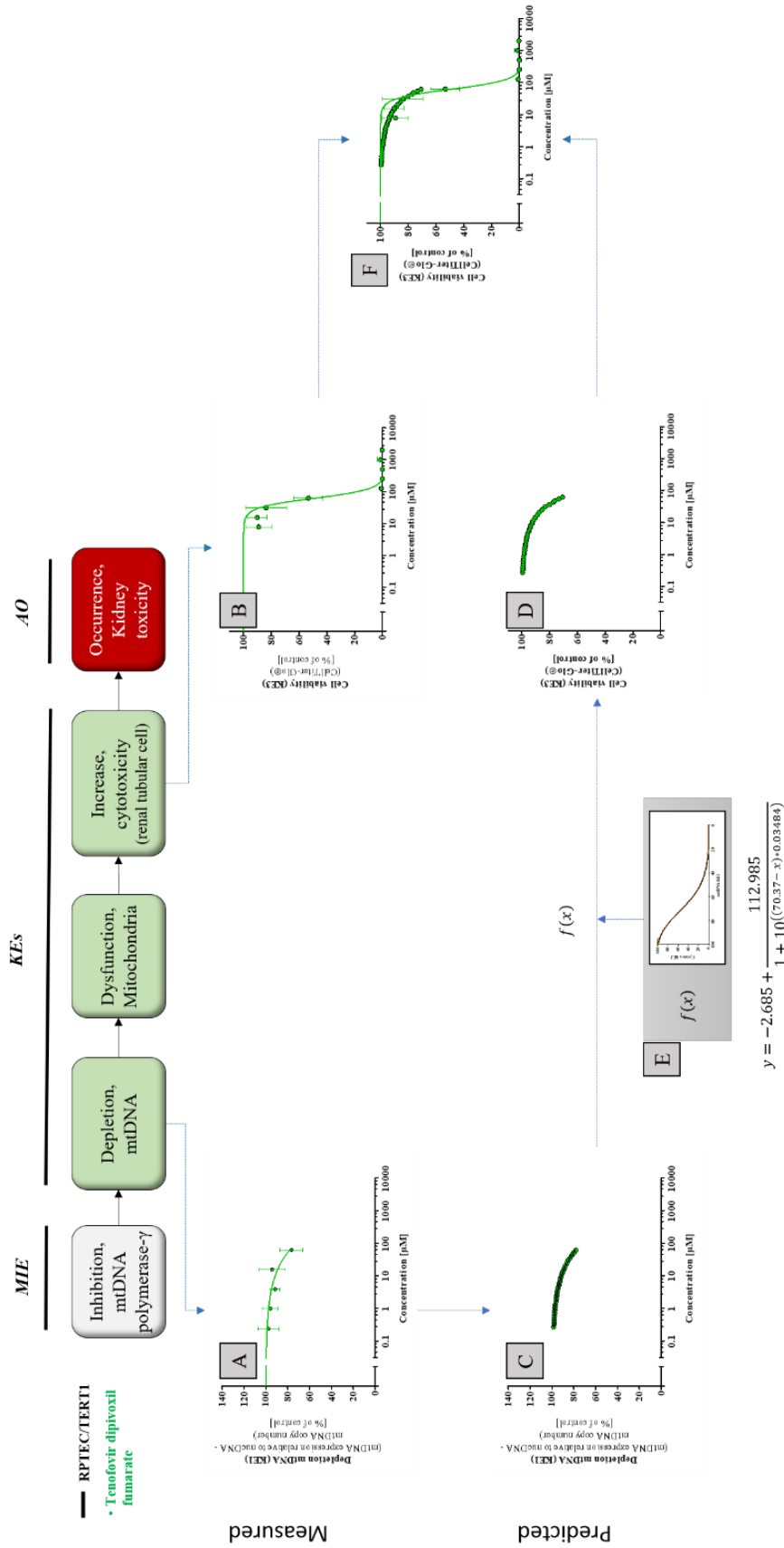


Figure 44

**Prediction of TDF cytotoxicity using response-response relationship based on ADV data in RPTEC/TERT1 cells excluding KE2 data**

(A) *in vitro* results from KE1 (Depletion of mtDNA copy number) after 14 d TDF treatment in RPTEC/TERT1 cells, (B) *in vitro* results from KE3 (Cell viability) after 14 d TDF treatment in RPTEC/TERT1 cells, (C) computed data points from the obtained mathematical equation for KE1 (Depletion of mtDNA copy number), (D) predicted data for KE3 (Cell viability), (E) response-response plot based on ADV data describing KE relationship between KE1 / KE3, (F) comparison of measured *in vitro* results from KE3 (Cell viability) and predicted data for KE3 (Cell viability)

By using the key event relationship between KE1 and KE3 (qKER<sub>1A</sub>), we were able to predict the cytotoxicity for TDF based on ADV data (Figure 44 (D) & (F)). Predicted cytotoxicity showed a concentration-dependent decrease in cell viability down to 70.8 % for the highest concentration used in the prediction (62.5  $\mu$ M), however, no further values could be predicted above this concentration (Figure 44 (D) & (F)). The pronounced cytotoxic effect of TDF in the *in vitro* assay for KE3 (Figure 38), was also the limiting factor for treatment with concentrations above 62.5  $\mu$ M, resulting in a poor response in KE1 after TDF treatment (Figure 44 (A)), which did not allow a calculation of a best-fit model resp. further data points, and we were restricted to the measured dose-response data. Overall, the prediction for TDF appeared to be good in the concentration range between 0 and 62.5  $\mu$ M, with a slightly weaker predicted cytotoxicity (70.8%) compared to the actual measured cytotoxicity (53.4%) predicted for the highest concentration used (62.5  $\mu$ M) (Figure 44 (F)).

### 4.3 Risk assessment based on *in vitro* results

After integrating suitable *in vitro* assays for the individual AOPs and experimentally supporting them with test substances, another important goal of the work was to obtain an estimate of risk based on the *in vitro* results. As a first estimate of risk, points of departure (PoD) derived from the *in vitro* assays were compared with serum and kidney concentrations achieved in humans and rats.

#### 4.3.1 *In vitro* points of departure related to the AOP – Receptor-mediated endocytosis and lysosomal overload

The following table shows serum concentrations obtained from human studies after administration of polymyxin antibiotics at therapeutic doses (Table 34) (Sorlí *et al.*, 2017, Falagas *et al.*, 2005, Falagas and Kasiakou, 2006, Santamaría *et al.*, 2009, Cheng *et al.*, 2010a, Sorlí *et al.*, 2013, Forrest *et al.*, 2014). Serum and kidney concentrations obtained from *in vivo* studies in rats were achieved after administration of polymyxin antibiotics doses based on therapeutically relevant exposure levels or suprathreshold exposure levels that induced renal injury representative of nephrotoxicity observed in patients and study results to determine the maximum tolerated dose (MTD) (Table 34) (Keirstead *et al.*, 2013, Nilsson *et al.*, 2015). The range of *in vivo* data was then visualized together with the determined PoDs derived from the *in vitro* assays in the human and rat cell lines (Figure 45). The recommended therapeutic dosage for polymyxin B when administered intravenously (*i.v.*) is 15,000 to 25,000 IU per kilogram of body weight per day in two doses where 10,000 IU is equivalent to 1 mg polymyxin B and thus 1.5 to 2.5 mg/kg/d is recommended (Falagas and Kasiakou, 2006, Kassamali *et al.*, 2015, Gupta *et al.*, 2009, Cai *et al.*, 2020b). Patients from the studies received polymyxin B at doses ranging from 4,500 to 33,800 IU per kilogram of body weight per day, which correspond to doses of



0.45 to 3.38 mg/kg/d, while in some cases dose levels above the recommended doses of 25,000 IU resp. 2.5 mg/kg/d were applied. Renal damage was observed in treated patients, occurring with increasing incidence at doses  $\geq 150$  mg polymyxin B per day (Sandri *et al.*, 2013, Rigatto *et al.*, 2015, Phe *et al.*, 2014). Depending on the severity of the infection, the recommended dose for colistin is between 50,000 to 150,000 IU per kg body weight per day, with 30,000 IU = 1 mg colistin, resulting in a recommended dose of 1.6 to 5 mg/kg body weight *i.v.* per day (Kaye *et al.*, 2015, Michalopoulos and Falagas, 2011). Patients were treated with colistin doses of 3 to 9 million IU per day, corresponding to 100 to 300 mg colistin per day (2.5 – 5 mg/kg/d), with observed nephrotoxicity after treatment (Sorlí *et al.*, 2017, Falagas *et al.*, 2005, Santamaría *et al.*, 2009, Cheng *et al.*, 2010a, Sorlí *et al.*, 2013, Forrest *et al.*, 2014). Polymyxin B treatment doses used from *in vivo* studies in rats were 3 to 4 mg per kilogram of body weight *i.v.* resp. 5 to 25 mg per kilogram of body weight per day as a subcutaneous injection (*s.c.*) (Manchandani *et al.*, 2016, Manchandani *et al.*, 2017, Nilsson *et al.*, 2015). The dose for colistin in the rat studies was reported to be 6.25 mg/kg given 4 times a day (QID) as a *s.c.* injection, which corresponds to a daily dose of 25 mg per kg body weight (Keirstead *et al.*, 2013, Nilsson *et al.*, 2015). Treatment doses for polymyxin B nonapeptide was selected as 10 mg/kg QID via *s.c.* injection, corresponding to a total daily dose of 40 mg/kg (Keirstead *et al.*, 2013, Nilsson *et al.*, 2015).

Table 34

**Serum and kidney concentrations of polymyxin antibiotics in humans and rats**

Serum and mean serum concentrations of polymyxin antibiotics in humans after administration of therapeutic doses of polymyxin B (0.45 - 3.38 mg/kg/d by *i.v.* injection), colistin (2.5 - 5 mg/kg/d by *i.v.* injection), and serum as well as kidney concentrations of polymyxins in rats after administration of polymyxin B (3 - 4 mg/kg/d by *i.v.* injection, resp. 5 - 25 mg/kg/d per *s.c.* injection), colistin (25 mg/kg/d per *s.c.* injection), and PBNP (40 mg/kg/d per *s.c.* injection) based on therapeutically relevant exposure levels to induce renal damages

	Human serum conc. [ $\mu\text{M}$ ]	Mean serum conc. [ $\mu\text{M}$ ]	Rat serum conc. [ $\mu\text{M}$ ]	Mean serum conc. [ $\mu\text{M}$ ]	Rat kidney conc. [ $\mu\text{M}$ ]	Mean kidney conc. [ $\mu\text{M}$ ]	References
<b>PB</b>	0.57 – 4.1	<b>2.31</b>	0.33 – 1.5	<b>0.93</b>	2.8 – 23.2	<b>12.99</b>	(Sandri <i>et al.</i> , 2013, Manchandani <i>et al.</i> , 2016, Manchandani <i>et al.</i> , 2017, Tran <i>et al.</i> , 2016)
<b>Col</b>	0.5 – 3.6	<b>2.05</b>	0.12 – 9.5	<b>4.82</b>	73.7 – 79.3	<b>76.50</b>	(Michalopoulos and Falagas, 2011, Keirstead <i>et al.</i> , 2013, Nilsson <i>et al.</i> , 2015, Markou <i>et al.</i> , 2008, Tran <i>et al.</i> , 2016, Sorlí <i>et al.</i> , 2017)
<b>PBNP</b>	<i>n.a.</i>	<b>n.a.</b>	6.2 – 28.0	<b>17.12</b>	38.0 – 41.1	<b>39.55</b>	(Keirstead <i>et al.</i> , 2013, Tran <i>et al.</i> , 2016)

The findings from the *in vitro* assays after treatment with polymyxin antibiotics were utilized to calculate *in vitro* points of departure (PoDs). Thereby, limitations appeared in the calculation of some PoDs such of the EC<sub>X</sub> approach or the NtC approach. For exponential dose-response curves with an exponential slope, as measured in KE1 (*Disturbance lysosomal functions*) (Figure 16 (A)), an EC<sub>10</sub> or EC<sub>20</sub> concentration was not determined because a maximum effect cannot be identified. Calculation of POD using the NtC approach proved unproblematic for sigmoidal dose-response curves, such as those observed for *in vitro* KE3 results (*Cell viability*)

(Figure 16 (C)) and could be determined quite straightforward. However, NtCs could not be calculated for non-sigmoidal dose-response curves. The NOEC, LOEC and BMC<sub>10</sub> approach proved to be unproblematic and reliable methods to derive an *in vitro* PoD and were thus determined for all KEs dose-response curves (Table 35). Since these PoDs could be derived for all KEs, the NOEC, LOEC, and BMC<sub>10</sub> were used to calculate the margin of exposure using the published mean serum and mean kidney concentrations obtained from *in vivo* studies, respectively (Table 34). Calculated MOEs for all KEs and all cell lines were displayed in tabular form, and low calculated MOEs representing very high risk (< 1) were highlighted in red, moderate MOEs representing moderate risk (1 - 10) were highlighted in yellow, and high MOEs representing low to no risk (10 - 100 and ≥ 100, respectively) were highlighted in green (Table 36).

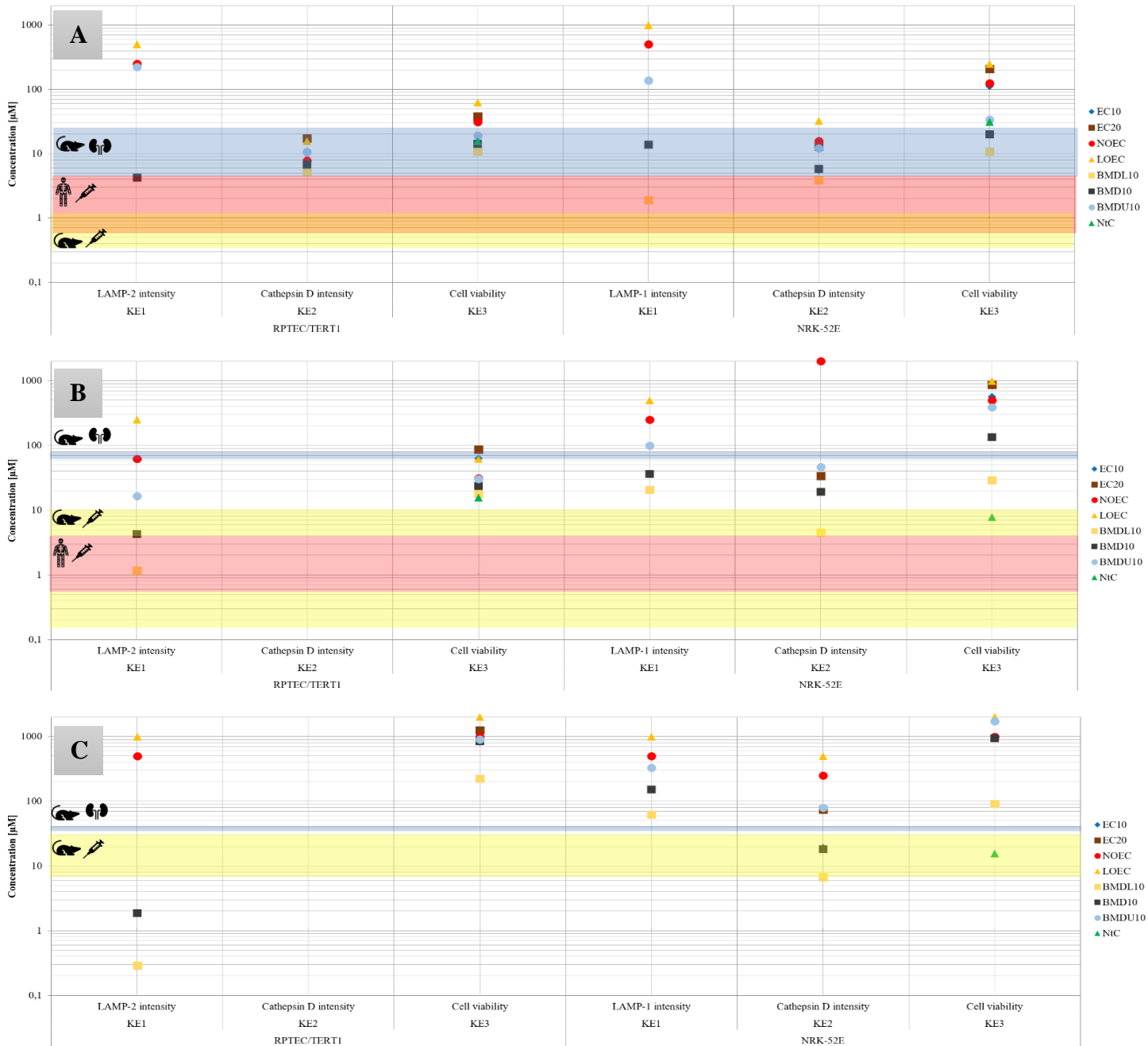
**Table 35**

**Calculated *in vitro* PoDs (NOEC, LOEC, BMC<sub>10</sub>) from *in vitro* assays for the AOP – Receptor-mediated endocytosis and lysosomal overload**

PoDs are given in μM for each key event (KE1 – 3) in both cell lines (RPTEC/TERT1 and NRK-52E) after treatment with polymyxin B (PB), colistin (Col) and polymyxin B nonapeptide (PBNP), n.a. not available *in vitro* data

<i>Key event</i>	<i>PoD</i>	<i>RPTEC/TERT1</i>			<i>NRK-52E</i>		
		<i>PB</i> [μM]	<i>Col</i> [μM]	<i>PBNP</i> [μM]	<i>PB</i> [μM]	<i>Col</i> [μM]	<i>PBNP</i> [μM]
<b>KE1</b>	<i>NOEC</i>	250	62.5	500	500	250	500
	<i>LOEC</i>	500	250	1000	1000	500	1000
	<i>BMC<sub>10</sub></i>	4.2	4.3	1.9	13.7	36.2	151.6
<b>KE2</b>	<i>NOEC</i>	7.8	n.a.	n.a.	15.62	2000	250
	<i>LOEC</i>	15.6	n.a.	n.a.	32.3	> 2000	500
	<i>BMC<sub>10</sub></i>	6.8	n.a.	n.a.	5.8	19.1	18.3
<b>KE3</b>	<i>NOEC</i>	31.3	31.3	1000	125	500	1000
	<i>LOEC</i>	62.5	62.5	2000	250	1000	2000
	<i>BMC<sub>10</sub></i>	14.2	23.5	847.2	19.9	135.5	944.9

## Results



**Figure 45**

**Visualization of different points of departure determined from *in vitro* assays after polyxim treatment in RPTEC/TERT1 and NRK-52E cells after 24 h and comparison with serum / kidney concentrations**

PoDs (EC<sub>10</sub> ◆; EC<sub>20</sub> ■; NOEC ●; LOEC ▲; BMCL<sub>10</sub> □; BMC<sub>10</sub> ■; BMCU<sub>10</sub> ●; NtC ▲) are described in the legend. Polyximins concentrations at therapeutic / suprathreshold exposure levels are plotted for rat kidney (blue range), rat serum (yellow range) and human serum concentration (red range) for (A) polymyxin B; (B) colistin; (C) PMBN

Table 36

Calculated margin of exposure (MOE) based on obtained *in vitro* PoDs (NOEC, LOEC, BMC<sub>10</sub>) for all key events (KE1 - KE3) from both cell lines (RPTEC/TERT1 & NRK-52E) and from published *in vivo* human serum, rat serum & rat kidney concentrations.

Calculated MOE (< 10) considered with a high risk are marked in red, MOE between 10 – 100 considered with a moderate risk are marked in yellow and MOE considered with low (> 100) are marked in green, n.a. not available *in vitro* or *in vivo* data

Key event	PoD	<i>in vivo</i> data	Margin of exposure					
			RPTEC/TERT1			NRK-52E		
			PB	Col	PBNP	PB	Col	PBNP
KE1 (Disturbance of lysosomal function)	NOEC	Human serum conc.	108	30	n.a.	216	122	n.a.
		Rat serum conc.	269	13	29	538	52	29
		Rat kidney conc.	19	0.81	13	38	3	13
	LOEC	Human serum conc.	216	122	n.a.	433	244	n.a.
		Rat serum conc.	538	52	58	1075	104	58
		Rat kidney conc.	38	3	25	77	7	25
	BMC <sub>10</sub>	Human serum conc.	2	2	n.a.	6	18	n.a.
		Rat serum conc.	5	0.88	0.11	15	8	9
		Rat kidney conc.	0.32	0.05	0.04	1	0.47	4
KE2 (Disruption of lysosomes)	NOEC	Human serum conc.	3	n.a.	n.a.	7	975	n.a.
		Rat serum conc.	8	n.a.	n.a.	17	415	15
		Rat kidney conc.	0.60	n.a.	n.a.	1	26	6
	LOEC	Human serum conc.	7	n.a.	n.a.	14	> 975	n.a.
		Rat serum conc.	17	n.a.	n.a.	35	> 410	29
		Rat kidney conc.	1	n.a.	n.a.	2	> 26	13
	BMC <sub>10</sub>	Human serum conc.	3	n.a.	n.a.	3	9	n.a.
		Rat serum conc.	7	n.a.	n.a.	6	4	1
		Rat kidney conc.	0.52	n.a.	n.a.	0.45	0.25	0.46
KE3 (Cytotoxicity of renal tubular cells)	NOEC	Human serum conc.	14	15	n.a.	54	244	n.a.
		Rat serum conc.	34	6	58	134	104	58
		Rat kidney conc.	2	0.41	25	10	7	25
	LOEC	Human serum conc.	27	30	n.a.	108	488	n.a.
		Rat serum conc.	67	13	117	269	207	117
		Rat kidney conc.	5	0.82	51	19	13	51
	BMC <sub>10</sub>	Human serum conc.	6	11	n.a.	9	66	n.a.
		Rat serum conc.	15	5	49	21	28	55
		Rat kidney conc.	1	0.31	21	2	2	24

A first estimate of human risk was obtained by comparing PoDs from the individual *in vitro* assays with plasma/kidney concentrations achieved in humans and rats. The visualization of the *in vitro* PoDs allows a better comparison between the individual PoDs as well as between the individual KEs (Figure 45). Visualization showed a high variability between the *in vitro* PoDs derived from assays covering different KEs and among the individual PoDs covering one KE. For a better assessment of the risk, the NOEC, LOEC and the BMC<sub>10</sub> as well as the serum and kidney concentrations from published *in vivo* studies were utilized to calculate the MOE. Margin of exposure calculations based on BMC<sub>10</sub> proved to be slightly more conservative compared to MOE based on LOEC or NOEC recognizable by MOEs being < 10 (red) and between 10 and 100 (yellow), respectively (Table 36). The lowest values for the MOE (< 1 or slightly above 1; red) resulted from the calculation using the renal concentrations from *in vivo* rat studies in combination with BMC<sub>10</sub> in particular. Data obtained from RPTEC/TERT1 cells tended to show a lower MOE that ranged from < 10 to 100 (red and yellow) compared to data obtained from NRK-52E cells, which would be representative for the observed renal damages from the *in vivo* studies, whereas the greater MOE obtained from NRK-52E data indicated lower to no concern for renal injuries (Table 36). Interestingly, using PoDs (especially NOEC / LOEC) from early key events (*e.g.*, KE1 - *Disturbance of lysosomal function*) for calculation, the MOE for *e.g.*, polymyxin B in both cell lines were partly > 100 or even > 1000 indicating low or no concern for renal injuries. Even MOE obtained from late key event (KE3 - *Cytotoxicity*) showed some moderate (10 - 100) or even low to no concern levels (> 100) for polymyxins, especially when using *in vitro* results from NRK-52E cells (Table 36). Overall, the risk assessment based on *in vitro* data implied a lower to no concern for renal injury associated with the polymyxin antibiotics.

### 4.3.2 *In vitro* points of departure related to the AOP –Inhibition of mtDNA polymerase- $\gamma$

*In vivo* data from pharmacokinetic studies (Bi 2005; Shida 2005, Yoon 2015, Nirogi 2012, Geboers 2015) were plotted together with PoDs derived from the *in vitro* assays to allow a first estimate of risk (Table 37; Figure 46). Serum concentrations obtained from *in vivo* studies in rats were achieved after administration of a single *i.v.* adefovir dose of 15  $\mu\text{mol/kg}$  (4 mg/kg) respectively a single oral (*p.o.*) dose of 36.6  $\mu\text{mol/kg}$  (10 mg/kg) (Yoon *et al.*, 2015). Pharmacokinetic studies in healthy volunteers and patients with chronic hepatitis B infection received single oral doses of 10 mg respectively 20 mg ADV (Bi *et al.*, 2005, Shida *et al.*, 2005). Dosages for TDF used for *in vivo* pharmacokinetics studies in rats were reported as 10 mg, 15 mg, and 30 mg per kg body weight (*p.o.*) (Nirogi *et al.*, 2012). *In vivo* pharmacokinetic study in healthy volunteers was carried out with a single dose of 300 mg TDF and were given oral (Geboers *et al.*, 2015).

**Table 37**

#### **Serum concentrations of adefovir and tenofovir in humans and rats**

Serum and mean serum concentrations of adefovir in humans after administration of therapeutic doses of ADV (10 mg, resp. 20 mg; *p.o.*) and serum concentrations in rats after *i.v.* administration (4 mg/kg) resp. after *p.o.* administration (10 mg/kg). Serum and mean serum concentrations of tenofovir in humans after single dose of 300 mg TDF (*p.o.*) and rats after *p.o.* administration of TDF (10 mg/kg, 15 mg/kg, 30 mg/kg)

	Human serum conc. [ $\mu\text{M}$ ]	Mean human serum conc. [ $\mu\text{M}$ ]	Rat serum conc. [ $\mu\text{M}$ ]	Mean rat serum conc. [ $\mu\text{M}$ ]	References
<b>Adefovir</b>	0.044 - 0.142	0.093	1.32 - 2.12	1.72	(Bi <i>et al.</i> , 2005, Shida <i>et al.</i> , 2005, Yoon <i>et al.</i> , 2015)
<b>Tenofovir</b>	0.771 - 0.978	0.875	0.36 - 1.05	0.71	(Nirogi <i>et al.</i> , 2012, Geboers <i>et al.</i> , 2015)

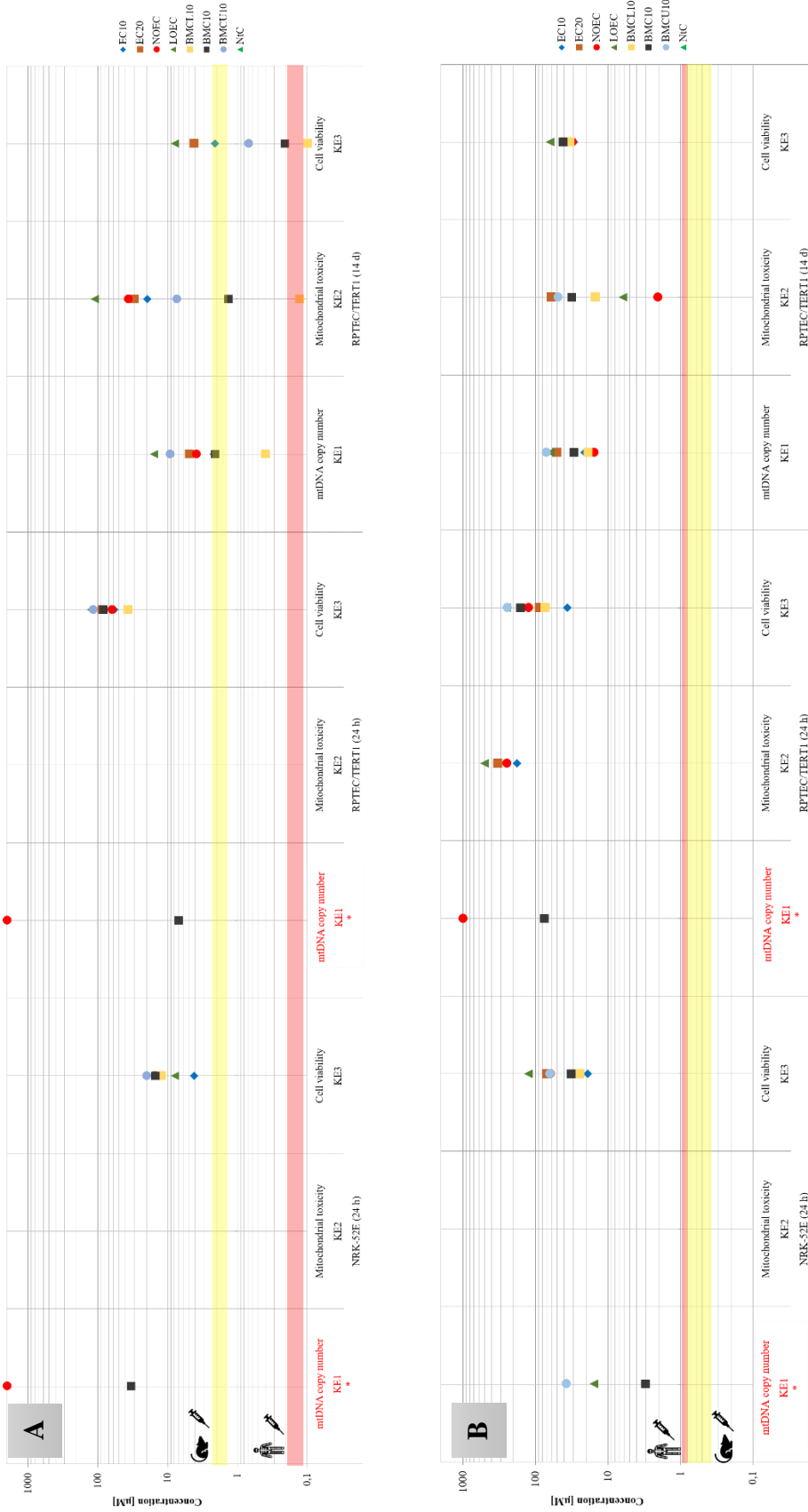
To use the most sensitive *in vitro* endpoints for risk assessment, the *in vitro* results for all key events (KE1 – 3) after 14 days of treatment in the RPTEC/TERT1 cells (Figure 38, Figure 46) were utilized to calculate *in vitro* points of departure (PoDs) (Table 38). *In vitro* data for the active metabolites adefovir and tenofovir and for the prodrugs ADV and TDF were selected as example model stressors for risk assessment to demonstrate the different sensitivity of the stressors (active metabolites vs. prodrugs) in the *in vitro* models.

**Table 38**  
**Calculated *in vitro* PoDs (NOEC, LOEC, BMC<sub>10</sub>) from *in vitro* assays for the**  
**AOP – Inhibition of mtDNA polymerase- $\gamma$**

PODs are given in  $\mu\text{M}$  for each key event (KE 1 – 3) from RPTEC/TERT1 cells after 14 d treatment with adefovir, tenofovir, adefovir dipivoxil (ADV) and tenofovir disoproxil fumarate (TDF), n.a. not available *in vitro* data

		<i>RPTEC/TERT1 (14 d)</i>			
<i>Key event</i>	<i>PoD</i>	<i>Adefovir</i> [ $\mu\text{M}$ ]	<i>Tenofovir</i> [ $\mu\text{M}$ ]	<i>ADV</i> [ $\mu\text{M}$ ]	<i>TDF</i> [ $\mu\text{M}$ ]
<b>KE1</b>	<i>NOEC</i>	2000	2000	3.9	15.6
	<i>LOEC</i>	> 2000	> 2000	15.6	62.5
	<i>BMC<sub>10</sub></i>	68.4	309.6	2.1	29.6
<b>KE2</b>	<i>NOEC</i>	1000	1000	36.6	2.05
	<i>LOEC</i>	> 1000	> 1000	110	6.2
	<i>BMC<sub>10</sub></i>	716	n.a.	1.35	31.55
<b>KE3</b>	<i>NOEC</i>	250	2000	n.a.	31.25
	<i>LOEC</i>	500	> 2000	7.8	62.5
	<i>BMC<sub>10</sub></i>	195	120.3	0.2	41.7





To overcome the limitations described in the calculation of some PoDs (Chapter 4.3.1), the NOEC, LOEC, and BMC<sub>10</sub> approaches were used, as in the previous AOP – *Receptor mediated endocytosis and lysosomal overload*, along with published *in vivo* rat and human serum concentrations to calculate the margins of exposure (MOE) (Table 39). MOEs for all KEs after 14 days of treatment in the RPTEC/TERT1 cells were tabulated, and low calculated MOEs representing very high risk (< 10) were highlighted in red, moderate MOEs representing moderate risk (10 - 100) were highlighted in yellow, and high MOEs representing low to no risk (> 100) were highlighted in green (Table 39). The calculated MOE for the active metabolites adefovir and tenofovir were found to be the highest calculated values with > 100, in some cases also with > 1,000 and > 10,000 and were thus marked in green with associated low to no risk (Table 39). With a few exceptions, the calculated MOEs for the prodrugs ADV and TDF were lower and ranked < 100 for the most values (Table 39). For all three key events, calculated MOEs for ADV and TDF were found to be even < 10 and were thus associated with a high risk. Similarly, the BMC<sub>10</sub> approach was found again to be the most conservative approach, since even MOE for ADV < 1 were calculated which are associated with high risk (Table 39). Overall, the risk assessment based on the *in vitro* results of the active metabolites adefovir and tenofovir implied no concern for renal damage as the MOEs were consistently > 100 and mostly > 1,000 to > 10,000. However, in cases of adefovir and tenofovir, it should be noted that these stressors may not be taken up into the cells and thus the conclusion would lead to a misinterpretation. Risk assessment for the prodrugs ADV and TDF showed a clearer tendency towards renal toxicity, since MOE values were found to be < 10, partly also for early key events with < 1 and thus associated with a high risk for renal toxicity. The majority of MOE values for ADV and TDF were in the range between 10 and 100 indicating moderate risk. For ADV, only 3 MOE values

> 100 resp. > 1000 were calculated associated with a low risk for renal toxicity and for TDF no MOE values were  $\geq 100$  (Table 39).

**Table 39**

**Calculated margin of exposure (MOE) based on *in vitro* PoDs (NOEC, LOEC, BMC<sub>10</sub>) for all key events (KE1 – 3) from RPTEC/TERT1 cells and from published *in vivo* human & rat serum concentrations**

Calculated MOE (< 10) considered with a high risk are marked in red, MOE between 10 – 100 considered with a moderate risk are marked in yellow and MOE considered with low or even no risk (> 100; > 1000) are marked in green, n.a. not available *in vitro* or *in vivo* data

Key event	PoD	<i>in vivo</i> data	Margin of exposure			
			RPTEC/TERT1 (14 d)			
			Adefovir	Tenofovir	ADV	TDF
KE1 (Depletion of mtDNA)	NOEC	Human serum conc.	> 20,000	> 2200	42	18
		Rat serum conc.	> 1000	> 2800	2.3	22
	LOEC	Human serum conc.	> 21,000	> 2280	> 160	71
		Rat serum conc.	> 1100	> 2800	9	88
	BMC <sub>10</sub>	Human serum conc.	> 700	> 350	22	34
		Rat serum conc.	40	> 430	1.2	42
KE2 (Dysfunction of mitochondria)	NOEC	Human serum conc.	> 10,000	> 1100	> 390	21
		Rat serum conc.	> 580	> 1400	21	26
	LOEC	Human serum conc.	> 10,700	> 1140	> 1100	7
		Rat serum conc.	> 580	> 1400	64	9
	BMC <sub>10</sub>	Human serum conc.	> 7000	n.a.	14.5	36
		Rat serum conc.	> 400	n.a.	0.8	44
KE3 (Cytotoxicity of renal tubular cells)	NOEC	Human serum conc.	> 2600	> 2200	n.a.	36
		Rat serum conc.	> 145	> 2800	n.a.	44
	LOEC	Human serum conc.	> 5300	> 2280	84	71
		Rat serum conc.	290	> 2800	4.5	88
	BMC <sub>10</sub>	Human serum conc.	> 2000	> 130	2.1	48
		Rat serum conc.	> 110	> 160	0.12	59

#### 4.4 <sup>4</sup>Integration of physiologically based pharmacokinetic modeling (PBPK) and quantitative *in vitro*-to-*in vivo* extrapolation (QIVIVE)

For prediction of more *in vivo* analogous pharmacokinetics of polymyxin B, a physiologically based pharmacokinetic (PBPK) model was established by the project partner at the University of Utrecht. After integration of the PBPK model with incorporated transporter kinetics that simulates active transport into the proximal tubule cells, *in vivo* plasma concentrations (Figure 47 – red line) achieved after 1-hour *i.v.* infusion with polymyxin B were more accurately

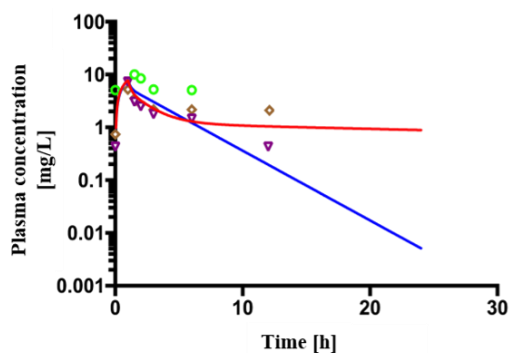


Figure 47

##### Physiologically based pharmacokinetic modeling of 1.0 mg/kg body weight (*i.v.*) polymyxin B

Polymyxin B administered per *i.v.* infusion over 1 h in humans. Polymyxin B plasma concentration without transporter kinetics assuming only glomerular filtration is presented in blue. Modeled polymyxin B plasma concentration including active transporter kinetics into proximal tubule cells are presented in red. Separated points represents *in vivo* data from published human study

<sup>4</sup> PBPK and QIVIVE modeling were performed by Dr. Nynke Kramer, Dr. Femke Taverne and Jiaqing Wu at the University of Utrecht - Institute for Risk Assessment Science (IRAS), in Utrecht, Netherlands, and kindly provided for this thesis.

predicted than in a simulation involving only glomerular filtration (Figure 47 – blue line) when compared with *in vivo* plasma concentrations achieved in patients after polymyxin B treatment (Figure 47 – separated points) (Zavascki *et al.*, 2008). Following PBPK modeling, the obtained *in vitro* data for KE1 (*Disturbance of lysosomal functions*) and for KE3 (*Cytotoxicity renal tubule cells*) were extrapolated to *in vivo* concentrations (Figure 48). A quantitative *in vitro*-to-*in vivo* extrapolation (QIVIVE) based on the nominal concentrations used in the *in vitro* assays resulted in modeled *in vivo* polymyxin B doses for KE1 and KE3 ranging from ~ 0.01 to 1 mg/kg body weight (Figure 48 – solid lines). These extrapolated *in vivo* doses, based on the nominal *in vitro* concentrations, were lower than the current polymyxin B doses used in clinical practice, which range from 0.75 - 1.25 mg/kg body weight (Falagas and Kasiakou, 2006, Kassamali *et al.*, 2015, Gupta *et al.*, 2009, Cai *et al.*, 2020a).

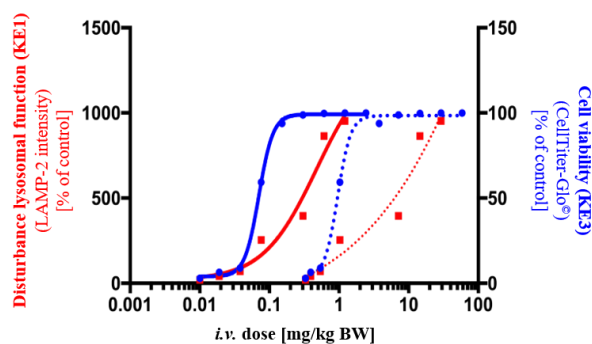


Figure 48

**Quantitative *in vitro*-to-*in vivo* extrapolation based on nominal and intracellular *in vitro* polymyxin B concentrations**

QIVIVE of polymyxin B concentrations obtained from KE1 (*Disturbance of lysosomal functions*) (solid red graph) and KE3 (*Cell toxicity*) (solid blue graph) from nominal *in vitro* polymyxin B concentrations used in *in vitro* assays. QIVIVE of polymyxin B concentrations obtained from KE1 (*Disturbance of lysosomal functions*) (dashed red graph) and KE3 (*Cell toxicity*) (dashed blue graph) from intracellular *in vitro* polymyxin B concentrations

In addition to extrapolation based on nominal concentrations, extrapolation based on intracellular concentrations was also performed. To determine a complete QIVIVE curve, the intracellular concentrations in RPTEC/TERT1 cells measured after treatment with 34  $\mu\text{M}$ , 62.5  $\mu\text{M}$ , and 125  $\mu\text{M}$  polymyxin B (see chapter 4.1.4.1; Figure 21 & Figure 22) were extrapolated (Figure 49 (B)). The modeling was based on an exponential increase in the concentration range between 0  $\mu\text{M}$  and 125  $\mu\text{M}$  and assumed a linear increase in the concentration range between 250  $\mu\text{M}$  and 2000  $\mu\text{M}$  (Figure 49 (B)). QIVIVE based on intracellular polymyxin B concentrations revealed *in vivo* doses between  $\sim 0.5$  to 1.5 mg/kg body weight that correspond well with the polymyxin B doses administered in clinical practice (0.75 - 1.25 mg/kg body weight) (Figure 48 – dashed lines).

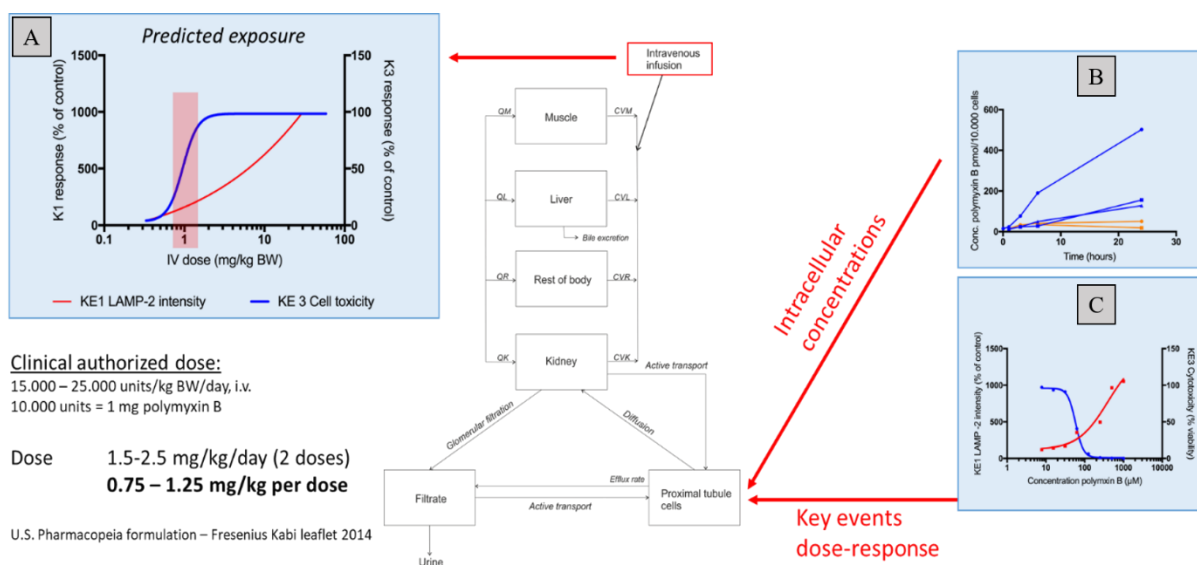


Figure 49

**Integration of *in vitro* biokinetic data, *in vitro* KE data and QIVIVE modeling for prediction of *in vivo* nephrotoxicity of polymyxin B**

(A) Predicted exposure for polymyxin B *in vivo* doses after integration of (B) *in vitro* biokinetic data and (C) *in vitro* KEs data resulted in more accurate extrapolated *in vivo* doses consistent with doses used in clinical practice

Integration of *in vitro* biokinetic data (Figure 49 (B)) as well as obtained data from *in vitro* KEs (Figure 49 (C)) supported the PBPK model to predict more accurately *in vivo* relevant human doses of polymyxin B (Figure 49 (A)). The obtained *in vitro* effect concentrations elicit an *in vivo* dose associated with nephrotoxicity and by modeling, *in vivo* nephrotoxic doses can thereby be predicted. The modeled polymyxin B data from the *in vitro* assays demonstrate that integration of biokinetic data and intracellular concentrations of model stressors is a prerequisite for extrapolation of human relevant *in vivo* doses from *in vitro* assays. This circumvents some limitations of *in vitro* assays such as altered intracellular uptake, which will in turn increase confidence for a risk assessment based on *in vitro* results.





## 5 Discussion

The goal of reducing animal testing in drug and chemical evaluation by integrating alternative animal-free methods has been the focus of toxicological research for years. Despite many efforts in the development of alternative methods, there are still several critical aspects of conventional *in vitro* methods in comparison to *in vivo* methods. The major points of criticism are altered metabolic activities (cancer cells), donor-to-donor variability (primary cells) and artificial, non-physiological conditions in cell cultivation (Hartung and Daston, 2009, Roggen, 2011). A further legitimate point of criticism, which is also regarded as a shortcoming of most *in vivo* methods, is the determination of apical endpoints. As a result, no information, or at most very limited information, can be obtained concerning the underlying mechanism leading to toxicity. However, bridging this mechanistic information gap can make a decisive contribution to a more scientifically based risk assessment (Rovida *et al.*, 2015b, Krewski *et al.*, 2009).

The present thesis aimed to examine whether the adverse outcome pathway concept is a strategic and targeted approach to develop more mechanism-based alternative methods useful for risk assessment. Therefore, AOPs were developed, describing kidney toxicity caused by (1) *Receptor-mediated endocytosis and lysosomal overload* and (2) *Inhibition of mtDNA polymerase- $\gamma$* , which served as case studies for systemic toxicity. Using publicly available information, key events were identified and integrated into the AOPs, which were subsequently quantified using model compounds and *in vitro* assays adapted to the key events. The dose-response data were then used to assess whether a prediction of the outcome is feasible using the key event relationship. *In vitro* points of departure were determined and compared with *in vivo* concen-

trations to demonstrate the comparability of both datasets regarding risk assessment. In the following sections the individual AOPs are discussed in more detail, as well as the use of *in vitro* data for a risk assessment.

### **5.1 AOP development for kidney injury due to *Receptor-mediated endocytosis and lysosomal overload* – a basis for an improved mechanistic *in vitro* approach**

The first presented AOP – *Receptor-mediated endocytosis and lysosomal overload*, focused on the mechanism leading to renal toxicity by polymyxin antibiotics, aminoglycosides or heavy metals bound to protein, such as the cadmium-metlothionein complex. Receptor-mediated endocytosis allows these compounds to enter the proximal tubule cells and the resulting disruption of lysosomal functions are decisive for the further progression of apoptosis and cell necrosis (Nielsen *et al.*, 2016, Oberle *et al.*, 2010, Quiros *et al.*, 2010). Based on the known and published knowledge about the mechanism leading to renal toxicity, a linear AOP was developed that includes important key events associated with the adverse outcome. With the application of model stressors for this pathway (polymyxin B, colistin, polymyxin B nonapeptide, CdCl<sub>2</sub>) (Nielsen *et al.*, 2016), the AOP and the *in vitro* assays were experimentally supported.

The MIE is defined as an interaction between a molecule (in this case that of polymyxin antibiotics and other stressors) and a biomolecule (in this AOP the cubilin:megalin complex), that lead to the adverse outcome (Allen *et al.*, 2014). Since the MIE is decisive for the further course of the pathway and indirectly responsible for the adverse outcome, a verification of biological plausibility as well as the essentiality of the MIE is of great interest and a necessary prerequisite for the establishment of AOPs (Coady *et al.*, 2019, Bal-Price and Meek, 2017, Edwards *et al.*, 2016, Patlewicz *et al.*, 2015).

### 5.1.1 Differences in cell line susceptibility due to different transporter expressions

Another important point of the AOP concept is to achieve a better understanding of the underlying mechanism in order to better compensate for possible differences and uncertainties (Ankley *et al.*, 2016). In particular, understanding the toxicological mechanism is essential when developing alternative methods for toxicological testing and risk assessment based on *in vitro* data (Sewell *et al.*, 2018). Results of the *in vitro* assays covering each KE (KE1 - *Disturbance of lysosomal function*, KE2 - *Disruption of lysosomes*, KE3 - *Cytotoxicity of renal tubule cells*) across the AOP – *Receptor-mediated endocytosis and lysosomal overload*, showed significant differences in the biological responses between NRK-52E and RPTEC/TERT1 cells after treatment with polymyxin antibiotics. Since not only differences between the cell lines were detected, but also a different biological response between the polymyxin antibiotics (PB > Col > PBNP) was measured, the question of the uptake of polymyxin antibiotics in the cells was of central interest. The different biological responses after treatment with polymyxin antibiotics in NRK-52E and RPTEC/TERT1 cells are consistent with published *in vitro* studies in kidney cells. Keirstead and colleagues showed the same biological ranking of polymyxins in HK-2 cells treated with PB, Col, and PBNP (Keirstead *et al.*, 2013). In order to test the hypothesis that cell line and compound related differences in the cytotoxicity of polymyxin antibiotics may be due to differences in the uptake of polymyxins into the cells, we analyzed intracellular concentrations of the different polymyxin derivatives in both cell lines. For this purpose, an intracellular time-concentration profile of polymyxin B and colistin in NRK-52E and RPTEC/TERT1 cells was generated using LC-MS/MS with prior purification of the analytes with SPE. A clear increase of both polymyxins was observed in the cell lines over time. It was particularly noticeable that accumulation of both polymyxin antibiotics (PB and Col) differed

significantly between RPTEC/TERT1 cells and NRK-52E cells. The intracellular polymyxin B and colistin levels after 24 h were up to 3.5 times higher in RPTEC/TERT1 cells compared to NRK-52E cells. The higher intracellular concentrations in the RPTEC/TERT1 cells compared to the NRK-52E cells, as well as the higher accumulation of polymyxin B compared to colistin in both cell lines support a direct correlation between compound uptake and toxic response. To further understand the relationship between intracellular concentrations of polymyxins and receptor-mediated endocytosis, uptake of Alexa-488 labeled aprotinin into RPTEC/TERT1 and NRK-52E cells was measured. Aprotinin is a small bovine pancreatic natural protein which is also known to be a ligand for megalin (Christensen *et al.*, 1998). With the labelled fluorescence dye Alexa-488, it was feasible to obtain fluorescence microscopic images of the absorbed and accumulated aprotinin in the cells. First fluorescence signals were measured 30 min after treatment with aprotinin. After 4 h a strong fluorescence signal was measurable in both cell lines. The images showed that Alexa-488 labeled aprotinin accumulated in punctual structures in the cytoplasm. These punctual staining indicated absorption and accumulation in lysosomes. A difference in fluorescence intensity between the cell lines was also visible, which was confirmed by the measurement of the intensity. RPTEC/TERT1 cells showed an almost two-fold higher intensity signal than the NRK-52E cells, which was congruent with the previous results with regard to the different uptake between the cell lines and which indicates a higher endocytosis activity in RPTEC/TERT1 cells.

Since the different uptake kinetics between the cell lines were demonstrated by LC-MS/MS and the aprotinin assay, we were interested to determine whether a different expression of the endocytic transporters is responsible for these effects. Because RPTEC/TERT1 cells have been

reported to express megalin, but immunofluorescence staining data were not convincing (Wieser *et al.*, 2008), we examined both cell lines for megalin expression.

In order to provide additional information about megalin expression and thus to allow a better comparison between both cell lines, fluorescence images of stained megalin were taken in both cell lines. Staining of megalin in the RPTEC/TERT1 cells was stronger than in the NRK-52E cells. These findings would underline the previous assumption of a higher megalin expression and activity in RPTEC/TERT1 cells compared to NRK-52E cells. Surprisingly, however, megalin staining in both cell lines was more prominent in the cytoplasm than on the cell membrane. Similar results in epithelial kidney cells were also observed by Nagai and (Nagai *et al.*, 2011). A Swedish program (The Human Protein Atlas), which started in 2003 with the aim of mapping all human proteins in cells, tissues and organs, showed similar results in CaCo-2, HEK293 and U-2 OS cells. The fluorescence images of megalin in CaCo-2, HEK293 and U-2 OS cells also showed localized staining to the mitochondria and vesicles but less signal at the cell membrane ([proteinatlas.org/ENSG00000081479-LRP2/cell#human](http://proteinatlas.org/ENSG00000081479-LRP2/cell#human)) (Uhlén *et al.*, 2005, Uhlén *et al.*, 2015, Uhlén *et al.*, 2010, Uhlén *et al.*, 2017, Thul *et al.*, 2017). Since the fluorescence images could not provide clear information about the expression of megalin in the cells, the expression of megalin was additionally measured at the mRNA level. Since specially designed primers for megalin and cubilin did not provide quantifiable results, TaqMan™ probes were used to increase the specificity of the quantitative PCR. In order to obtain a direct comparison to *in vivo* megalin mRNA expression, the mRNA level of megalin from rat kidney was analyzed in addition to the two cell lines. In addition, megalin mRNA expressions in HK-2 and CaCo-2 cells was determined, as information from the Human Protein Atlas indicated that CaCo-2 cells express megalin mRNA (Uhlén *et al.*, 2005, Uhlén *et al.*, 2015, Uhlén *et al.*, 2010, Uhlén *et al.*,

2017, Thul *et al.*, 2017). Megalin mRNA was detected in the rat kidney and in CaCo-2 cells, however no signals were evident in the other kidney cell-lines examined (NRK-52E, RPTEC/TERT1 and HK-2). These results in RPTEC/TERT1 and CaCo-2 cells are in line with the mRNA expression levels contained in the human protein atlas, which reports megalin mRNA expression in CaCo-2 cells but not in RPTEC/TERT1 cells (proteinatlas.org/ENSG00000081479-LRP2/cell#human) (Uhlén *et al.*, 2005, Uhlén *et al.*, 2015, Uhlén *et al.*, 2010, Uhlén *et al.*, 2017, Thul *et al.*, 2017). Interestingly, mRNA expression of cubilin was negative in rat kidney and all examined cell models. To support our immunocytochemical fluorescence imaging and the mRNA expression of megalin, immunoblotting experiments were performed.

Western blot analysis from cell lysate of NRK-52E cells showed no bands that could be associated with megalin, but clear bands in the range between 35 - 40 kDa could be detected from the cell lysate of rat kidney. Since the anti-megalin antibody used in this work is directed against the cytosolic domain of megalin, the bands between 35 - 40 kDa could be associated with the megalin carboxyl terminal fragment (MCTF) (Zou *et al.*, 2004). Recent studies show that this fragment is produced by regulated intramembrane proteolysis (RIP) of megalin. This process combines the receptor function of megalin with transcriptional regulation, similar to that of the Notch pathway (Biemesderfer, 2006). It has been demonstrated that megalin produces this 35 - 40 kDa C-terminal fragment (MCTF) by a protein kinase with C-regulated, metalloprotease-mediated ectodomain shedding (Zou *et al.*, 2004). This C-terminal megalin fragment serves as a substrate for membrane-resident secretase activity, which subsequently releases the free megalin intracellular domain (MICD) into the cytosol, whereupon the domain is transferred into the cell nucleus and acts as a transcription regulator (Biemesderfer, 2006, De *et al.*, 2014, Alan *et*

*al.*, 2019). This finding is also congruent with the fluorescence images from the NRK-52E and RPTEC/TERT1 cells. The staining with the anti-megalin antibody directed against the C-terminal end showed a strong punctured signal in the cytoplasm, which might indicate this C-terminal fragment.

The exact transcriptional function of this fragment has not yet been fully clarified, but it has been shown in cultured OKP cells (proximal tubule cells from the opossum kidney) that the C-terminal megalin fragment serves as a transcription regulator, thereby down-regulating megalin expression and other megalin regulating proteins such as sodium-hydrogen antiporter 3 (NHE3) (Li *et al.*, 2008). Biemesderfer and colleagues also showed that the shedding process and the megalin signaling pathway can be activated by megalin ligands such as vitamin D-binding protein (VDBP) and raised the legitimate question: which other megalin ligands might be involved in this activation process (Biemesderfer, 2006). Other megalin ligands that might be involved in the regulation are other (vitamin-) carrier proteins such as retinol-binding protein, albumin or hemoglobin as well as hormones and signaling proteins such as insulin, transferrin, epidermal growth factor (EGF) or angiotensin II (Marzolo and Farfán, 2011, Christensen *et al.*, 2012). Marzolo and Farfán showed that megalin mRNA expression is positively influenced by *e.g.*, retinoic acid, vitamin D or PPAR  $\alpha$  and  $\gamma$  (Marzolo and Farfán, 2011). However, it was also shown that transforming growth factor (TGF) has an important influence on megalin expression. Several recent *in vitro* studies in different epithelial cell lines have shown that TGF- $\beta$  has a negative effect on the expression of megalin. In OK cells (opossum kidney) it was shown that TGF- $\beta_1$  down-regulates the mRNA and protein level for megalin and cubilin (Gekle *et al.*, 2003). In RLE-6TN cells (rat lung epithelial-T-antigen negative) a reduced gene expression and a reduced cell surface stability of megalin was observed after TGF- $\beta_1$  exposure (Mazzocchi *et*

*al.*, 2017). Likewise, in LLC-PK1 cells (porcine kidney epithelial) and dGBEC cells (dog gallbladder epithelial) a correlation was observed between TGF- $\beta_1$  and a decrease in megalin mRNA as well as decrease at protein level (Cabezas *et al.*, 2019a). Furthermore, *in vitro* experiments have shown that epithelial cells, especially proximal tubule cells, are able to secrete TGF- $\beta_1$  (Phillips *et al.*, 1997, Fraser *et al.*, 2003, Briffa *et al.*, 2015, Cabezas *et al.*, 2019b). The release of TGF- $\beta_1$  in epithelial cells can be activated and further enhanced by the presence of albumin, as shown in OK cells (Gekle *et al.*, 2003, Diwakar *et al.*, 2007, Slattery *et al.*, 2013). Results from another study in OK cells showed that megalin expression decreased significantly under high albumin concentrations (Caruso-Neves *et al.*, 2006). In addition to albumin, it was also observed that long term treatment with glucose in HK-2 cells leads to activation of p38MAP kinase, which in turn leads to an increase in TGF- $\beta_1$  synthesis and thus to a decrease in megalin expression (Fraser *et al.*, 2003). De Barros Peruchetti and colleagues demonstrated that high glucose conditions inhibited megalin expression and albumin endocytosis in LLC-PK1 cells (de Barros Peruchetti *et al.*, 2018). More interestingly, in OK cells it was demonstrated that under high glucose conditions and insulin treatment the megalin expression at protein and mRNA level was significantly increased (Russo *et al.*, 2007, Bryniarski *et al.*, 2018). Further investigations showed that other ligands of megalin also play a role in the regulation of megalin. For instance, angiotensin II was also associated with a negative influence on the expression of megalin mRNA in OK cells (Hosojima *et al.*, 2009). Epidermal growth factor (EGF), which has a structural homology with TGF, is also a ligand for megalin and could therefore also be involved in the regulation of the shedding process (Todaro *et al.*, 1980, Christensen *et al.*, 2012). Detailed studies on the connection between EGF and the expression of megalin in epithelial cells are not available. However, studies in astrocytic tumor cells (U-251 MG and U-



1242 MG) showed that functional megalin on the cell surface was downregulated by EGF compared to control and megalin-mediated endocytosis was reduced by 50 – 60 %. This decrease was demonstrated by reduced megalin mRNA transcription and these data suggest that EGF mediates megalin down-regulation at least in astrocytic cells (Hussaini *et al.*, 1999).

The extent to which the ligands insulin and transferrin are involved in the expression of the transporters is open to question. More detailed studies on this relationship are lacking but should be questioned with regard to the other ligands associated with the regulation of the expression of megalin, such as glucose, EGF or vitamin D. Especially with regard to the composition of the culture media, which contains a number of these ligands but is nevertheless essential for the cultivation of the cells, should be critically questioned.

Unphysiological cultivation conditions, in particular for toxicological testing and risk assessment based on *in vitro* data, have often been critically reviewed (Pamies and Hartung, 2016). Aside from the composition of the culture media, the cultivation method, especially that of 2D cultivation, is also of great importance. There are many advantages of 2D cell culture systems, such as easy and cost-effective maintenance of cell cultures, ease of use, and ease of downstream processing (Ryan *et al.*, 2016, Kapałczyńska *et al.*, 2018). Furthermore, 2D systems are well established, well-proven and widely accepted, which is also the reason why they form the basis for a major part of current *in vitro* routine assays (Duval *et al.*, 2017, Kapałczyńska *et al.*, 2018). Moreover, a further important aspect and an additional argument for the use of 2D cultivation, also in this study is, that a large amount of information and literature are available (Joseph *et al.*, 2018, Edmondson *et al.*, 2014). However, if the more detailed circumstances of 2D cultivation are considered, elementary and essential differences are apparent. Under physiological conditions, the epithelial cells of the proximal tubule grow to a tube along with close

cell-cell contact and are perfused on the basolateral side as well as on the luminal side (Smith, 1951). There is therefore no cell contact to plastic or glass surfaces, as is the case in conventional 2D cultivation, and therefore no one-sided perfusion of the cells. This could have an influence on the orientation of the cells, which side of the cell is regarded as the luminal or basolateral side and thus also on the orientation of the influx and efflux transporters, which differ from the respective sides (Chu *et al.*, 2016, Zennaro *et al.*, 2014, Lash *et al.*, 2006). Among others, the Predict IV project (European Union's seventh Framework Programme (FP7 / 2007 - 2013)) showed that in RPTEC/TERT1 cells some transporters were expressed at mRNA and / or protein level (Aschauer *et al.*, 2015a, Wieser *et al.*, 2008), but the establishment of transporter assays was not successful (Tiong *et al.*, 2014). Also, cells after treatment were examined for the expression of known acute kidney injury (AKI) biomarkers such as clusterin (Vinken *et al.*, 2012, Dieterle *et al.*, 2010, Vaidya *et al.*, 2008) and KIM-1 (Pavkovic *et al.*, 2016, Huo *et al.*, 2010, Ichimura *et al.*, 1998). However, no upregulation of these AKI biomarkers after treatment were measured and it was concluded that possible cultivation conditions in 2D monolayers or membrane inserts were insufficient (Tiong *et al.*, 2014). A recently published study by the University of Constance, Germany, showed that the *in vitro* cultivation of RPTEC/TERT1 cells in a stable 3D tubular structure offers advantages over conventional 2D monolayer cultivation or cultivation on membrane inserts. The cells in 3D cultivation showed enhanced mRNA expression of transporters such as OCTs and MATEs and *de novo* expression of OAT3 compared to conventional cultivation methods (Secker *et al.*, 2018). In summary, it can be said that TGF- $\beta$  induced proteolysis as well as the presence of further megalin ligands in the culture medium, which can support intramembrane proteolysis, as well as

the cultivation method, does not exclude an altered or even disturbed megalin expression. This could also explain the absence of megalin mRNA in the cells.

Since an increase of intracellular concentration of polymyxin B and colistin was measured over time, the legitimate question arises as to how the model substances entered the cells. Furthermore, other potential or unknown mechanisms leading to polymyxin uptake should not be ignored. An *in vivo* study with megalin knockout rats showed that accumulation of polymyxin antibiotics was only slightly reduced in the kidney as compared to megalin expressing rats, suggesting other mechanisms responsible for the uptake into renal tubular cells (Suzuki *et al.*, 2013).

Besides receptor-mediated endocytosis via the megalin:cubilin complex, another uptake pathway into the proximal tubule cells has been described. Nonspecific fluid phase endocytosis is an additional uptake pathway for macromolecules along the proximal tubule (especially in the S1 and S2 segment) (Eshbach and Weisz, 2017, Schuh *et al.*, 2018). *In vivo* experiments in mice demonstrated that nonspecific fluid phase endocytosis was responsible for the uptake of dextran molecules (10 kD) which occurred equally in both S1 and S2 segments (Schuh *et al.*, 2018). This may explain the uptake of aprotinin and the polymyxin antibiotics into RPTEC/TERT1 and NRK-52E cells by a receptor independent uptake pathway.

From a structural point of view, polymyxin antibiotics are polypeptides, hence it is reasonable to assume that the peptide transporter 2 (PEPT2) in the proximal tubule, responsible for the reuptake of peptides, is also involved in the uptake of polymyxin B and colistin, as shown in several studies (Ma *et al.*, 2009, Lu *et al.*, 2015, Zavascki and Nation, 2017). Within the Human Protein Atlas project, it was shown that the expression of PEPT2 transporters is present in RPTEC/TERT1 cells at least at the mRNA level (Uhlén *et al.*, 2005, Uhlén *et al.*, 2010, Uhlén

*et al.*, 2015, Uhlén *et al.*, 2017, Thul *et al.*, 2017) (proteinatlas.org/ENSG000001 63406-SLC15A2/cell). This finding suggests an additional potential uptake pathway of polymyxins into the cells besides nonspecific fluid phase endocytosis and the megalin:cubilin complex.

Apart from the kidney, megalin is also expressed in many other tissues, such as parts of the brain and central nervous system, intestinal brush border, gall bladder, thyroid gland, eye, fallopian tubes, uterus and yolk sacs (De *et al.*, 2014, Fisher and Howie, 2006). Megalin thus has an important physiological importance in many tissues, but nevertheless the regulation and expression are still poorly understood, especially in the *in vitro* situation (Marzolo and Farfán, 2011). In addition, there are still open questions regarding polymyxin antibiotics that need to be answered. Especially with regard to the uptake of substances into the cells. As mentioned above, there is also evidence that polymyxins can be taken up into cells via PEPT2 transporters (Zavascki and Nation, 2017, Lu *et al.*, 2015, Ma *et al.*, 2009) or nonspecific fluid phase endocytosis (Schuh *et al.*, 2018), which leads to a different understanding of the pharmacokinetics. This data could also be included in the assessment to improve the understanding of the key event relationship between the MIE and the downstream KEs and finally to the adverse outcome. This is also of great relevance with regard to the necessary implementation of quantitative *in vitro* to *in vivo* extrapolation (QIVIVE), which will be discussed in more detail in the later part of the discussion. To answer the question about the biological relevance and essentiality of the MIE, a clear answer might be obtained by measuring the intracellular concentration of model substances after treatment of megalin knock-out cells, which could also provide a better indication of the essentiality of downstream KEs. However, in the absence of megalin/cubilin in the *in vitro* systems, perhaps a refinement strategy for the AOP would be appropriate, defining the MIE simply as “*Endocytosis*” rather than as “*Receptor-mediated endocytosis*”.

It is important to note that in this linear AOP not all KE that lead to a reduction of cell viability were included. For example, the caspase pathway, which leads to polymyxin B mediated apoptosis (Quiros *et al.*, 2010), is a potential mechanism that should not be disregarded and might also be included in the AOP. It has already been shown that cellular apoptosis mediated by polymyxin B is triggered by a temporal and concentration-dependent activation of the caspase pathways (Azad *et al.*, 2013, Azad *et al.*, 2015). The addition of further MIEs and KEs to the AOP is essential for mechanistic reasons, but this makes the AOP more complex and a prediction of the downstream KEs, as discussed in the later chapter, more difficult.

### **5.1.2 Predicting downstream key events by using key event relationships from the AOP – Receptor-mediated endocytosis and lysosomal overload**

Another important part of this work was to use the developed mechanistic framework and the *in vitro* results obtained from the individual KEs to establish quantitative relationships between KEs in order to test whether a prediction of downstream KEs is possible. One way to establish the quantitative relationship between KEs is to build response-response plots as described in the open-knowledge and structured platform Effectopedia (OECD, 2016). This method of response-response plots to describe the quantitative relationship between the KEs was also described in the work of Conolly and colleagues (Conolly *et al.*, 2017). In order to generate response-response plots, a sufficient amount of data from two dose-response curves measured on both sides of a relationship has to be available. Ideally, these data come from a single study conducted under the same experimental conditions and using the same tested concentrations from the same chemical substance (OECD, 2016). Since the prerequisites were fulfilled in the AOP – *Receptor-mediated endocytosis and lysosomal overload* after treatment with polymyxin B, response-response plots were generated based on these computed data. Before, response-response plots were generated, additional data were computed to generate a sufficient amount of data in order to obtain a better description of the dose-response curves. Therefore, the best fit function of the dose-response curves for KE1-3 was determined using the online application PROAST and additional data were calculated from the resulting mathematical equation. The advantage of this procedure is that additional non-tested concentrations can be included in the response-response plots, especially lower and higher concentrations and also larger gaps between the concentrations can be compensated. The disadvantage is, however, that if there is a missing response at higher concentrations, it is not clear whether the curve description takes on *e.g.*, an exponential function or a sigmoid function, the calculation of further data becomes

purely speculative. This makes it very difficult or in some cases even impossible to determine a best fit model. Thus, the dose-response curves should cover a wide range in order to obtain a correct dose-response curve description. With the additional computed data after polymyxin B treatment, response-response plots were generated. For this calculation, the data of the dose-response from KE2 - *Disruption of lysosomes* was generated as a function of the data of the dose-response from KE1 - *Disturbance of lysosomal function*. The resulting curve describes the quantitative relationship between KE1 and KE2 (qKER<sub>1</sub>). Likewise, the response-response curve and thus the quantitative relationship between KE2 and KE3 (qKER<sub>2</sub>) was created from KE3 - *Cytotoxicity of renal tubule cells* data as a function of KE2 - *Disruption of lysosomes*. From both response-response plots obtained, a best fit model was then determined using PROAST and the resulting mathematical function describes the quantitative relationship of the KEs. With these mathematical descriptions of the relationships of the KEs, it was possible to calculate how much change in KE1 leads to a change in KE2, which in turn triggers a change in KE3.

In order to test whether this quantitative relationship, based on polymyxin B data, can be used to predict downstream KEs for other stressors associated with the same AOP, data from KE1 after colistin, PBNP treatment and data after CdCl<sub>2</sub> treatment were used. Additional data points from KE1 after colistin, PBNP and CdCl<sub>2</sub> treatment were calculated using the same procedure as described above. These data from KE1 were then used to predict the response in KE2 and the response in KE3 using the mathematical description of the KERs based on polymyxin B data. The predicted response for colistin in KE3 in RPTEC/TERT1 cells was close to the experimentally determined cytotoxicity. The overall measured cytotoxicity of PBNP was low and was also predicted as such, with minor variations at the highest tested concentrations.

Since the response in KE1 after PBNP treatment was found to be extremely low compared to colistin and polymyxin B, the predicted effects in downstream KE2 and KE3 were also found to be very low. More clearly, these effects were seen in the NRK-52E cells. Based on the polymyxin B data, the downstream KEs for colistin and PBNP could also be predicted for the NRK-52E cells, but lower cytotoxicity was predicted for both compounds compared with the cytotoxicity that were measured from the *in vitro* assays. A further reason for the poorer prediction in KE3 could be that not all KEs leading to cytotoxicity were part of the AOP and were therefore missed in the prediction calculation. As mentioned at the beginning of the chapter on the mechanism (see chapter 1.3.1), other pathways may contribute to cytotoxicity in proximal tubule cells, *e.g.*, oxidative stress or activation of caspase may be an essential part of this mechanism but are missing in the calculation respectively prediction.

In the AOP – *Receptor-mediated endocytosis and lysosomal overload* the first effects associated with the KEs were observed after a few hours. If cellular effects associated with the AO can be detected in a shorter time than the usual 24 h, *in vitro* assays can be performed faster, which would be a massive time and cost saving. The biggest challenge here will be the integration of all MIEs that are directly or indirectly linked to the AO. Especially when MIEs are events that describe the uptake of substances into the cells, as demonstrated by the example of the AOP – *Receptor-mediated endocytosis and lysosomal overload*. If, substances can be taken up into the cells via several transport pathways, *e.g.*, not only via the megalin: cubilin complex but possibly also as described above in the case of the AOP – *Receptor-mediated endocytosis and lysosomal overload* via unspecific fluid phase endocytosis (Schuh *et al.*, 2018) and PEPT transporters (Zavascki and Nation, 2017, Lu *et al.*, 2015, Ma *et al.*, 2009), a thorough evaluation of the MIEs should be performed. One limitation of the AOP concept is the lack of kinetics, which is not



included in an AOP. But especially here in the example of AOP - Receptor-mediated endocytosis and lysosomal overload, kinetic proved to be an important factor, since the affinity of stressors to the megalin:cubilin complex is essential for accumulation in lysosomes. It becomes particularly interesting for substances that trigger the same mechanism and KEs leading to the AO but can be taken up into the cells via many different uptake pathways. A prominent example of its toxicity in the proximal tubule cells is cadmium. After absorption into the organism, cadmium is transported to the liver and induces the synthesis of metallothionein in the hepatocytes, which bind cadmium and thus buffer the toxic effect. This Cd-metallothionein complex can then be absorbed into the proximal tubule cells via the megalin:cubilin complex (Sabolić *et al.*, 2010). Also, the high affinity of cadmium to thiol-groups allows cadmium to form conjugates with cysteine and glutathione and these Cd-thiol conjugates can in turn be taken up into the proximal tubule cells via the same mechanism (Prozialeck and Edwards, 2012). Further uptake pathways of cadmium into the proximal tubule cells have been described via zinc and calcium transporters and via DMT1 and OCT1/2 transporters (Yang and Shu, 2015). The prediction for the polymyxin antibiotics based on polymyxin B in general looked good and reflected the observed cytotoxicity well. However, the example of CdCl<sub>2</sub> showed that the prediction of downstream key events was poorer for a stressor potentially involving multiple mechanisms leading to the adverse outcome. Thus, CdCl<sub>2</sub> was predicted to have much weaker cytotoxicity in both cell lines based on the key event relationships of polymyxin B, compared with the measured cytotoxicity obtained from the *in vitro* assay. Notable here is that in the *in vivo* situation, cadmium is presumably predominantly bound to metallothionein and this Cd-metallothionein complex is taken up into the cells via megalin:cubilin complex (Klaassen *et al.*, 2009, Sabolić *et al.*, 2010, Prozialeck and Edwards, 2012, Järup *et al.*, 2000, Simon *et al.*, 2014b, Wolff *et al.*, 2011),

whereas in this *in vitro* study the cells were simply treated with CdCl<sub>2</sub>. Hence, it might be reasonable to assume that KE1 describes the *in vivo* toxicity more accurately than the *in vitro* toxicity. These findings of the different uptake pathways are not only important with regard to kinetics and for the construction of the AOP, but also show in advance direct requirements for the *in vitro* assays. The absence of metallothionein could have an effect on the intracellular concentration and consequently on the adverse outcome (Perkins *et al.*, 2019).

### **5.1.3 Estimation of risk using *in vitro* data obtained from the AOP – Receptor-mediated endocytosis and lysosomal overload**

Another focus of this thesis was to obtain a first rough estimate for a risk assessment based on *in vitro* results. The question of a suitable *in vitro* point of departure (PoD) to receive a starting point for risk assessment posed the first challenge. Since there is no consensus in the scientific community about an appropriate PoD (Green *et al.*, 2013), the most common PoDs, such the Benchmark approach (BMC<sub>10</sub>) and the no / lowest observed effect concentration (NOEC / LOEC) were applied. The advantages and disadvantages of this strategy quickly became apparent. Due to the fact that not each approach was suitable for the calculation of a PoD, *e.g.*, the non-toxic concentration (NtC) approach, which does not calculate a non-toxic concentration for a non-sigmoid dose-response, or the effective concentration (EC<sub>x</sub>) approach, which is unsuitable for an exponentially increasing dose-response curve, the LOEC / NOEC or the BMC<sub>10</sub> approach were able to close the gaps. As different as the individual approaches are, the deviations between the individual PoDs were also varying. In some cases, 1000-fold concentration differences were observed between the PoDs. This broad variation was particularly noticeable in KE1 – *Disturbance of lysosomal function*. The NOEC / LOEC approach typically resulted in the PoD at the highest concentrations, while the BMC<sub>10</sub> / BMCL<sub>10</sub> were more conservative and

resulted in lower PoD. The NOEC, LOEC, and BMC<sub>10</sub> approaches were selected for MOE calculation since they were determinable across all *in vitro* assays, capture the range of all other PoDs, and represent the most common PoDs used in practice. After calculating the MOEs for all three key events in both cell lines based on the three selected PoDs as well as serum and kidney concentrations from *in vivo* studies, the range of MOEs was very broad, with values ranging *e.g.*, from 0.32 to 1075 for polymyxin B. The increased susceptibility of the RPTEC/TERT1 cells became noticeable, as the overall MOEs values from the RPTEC/TERT1 cells were lower compared to the overall MOEs from the NRK-52E cells. The lowest MOE values associated with a risk of renal toxicity were obtained using the more conservative BMC<sub>10</sub> approach in combination with *in vivo* kidney concentrations, as in the kidney tissue higher polymyxin antibiotic concentrations were found compared to serum. Interestingly, apart from the MOE calculated based on BMC<sub>10</sub> values, the MOE values of the early key event KE1 - *Disturbance of lysosomal function*, revealed higher MOE values and were thus associated with lower risk for kidney toxicity than those of the late key event KE3 - *Cytotoxicity of renal tubular cells*. Usually, it would be expected that the MOE values of an earlier key event are lower than those of a later key event, since the response must occur earlier temporally even before a later key event is triggered and, accordingly, the *in vitro* response must be more pronounced. However, the different sensitivity of the applied *in vitro* assays should be considered, as their sensitivity may have a significant influence on the risk assessment. For example, if a very sensitive *in vitro* assay is used for KE3 compared to a less sensitive *in vitro* assay for KE1, lower PoDs will result from KE3, resulting in a lower MOE for the late key event. In particular, considering the high sensitivity of modern and improved bioassays, which are now able to detect effects at sub-femtomole levels and are not only limited to omics analyses, but are now also used as *in*

*in vitro* spectroscopy assays or enzyme-linked immunosorbent assays (Cohen *et al.*, 2020, Huang and Chen, 2018, Yu *et al.*, 2004).

In general, an improved strategy should be applied, the so called Next Generation Risk Assessment (NGRA) (Gilmour *et al.*, 2020, Dent *et al.*, 2018). Accordingly, a human equivalent concentration should be extrapolated from the *in vitro* data by using suitable PBPK models and QIVIVE as demonstrated for polymyxin B (Moxon *et al.*, 2020, Mallick *et al.*, 2020, Yu *et al.*, 2020, Poet *et al.*, 2016). After integration of safety factors, this PoD could be used as a basis to arrive at a human reference dose (RfD) (Crump *et al.*, 2010).

## **5.2 AOP development for kidney injury due to *Inhibition of mtDNA polymerase- $\gamma$* – a basis for an improved mechanistic *in vitro* approach**

The second AOP – *Inhibition of mtDNA polymerase- $\gamma$*  presented here describes the mechanism leading to renal toxicity by inhibition of mitochondrial DNA polymerase- $\gamma$ . This inhibition is mostly associated with antiviral drugs from the group of acyclic nucleoside phosphonates (Fernandez-Fernandez *et al.*, 2011). Prominent representatives of this group are drugs used against hepatitis or HI viruses such as cidofovir, adefovir, tenofovir and the associated prodrugs adefovir dipivoxil or tenofovir disoproxil fumarate (Reynaud *et al.*, 2009, De Clercq, 2003). Via organic anion transporters such as OAT1 and OAT3, these drugs enter the cells, incorporate into the mtDNA, inhibit the mitochondrial DNA polymerase- $\gamma$  and finally lead to a reduction of the mtDNA copy number (Fernandez-Fernandez *et al.*, 2011, Hagos and Wolff, 2010). As a result, essential proteins of the respiratory chain are insufficiently expressed or not expressed at all, leading to damage in the proximal tubule cells (Perazella, 2010, Markowitz and Perazella, 2005, Tanji *et al.*, 2001). The development of this linear AOP focused on current knowledge of the mechanism leading to cytotoxicity in proximal tubule cells by antiviral drugs. After *in vitro* assays were established for the individual KEs, this AOP and the *in vitro* assays were experimentally evaluated with model substances (adefovir, cidofovir, tenofovir, adefovir dipivoxil, tenofovir disoproxil fumarate).

After 24 h treatment with the model compounds, the response of the first KE (*Depletion of mtDNA copy number*) in both cell lines was unexpected. Contrary to what is known from *in vivo* studies (Menezes *et al.*, 2013, Lebrecht *et al.*, 2009, Markowitz and Perazella, 2005, Tanji *et al.*, 2001), there was no decrease in the mtDNA copy number in the first KE. In contrast, cidofovir, tenofovir and tenofovir disoproxil fumarate resulted in an increase in mtDNA copy

number, whereas a concentration-dependent decrease in cell viability was observed only for TDF. More importantly, a concentration-dependent decrease in cell viability was measured for the prodrugs ADV and TDF in the absence of biological effects on KE1. No or only low toxicity was observed for the other model substances. The assumption was that a treatment for 24 h was not sufficient to reflect the *in vivo* results after long-term treatment. This is partly due to the fact that the active metabolites adefovir, cidofovir and tenofovir may not be sufficiently taken up by the cells due to the absence of relevant transporters (*e.g.*, OAT1/3) in the cells, which is essential for the uptake of these substances resulting in the absence of toxicity. On the other hand, the treatment time of 24 h for the membrane-permeable prodrugs was insufficient to express effects on the mtDNA copy number. However, other studies also suggest that an increase in mtDNA copy number may be a protective mechanism of epithelial cells against apoptosis and could occur before a decrease in mtDNA copy number results (Mei *et al.*, 2015). These results also highlight the need for long-term treatment beyond the usual 24 h to simulate long-term effects in *in vitro* systems observed in *in vivo* studies. One advantage of RPTEC/TERT1 cells over most cell lines is that they can be cultivated over a longer period of time, allowing treatment times up to 14 days (Crean *et al.*, 2015, Limonciel *et al.*, 2011). Daily treatment with prodrugs over 14 days in RPTEC/TERT1 cells showed a decrease in mtDNA copy numbers in response to the prodrugs ADV and TDF. Following treatment with tenofovir and adefovir, however, only a very slight decrease was observed. Treatment with cidofovir for 14 days resulted in an increase in mtDNA copy number, whereas no effects in mtDNA copy number were observed during 24 h treatment, which might be due to the long-term treatment. With the exception of tenofovir, all model compounds resulted in a concentration-dependent decrease in cell viability, which was most pronounced after treatment with the prodrugs since they are expected

to be better taken up into the cells over time and uptake is not transporter-dependent as in the case of the active metabolites.

With regard to the mechanistic background, the *in vitro* results for KE1 and KE3 obtained after adefovir, cidofovir and tenofovir treatment were of particular interest. Based on the results, in particular those of the mtDNA copy number, the question arose about the uptake of the substances into the cells. It is known that antiviral drugs of the acyclic nucleoside phosphonates group are taken up into proximal tubule cells via organic anion transporters such as OAT1 / OAT3 (Nieskens *et al.*, 2016, Ortiz *et al.*, 2005, Cihlar *et al.*, 2001, Ho *et al.*, 2000). *In vitro* studies with cells overexpressing OAT1/3 or with stable transfected OAT1 and OAT3 transporters showed higher cytotoxicity after treatment with adefovir, cidofovir or tenofovir than cells without these transporters (Nieskens *et al.*, 2016, Zhang *et al.*, 2015, Ho *et al.*, 2000). As in the AOP – *Receptor-mediated endocytosis and lysosomal overload*, the question about the expression pattern of transporters is of central relevance for the biokinetic understanding. Although expression of some transporters at mRNA or protein level was reported in RPTEC/TERT1 cells (Aschauer *et al.*, 2015a), establishment of transporter assays was not successful (Tiong *et al.*, 2014), which may imply downregulated expression or impaired expression with non-functional transporters. Of note, rapid loss of OAT1/3 transporters was observed in cultured proximal tubule epithelial cells (Nieskens *et al.*, 2016). Furthermore, several studies, including the Human Protein Atlas project failed to detect expression of OAT1 (SLC22A6) and OAT3 (SLC22A8) transporters in NRK-52E and RPTEC/TERT1, suggesting the absence of these transporters (Uhlén *et al.*, 2005, Uhlén *et al.*, 2015, Uhlén *et al.*, 2010, Uhlén *et al.*, 2017,

Thul *et al.*, 2017, Lash *et al.*, 2007, Heussner and Dietrich, 2013, Lechner, 2014) (proteinatlas.org/ENSG00000197901-SLC22A6/cell) and (proteinatlas.org /ENSG00000149452-SLC22A8/cell).

In addition to the expression of influx transporters, expression of efflux transporters such as the multidrug resistance protein (MRP4 or ABCC4) could also play a decisive role in the excretion of antiviral drugs (Rodríguez-Nóvoa *et al.*, 2010, Ray *et al.*, 2006, Izzedine *et al.*, 2005). In MRP4 knockout (KO) mice, accumulation of adefovir and tenofovir in the kidney was reported to be significantly increased compared to wild type mice (Imaoka *et al.*, 2007). With regard to the accumulation time of the stressors in the cells, it is important to know how and to what extent the substances enter the cells, but also how long they accumulate in the cells and how and to what extent they are excreted. This was also clearly demonstrated in the study by Kohler and colleagues who showed the roles of OAT1 and MRP4 in the transport and regulation of tenofovir in the proximal tubule. They evaluated renal toxicity of tenofovir in OAT1 KO or MRP4 KO mice compared to wild type mice. A change in mtDNA content remained unchanged in the OAT1 KO mice indicating a loss of tenofovir transport. In contrast, the renal proximal tubules of MRP4 KO mice after tenofovir treatment showed an increased mtDNA abundance indicating compensation (Kohler *et al.*, 2011). These correlations of equilibrating transport processes, which play a role in the intracellular accumulation of foreign substances and cytotoxicity, were also illustrated *in vitro*. Stray and co-workers showed that overexpression of OAT1 and OAT3 increased cytotoxicity in HEK293T embryonic kidney cells, while co-transfection of MRP4 led to a decrease in cytotoxicity (Stray *et al.*, 2013). Studies with RPTEC/TERT1 cells showed overexpression of MRP4 transporter (Uhlén *et al.*, 2005, Uhlén *et al.*, 2015, Uhlén



*et al.*, 2010, Uhlén *et al.*, 2017, Thul *et al.*, 2017, Aschauer *et al.*, 2015a) (proteinatlas.org/ENSG00000125257-ABCC4/cell) and thus an increased efflux of xenobiotics can be assumed.

These two examples show the importance of the balance between influx and efflux transporter, hence the biokinetics. This is also an important source of uncertainty from *in vitro* systems that needs to be known in order to implement target-specific tools to overcome them. Of particular importance here is the fact that substances can thus have a short mean residence time (MRT) in the cells, which is an important pharmacokinetic parameter (Ďurišová, 2012). The resulting altered biokinetics leads to a shift in the sensitivity of the *in vitro* systems compared to the *in vivo* situation and results in less toxic effects or even lack of toxic effects.

This AOP is an exemplary case in which the limitations of short-term exposure in *in vitro* systems become obvious. On the one hand, conventional cell models do not always allow to mimic long-term effects that occur *in vivo* after chronic application due to limited cultivation time. On the other hand, modified pharmacokinetic, caused by an altered expression of relevant transport systems in comparison to the *in vivo* situation, is also crucial for the outcome. Nevertheless, after identifying such limitations and the differences in pharmacokinetics, it is possible to overcome them with, for example, by using the prodrugs, *in vitro* biokinetics data, and targeted PBPK modeling.

Another point that should not be disregarded and was also discussed in the previous chapter (see chapter 5.1.1) in the case of the AOP – *Receptor-mediated endocytosis and lysosomal overload*, is the cultivation method. The cultivation of RPTEC/TERT1 cells in a 3D model showed that a more *in vivo* like environment could be advantageous for cell orientation and differentiation. Expression of important influx transporters that could not or only partially be

detected in 2D monolayer cultured cells could be detected in the 3D model (*e.g.*, *de novo* expression of OAT3). The 3D cultured RPTEC/TERT1 cells also showed a slight decrease of MRP4 mRNA compared to the differentiated cells in the 2D culture (Secker *et al.*, 2018). Based on the mRNA expression results of the 3D culture, an investigation of the biokinetics of adefovir, cidofovir and tenofovir would now be of great interest and could provide further understanding of the mechanism. The results from the present AOP – *Inhibition of mtDNA polymerase- $\gamma$* , however, suggest possible further pathways respectively key events related to the AO that may lead to a better understanding of the mechanism. Especially the results of the prodrugs (ADV and TDF) after 24 h treatment are of interest. The response in KE3 showed a strong concentration-dependent decrease of cell viability in both cell lines treated with prodrugs after 24 h, whereas no effects on KE1 is contradictory to the *in vivo* findings. Therefore, a causal relationship between depletion of mtDNA and cytotoxicity is not supported by these data. The uptake of prodrugs into the cells does not take place via organic anion transporter as in the case of the parent compounds adefovir and tenofovir, but rather via passive diffusion (Darsazan *et al.*, 2018, Taneva *et al.*, 2016, Ming and Thakker, 2010). Absorbed in the cells, the prodrugs undergo an enzymatic degradation to their active forms adefovir respectively tenofovir. Enzymatic degradation requires the presence of carboxylesterases (CES) and phosphodiesterases (PDE) (Geboers *et al.*, 2015). Although not all but most phosphodiesterases are expressed in RPTEC/TERT1 cells (PDE1A / C, 3A - 11A, 4B / C / D, 6B / D, 7B, and 12) (proteintlas.org/search/phosphodiesterase), only the expression of CES2 and a very weak expression of CES3 (proteintlas.org/search/carboxylesterase) was measured on the carboxylesterase side, which represents the first step of hydrolysis of the prodrugs (Uhlén *et al.*, 2005, Uhlén *et al.*, 2015, Uhlén *et al.*, 2010, Uhlén *et al.*, 2017, Thul *et al.*, 2017). In order to incorporate into the

mtDNA, the prodrugs must first be hydrolyzed by CES (Geboers *et al.*, 2015). Due to the low expression of CES and an imbalance of the enzymes to the disadvantage of the first hydrolyzing step, only a small fraction of prodrugs may be hydrolyzed, and the prodrugs may not be recognized as substrate for the DNA polymerase due to their phosphate groups. Therefore, the cytotoxicity observed in response to antivirals may be induced by additional mechanisms. An *in vivo* study with male rats treated with TDF to induce renal injury showed an activation of caspase 3 and the release of cytochrome C in the cells that leads to the activation of the intrinsic pathway of apoptosis (Ramamoorthy *et al.*, 2019, Quiros *et al.*, 2010). Increased production of reactive oxygen species (ROS) and reactive nitrogen species (RNS) was also observed, leading to increased mitochondrial damage (Abraham *et al.*, 2013, Ramamoorthy *et al.*, 2014, Ramamoorthy *et al.*, 2012). According to the *in vitro* results describing KE1 – KE3 in the AOP – *Inhibition of mtDNA polymerase- $\gamma$* , there are similarly open questions about the mechanism, as noted in the AOP – *Receptor-mediated endocytosis and lysosomal overload*, presented above. Additional mechanisms and thus also further KEs in connection with the AO cannot be completely excluded. The sequence of KEs in this AOP may well be correct and equally biologically plausible, but a suspected stressor of this AOP may also act via other mechanisms respectively AOPs as well, so that the *in vitro* results obtained for this stressor might not or only partially support this AOP. This does not immediately imply that this sequence of KEs is incorrect, but rather suggests that the stressor is not specifically acting only via this sequence of KEs. Which KEs finally have a key role with regard to the AO or whether an activation of several KEs is necessary that eventually lead to the AO must then be clarified and is open to question. Especially with regard to regulatory endpoints, an exact mechanistic understanding of the toxicity pathway is of major relevance (Sachana, 2019, Leist *et al.*, 2017).

### **5.2.1 Predicting downstream key events by using key event relationships from the AOP – Inhibition of mtDNA polymerase- $\gamma$**

For the AOP – *Inhibition of mtDNA polymerase- $\gamma$*  the same strategy as for the AOP – *Receptor-mediated endocytosis and lysosomal overload* was applied to test if a prediction of downstream KEs is feasible using the key event relationship. Quantitative relationships between key events were also generated via response-response plots as described on the open-knowledge and structured platform Effectopedia (OECD, 2016). The *in vitro* results showed that only the data obtained from RPTEC/TERT1 cells after 14 d treatment with adefovir dipivoxil were suitable for the generation of response-response plots, since responses across all key events were measured that enable to generate key event relationships. The data sets of the dose-response curves after 14 d treatment showed sufficient responses to determine best fit functions using the online application PROAST. This allowed to calculate further data which were used to generate a description of the dose-response curve. With the additional data obtained, response-response plots were generated, which covered a wide concentration range and allowed a prediction. Since 24 h treatment showed an increase rather than a decrease in mtDNA copy number, the *in vitro* results from RPTEC/TERT1 cells after 14 days' treatment with tenofovir disoproxil fumarate corresponded more to observations made in *in vivo* studies in which a decrease was also shown and were more suitable for the prediction of downstream key events. However, this case showed the first limitations. A best-fit function and thus a calculation of additional data for TDF describing the KE1 - *Depletion of mtDNA*, proved not to be feasible, because the results from the *in vitro* assay contained a response that was too low to determine a best-fit function. To obtain additional data in the measurement range of the KE1 - *Depletion of mtDNA*, data of the dose-response curve in the tested range from 0.24 to 62.5  $\mu\text{M}$  were manually selected and plotted. This ensured, at least for a prediction, that sufficient data sets for TDF were available in this

concentration range. A further limitation was revealed in the prediction of KE3 of TDF utilizing the key event relationship between KE2 and KE3 (qKER2) based on the ADV data. Predicted cytotoxicity of TDF resulted in values  $> 50,000\%$  and were far out of the measurable range. Closer examination of the *in vitro* results revealed that cytotoxicity was measured in the late key event (KE3) even before mitochondrial toxicity was measured in KE2. Predicting based on this key event relationship in order to quantify how much effect is needed in the upstream key event to achieve an effect in the downstream key event can therefore not be made. A reason for this limitation might be the sensitivity of the *in vitro* assays applied. If a highly sensitive assay is used for a downstream key event and a less sensitive assay is used for an upstream key event, and effects are observed in the late key event before effects are measured in the earlier key event, a prediction cannot be made based on this established key event relationship. Nevertheless, to allow prediction of the cytotoxicity of TDF, a key event relationship was established between KE1 and KE3 and KE2 was skipped.

The prediction of KE3 – *Cytotoxicity* was therefore limited to the tested concentration range in which a response was observed for TDF in KE1 – *Depletion of mtDNA* and to the key event relationship between KE1 and KE3 (qKER<sub>1A</sub>) based on ADV data. The range in KE3 – *Cytotoxicity*, where the strongest decrease was measured, could therefore not be predicted. As a result, important information about key downstream events may be lost, since it is precisely in this concentration range that the greatest decrease in cell viability was measured. It is important on one hand to identify exactly this range where toxicity starts, but on the other hand an entire dose response curve is an essential prerequisite for the accurate calculation of PoDs. Time-resolved dose-response analyses might circumvent this limitation. Consequently, the calcula-

tion of PoDs is becoming progressively more difficult. Moreover, based on the predicted results, false conclusions may be drawn, such as a lower toxicity or even lack of cytotoxicity. The AOP – *Inhibition of mtDNA polymerase- $\gamma$*  showed in an exemplary way that in some cases longer treatment times are necessary to mimic effects observed in *in vivo* studies. Therefore, for a better quantitative characterization it would be advantageous if not only dose-dependent but also time-dependent data were tested and integrated into the AOPs (Leist *et al.*, 2017). From these time-dependent data, adaptive or compensatory effects of upstream key events could be detected earlier, even before excessive cytotoxicity occurs (Spinu *et al.*, 2019).

### **5.2.2 Estimation of risk using *in vitro* data obtained from the AOP – *Inhibition of mtDNA polymerase- $\gamma$***

As in the AOP – *Receptor-mediated endocytosis and lysosomal overload* the *in vitro* results of the AOP – *Inhibition of mtDNA polymerase- $\gamma$*  were used to obtain a first rough estimation of risk. Parallel to the strategy applied in the AOP – *Receptor-mediated endocytosis and lysosomal overload*, different points of departure from each key event were calculated and compared with serum concentrations from human and rat studies achieved after therapeutic treatment. For completeness, the results after 24 hours of treatment were also used to calculate points of departure. However, special consideration is required regarding the first key event – *Depletion of mtDNA copy number*. After 24 hours of treatment, the first key event showed an increase of mitochondrial DNA copy numbers, which were contrary to the reported *in vivo* findings and which might indicate a cellular defense mechanism (Mei *et al.*, 2015, Kohler *et al.*, 2011). However, they are observed *in vitro* effects after all, and these results may thus be of great interest for risk assessment. This raises important questions: which key events should be considered for risk

assessment? When must a key event be classified as an adverse effect and when as a non-adverse effect, an adaptive effect, or a compensatory effect? Should adaptive or compensatory events be included in the AOP and in the evaluation? If compensatory or adaptive effects are included in a linear AOP, and the cells have thus built up a protective function, there will be none or at least a reduced response in the subsequent key event(s). Thus, for example, cytotoxicity would not occur or would at least be less significant. However, it would be of high interest and benefit to know when a compensatory effect changes and an adverse outcome occurs, since this effect must take place before the first effect of the following key event emerges, which highlights the need for quantitative AOPs and quantitative information about key event relationships (Spinu *et al.*, 2019, Sewell *et al.*, 2018, Leist *et al.*, 2017).

After 14 days of treatment in RPTEC/TERT1 cells, the data showed that PoDs for ADV were lower and were now clearly in the range of rat and human serum concentrations compared to PoDs obtained after 24 h treatment. In contrast, after 14 days of treatment with TDF the PoDs, especially those for KE3 (cytotoxicity), showed little changes compared to PoDs obtained after 24 h treatment and were still between 10 - 100 times above the serum concentrations. Mostly calculated MOE values for adefovir and tenofovir were above 1000 for all 3 KEs, with only a few exceptions, and in some cases even for early KEs well above 10,000 and can thus be interpreted as a low risk for renal toxicity. In comparison, the calculated MOE values for the prodrugs ADV and TDF were clearly lower, averaging in ranges < 100, with a few exceptions. In some cases, calculated MOE values by using the conservative BMC<sub>10</sub> approach ranged < 10 and even < 1, respectively, and were thus associated with moderate or high risk of renal toxicities, respectively. However, with two exceptions, the MOE values for TDF were not below a range of 10 – 100, but still significantly lower than the MOE values for the active metabolite

tenofovir. The risk assessment based on the *in vitro* results showed that chronic effects observed in *in vivo* studies are poorly replicated in short-term *in vitro* testing. Although effects could be better mimicked in a suitable cell system by longer treatment duration with membrane permeable prodrugs over 14 days, and thus limitations could be partially circumvented, nevertheless biokinetic aspects were left aside at this point. Suitable *in silico* methods such as PBPK modeling and QIVIVE should also be integrated to overcome limitations of altered biokinetic factors, and also possible others like plastic binding, protein binding evaporation *etc.*, should be included in the assessment using suitable PBPK models and QIVIVE (Blaauboer, 2010). Likewise, it was again evident that not only dose-dependent data should be considered in the AOPs, but also time-resolved data need to be incorporated into the assessment (Leist *et al.*, 2017).

Nevertheless, a linear AOP does not reflect the complexity of biological processes, which are strongly characterized by negative / positive feedback and feed forward loops (Spinu *et al.*, 2019, Knapen *et al.*, 2018, Leist *et al.*, 2017). With regard to the AOP concept, which has the establishment of an AOP network as its central idea, adaptive and compensatory effects should also be included, not only for reasons concerning completeness but also through the resulting gain in knowledge about toxic mechanisms to increase the information content for future research, development of animal-free methods, and for regulatory decision making (Knapen *et al.*, 2018, Sewell *et al.*, 2018, Vinken *et al.*, 2017, Leist *et al.*, 2017). Which effects finally are decisive for a risk determination, is still open for discussion and should be evaluated individually for each AOP respectively AO.



### **5.3 Adverse Outcome Pathway concept – a feasible approach for toxicity testing?**

In order to advance the worldwide efforts to reduce animal studies in toxicity testing and to steer the tests into a more mechanistic direction, the AOP concept was adopted as a supporting tool. The development of AOPs revealed gaps in knowledge about toxicological pathways and reveals weaknesses of *in vitro* systems, such as altered biokinetics, which are relevant for risk assessment (Leist *et al.*, 2017). By this point alone, the visualization of knowledge gaps, the concept of the Adverse Outcome Pathway stands out as useful and helpful. By identifying and establishing key events, an implementation of *in vitro* assays is more specific, and target oriented. Key events in an AOP can also prove to be adaptive or compensatory, as in the example of the AOP – *Inhibition of mtDNA polymerase- $\gamma$*  in KE1 – *Depletion of mtDNA copy number*. Especially with regard to chronic effects, such compensatory KEs are of great interest and should be included in the AOPs (Leist *et al.*, 2017). From a mechanistic point of view, the implementation of all KEs associated with the AO is recommended, but it is also a time consuming and costly matter to prove the biological plausibility and essentiality of each individual KE. As a consequence, AOPs become increasingly large and more comprehensive, which also increases the complexity of response-response plots and quantitative key event relationships, making calculation and prediction based on these key event relationships a mathematical challenge.

However, both AOPs exemplarily demonstrate that time, besides test concentrations, is a further important factor. These concentration-time profiles can then be used as starting points for developing mathematical models to optimize prediction probabilities (Bal-Price and Meek, 2017). Strategically beneficial in the construction of AOPs, would be to first establish the connection

between MIE and AO and to completely verify the MIE for its biological plausibility and for its essentiality, especially when using *in vitro* models. Based on this connection, the AOP can then be successively expanded and extended by adding relevant KEs (Patlewicz *et al.*, 2015, Simon *et al.*, 2014a). Another approach that could help to reduce complexity in AOP development is the right to left or reverse engineering approach (Sewell *et al.*, 2018, Villeneuve *et al.*, 2014, Perkins *et al.*, 2011). Here the AOP is built up backwards starting with the AO. This strategy can be very helpful in the development of AOPs where data on the mechanism are missing or where it is not clear whether a key event leads to an adverse outcome (Sewell *et al.*, 2018). Kimber and colleagues described this reverse engineering approach for the development of the AOP for chemical respiratory allergy (Kimber *et al.*, 2014).

The AOP concept is a first important approach to build a knowledge base for toxic mechanisms with a uniform nomenclature for the individual MIEs, KEs, and AOs based on the Mode of Action approach that has been known and applied for decades (Leist *et al.*, 2017). For the intended paradigm shift in toxicology towards a more mechanistic approach, the AOP concept proves to be a very helpful tool. The more detailed identification of KEs allows a more targeted application of *in vitro* assays. However, some points need to be discussed, especially with regard to the rapidly growing complexity of AOPs. Besides dose-dependent data, time-dependent data needs to be included in the AOPs. The experimental data from the AOPs only provide a snapshot of effects for a certain point in time, such as usually 24 h for a cytotoxicity *in vitro* assay. Effects in upstream KEs can also occur and be measured after a far shorter time. Therefore, the question should be clarified which effects are triggered over time beginning with the starting point of the treatment. Furthermore, it has to be clarified how to proceed in case of different AOPs that lead to the same AO or with branched KEs. For linear AOPs, the generation

of KERs proved to be relatively simple. With more complex AOPs or even AOP-networks the generation of KERs turns into a real challenge.

#### **5.4 *In vitro* PoDs for *in vitro* risk assessment – fit for purpose?**

In order to obtain a first rough estimate of the risk, the question arose of a suitable *in vitro* PoD as a starting point for comparison with concentrations obtained from *in vivo* studies. Already during the selection of a suitable *in vitro* PoD, some challenges became apparent. A clear agreement on the use of an appropriate *in vitro* PoD does not exist (Green *et al.*, 2013). For completeness, the most common PoDs for the individual *in vitro* assays and KEs were used in this study. Limitations quickly became apparent in the use of individual PoDs, such as those of the EC<sub>X</sub> approach. With a dose-response curve that has an exponential slope (*e.g.*, KE1 – *Depletion of mtDNA copy number*), it is mathematically challenging to determine the maximum effect and thus also to determine an X % - effect (Green *et al.*, 2013). The new NtC approach described by Stadnicka-Michalak and colleagues (Stadnicka-Michalak *et al.*, 2018) also reached its limitations and non-toxic concentrations could only be calculated for sigmoid dose-response curves. In contrast, the approaches of the benchmark concentration and those of the NOEC / LOEC proved to be unproblematic to determine and were used to calculate MOE values. It was shown that the BMC<sub>10</sub> approach was consistently more conservative and calculated values were always below the calculated NOEC / LOEC values. Most of the PoDs for the individual key events were located in this range, which provided a further argument for conducting the risk assessment based on these PoDs. But in order to perform a risk assessment based on *in vitro* data in the future, a decision has to be made about which *in vitro* PoD is the most appropriate. To support and underpin the decision of an appropriate *in vitro* PoD, further *in vitro* data, such as

from this study, are required to identify and quantify additional sources of uncertainty to eventually incorporate and compensate for by targeted modeling tools. The quantity and calculation of points of departure based on *in vitro* approaches within the AOP concept will inevitably assume larger and more complex dimensions than PoD determinations based on *in vivo* data. Due to the large number of possible pathways and KEs within an AOP or AOP network, as well as the need to generate and integrate time-resolved data, complexity increases rapidly. For this purpose, it is essential to understand how well the measured *in vitro* endpoints reflect the integrated key events in the AOPs, even before a decision can be made on which key events and PoDs should be included in the evaluation in order to exclude possible false-positive results from non-adverse effects (Crump *et al.*, 2010).

It was already pointed out in the chapters above that *in vitro* systems are associated with certain limitations and restrictions. Differences between *in vitro* and *in vivo* systems such as in xenobiotic metabolism or expression pattern of transporters and the resulting impact on biokinetics pose several challenges for risk assessment based on *in vitro* data. Thus, factors which can influence the kinetics of a compound within an *in vitro* system need to be considered. The assumption that the nominal *in vitro* concentration and the resulting point of departure is equivalent to the *in vivo* plasma or tissue concentration is a source of uncertainty (Thomas *et al.*, 2018, Zhang *et al.*, 2018b). In fact, it is uncertain to which degree the nominal concentration of the test substance can be disturbed and altered through, *e.g.*, evaporation of the culture medium, evaporation of the test substance itself, or through metabolic processes in the culture medium (Zhang *et al.*, 2018b, Kramer *et al.*, 2012). In some cases, many test substances are also instable in culture media and / or have a strong binding affinity to plastic of the cultivation wells, which can significantly reduce the effective free concentration, especially during repeated treatment

(Kramer *et al.*, 2015). Some limitations of *in vitro* systems can only be minimized partially, for example by using suitable and very well-established cell lines and advanced optimized culture conditions, such as 3D cultivation. However, other factors are very difficult or impossible to eliminate (*e.g.*, plastic binding, evaporation, medium protein binding). The demand for suitable tools to compensate uncertainties is therefore increasing. Quantitative *in vitro* to *in vivo* extrapolation (QIVIVE) can be one tool. To this end, understanding the limitations and uncertainties of the models and approaches applied is crucial. These uncertainties can then be overcome by combining *e.g.*, *in vitro* biokinetics, omics data and modeling to improve the prediction (Yoon *et al.*, 2012). Especially now, in times of big data, computational modeling and the collection of affordable omics data sets, there are many opportunities to combine the obtained information and incorporate it into mechanistically based risk assessments, which are urgently needed by regulatory agencies (Ciallella and Zhu, 2019). Even better, this would allow AOPs and the information sources they contain to be used more widely in AOP-networks. Pathways that share the same mechanism and KEs in other tissues or cells could be linked to it. The first AOP – *Receptor mediated endocytosis and lysosomal overload*, had the focus on the pathway leading to kidney toxicity. For example, the AOP could also be transferred to other epithelial tissues in which the megalin/cubilin transporters are expressed, such as in the thyroid, parathyroid gland (Shah *et al.*, 2013), in the neonatal inner ear (Tauris *et al.*, 2009), or in the placenta (Storm *et al.*, 2016). However, AOPs by definition do not incorporate kinetics, and this is a shortcoming when it comes to toxicity prediction and risk assessment, as kinetics often determines the target. Especially here, an integration of PBPK models and QIVIVE is indispensable, since important parameters that are important for a quantitative assessment such as liberation, absorption, distribution, metabolism, and excretion (LADME - principle) can vary in other types of tissue.

Without this integration, the data obtained from the *in vitro* assays are not target oriented for a quantitative risk assessment, as important parameters relevant to the doses received *in vivo* are not considered or even altered (Yoon *et al.*, 2012). One of the most important and beneficial aspects in the development of AOPs is the identification of limitations, especially when using *in vitro* models. A general drawback of adverse outcome pathways is that they do not take biokinetics into account. This is especially relevant with regard to the *in vitro* systems applied, which may reveal altered intracellular uptake as well as altered metabolic activities. The time-limited cultivation of cell cultures inevitably results in limitations of short-term assays when it comes to detecting long-term effects. Therefore, the information content of dose-dependent generated *in vitro* data, which are obtained routinely after 24 hours, is not sufficient, which emphasizes the additional requirement for time-resolved data. With the benefit of such time-resolved data, it will improve identification of how well the *in vitro* assays reflect the key events to distinguish adverse effects from non-adverse effects or to determine when compensatory or adaptive effects turn into relevant adverse effects. Only after these limitations are identified, additional tools such as physiologically based pharmacokinetic modeling and toxicokinetic-toxicodynamic models can be specifically included in the AOPs to counteract uncertainties and limitations (Punt *et al.*, 2017, Zhang *et al.*, 2018b).

## 6 Summary and conclusion

The aim of this thesis was to apply the AOP concept as a basis for the development of mechanism based *in vitro* assays for systemic toxicity testing. The kidney, more precisely the proximal tubule cells, which are a major target of toxicity of numerous drugs and chemicals, served as an exemplary target. Based on two mechanisms described in the literature leading to toxicity of proximal tubule cells by polymyxin antibiotics and antiviral drugs, AOPs were established, which in turn were used as basis for the implementation of suitable *in vitro* tests. The systematic mapping of AOPs provides a useful opportunity to develop mechanistically based *in vitro* tests for systemic toxicity testing and the development of AOPs reveals gaps about understanding of the underlying mechanism leading to toxicity. AOPs were established using published information available from publications and databases (*e.g.*, PubMed, Comparative Toxicogenomics Database). It revealed that public information is readily available for questions related to the AOPs or the underlying mechanisms and were helpful for identifying KEs. However, for specific questions respectively key events, no adequate information could be retrieved. OMICS data can provide support to obtain increased information in order to improve the design of AOPs and can bring them to the next level. The AOP *Receptor-mediated endocytosis and lysosomal overload* can be considered as a good representative example. The literature describes the uptake of polymyxins into the proximal tubule cells via the megalin/cubilin complex, but it was found that, at least in the *in vitro* situation, further possible mechanisms are relevant for the uptake. Apart from receptor-mediated endocytosis, receptor-independent uptake or uptake via protein transporters are considered to play potential (further) important roles. To address such issues, *e.g.*, OMICS data could improve the information content and should be included in the

development of AOPs, combined with expert knowledge (Ball *et al.*, 2021). Edward Osborne Wilson's statement, "*We are drowning in information, while starving for wisdom*" exemplifies the development of adverse outcome pathways in this context and was also cited in this manner in a current paper regarding adverse outcome pathways (Ball *et al.*, 2021). The most important advantage in developing AOPs is that they are very well adapted to provide simply a better and clearer structure to toxicological mechanisms, to integrate the existing information in a meaningful way, and to point out knowledge gaps that still exist. Thus, the integration of *in vitro* assays can also become more effective and straightforward. Indeed, following the establishment and integration of *in vitro* assays for each of the key events in the AOPs presented here, questions emerged as to which extent the *in vitro* assays reflected the key events. It also became apparent that a need exists for time-resolved *in vitro* data to answer such issues. Time-resolved data offers further benefits in terms of being able to support kinetics models. What continues to be a challenge, however, is the ability to measure long-term effects. Associated with the detection of long-term effects, it again underlines the need for time-resolved *in vitro* data. By integrating dose-dependent and time-resolved *in vitro* data, possible compensatory effects will be better revealed to detect when they may turn into adverse effects and thus distinguish them from non-adverse effects. As in KE1 - *Depletion of mtDNA copy number* (AOP - *Inhibition of mtDNA polymerase- $\gamma$* ) demonstrated, after short-term treatment, initially an increase in mtDNA copy number was observed, due to possible compensatory effects, which, after prolonged treatment, changed into a decrease in mtDNA copy number, which might be relevant for the further toxic course. Thus, a better understanding of how well the *in vitro* assays reflect key events can be obtained and thus better decision making for a risk assessment based on *in vitro* data. Fundamental, for better decision making for risk assessment are also the obtained *in vitro* data.



Entire dose-response plots are needed and supportive to construct entire response-response plots and to estimate a correct and conclusive POD. We also showed that predictions of downstream key events, at least in a linear AOP, were feasible via the response-response plots and key event relationships. However, not all information is included in a linear AOP, since toxicological pathways are not linear and simple in nature, rather they are branched and complex in nature with multiple dose- and time-dependent effects, partly accompanied by negative / positive feedback and feed forward loops (Spinu *et al.*, 2019, Knapen *et al.*, 2018, Leist *et al.*, 2017). In addition, activated KEs within an AOP can also lead to different AOs and are therefore not necessarily coupled to only one AO. Thus, establishing key event relationships and prediction via response-response plots in a branching AOP becomes more complex and turns into a mathematical challenge. Also, a critical point to note is that AOPs by definition should be stressor independent. In particular, it becomes critical when key events are integrated in an AOP, such as uptake mechanisms into cells via transporters, but these transporters are substance specific. Relevant differences in biokinetics between cell lines and between the *in vitro* and *in vivo* situation also became evident. Especially, when altered expression of transporters can be assumed in the *in vitro* situation compared to the *in vivo* situation. Such differences can be circumvented by appropriate *in silico* models, as shown in the example of polymyxin B, but must be detected and identified, especially if unknown stressors need to be tested. In this way, the modeled *in vitro* results can be used to extrapolate an *in vivo* equivalent dose, which provides a more appropriate basis for risk assessment. However, in order to subsequently be able to decide which *in vitro* POD is most appropriate for a risk assessment, further *in vitro* data such as ours are needed to support the decision. The determination of the NOEL/LOEL and

BMC approach proved to be straightforward in practice, and precisely such simple and pragmatic methods are needed to increase the predictive potential of an *in vitro* strategy.

However, the central aspect of the Tox21 program, with the vision of shifting the apical endpoints in animals to *in vitro* high-throughput methods in predominantly human cells, is at the beginning of a long-term development. Due to the limitations of *in vitro* systems, it is currently not feasible to completely avoid safety testing on animals. Nevertheless, a first pragmatic step towards a multi-step test strategy (Figure 1), combined with modern *in silico* methods, improved *in vitro* assays coupled with PBPK modeling and QIVIVE, followed by a second test step with alternative model organisms, is an important step in the correct direction. Finally, the AOP concept and the paradigm shift in toxicology is a good chance to steer toxicity testing into a more mechanistic path in order to understand which pathways are relevant and to obtain a better mechanistic understanding in toxicology. It was therefore astonishing and applaudable at once when Simon Upton (Environment Director at the OECD) said about the work on Adverse Outcome Pathways:

*“I naively believed that we tested things because we knew what the mechanism was.*

*We don’t.”*

In other words:

If we understand the mechanisms of toxicity, we have more trust in the prediction.

---

## 7 References

- ABBOTT, A. 2005. More than a cosmetic change. *Nature*, 438, 144-146.
- ABDELRAOUF, K., BRAGGS, K. H., YIN, T., TRUONG, L. D., HU, M. & TAM, V. H. 2012a. Characterization of polymyxin B-induced nephrotoxicity: implications for dosing regimen design. *Antimicrobial agents chemotherapy*, 56, 4625-4629.
- ABDELRAOUF, K., CHANG, K.-T., YIN, T., HU, M. & TAM, V. H. 2014. Uptake of polymyxin B into renal cells. *Antimicrobial agents chemotherapy*, 58, 4200-4202.
- ABDELRAOUF, K., HE, J., LEDESMA, K. R., HU, M. & TAM, V. H. 2012b. Pharmacokinetics and renal disposition of polymyxin B in an animal model. *Antimicrobial agents chemotherapy*, 56, 5724-5727.
- ABRAHAM, P., RAMAMOORTHY, H. & ISAAC, B. 2013. Depletion of the cellular antioxidant system contributes to tenofovir disoproxil fumarate-induced mitochondrial damage and increased oxido-nitrosative stress in the kidney. *Journal of biomedical science*, 20, 61.
- ADKINS, J. C., PETERS, D. H. & FAULDS, D. 1997. Zalcitabine. *Drugs*, 53, 1054-1080.
- ADLER, S., BASKETTER, D., CRETON, S., PELKONEN, O., VAN BENTHEM, J., ZUANG, V., ANDERSEN, K. E., ANGERS-LOUSTAU, A., APTULA, A. & BAL-PRICE, A. 2011. Alternative (non-animal) methods for cosmetics testing: current status and future prospects—2010. *Archives of toxicology*, 85, 367-485.
- AKAJAGBOR, D. S., WILSON, S. L., SHERE-WOLFE, K. D., DAKUM, P., CHARURAT, M. E. & GILLIAM, B. L. 2013. Higher incidence of acute kidney injury with intravenous colistimethate sodium compared with polymyxin B in critically ill patients at a tertiary care medical center. *Clinical infectious diseases*, 57, 1300-1303.
- ALAN, S., CHERTOW, G. M., LUYCKX, V., MARSDEN, P. A., SKORECKI, K. & TAAL, M. W. 2019. *Brenner and Rector's The Kidney E-Book*, Elsevier Health Sciences.
- ALLEN, T. E., GOODMAN, J. M., GUTSELL, S. & RUSSELL, P. J. 2014. Defining molecular initiating events in the adverse outcome pathway framework for risk assessment. *Chemical research in toxicology*, 27, 2100-2112.
- AMET, Y., BERTHOU, F., FOURNIER, G., DRÉANO, Y., BARDOU, L., CLÈDES, J. & MÉNEZ, J.-F. 1997. Cytochrome P450 4A and 2E1 expression in human kidney microsomes. *Biochemical pharmacology*, 53, 765-771.
- ANKLEY, G., ESCHER, B. I., HARTUNG, T. & SHAH, I. 2016. Pathway-based approaches for environmental monitoring and risk assessment. ACS Publications.
- ANKLEY, G. T., BENNETT, R. S., ERICKSON, R. J., HOFF, D. J., HORNUNG, M. W., JOHNSON, R. D., MOUNT, D. R., NICHOLS, J. W., RUSSOM, C. L. & SCHMIEDER, P. K. 2010. Adverse outcome pathways: a conceptual framework to support ecotoxicology research and risk assessment. *Environmental Toxicology Chemistry: An International Journal*, 29, 730-741.
- APPELQVIST, H., JOHANSSON, A.-C., LINDEROTH, E., JOHANSSON, U., ANTONSSON, B., STEINFELD, R., KÅGEDAL, K. & ÖLLINGER, K. 2012. Lysosome-mediated apoptosis is associated with cathepsin D-specific processing of bid at Phe24, Trp48, and Phe183. *Annals of Clinical Laboratory Science*, 42, 231-242.

- APPELQVIST, H., NILSSON, C., GARNER, B., BROWN, A. J., KÅGEDAL, K. & ÖLLINGER, K. 2011. Attenuation of the lysosomal death pathway by lysosomal cholesterol accumulation. *The American journal of pathology*, 178, 629-639.
- ARAÚJO, G. L. D., CAMPOS, M. A. A., VALENTE, M. A. S., SILVA, S. C. T., FRANÇA, F. D., CHAVES, M. M. & TAGLIATI, C. A. J. B. J. O. P. S. 2014. Alternative methods in toxicity testing: the current approach. 50, 55-62.
- ARNAUDO, E., SHANSKE, S., DIMAURO, S., SCHON, E., MORAES, C. T. & DALAKAS, M. 1991. Depletion of muscle mitochondrial DNA in AIDS patients with zidovudine-induced myopathy. *The Lancet*, 337, 508-510.
- ASCHAUER, L., CARTA, G., VOGELSANG, N., SCHLATTER, E. & JENNINGS, P. 2015a. Expression of xenobiotic transporters in the human renal proximal tubule cell line RPTEC/TERT1. *Toxicology In Vitro*, 30, 95-105.
- ASCHAUER, L., LIMONCIEL, A., WILMES, A., STANZEL, S., KOPP-SCHNEIDER, A., HEWITT, P., LUKAS, A., LEONARD, M. O., PFALLER, W. & JENNINGS, P. 2015b. Application of RPTEC/TERT1 cells for investigation of repeat dose nephrotoxicity: a transcriptomic study. *Toxicology in Vitro*, 30, 106-116.
- AVEDISSIAN, S. N., LIU, J., RHODES, N. J., LEE, A., PAIS, G. M., HAUSER, A. R. & SCHEETZ, M. H. 2019. A review of the clinical pharmacokinetics of polymyxin B. *Antibiotics*, 8, 31.
- AZAD, M. A., AKTER, J., ROGERS, K. L., NATION, R. L., VELKOV, T. & LI, J. 2015. Major pathways of polymyxin-induced apoptosis in rat kidney proximal tubular cells. *Antimicrobial agents chemotherapy*, 59, 2136-2143.
- AZAD, M. A., FINNIN, B. A., POU DYAL, A., DAVIS, K., LI, J., HILL, P. A., NATION, R. L., VELKOV, T. & LI, J. 2013. Polymyxin B induces apoptosis in kidney proximal tubular cells. *Antimicrobial agents chemotherapy*, 57, 4329-4335.
- BAJAJ, P., CHOWDHURY, S. K., YUCHA, R., KELLY, E. J. & XIAO, G. 2018. Emerging kidney models to investigate metabolism, transport, and toxicity of drugs and xenobiotics. *Drug Metabolism Disposition*, 46, 1692-1702.
- BAL-PRICE, A. & MEEK, M. B. 2017. Adverse outcome pathways: application to enhance mechanistic understanding of neurotoxicity. *Pharmacology therapeutics*, 179, 84-95.
- BALE, A. S., KENYON, E., FLYNN, T. J., LIPSCOMB, J. C., NEDRICK, D. L., HARTUNG, T. & PATTON, G. W. 2014. Correlating in vitro data to in vivo findings for risk assessment. *Alternatives to Animal Experimentation: ALTEX*, 31, 79-90.
- BALL, T., BARBER, C. G., CAYLEY, A., CHILTON, M. L., FOSTER, R., FOWKES, A., HEGHES, C., HILL, E., HILL, N. & KANE, S. 2021. Beyond adverse outcome pathways: making toxicity predictions from event networks, SAR models, data and knowledge. *Toxicology Research*, 10, 102-122.
- BARBIER, O., JACQUILLET, G., TAUC, M., COUGNON, M. & POUJEOL, P. 2005. Effect of heavy metals on, and handling by, the kidney. *Nephron Physiology*, 99, p105-p110.
- BARDITCH-CROVO, P., TOOLE, J., HENDRIX, C., CUNDY, K., EBELING, D., JAFFE, H. & LIETMAN, P. 1997. Anti-human immunodeficiency virus (HIV) activity, safety, and pharmacokinetics of adefovir dipivoxil (9-[2-(bis-pivaloyloxymethyl)-phosphonylmethoxyethyl] adenine) in HIV-infected patients. *Journal of Infectious Diseases*, 176, 406-413.
- BEAUCHAMP, D., GOURDE, P., SIMARD, M. & BERGERON, M. 1992. Subcellular localization of tobramycin and vancomycin given alone and in combination in proximal

- tubular cells, determined by immunogold labeling. *Antimicrobial agents chemotherapy*, 36, 2204-2210.
- BENBRIK, E., CHARIOT, P., BONAUAUD, S., AMMI-SAÏD, M., FRISDAL, E., REY, C., GHERARDI, R. & BARLOVATZ-MEIMON, G. 1997. Cellular and mitochondrial toxicity of zidovudine (AZT), didanosine (ddI) and zalcitabine (ddC) on cultured human muscle cells. *Journal of the neurological sciences*, 149, 19-25.
- BENFENATI, E., CHAUDHRY, Q., GINI, G. & DORNE, J. L. 2019. Integrating in silico models and read-across methods for predicting toxicity of chemicals: A step-wise strategy. *Environment international*, 131, 105060.
- BESSEMS, J. G. & VERMEULEN, N. P. 2001. Paracetamol (acetaminophen)-induced toxicity: molecular and biochemical mechanisms, analogues and protective approaches. *Critical reviews in toxicology*, 31, 55-138.
- BI, H. C., ZHONG, G. P., ZHOU, S., CHEN, X. & HUANG, M. 2005. Determination of adefovir in human plasma by liquid chromatography/tandem mass spectrometry: application to a pharmacokinetic study. *Rapid Communications in Mass Spectrometry: An International Journal Devoted to the Rapid Dissemination of Up-to-the-Minute Research in Mass Spectrometry*, 19, 2911-2917.
- BIEMESDERFER, D. 2006. Regulated intramembrane proteolysis of megalin: linking urinary protein and gene regulation in proximal tubule? *Kidney international*, 69, 1717-1721.
- BIESECKER, G., KARIMI, S., DESJARDINS, J., MEYER, D., ABBOTT, B., BENDELE, R. & RICHARDSON, F. 2003. Evaluation of mitochondrial DNA content and enzyme levels in tenofovir DF-treated rats, rhesus monkeys and woodchucks. *Antiviral research*, 58, 217-225.
- BIRKUS, G., HITCHCOCK, M. J. & CIHLAR, T. 2002. Assessment of mitochondrial toxicity in human cells treated with tenofovir: comparison with other nucleoside reverse transcriptase inhibitors. *Antimicrobial agents chemotherapy*, 46, 716-723.
- BLAAUBOER, B. J. 2010. Biokinetic modeling and in vitro–in vivo extrapolations. *Journal of Toxicology Environmental Health Part B*, 13, 242-252.
- BOOGAARD, P. J., NAGELKERKE, J. F. & MULDER, G. J. 1990. Renal proximal tubular cells in suspension or in primary culture as in vitro models to study nephrotoxicity. *Chemico-biological interactions*, 76, 251-291.
- BOYA, P. & KROEMER, G. 2008. Lysosomal membrane permeabilization in cell death. *Oncogene*, 27, 6434-6451.
- BRELJAK, D., LJUBOJEVIĆ, M., HAGOS, Y., MICEK, V., BALEN EROR, D., VRHOVAC MADUNIĆ, I., BRZICA, H., KARAICA, D., RADOVIĆ, N. & KRAUS, O. 2016. Distribution of organic anion transporters NaDC3 and OAT1-3 along the human nephron. *American Journal of Physiology-Renal Physiology*, 311, F227-F238.
- BRIFFA, J. F., GRINFELD, E., MATHAI, M. L., PORONNIK, P., MCAINCH, A. J. & HRYCIW, D. H. 2015. Acute leptin exposure reduces megalin expression and upregulates TGFβ1 in cultured renal proximal tubule cells. *Molecular cellular endocrinology*, 401, 25-34.
- BRINKMAN, K., TER HOFSTEDÉ, H. J., BURGER, D. M., SMEITINK, J. A. & KOOPMANS, P. P. 1998. Adverse effects of reverse transcriptase inhibitors: mitochondrial toxicity as common pathway. *Aids*, 12, 1735-1744.
- BROWN, A. E. C., COHEN, M. N., TONG, S., BRAVERMAN, R. S., ROONEY, J. F., GILLER, R. & LEVIN, M. J. 2015. Pharmacokinetics and safety of intravenous

- cidofovir for life-threatening viral infections in pediatric hematopoietic stem cell transplant recipients. *Antimicrobial agents chemotherapy*, 59, 3718-3725.
- BROWN, C. C. 1984. High-to low-dose extrapolation in animals. ACS Publications.
- BRYNIARSKI, M. A., YEE, B. M., JAFFRI, I., CHAVES, L. D., YU, J. A., GUAN, X., GHAVAM, N., YACOUB, R. & MORRIS, M. E. 2018. Increased megalin expression in early type 2 diabetes: role of insulin-signaling pathways. *American Journal of Physiology-Renal Physiology*, 315, F1191-F1207.
- CABEZAS, F., FARFÁN, P. & MARZOLO, M.-P. 2019a. The down regulation of megalin/LRP2 by transforming growth factor beta (TGF- $\beta$ 1) is mediated by the SMAD2/3 signalling pathway. *bioRxiv*, 553974.
- CABEZAS, F., FARFÁN, P. & MARZOLO, M.-P. 2019b. Participation of the SMAD2/3 signalling pathway in the down regulation of megalin/LRP2 by transforming growth factor beta (TGF- $\beta$ 1). *PloS one*, 14, e0213127.
- CAI, Y., LECK, H., TAN, R. W., TEO, J. Q., LIM, T.-P., LEE, W., CHLEBICKI, M. P. & KWA, A. L. 2020a. Clinical Experience with High-Dose Polymyxin B against Carbapenem-Resistant Gram-Negative Bacterial Infections—A Cohort Study. *Antibiotics*, 9, 451.
- CAI, Y., LECK, H., TAN, R. W., TEO, J. Q., LIM, T.-P., LEE, W., CHLEBICKI, M. P. & KWA, A. L. J. A. 2020b. Clinical Experience with High-Dose Polymyxin B against Carbapenem-Resistant Gram-Negative Bacterial Infections—A Cohort Study. 9, 451.
- CARROLL, R. G. & ABDEL-RAHMAN, A. A. 2014. Glomerular Filtration. *Biomedical Sciences*. Elsevier.
- CARUSO-NEVES, C., PINHEIRO, A. A. S., CAI, H., SOUZA-MENEZES, J. & GUGGINO, W. B. 2006. PKB and megalin determine the survival or death of renal proximal tubule cells. *Proceedings of the National Academy of Sciences*, 103, 18810-18815.
- CASHMAN, J. R. & ZHANG, J. 2006. Human flavin-containing monooxygenases. *Annu. Rev. Pharmacol. Toxicol.*, 46, 65-100.
- CHEN, J. W., MADAMANCHI, N., MADAMANCHI, N. R., TRIER, T. T. & KEHERLY, M. J. 2001. Lamp-1 is upregulated in human glioblastoma cell lines induced to undergo apoptosis. *Journal of biomedical science*, 8, 365-374.
- CHENG, C.-Y., SHENG, W.-H., WANG, J.-T., CHEN, Y.-C. & CHANG, S.-C. 2010a. Safety and efficacy of intravenous colistin (colistin methanesulphonate) for severe multidrug-resistant Gram-negative bacterial infections. *International journal of antimicrobial agents*, 35, 297-300.
- CHENG, C., LIU, S., XIAO, D., HOLLEMBAEK, J., YAO, L., LIN, J. & HANSEL, S. 2010b. LC-MS/MS method development and validation for the determination of polymyxins and vancomycin in rat plasma. *Journal of Chromatography B*, 878, 2831-2838.
- CHERRINGTON, J., ALLEN, S., BISCHOFBERGER, N. & CHEN, M. 1995. Kinetic interaction of the diphosphates of 9-(2-phosphonylmethoxyethyl) adenine and other anti-HIV active purine congeners with HIV reverse transcriptase and human DNA polymerases  $\alpha$ ,  $\beta$  and  $\gamma$ . *Antiviral Chemistry Chemotherapy*, 6, 217-221.
- CHRISTENSEN, E. I., BIRN, H., STORM, T., WEYER, K. & NIELSEN, R. 2012. Endocytic receptors in the renal proximal tubule. *Physiology*, 27, 223-236.
- CHRISTENSEN, E. I., BIRN, H., VERRONST, P. & MOESTRUP, S. K. 1998. Megalin-mediated endocytosis in renal proximal tubule. *Renal failure*, 20, 191-199.

- CHU, X., BLEASBY, K., CHAN, G. H., NUNES, I. & EVERS, R. 2016. The complexities of interpreting reversible elevated serum creatinine levels in drug development: does a correlation with inhibition of renal transporters exist? *Drug Metabolism Disposition*, 44, 1498-1509.
- CHWIERALSKI, C., WELTE T & F, B. 2006. Cathepsin-regulated apoptosis. *Apoptosis*, 11, 143-149.
- CIALLELLA, H. L. & ZHU, H. 2019. Advancing computational toxicology in the big data era by artificial intelligence: data-driven and mechanism-driven modeling for chemical toxicity. *Chemical research in toxicology*, 32, 536-547.
- CIHLAR, T., HO, E. S., LIN, D. C. & MULATO, A. S. 2001. Human renal organic anion transporter 1 (hOAT1) and its role in the nephrotoxicity of antiviral nucleotide analogs. *Nucleosides, Nucleotides Nucleic Acids*, 20, 641-648.
- CIHLAR, T., LAFLAMME, G., FISHER, R., CAREY, A. C., VELA, J. E., MACKMAN, R. & RAY, A. S. 2009. Novel nucleotide human immunodeficiency virus reverse transcriptase inhibitor GS-9148 with a low nephrotoxic potential: characterization of renal transport and accumulation. *Antimicrobial agents chemotherapy*, 53, 150-156.
- CLEWELL I, H. J. & ANDERSEN, M. E. 1987. Dose, species, and route extrapolation using physiologically based pharmacokinetic models. *Drinking Water Health, Volume 8: Pharmacokinetics in Risk Assessment*, 8, 111-131.
- COADY, K., BROWNE, P., EMBRY, M., HILL III, T., LEINALA, E., STEEGER, T., MAŚLANKIEWICZ, L. & HUTCHINSON, T. 2019. When are Adverse Outcome Pathways and Associated Assays “Fit for Purpose” for Regulatory Decision-Making and Management of Chemicals? *Integrated environmental assessment management*.
- COCCHIARO, P., FOX, C., TREGIDGO, N. W., HOWARTH, R., WOOD, K. M., SITUMORANG, G. R., PAVONE, L. M., SHEERIN, N. S. & MOLES, A. 2016. Lysosomal protease cathepsin D; a new driver of apoptosis during acute kidney injury. *Scientific reports*, 6, 1-15.
- COHEN, L., CUI, N., CAI, Y., GARDEN, P. M., LI, X., WEITZ, D. A. & WALT, D. R. 2020. Single Molecule Protein Detection with Attomolar Sensitivity Using Droplet Digital Enzyme-Linked Immunosorbent Assay. *ACS nano*, 14, 9491-9501.
- COLLIER, A. C., COOMBS, R. W., SCHOENFELD, D. A., BASSETT, R. L., TIMPONE, J., BARUCH, A., JONES, M., FACEY, K., WHITACRE, C. & MCAULIFFE, V. 1996. Treatment of human immunodeficiency virus infection with saquinavir, zidovudine, and zalcitabine. *New England Journal of Medicine*, 334, 1011-1018.
- CONOLLY, R. B., ANKLEY, G. T., CHENG, W., MAYO, M. L., MILLER, D. H., PERKINS, E. J., VILLENEUVE, D. L., WATANABE, K. H. J. E. S. & TECHNOLOGY 2017. Quantitative adverse outcome pathways and their application to predictive toxicology. 51, 4661-4672.
- COOPER, R. D., WIEBE, N., SMITH, N., KEISER, P., NAICKER, S. & TONELLI, M. 2010. Systematic review and meta-analysis: renal safety of tenofovir disoproxil fumarate in HIV-infected patients. *Clinical Infectious Diseases*, 51, 496-505.
- CÔTÉ, H. C., MAGIL, A. B., HARRIS, M., SCARTH, B. J., GADAWSKI, I., WANG, N., YU, E., YIP, B., ZALUNARDO, N. & WERB, R. 2006. Exploring mitochondrial nephrotoxicity as a potential mechanism of kidney dysfunction among HIV-infected patients on highly active antiretroviral therapy. *Antiviral therapy*, 11, 79.

- CREAN, D., BELLWON, P., ASCHAUER, L., LIMONCIEL, A., MOENKS, K., HEWITT, P., SCHMIDT, T., HERRGEN, K., DEKANT, W. & LUKAS, A. 2015. Development of an in vitro renal epithelial disease state model for xenobiotic toxicity testing. *Toxicology in Vitro*, 30, 128-137.
- CRISTOFORI, P., ZANETTI, E., FREGONA, D., PIAIA, A. & TREVISAN, A. 2007. Renal proximal tubule segment-specific nephrotoxicity: an overview on biomarkers and histopathology. *Toxicologic pathology*, 35, 270-275.
- CRUMP, K. S. 1984. A new method for determining allowable daily intakes. *Toxicological Sciences*, 4, 854-871.
- CRUMP, K. S., CHEN, C. & LOUIS, T. A. 2010. The future use of in vitro data in risk assessment to set human exposure standards: challenging problems and familiar solutions. *Environmental health perspectives*, 118, 1350-1354.
- CUI, G., XU, X. & DIAO, H. 2015. Comparative Meta-analysis of tenofovir disoproxil fumarate versus emtricitabine and tenofovir disoproxil fumarate as treatments for patients with chronic hepatitis B. *Scientific reports*, 5, 11854.
- CULLEN, J. T. & MALDONADO, M. T. 2013. Biogeochemistry of cadmium and its release to the environment. *Cadmium: from toxicity to essentiality*, 31-62.
- CUMMINGS, B. S. & LASH, L. H. 2000. Metabolism and toxicity of trichloroethylene and S-(1, 2-dichlorovinyl)-L-cysteine in freshly isolated human proximal tubular cells. *Toxicological Sciences*, 53, 458-466.
- CUMMINGS, B. S., LASKER, J. M. & LASH, L. H. 2000a. Expression of glutathione-dependent enzymes and cytochrome P450s in freshly isolated and primary cultures of proximal tubular cells from human kidney. *Journal of Pharmacology Experimental Therapeutics*, 293, 677-685.
- DAI, Y. J., JIA, Y. F., CHEN, N., BIAN, W. P., LI, Q. K., MA, Y. B., CHEN, Y. L. & PEI, D. S. 2014. Zebrafish as a model system to study toxicology. *Environmental toxicology chemistry*, 33, 11-17.
- DAMAGHI, M., TAFRESHI, N. K., LLOYD, M. C., SPRUNG, R., ESTRELLA, V., WOJTKOWIAK, J. W., MORSE, D. L., KOOMEN, J. M., BUI, M. M. & GATENBY, R. A. 2015. Chronic acidosis in the tumour microenvironment selects for overexpression of LAMP2 in the plasma membrane. *Nature communications*, 6, 1-13.
- DANNER, R. L., JOINER, K. A., RUBIN, M., PATTERSON, W., JOHNSON, N., AYERS, K. & PARRILLO, J. 1989. Purification, toxicity, and antiendotoxin activity of polymyxin B nonapeptide. *Antimicrobial Agents Chemotherapy*, 33, 1428-1434.
- DARSAZAN, B., SHAFATI, A., ZARGHI, A. & MORTAZAVI, S. A. 2018. Evaluation of Ion-pair Formation of Adefovir to Improve Permeation across Artificial and Biological Membranes. *Journal of Pharmacy Pharmaceutical Sciences*, 21, 160-170.
- DAUCHY, F.-A., LAWSON-AYAYI, S., DE LA FAILLE, R., BONNET, F., RIGOTHIER, C., MEHSEN, N., MIREMONT-SALAMÉ, G., CAZANAVE, C., GREIB, C. & DABIS, F. 2011. Increased risk of abnormal proximal renal tubular function with HIV infection and antiretroviral therapy. *Kidney international*, 80, 302-309.
- DAUGAS, E., ROUGIER, J.-P. & HILL, G. 2005. HAART-related nephropathies in HIV-infected patients. *Kidney international*, 67, 393-403.
- DAVIS, A. P., MURPHY, C. G., JOHNSON, R., LAY, J. M., LENNON-HOPKINS, K., SARACENI-RICHARDS, C., SCIAKY, D., KING, B. L., ROSENSTEIN, M. C. &



- WIEGERS, T. C. 2013. The comparative toxicogenomics database: update 2013. *Nucleic acids research*, 41, D1104-D1114.
- DAVIS, A. P., WIEGERS, T. C., MURPHY, C. G. & MATTINGLY, C. J. 2011. The curation paradigm and application tool used for manual curation of the scientific literature at the Comparative Toxicogenomics Database. *Database*, 2011.
- DE BARROS PERUCHETTI, D., SILVA-AGUIAR, R. P., SIQUEIRA, G. M., DIAS, W. B. & CARUSO-NEVES, C. 2018. High glucose reduces megalin-mediated albumin endocytosis in renal proximal tubule cells through protein kinase B O-GlcNAcylation. *Journal of Biological Chemistry*, 293, 11388-11400.
- DE CLERCQ, E. 2003. Clinical potential of the acyclic nucleoside phosphonates cidofovir, adefovir, and tenofovir in treatment of DNA virus and retrovirus infections. *Clinical microbiology reviews*, 16, 569-596.
- DE LARCO, J. E. & TODARO, G. J. 1978. Epithelioid and fibroblastic rat kidney cell clones: epidermal growth factor (EGF) receptors and the effect of mouse sarcoma virus transformation. *Journal of cellular physiology*, 94, 335-342.
- DE, S., KUWAHARA, S. & SAITO, A. 2014. The endocytic receptor megalin and its associated proteins in proximal tubule epithelial cells. *Membranes*, 4, 333-355.
- DENT, M., AMARAL, R. T., DA SILVA, P. A., ANSELL, J., BOISLEVE, F., HATAO, M., HIROSE, A., KASAI, Y., KERN, P. & KREILING, R. 2018. Principles underpinning the use of new methodologies in the risk assessment of cosmetic ingredients. *Computational Toxicology*, 7, 20-26.
- DIETERLE, F., PERENTES, E., CORDIER, A., ROTH, D. R., VERDES, P., GRENET, O., PANTANO, S., MOULIN, P., WAHL, D. & MAHL, A. 2010. Urinary clusterin, cystatin C,  $\beta$ 2-microglobulin and total protein as markers to detect drug-induced kidney injury. *Nature biotechnology*, 28, 463.
- DIRECTIVE\_2010/63/EU 2010. Directive 2010/63/EU of the European Parliament and of the Council of 22 September 2010 on the protection of animals used for scientific purposes. *Off J Eur Union L*, 276, 33-76.
- DIWAKAR, R., PEARSON, A. L., COLVILLE-NASH, P., BRUNSKILL, N. J. & DOCKRELL, M. E. 2007. The role played by endocytosis in albumin-induced secretion of TGF- $\beta$ 1 by proximal tubular epithelial cells. *American Journal of Physiology-Renal Physiology*, 292, F1464-F1470.
- DUC-NGUYEN, H., ROSENBLUM, E. N. & ZEIGEL, R. F. 1966. Persistent infection of a rat kidney cell line with Rauscher murine leukemia virus. *Journal of bacteriology*, 92, 1133-1140.
- ĎURIŠOVÁ, M. 2012. Physiologically based structure of mean residence time. *The Scientific World Journal*, 2012.
- DUVAL, K., GROVER, H., HAN, L.-H., MOU, Y., PEGORARO, A. F., FREDBERG, J. & CHEN, Z. 2017. Modeling physiological events in 2D vs. 3D cell culture. *Physiology*, 32, 266-277.
- EDMONDSON, R., BROGLIE, J. J., ADCOCK, A. F., YANG, L. J. A. & TECHNOLOGIES, D. D. 2014. Three-dimensional cell culture systems and their applications in drug discovery and cell-based biosensors. 12, 207-218.
- EDWARDS, S. W., TAN, Y.-M., VILLENEUVE, D. L., MEEK, M. & MCQUEEN, C. A. 2016. Adverse outcome pathways—organizing toxicological information to improve decision making. *Journal of Pharmacology Experimental Therapeutics*, 356, 170-181.

- EFSA, S. C. 2005. Opinion of the Scientific Committee on a request from EFSA related to a harmonised approach for risk assessment of substances which are both genotoxic and carcinogenic. *EFSA Journal*, 3, 282.
- EFSA, S. C., HARDY, A., BENFORD, D., HALLDORSSON, T., JEGER, M. J., KNUTSEN, K. H., MORE, S., MORTENSEN, A., NAEGELI, H. & NOTEBORN, H. 2017. Update: use of the benchmark dose approach in risk assessment. *EFSA Journal*, 15, e04658.
- EPA, U. 1991. Technical support document for water quality-based toxics control. *EPA/505/2-90-001*.
- EPA, U. 2012. Benchmark dose technical guidance. *US Environmental Protection Agency*.
- ESCHER, S. E., KAMP, H., BENNEKOU, S. H., BITSCH, A., FISHER, C., GRAEPEL, R., HENGSTLER, J. G., HERZLER, M., KNIGHT, D. & LEIST, M. 2019. Towards grouping concepts based on new approach methodologies in chemical hazard assessment: the read-across approach of the EU-ToxRisk project. *Archives of toxicology*, 93, 3643-3667.
- ESHBACH, M. L. & WEISZ, O. A. 2017. Receptor-mediated endocytosis in the proximal tubule. *Annual review of physiology*, 79, 425-448.
- EUROPEAN\_COMMISSION 2015. Test No. 404: Acute Dermal Irritation/Corrosion. *OECD Guidelines for the Testing of Chemicals, Section 4: Health Effects*.
- EUROPEAN\_COMMISSION 2017. Test No. 405: Acute Eye Irritation/Corrosion. *OECD Guidelines for the Testing of Chemicals, Section 4: Health Effects*.
- FALAGAS, M. E., FRAGOULIS, K. N., KASIAKOU, S. K., SERMAIDIS, G. J. & MICHALOPOULOS, A. 2005. Nephrotoxicity of intravenous colistin: a prospective evaluation. *International journal of antimicrobial agents*, 26, 504-507.
- FALAGAS, M. E. & KASIAKOU, S. K. 2006. Toxicity of polymyxins: a systematic review of the evidence from old and recent studies. *Critical care*, 10, 1-13.
- FARIA, J., AHMED, S., GERRITSEN, K. G., MIHAILA, S. M. & MASEREEUW, R. J. A. O. T. 2019. Kidney-based in vitro models for drug-induced toxicity testing. 1-22.
- FERNANDEZ-FERNANDEZ, B., MONTOYA-FERRER, A., SANZ, A. B., SANCHEZ-NINO, M. D., IZQUIERDO, M. C., POVEDA, J., SAINZ-PRESTEL, V., ORTIZ-MARTIN, N., PARRA-RODRIGUEZ, A. & SELGAS, R. 2011. Tenofovir nephrotoxicity: 2011 update. *AIDS research treatment*, 2011.
- FISHER, C. E. & HOWIE, S. E. 2006. The role of megalin (LRP-2/Gp330) during development. *Developmental biology*, 296, 279-297.
- FONTANA, R. J. 2009. Side effects of long-term oral antiviral therapy for hepatitis B. *Hepatology*, 49, S185-S195.
- FORREST, A., SILVEIRA, F., THAMLIKITKUL, V., GARONZIK, S., MANDRAGOS, K., SHOHAM, S., PATERSON, D., LI, J. & NATION, R. Toxicodynamics for colistin-associated changes in creatinine clearance. Interscience Conference on Antimicrobial Agents and Chemotherapy, 2014. 5-9.
- FOX, C., COCCHIARO, P., OAKLEY, F., HOWARTH, R., CALLAGHAN, K., LESLIE, J., LULI, S., WOOD, K. M., GENOVESE, F. & SHEERIN, N. S. 2016. Inhibition of lysosomal protease cathepsin D reduces renal fibrosis in murine chronic kidney disease. *Scientific reports*, 6, 1-15.
- FRASER, D., BRUNSKILL, N., ITO, T. & PHILLIPS, A. 2003. Long-term exposure of proximal tubular epithelial cells to glucose induces transforming growth factor- $\beta$ 1

- synthesis via an autocrine PDGF loop. *The American journal of pathology*, 163, 2565-2574.
- FUKUDA, M. 1991. Lysosomal membrane glycoproteins. Structure, biosynthesis, and intracellular trafficking. *Journal of Biological Chemistry*, 266, 21327-21330.
- GALES, A. C., JONES, R. N. & SADER, H. S. 2011. Contemporary activity of colistin and polymyxin B against a worldwide collection of Gram-negative pathogens: results from the SENTRY Antimicrobial Surveillance Program (2006–09). *Journal of Antimicrobial Chemotherapy*, 66, 2070-2074.
- GALLANT, J. E. & DERESINSKI, S. 2003. Tenofovir disoproxil fumarate. *Clinical Infectious Diseases*, 37, 944-950.
- GALLANT, J. E., STASZEWSKI, S., POZNIAK, A. L., DEJESUS, E., SULEIMAN, J. M., MILLER, M. D., COAKLEY, D. F., LU, B., TOOLE, J. J. & CHENG, A. K. 2004. Efficacy and safety of tenofovir DF vs stavudine in combination therapy in antiretroviral-naïve patients: a 3-year randomized trial. *Jama*, 292, 191-201.
- GEBOERS, S., HAENEN, S., MOLS, R., BROUWERS, J., TACK, J., ANNAERT, P. & AUGUSTIJNS, P. 2015. Intestinal behavior of the ester prodrug tenofovir DF in humans. *International journal of pharmaceutics*, 485, 131-137.
- GEKLE, M., KNAUS, P., NIELSEN, R., MILDENBERGER, S., FREUDINGER, R., WOHLFARTH, V., SAUVANT, C. & CHRISTENSEN, E. I. 2003. Transforming growth factor- $\beta$ 1 reduces megalin-and cubilin-mediated endocytosis of albumin in proximal-tubule-derived opossum kidney cells. *The Journal of physiology*, 552, 471-481.
- GIFFIN, R., ROBINSON, S. & OLSON, S. 2009. *Accelerating the development of biomarkers for drug safety: workshop summary*, National Academies Press.
- GILMOUR, N., KERN, P. S., ALÉPÉE, N., BOISLÈVE, F., BURY, D., CLOUET, E., HIROTA, M., HOFFMANN, S., KÜHNEL, J. & LALKO, J. F. 2020. Development of a next generation risk assessment framework for the evaluation of skin sensitisation of cosmetic ingredients. *Regulatory Toxicology Pharmacology*, 116, 104721.
- GINET, V., PUYAL, J., CLARKE, P. G. & TRUTTMANN, A. C. 2009. Enhancement of autophagic flux after neonatal cerebral hypoxia-ischemia and its region-specific relationship to apoptotic mechanisms. *The American journal of pathology*, 175, 1962-1974.
- GOLSTEIN, P. & KROEMER, G. 2007. Cell death by necrosis: towards a molecular definition. *Trends in biochemical sciences*, 32, 37-43.
- GREEN, J. W., SPRINGER, T. A. & STAVELEY, J. P. 2013. The drive to ban the NOEC/LOEC in favor of ECx is misguided and misinformed. *Integrated environmental assessment management*, 9, 12-16.
- GROTH-PEDERSEN, L., JÄÄTTELÄ, M. & NYLANDSTED, J. 2015. A method to monitor lysosomal membrane permeabilization by immunocytochemistry. *Cold Spring Harbor Protocols*, 2015, pdb. prot086181.
- GUBBELS-VAN HAL, W., BLAAUBOER, B., BARENTSEN, H., HOITINK, M., MEERTS, I., VAN DER HOEVEN, J. J. R. T. & PHARMACOLOGY 2005. An alternative approach for the safety evaluation of new and existing chemicals, an exercise in integrated testing. 42, 284-295.
- GUISHUANG, W. & HAODONG, C. 2010. Adefovir dipivoxil and tenofovir-associated tubulopathy. *Adverse Drug Reactions Journal*, 1.

- GUPTA, S., GOVIL, D., KAKAR, P. N., PRAKASH, O., ARORA, D., DAS, S., GOVIL, P. & MALHOTRA, A. 2009. Colistin and polymyxin B: a re-emergence. *Indian journal of critical care medicine: peer-reviewed, official publication of Indian Society of Critical Care Medicine*, 13, 49.
- HAGOS, Y. & WOLFF, N. A. 2010. Assessment of the role of renal organic anion transporters in drug-induced nephrotoxicity. *Toxins*, 2, 2055-2082.
- HALAPPANAVAR, S., VAN DEN BRULE, S., NYMARK, P., GATÉ, L., SEIDEL, C., VALENTINO, S., ZHERNOVKOV, V., HØGH DANIELSEN, P., DE VIZCAYA, A. & WOLFF, H. 2020. Adverse outcome pathways as a tool for the design of testing strategies to support the safety assessment of emerging advanced materials at the nanoscale. *Particle Fibre Toxicology*, 17, 1-24.
- HALL, A. M. 2013. Update on tenofovir toxicity in the kidney. *Pediatric nephrology*, 28, 1011-1023.
- HARTUNG, T. 2017. Evolution of toxicological science: The need for change. *International Journal of Risk Assessment Management*, 20, 21-45.
- HARTUNG, T. & DASTON, G. 2009. Are in vitro tests suitable for regulatory use? *Toxicological sciences*, 111, 233-237.
- HASCHEK, W. M., ROUSSEAU, C. G. & WALLIG, M. A. 2013a. *Haschek and Rousseaux's handbook of toxicologic pathology*, Academic Press.
- HASCHEK, W. M., ROUSSEAU, C. G., WALLIG, M. A., BOLON, B. & OCHOA, R. 2013b. *Haschek and Rousseaux's handbook of toxicologic pathology*, Academic Press.
- HASHINO, E., SHERO, M. & SALVI, R. J. 1997. Lysosomal targeting and accumulation of aminoglycoside antibiotics in sensory hair cells. *Brain research*, 777, 75-85.
- HERLITZ, L. C., MOHAN, S., STOKES, M. B., RADHAKRISHNAN, J., D'AGATI, V. D. & MARKOWITZ, G. S. 2010. Tenofovir nephrotoxicity: acute tubular necrosis with distinctive clinical, pathological, and mitochondrial abnormalities. *Kidney international*, 78, 1171-1177.
- HEUSSNER, A. H. & DIETRICH, D. R. 2013. Primary porcine proximal tubular cells as an alternative to human primary renal cells in vitro: an initial characterization. *BMC cell biology*, 14, 55.
- HEYBELI, C., OKTAN, M. A. & ÇAVDAR, Z. 2019. Rat models of colistin nephrotoxicity: previous experimental researches and future perspectives. *European Journal of Clinical Microbiology Infectious Diseases*, 1-7.
- HITCHCOCK, M., JAFFE, H., MARTIN, J. & STAGG, R. 1996. Cidofovir, a new agent with potent anti-herpesvirus activity. *Antiviral Chemistry Chemotherapy*, 7, 115-127.
- HO, E. S., LIN, D. C., MENDEL, D. B. & CIHLAR, T. 2000. Cytotoxicity of antiviral nucleotides adefovir and cidofovir is induced by the expression of human renal organic anion transporter 1. *Journal of the American Society of Nephrology*, 11, 383-393.
- HONG, F., JIN, T. & ZHANG, A. 2004. Risk assessment on renal dysfunction caused by co-exposure to arsenic and cadmium using benchmark dose calculation in a Chinese population. *Biometals*, 17, 573-580.
- HORI, Y., AOKI, N., KUWAHARA, S., HOSOJIMA, M., KASEDA, R., GOTO, S., IIDA, T., DE, S., KABASAWA, H. & KANEKO, R. 2017. Megalin blockade with cilastatin suppresses drug-induced nephrotoxicity. *Journal of the American Society of Nephrology*, 28, 1783-1791.

- HOSOJIMA, M., SATO, H., YAMAMOTO, K., KASEDA, R., SOMA, T., KOBAYASHI, A., SUZUKI, A., KABASAWA, H., TAKEYAMA, A. & IKUYAMA, K. 2009. Regulation of megalin expression in cultured proximal tubule cells by angiotensin II type 1A receptor-and insulin-mediated signaling cross talk. *Endocrinology*, 150, 871-878.
- HRISTEV, H., BAYKOV, D., PENKOV, D., WILLEKE-WETSTEIN, C. & STEINBACH, J. 2003. STUDY ON THE CHEMICAL HETEROGENEITY OF CADMIUM AND LEAD IN THE BIOSPHERE-BIOACCUMULATION OF CADMIUM AND LEAD IN THE ORGANISM OF YOUNG RUMINANTS FROM ANTHROPOGENIC ECOSYSTEMS WITH AN INCREASED TECHNOGENIC CLARC. *Journal of Central European Agriculture*.
- HUA, C. T., HOPWOOD, J. J., CARLSSON, S. R., HARRIS, R. J. & MEIKLE, P. J. 1998. Evaluation of the lysosome-associated membrane protein LAMP-2 as a marker for lysosomal storage disorders. *Clinical chemistry*, 44, 2094-2102.
- HUANG, C.-C. & CHEN, W. 2018. A SERS method with attomolar sensitivity: a case study with the flavonoid catechin. *Microchimica Acta*, 185, 120.
- HUANG, J. X., KAESLIN, G., RANALL, M. V., BLASKOVICH, M. A., BECKER, B., BUTLER, M. S., LITTLE, M. H., LASH, L. H. & COOPER, M. A. 2015. Evaluation of biomarkers for in vitro prediction of drug-induced nephrotoxicity: comparison of HK-2, immortalized human proximal tubule epithelial, and primary cultures of human proximal tubular cells. *Pharmacology research perspectives*, 3, e00148.
- HUNT, P. R. 2017. The *C. elegans* model in toxicity testing. *Journal of Applied Toxicology*, 37, 50-59.
- HUO, W., ZHANG, K., NIE, Z., LI, Q. & JIN, F. 2010. Kidney injury molecule-1 (KIM-1): a novel kidney-specific injury molecule playing potential double-edged functions in kidney injury. *Transplantation Reviews*, 24, 143-146.
- HUSSAINI, I. M., BROWN, M. D., KARNS, L. R., CARPENTER, J., REDPATH, G. T., GONIAS, S. L. & VANDENBERG, S. R. 1999. Epidermal growth factor differentially regulates low density lipoprotein receptor-related protein gene expression in neoplastic and fetal human astrocytes. *Glia*, 25, 71-84.
- ICHIMURA, T., BONVENTRE, J. V., BAILLY, V., WEI, H., HESSION, C. A., CATE, R. L. & SANICOLA, M. 1998. Kidney injury molecule-1 (KIM-1), a putative epithelial cell adhesion molecule containing a novel immunoglobulin domain, is up-regulated in renal cells after injury. *Journal of Biological Chemistry*, 273, 4135-4142.
- IMAOKA, T., KUSUHARA, H., ADACHI, M., SCHUETZ, J. D., TAKEUCHI, K. & SUGIYAMA, Y. 2007. Functional involvement of multidrug resistance-associated protein 4 (MRP4/ABCC4) in the renal elimination of the antiviral drugs adefovir and tenofovir. *Molecular pharmacology*, 71, 619-627.
- ISSUANCE, E. P. N. P. 2005. The US Environmental Protection Agency (EPA) Plans To Issue A Wastewater Discharge Permit To: Concha Holdings, Ltd.
- IZZEDINE, H., LAUNAY-VACHER, V. & DERAY, G. 2005. Antiviral drug-induced nephrotoxicity. *American journal of kidney diseases*, 45, 804-817.
- JANG, K.-J., MEHR, A. P., HAMILTON, G. A., MCPARTLIN, L. A., CHUNG, S., SUH, K.-Y. & INGBER, D. E. 2013. Human kidney proximal tubule-on-a-chip for drug transport and nephrotoxicity assessment. *Integrative Biology*, 5, 1119-1129.
- JANSSON, B., KARVANEN, M., CARLSON, O., PLACHOURAS, D. & FRIBERG, L. E. 2009. Quantitative analysis of colistin A and colistin B in plasma and culture medium using a

- simple precipitation step followed by LC/MS/MS. *Journal of pharmaceutical biomedical analysis*, 49, 760-767.
- JÄRUP, L., HELLSTRÖM, L., ALFVÉN, T., CARLSSON, M. D., GRUBB, A., PERSSON, B., PETTERSSON, C., SPÅNG, G., SCHÜTZ, A. & ELINDER, C.-G. 2000. Low level exposure to cadmium and early kidney damage: the OSCAR study. *Occupational environmental medicine*, 57, 668-672.
- JIANG, H., SHA, S., FORGE, A. & SCHACHT, J. 2006. Caspase-independent pathways of hair cell death induced by kanamycin in vivo. *Cell Death Differentiation*, 13, 20-30.
- JOHANSSON, A.-C., APPELQVIST, H., NILSSON, C., KÅGEDAL, K., ROBERG, K. & ÖLLINGER, K. 2010. Regulation of apoptosis-associated lysosomal membrane permeabilization. *Apoptosis*, 15, 527-540.
- JOSEPH, J. S., MALINDISA, S. T. & NTWASA, M. 2018. Two-dimensional (2D) and three-dimensional (3D) cell culturing in drug discovery. *Cell Culture*, 2, 1-22.
- KÅGEDAL, K., JOHANSSON, A. C., JOHANSSON, U., HEIMLICH, G., ROBERG, K., WANG, N. S., JÜRGENSMEIER, J. M. & ÖLLINGER, K. 2005. Lysosomal membrane permeabilization during apoptosis-involvement of Bax? *International journal of experimental pathology*, 86, 309-321.
- KAHN, J., LAGAKOS, S., WULFSOHN, M., CHERNG, D., MILLER, M., CHERRINGTON, J., HARDY, D., BEALL, G., COOPER, R. & MURPHY, R. 1999. Efficacy and safety of adefovir dipivoxil with antiretroviral therapy: a randomized controlled trial. *Jama*, 282, 2305-2312.
- KAPALCZYŃSKA, M., KOLENDA, T., PRZYBYŁA, W., ZAJĄCZKOWSKA, M., TERESIAK, A., FILAS, V., IBBS, M., BLIŹNIAK, R., ŁUCZEWSKI, Ł. & LAMPERSKA, K. 2018. 2D and 3D cell cultures—a comparison of different types of cancer cell cultures. *Archives of medical science: AMS*, 14, 910.
- KARASAWA, T. & STEYGER, P. S. 2011. Intracellular mechanisms of aminoglycoside-induced cytotoxicity. *Integrative Biology*, 3, 879-886.
- KARIM, Q. A., KARIM, S. S. A., FROHLICH, J. A., GROBLER, A. C., BAXTER, C., MANSOOR, L. E., KHARSANY, A. B., SIBEKO, S., MLISANA, K. P. & OMAR, Z. 2010. Effectiveness and safety of tenofovir gel, an antiretroviral microbicide, for the prevention of HIV infection in women. *Science*, 329, 1168-1174.
- KASSAMALI, Z., JAIN, R. & DANZIGER, L. H. 2015. An update on the arsenal for multidrug-resistant *Acinetobacter* infections: polymyxin antibiotics. *International Journal of Infectious Diseases*, 30, 125-132.
- KAYE, K. S., POGUE, J. M. & KAYE, D. 2015. Polymyxins (polymyxin B and colistin). *Mandell, Douglas, and Bennett's principles and practice of infectious diseases*. Elsevier.
- KEIRSTEAD, N. D., WAGONER, M. P., BENTLEY, P., BLAIS, M., BROWN, C., CHEATHAM, L., CIACCIO, P., DRAGAN, Y., FERGUSON, D. & FIKES, J. 2013. Early prediction of polymyxin-induced nephrotoxicity with next-generation urinary kidney injury biomarkers. *Toxicological sciences*, 137, 278-291.
- KELESIDIS, T. & FALAGAS, M. E. 2015. The safety of polymyxin antibiotics. *Expert opinion on drug safety*, 14, 1687-1701.
- KIM, S. & TAKAYAMA, S. 2015. Organ-on-a-chip and the kidney. *Kidney research clinical practice*, 34, 165-169.

- KIMBER, I., DEARMAN, R. J., BASKETTER, D. A. & BOVERHOF, D. R. 2014. Chemical respiratory allergy: reverse engineering an adverse outcome pathway. *Toxicology*, 318, 32-39.
- KIRKEGAARD, T. & JÄÄTTELÄ, M. 2009. Lysosomal involvement in cell death and cancer. *Biochimica et Biophysica Acta - Molecular Cell Research*, 1793, 746-754.
- KLAASSEN, C. D., LIU, J. & DIWAN, B. A. 2009. Metallothionein protection of cadmium toxicity. *Toxicology applied pharmacology*, 238, 215-220.
- KNAPEN, D., ANGRISH, M. M., FORTIN, M. C., KATSIADAKI, I., LEONARD, M., MARGIOTTA-CASALUCI, L., MUNN, S., O'BRIEN, J. M., POLLESCH, N., SMITH, L. C. J. E. T. & CHEMISTRY 2018. Adverse outcome pathway networks I: development and applications. 37, 1723-1733.
- KNIGHT, A., BAILEY, J. & BALCOMBE, J. 2006. Animal carcinogenicity studies: 1. Poor human predictivity.
- KODELL, R. L. & GAYLOR, D. W. 1997. Uncertainty of estimates of cancer risks derived by extrapolation from high to low doses and from animals to humans. *International Journal of Toxicology*, 16, 449-460.
- KOHLER, J. J., HOSSEINI, S. H., GREEN, E., ABUIN, A., LUDAWAY, T., RUSS, R., SANTOIANNI, R. & LEWIS, W. 2011. Tenofovir renal proximal tubular toxicity is regulated by OAT1 and MRP4 transporters. *Laboratory investigation*, 91, 852.
- KOHLER, J. J., HOSSEINI, S. H., HOYING-BRANDT, A., GREEN, E., JOHNSON, D. M., RUSS, R., TRAN, D., RAPER, C. M., SANTOIANNI, R. & LEWIS, W. 2009a. Tenofovir renal toxicity targets mitochondria of renal proximal tubules. *Laboratory investigation*, 89, 513-519.
- KOHLER, J. J., HOSSEINI, S. H., HOYING-BRANDT, A., GREEN, E., JOHNSON, D. M., RUSS, R., TRAN, D., RAPER, C. M., SANTOIANNI, R. & LEWIS, W. J. L. I. 2009b. Tenofovir renal toxicity targets mitochondria of renal proximal tubules. 89, 513-519.
- KRAMER, N. I., DI CONSIGLIO, E., BLAAUBOER, B. J. & TESTAI, E. 2015. Biokinetics in repeated-dosing in vitro drug toxicity studies. *Toxicology in Vitro*, 30, 217-224.
- KRAMER, N. I., KRISMARTINA, M., RICO-RICO, A. N., BLAAUBOER, B. J. & HERMENS, J. L. 2012. Quantifying processes determining the free concentration of phenanthrene in basal cytotoxicity assays. *Chemical research in toxicology*, 25, 436-445.
- KRASICH, R. & COPELAND, W. C. 2017. DNA polymerases in the mitochondria: a critical review of the evidence. *Frontiers in bioscience*, 22, 692.
- KRAUSE, R. J., LASH, L. H. & ELFARRA, A. A. 2003. Human kidney flavin-containing monooxygenases and their potential roles in cysteine S-conjugate metabolism and nephrotoxicity. *Journal of Pharmacology Experimental Therapeutics*, 304, 185-191.
- KREWSKI, D., ANDERSEN, M. E., MANTUS, E. & ZEISE, L. 2009. Toxicity testing in the 21st century: implications for human health risk assessment. *Risk Analysis: An International Journal*, 29, 474-479.
- KROEMER, G. & JÄÄTTELÄ, M. 2005. Lysosomes and autophagy in cell death control. *Nature Reviews Cancer*, 5, 886-897.
- KUBIN, C. J., ELLMAN, T. M., PHADKE, V., HAYNES, L. J., CALFEE, D. P. & YIN, M. T. 2012. Incidence and predictors of acute kidney injury associated with intravenous polymyxin B therapy. *Journal of Infection*, 65, 80-87.

- LACY, S. A., HITCHCOCK, M. J., LEE, W. A., TELLIER, P. & CUNDY, K. C. 1998. Effect of oral probenecid coadministration on the chronic toxicity and pharmacokinetics of intravenous cidofovir in cynomolgus monkeys. *Toxicological Sciences*, 44, 97-106.
- LALEZARI, J., DREW, W., GLUTZER, E., JAMES, C., MINER, D., FLAHERTY, J., FISHER, P., CUNDY, K., HANNIGAN, J. & MARTIN, J. 1995. (S)-1-[3-hydroxy-2-(phosphonylmethoxy) propyl] cytosine (cidofovir): results of a phase I/II study of a novel antiviral nucleotide analogue. *Journal of Infectious Diseases*, 171, 788-796.
- LALEZARI, J. P., STAGG, R. J., KUPPERMANN, B. D., HOLLAND, G. N., KRAMER, F., IVES, D. V., YOULE, M., ROBINSON, M. R., DREW, W. L. & JAFFE, H. S. 1997. Intravenous cidofovir for peripheral cytomegalovirus retinitis in patients with AIDS: a randomized, controlled trial. *Annals of Internal Medicine*, 126, 257-263.
- LANDIS, W. G. & CHAPMAN, P. M. 2011. Well past time to stop using NOELs and LOELs. *Integrated Environmental Assessment Management*, 7, vi-viii.
- LASH, L. H. & PARKER, J. C. 2001. Hepatic and renal toxicities associated with perchloroethylene. *Pharmacological reviews*, 53, 177-208.
- LASH, L. H., PUTT, D. A. & CAI, H. 2006. Membrane transport function in primary cultures of human proximal tubular cells. *Toxicology*, 228, 200-218.
- LASH, L. H., PUTT, D. A., HUENI, S. E., CAO, W., XU, F., KULIDJIAN, S. J. & HORWITZ, J. P. 2002. Cellular energetics and glutathione status in NRK-52E cells: toxicological implications. *Biochemical pharmacology*, 64, 1533-1546.
- LASH, L. H., PUTT, D. A., XU, F. & MATHERLY, L. H. 2007. Role of rat organic anion transporter 3 (Oat3) in the renal basolateral transport of glutathione. *Chemico-biological interactions*, 170, 124-134.
- LASKOWSKI, R. 1995. Some good reasons to ban the use of NOEC, LOEC and related concepts in ecotoxicology. *Oikos*, 140-144.
- LEBRECHT, D., VENHOFF, A. C., KIRSCHNER, J., WIECH, T., VENHOFF, N. & WALKER, U. A. 2009. Mitochondrial tubulopathy in tenofovir disoproxil fumarate-treated rats. *JAIDS Journal of Acquired Immune Deficiency Syndromes*, 51, 258-263.
- LECHNER, C. A. 2014. *Nierenzellen als In-vitro-Modell zur Evaluierung der renalen Sekretion von Arzneistoffkandidaten*.
- LEE, J. & KIM, S. 2018. Kidney-on-a-chip: a new technology for predicting drug efficacy, interactions, and drug-induced nephrotoxicity. *Current drug metabolism*, 19, 577-583.
- LEIST, M., GHALLAB, A., GRAEPEL, R., MARCHAN, R., HASSAN, R., BENNEKOU, S. H., LIMONCIEL, A., VINKEN, M., SCHILDKNECHT, S. & WALDMANN, T. J. A. O. T. 2017. Adverse outcome pathways: opportunities, limitations and open questions. 91, 3477-3505.
- LENHARD, J. R., BULMAN, Z. P., TSUJI, B. T. & KAYE, K. S. 2019. Shifting gears: the future of polymyxin antibiotics. *Antibiotics*, 8, 42.
- LEWIS, W. 2003b. Mitochondrial dysfunction and nucleoside reverse transcriptase inhibitor therapy: experimental clarifications and persistent clinical questions. *Antiviral research*, 58, 189-197.
- LEWIS, W., COPELAND, W. C. & DAY, B. J. 2001. Mitochondrial DNA depletion, oxidative stress, and mutation: Mechanisms Of dysfunction from nucleoside reverse transcriptase inhibitors. *Laboratory investigation*, 81, 777-790.
- LEWIS, W. & DALAKAS, M. C. 1995. Mitochondrial toxicity of antiviral drugs. *Nature medicine*, 1, 417-422.



- LEWIS, W., DAY, B. J. & COPELAND, W. C. 2003a. Mitochondrial toxicity of NRTI antiviral drugs: an integrated cellular perspective. *Nature Reviews Drug Discovery*, 2, 812.
- LI, Y., CONG, R. & BIEMESDERFER, D. 2008. The COOH terminus of megalin regulates gene expression in opossum kidney proximal tubule cells. *American Journal of Physiology-Cell Physiology*, 295, C529-C537.
- LIBORIO, A. B., ANDRADE, L., PEREIRA, L. V., SANCHES, T. R., SHIMIZU, M. H. & SEGURO, A. C. 2008. Rosiglitazone reverses tenofovir-induced nephrotoxicity. *Kidney international*, 74, 910-918.
- LIMONCIEL, A., ASCHAUER, L., WILMES, A., PRAJCZER, S., LEONARD, M. O., PFALLER, W. & JENNINGS, P. 2011. Lactate is an ideal non-invasive marker for evaluating temporal alterations in cell stress and toxicity in repeat dose testing regimes. *Toxicology in Vitro*, 25, 1855-1862.
- LIU, Z., HUANG, R., ROBERTS, R. & TONG, W. 2019. Toxicogenomics: a 2020 vision. *Trends in Pharmacological Sciences*, 40, 92-103.
- LOCK, E. A. & REED, C. J. 2006. Trichloroethylene: mechanisms of renal toxicity and renal cancer and relevance to risk assessment. *Toxicological sciences*, 91, 313-331.
- LOENS, C., AMET, S., ISNARD-BAGNIS, C., DERAY, G. & TOURRET, J. 2018. Néphrotoxicité des antirétroviraux autres que le ténofovir. *Nephrologie thérapeutique*, 14, 55-66.
- LU, S., SUNG, T., LIN, N., ABRAHAM, R. T. & JESSEN, B. A. 2017. Lysosomal adaptation: How cells respond to lysosomotropic compounds. *PLoS One*, 12.
- LU, X., CHAN, T., XU, C., ZHU, L., ZHOU, Q. T., ROBERTS, K. D., CHAN, H.-K., LI, J. & ZHOU, F. 2015. Human oligopeptide transporter 2 (PEPT2) mediates cellular uptake of polymyxins. *Journal of Antimicrobial Chemotherapy*, 71, 403-412.
- LUNDHOLM, C. & ANDERSSON, L. 1985. Biosphere levels of cadmium, zinc and copper around an old Swedish copper mine. *Ambio*, 167-172.
- LUNGKAPHIN, A., LEWCHALERMWONGSE, B. & CHATSUDTHIPONG, V. 2006. Relative contribution of OAT1 and OAT3 transport activities in isolated perfused rabbit renal proximal tubules. *Biochimica et Biophysica Acta - Biomembranes*, 1758, 789-795.
- LUO, Q., DENG, Y., CHENG, F., KANG, J., ZHONG, S., ZHANG, D. & ZENG, W. 2016. Relationship between nephrotoxicity and long-term adefovir dipivoxil therapy for chronic hepatitis B: A meta-analysis. *Medicine*, 95.
- LUZIO, J. P., HACKMANN, Y., DIECKMANN, N. M. & GRIFFITHS, G. M. 2014. The biogenesis of lysosomes and lysosome-related organelles. *Cold Spring Harbor perspectives in biology*, 6, a016840.
- LUZIO, J. P., PRYOR, P. R. & BRIGHT, N. A. 2007. Lysosomes: fusion and function. *Nature reviews Molecular cell biology*, 8, 622-632.
- MA, Z., WANG, J., GERBER, J. P. & MILNE, R. W. 2008. Determination of colistin in human plasma, urine and other biological samples using LC-MS/MS. *Journal of Chromatography B*, 862, 205-212.
- MA, Z., WANG, J., NATION, R. L., LI, J., TURNIDGE, J. D., COULTHARD, K. & MILNE, R. W. 2009. Renal disposition of colistin in the isolated perfused rat kidney. *Antimicrobial agents chemotherapy*, 53, 2857-2864.
- MALLICK, P., SONG, G., EFREMENKO, A. Y., PENDSE, S. N., CREEK, M. R., OSIMITZ, T. G., HINES, R. N., HINDERLITER, P., CLEWELL, H. J. & LAKE, B. G. 2020.

- Physiologically Based Pharmacokinetic Modeling in Risk Assessment: Case Study With Pyrethroids. *Toxicological Sciences*, 176, 460-469.
- MANCHANDANI, P., ZHOU, J., BABIC, J. T., LEDESMA, K. R., TRUONG, L. D. & TAM, V. H. 2017. Role of renal drug exposure in polymyxin B-Induced nephrotoxicity. *Antimicrobial agents chemotherapy*, 61, e02391-16.
- MANCHANDANI, P., ZHOU, J., LEDESMA, K. R., TRUONG, L. D., CHOW, D. S.-L., ERIKSEN, J. L. & TAM, V. H. 2016. Characterization of polymyxin B biodistribution and disposition in an animal model. *Antimicrobial agents chemotherapy*, 60, 1029-1034.
- MARCELLIN, P., CHANG, T.-T., LIM, S. G., TONG, M. J., SIEVERT, W., SHIFFMAN, M. L., JEFFERS, L., GOODMAN, Z., WULFSOHN, M. S. & XIONG, S. 2003. Adefovir dipivoxil for the treatment of hepatitis B e antigen–positive chronic hepatitis B. *New England Journal of Medicine*, 348, 808-816.
- MARKOU, N., MARKANTONIS, S. L., DIMITRAKIS, E., PANIDIS, D., BOUTZOUKA, E., KARATZAS, S., RAFAILIDIS, P., APOSTOLAKOS, H. & BALTOPOULOS, G. 2008. Colistin serum concentrations after intravenous administration in critically ill patients with serious multidrug-resistant, gram-negative bacilli infections: a prospective, open-label, uncontrolled study. *Clinical therapeutics*, 30, 143-151.
- MARKOWITZ, G. S. & PERAZELLA, M. A. 2005. Drug-induced renal failure: a focus on tubulointerstitial disease. *Clinica Chimica Acta*, 351, 31-47.
- MARTIN, J. L., BROWN, C. E., MATTHEWS-DAVIS, N. & REARDON, J. E. 1994. Effects of antiviral nucleoside analogs on human DNA polymerases and mitochondrial DNA synthesis. *Antimicrobial agents chemotherapy*, 38, 2743-2749.
- MARZOLO, M.-P. & FARFÁN, P. 2011. New insights into the roles of megalin/LRP2 and the regulation of its functional expression. *Biological research*, 44, 89-105.
- MASANÉS, F., BARRIENTOS, A., CEBRIÁN, M., PEDROL, E., MIRÓ, O., CASADEMONT, J. & GRAU, J. M. 1998. Clinical, histological and molecular reversibility of zidovudine myopathy. *Journal of the neurological sciences*, 159, 226-228.
- MAZZOCCHI, L. C., VOHWINKEL, C. U., MAYER, K., HEROLD, S., MORTY, R. E., SEEGER, W. & VADÁSZ, I. 2017. TGF- $\beta$  inhibits alveolar protein transport by promoting shedding, regulated intramembrane proteolysis, and transcriptional downregulation of megalin. *American Journal of Physiology-Lung Cellular Molecular Physiology*, 313, L807-L824.
- MEI, H., SUN, S., BAI, Y., CHEN, Y., CHAI, R. & LI, H. 2015. Reduced mtDNA copy number increases the sensitivity of tumor cells to chemotherapeutic drugs. *Cell death disease*, 6, e1710.
- MEIKLE, P. J., BROOKS, D. A., RAVENSCROFT, E. M., YAN, M., WILLIAMS, R. E., JAUNZEMS, A. E., CHATAWAY, T. K., KARAGEORGOS, L. E., DAVEY, R. C. & BOULTER, C. D. 1997. Diagnosis of lysosomal storage disorders: evaluation of lysosome-associated membrane protein LAMP-1 as a diagnostic marker. *Clinical chemistry*, 43, 1325-1335.
- MENEZES, C., DUARTE, R., DICKENS, C., DIX-PEEK, T., VAN AMSTERDAM, D., JOHN, M. A., IVE, P., MASKEW, M., MACPHAIL, P. & FOX, M. 2013. The early effects of stavudine compared with tenofovir on adipocyte gene expression,

- mitochondrial DNA copy number and metabolic parameters in South African HIV-infected patients: a randomized trial. *HIV medicine*, 14, 217-225.
- MICHALOPOULOS, A. S. & FALAGAS, M. E. 2011. Colistin: recent data on pharmacodynamics properties and clinical efficacy in critically ill patients. *Annals of intensive care*, 1, 30.
- MINER, J. H. 2011. Glomerular basement membrane composition and the filtration barrier. *Pediatric nephrology*, 26, 1413-1417.
- MING, X. & THAKKER, D. R. 2010. Role of basolateral efflux transporter MRP4 in the intestinal absorption of the antiviral drug adefovir dipivoxil. *Biochemical pharmacology*, 79, 455-462.
- MOESTRUP, S. K., CUI, S., VORUM, H., BREGENGÅRD, C., BJØRN, S., NORRIS, K., GLIEMANN, J. & CHRISTENSEN, E. I. 1995. Evidence that epithelial glycoprotein 330/megalin mediates uptake of polybasic drugs. *The Journal of clinical investigation*, 96, 1404-1413.
- MORAES, C. B., WITT, G., KUZIKOV, M., ELLINGER, B., CALOGEROPOULOU, T., PROUSIS, K. C., MANGANI, S., DI PISA, F., LANDI, G. & IACONO, L. D. 2019. Accelerating drug discovery efforts for trypanosomatid infections using an integrated transnational academic drug discovery platform. *SLAS DISCOVERY: Advancing Life Sciences R*, 24, 346-361.
- MORTON, D. M. 1998. Importance of species selection in drug toxicity testing. *Toxicology letters*, 102, 545-550.
- MOXON, T. E., LI, H., LEE, M.-Y., PIECHOTA, P., NICOL, B., PICKLES, J., PENDLINGTON, R., SORRELL, I. & BALTAZAR, M. T. 2020. Application of physiologically based kinetic (PBK) modelling in the next generation risk assessment of dermally applied consumer products. *Toxicology in Vitro*, 63, 104746.
- MRSCHTIK, M. & RYAN, K. M. 2015. Lysosomal proteins in cell death and autophagy. *The FEBS journal*, 282, 1858-1870.
- MUDGE, G., GEMBORYS, M. W. & DUGGIN, G. 1978. Covalent binding of metabolites of acetaminophen to kidney protein and depletion of renal glutathione. *Journal of Pharmacology Experimental Therapeutics*, 206, 218-226.
- MURADO, M. & PRIETO, M. J. S. O. T. T. E. 2013. NOEC and LOEC as merely concessive expedients: Two unambiguous alternatives and some criteria to maximize the efficiency of dose–response experimental designs. 461, 576-586.
- MURPHY, R. A. 2017. Tenofovir Induced Nephrotoxicity: A Mechanistic Study.
- NAGAI, J., SATO, K., YUMOTO, R. & TAKANO, M. 2011. Megalin/cubilin-mediated uptake of FITC-labeled IgG by OK kidney epithelial cells. *Drug metabolism pharmacokinetics*, 1106230197-1106230197.
- NAGAI, J. & TAKANO, M. 2014. Entry of aminoglycosides into renal tubular epithelial cells via endocytosis-dependent and endocytosis-independent pathways. *Biochemical pharmacology*, 90, 331-337.
- NATION, R. L., VELKOV, T. & LI, J. 2014. Colistin and polymyxin B: peas in a pod, or chalk and cheese? *Clinical infectious diseases*, 59, 88-94.
- NATIONAL\_RESEARCH\_COUNCIL 1994. *Science and judgment in risk assessment*, National Academies Press.
- NATIONAL\_RESEARCH\_COUNCIL 2007. *Toxicity Testing in the 21st Century: A Vision and a Strategy*. Washington, DC: The National Academies Press.

- NELSON, L. S., HOFFMAN, R. S., HOWLAND, M. A., LEWIN, N. A. & GOLDFRANK, L. R. 2018. *Goldfrank's toxicologic emergencies*, McGraw Hill Professional.
- NIELSEN, R., CHRISTENSEN, E. I. & BIRN, H. 2016. Megalin and cubilin in proximal tubule protein reabsorption: from experimental models to human disease. *Kidney international*, 89, 58-67.
- NIESKENS, T. T., PETERS, J. G., SCHREURS, M. J., SMITS, N., WOESTENENK, R., JANSEN, K., VAN DER MADE, T. K., RÖRING, M., HILGENDORF, C. & WILMER, M. J. 2016. A human renal proximal tubule cell line with stable organic anion transporter 1 and 3 expression predictive for antiviral-induced toxicity. *The AAPS journal*, 18, 465-475.
- NILSSON, A., GOODWIN, R. J., SWALES, J. G., GALLAGHER, R., SHANKARAN, H., SATHE, A., PRADEEPAN, S., XUE, A., KEIRSTEAD, N. & SASAKI, J. C. 2015. Investigating nephrotoxicity of polymyxin derivatives by mapping renal distribution using mass spectrometry imaging. *Chemical research in toxicology*, 28, 1823-1830.
- NIROGI, R., BHYRAPUNENI, G., KANDIKERE, V., MUDDANA, N., SARALAYA, R., KOMARNENI, P., MUDIGONDA, K. & MUKKANTI, K. 2012. Pharmacokinetic profiling of efavirenz–emtricitabine–tenofovir fixed dose combination in pregnant and non-pregnant rats. *Biopharmaceutics drug disposition*, 33, 265-277.
- NISHIMURA, M. & NAITO, S. 2006. Tissue-specific mRNA expression profiles of human phase I metabolizing enzymes except for cytochrome P450 and phase II metabolizing enzymes. *Drug metabolism pharmacokinetics*, 21, 357-374.
- OBERLE, C., HUAI, J., REINHECKEL, T., TACKE, M., RASSNER, M., EKERT, P. G., BUELLESBACH, J. & BORNER, C. 2010. Lysosomal membrane permeabilization and cathepsin release is a Bax/Bak-dependent, amplifying event of apoptosis in fibroblasts and monocytes. *Cell death differentiation*, 17, 1167.
- OECD 2006. Current approaches in the statistical analysis of ecotoxicology data: A guidance to application.
- OECD 2016. *Users' Handbook Supplement to the Guidance Document for Developing and Assessing Adverse Outcome Pathways*, OECD publishing.
- ORTIZ, A., JUSTO, P., SANZ, A., MELERO, R., CAMELO, C., GUERRERO, M. F., STRUTZ, F., MÜLLER, G., BARAT, A. & EGIDO, J. 2005. Short communication tubular cell apoptosis and cidofovir-induced acute renal failure. *Antivir Ther*, 10, 185-190.
- PAMIES, D. & HARTUNG, T. 2016. 21st century cell culture for 21st century toxicology. *Chemical research in toxicology*, 30, 43-52.
- PATLEWICZ, G., SIMON, T. W., ROWLANDS, J. C., BUDINSKY, R. A. & BECKER, R. A. 2015. Proposing a scientific confidence framework to help support the application of adverse outcome pathways for regulatory purposes. *Regulatory Toxicology Pharmacology*, 71, 463-477.
- PAVELKA, M. & ROTH, J. 2015. *Functional ultrastructure: atlas of tissue biology and pathology*, Springer.
- PAVKOVIC, M., ROBINSON-COHEN, C., CHUA, A. S., NICOARA, O., CÁRDENAS-GONZÁLEZ, M., BIJOL, V., RAMACHANDRAN, K., HAMPSON, L., PIRMOHAMED, M. & ANTOINE, D. J. 2016. Detection of drug-induced acute kidney injury in humans using urinary KIM-1, miR-21, -200c, and -423. *Toxicological Sciences*, 152, 205-213.

- PERAZELLA, M. A. J. K. I. 2010. Tenofovir-induced kidney disease: an acquired renal tubular mitochondriopathy. *78*, 1060-1063.
- PERKINS, E. J., ASHAUER, R., BURGOON, L., CONOLLY, R., LANDESMANN, B., MACKAY, C., MURPHY, C. A., POLLESCH, N., WHEELER, J. R. & ZUPANIC, A. 2019. Building and applying quantitative adverse outcome pathway models for chemical hazard and risk assessment. *Environmental toxicology chemistry*, *38*, 1850-1865.
- PERKINS, E. J., CHIPMAN, J. K., EDWARDS, S., HABIB, T., FALCIANI, F., TAYLOR, R., VAN AGGELEN, G., VULPE, C., ANTCZAK, P. & LOGUINOV, A. 2011. Reverse engineering adverse outcome pathways. *Environmental toxicology chemistry*, *30*, 22-38.
- PEZESHKPOUR, G., ILLA, I. & DALAKAS, M. C. 1991. Ultrastructural characteristics and DNA immunocytochemistry in human immunodeficiency virus and zidovudine-associated myopathies. *Human pathology*, *22*, 1281-1288.
- PHE, K., LEE, Y., MCDANELD, P. M., PRASAD, N., YIN, T., FIGUEROA, D. A., MUSICK, W. L., COTTREAU, J. M., HU, M. & TAM, V. H. 2014. In vitro assessment and multicenter cohort study of comparative nephrotoxicity rates associated with colistimethate versus polymyxin B therapy. *Antimicrobial agents chemotherapy*, *58*, 2740-2746.
- PHILLIPS, A. O., STEADMAN, R., MORRISEY, K. & WILLIAMS, J. D. 1997. Polarity of stimulation and secretion of transforming growth factor-beta 1 by cultured proximal tubular cells. *The American journal of pathology*, *150*, 1101.
- PIEGORSCH, W. W. 2014. Low-Dose Extrapolation. *Wiley StatsRef: Statistics Reference Online*.
- POET, T., SCHLOSSER, P., RODRIGUEZ, C., PAROD, R., RODWELL, D. & KIRMAN, C. 2016. Using physiologically based pharmacokinetic modeling and benchmark dose methods to derive an occupational exposure limit for N-methylpyrrolidone. *Regulatory Toxicology Pharmacology*, *76*, 102-112.
- POGUE, J. M., LEE, J., MARCHAIM, D., YEE, V., ZHAO, J. J., CHOPRA, T., LEPHART, P. & KAYE, K. S. 2011. Incidence of and risk factors for colistin-associated nephrotoxicity in a large academic health system. *Clinical infectious diseases*, *53*, 879-884.
- POLESEL, M. & HALL, A. M. 2019. Axial differences in endocytosis along the kidney proximal tubule. *American Journal of Physiology-Renal Physiology*, *317*, F1526-F1530.
- PREUSS, H. G. 1993. Basics of renal anatomy and physiology. *Clinics in laboratory medicine*, *13*, 1-11.
- PRIOR, H., CASEY, W., KIMBER, I., WHELAN, M. & SEWELL, F. 2019. Reflections on the progress towards non-animal methods for acute toxicity testing of chemicals. *Regulatory Toxicology Pharmacology*, *102*, 30-33.
- PROZIALECK, W. C. & EDWARDS, J. R. 2012. Mechanisms of cadmium-induced proximal tubule injury: new insights with implications for biomonitoring and therapeutic interventions. *Journal of Pharmacology Experimental Therapeutics*, *343*, 2-12.
- PUNT, A., PEIJNENBURG, A. A., HOOGENBOOM, R. L. & BOUWMEESTER, H. 2017. Non-animal approaches for toxicokinetics in risk evaluations of food chemicals. *ALTEX-Alternatives to animal experimentation*, *34*, 501-514.

- PUYAL, J., VASLIN, A., MOTTIER, V., CLARKE, P. G. J. A. O. N. O. J. O. T. A. N. A. & SOCIETY, T. C. N. 2009. Postischemic treatment of neonatal cerebral ischemia should target autophagy. *66*, 378-389.
- QUIROS, Y., VICENTE-VICENTE, L., MORALES, A. I., LÓPEZ-NOVOA, J. M. & LÓPEZ-HERNÁNDEZ, F. J. 2010. An integrative overview on the mechanisms underlying the renal tubular cytotoxicity of gentamicin. *Toxicological sciences*, *119*, 245-256.
- QUIROS, Y., VICENTE-VICENTE, L., MORALES, A. I., LÓPEZ-NOVOA, J. M. & LÓPEZ-HERNÁNDEZ, F. J. 2011. An integrative overview on the mechanisms underlying the renal tubular cytotoxicity of gentamicin. *Toxicological sciences*, *119*, 245-256.
- RALL, D. P. & POPE, A. M. 1995. *Environmental medicine: integrating a missing element into medical education*, National Academies Press.
- RAMAMOORTHY, H., ABRAHAM, P. & ISAAC, B. 2014. Mitochondrial dysfunction and electron transport chain complex defect in a rat model of tenofovir disoproxil fumarate nephrotoxicity. *Journal of biochemical molecular toxicology*, *28*, 246-255.
- RAMAMOORTHY, H., ABRAHAM, P., ISAAC, B. & SELVAKUMAR, D. 2019. Mitochondrial pathway of apoptosis and necrosis contribute to tenofovir disoproxil fumarate-induced renal damage in rats. *Human experimental toxicology*, *38*, 288-302.
- RAMAMOORTHY, H., ISSAC, B. & ABRAHAM, P. 2012. Evidence for the roles of oxidative stress, nitrosative stress and Nf-Kb activation in Tenofovir Disoproxil Fumarate (TDF) induced renal damage in rats. *BMC infectious diseases*, *12*, P6.
- RAND, M. D., MONTGOMERY, S. L., PRINCE, L. & VOROJEIKINA, D. 2014. Developmental toxicity assays using the Drosophila model. *Current protocols in toxicology*, *59*, 1.12. 1-1.12. 20.
- RAY, A. S., CIHLAR, T., ROBINSON, K. L., TONG, L., VELA, J. E., FULLER, M. D., WIEMAN, L. M., EISENBERG, E. J. & RHODES, G. R. 2006. Mechanism of active renal tubular efflux of tenofovir. *Antimicrobial agents chemotherapy*, *50*, 3297-3304.
- REISER, J., ADAIR, B. & REINHECKEL, T. 2010. Specialized roles for cysteine cathepsins in health and disease. *The Journal of clinical investigation*, *120*, 3421-3431.
- REPNIK, U., STOKA, V., TURK, V. & TURK, B. 2012. Lysosomes and lysosomal cathepsins in cell death. *Biochimica et Biophysica Acta -Proteins Proteomics*, *1824*, 22-33.
- REYNAUD, L., CARLEO, M. A., TALAMO, M., BORGIA, G. J. T. & MANAGEMENT, C. R. 2009. Tenofovir and its potential in the treatment of hepatitis B virus. *5*, 177.
- RIGATTO, M. H., BEHLE, T. F., FALCI, D. R., FREITAS, T., LOPES, N. T., NUNES, M., COSTA, L. W. & ZAVASCKI, A. P. 2015. Risk factors for acute kidney injury (AKI) in patients treated with polymyxin B and influence of AKI on mortality: a multicentre prospective cohort study. *Journal of Antimicrobial Chemotherapy*, *70*, 1552-1557.
- RODRÍGUEZ-NÓVOA, S., LABARGA, P., D'AVOLIO, A., BARREIRO, P., ALBALATE, M., VISPO, E., SOLERA, C., SICCARDI, M., BONORA, S. & DI PERRI, G. 2010. Impairment in kidney tubular function in patients receiving tenofovir is associated with higher tenofovir plasma concentrations. *Aids*, *24*, 1064-1066.
- ROGGEN, E. L. 2011. In vitro toxicity testing in the twenty-first century. *Frontiers in pharmacology*, *2*, 3.
- ROONEY, J. P., RYDE, I. T., SANDERS, L. H., HOWLETT, E. H., COLTON, M. D., GERM, K. E., MAYER, G. D., GREENAMYRE, J. T. & MEYER, J. N. 2015. PCR based determination of mitochondrial DNA copy number in multiple species. *Mitochondrial Regulation*. Humana Press: Springer.

- ROVIDA, C., ALÉPÉE, N., API, A. M., BASKETTER, D. A., BOIS, F. Y., CALONI, F., CORSINI, E., DANESHIAN, M., ESKES, C. & EZENDAM, J. 2015a. Integrated Testing Strategies (ITS) for safety assessment. *ALTEX-Alternatives to Animal Experimentations*, 32, 25-40.
- ROVIDA, C., ASAKURA, S., DANESHIAN, M., HOFMAN-HUETHER, H., LEIST, M., MEUNIER, L., REIF, D., ROSSI, A., SCHMUTZ, M. & VALENTIN, J.-P. 2015b. Toxicity testing in the 21st century beyond environmental chemicals. *ALTEX-Alternatives to animal experimentation*, 32, 171.
- RUAN, B., LU, X. & LIN, Y. 2013. Evaluation of adverse reactions induced by adefovir dipivoxil in 85 chronic hepatitis B patients. *Clin Hepatol*, 29, 104-6.
- RUSSELL, W. M. S. & BURCH, R. L. 1959. *The principles of humane experimental technique*, Methuen London.
- RUSSO, L. M., DEL RE, E., BROWN, D. & LIN, H. Y. 2007. Evidence for a role of transforming growth factor (TGF)- $\beta$ 1 in the induction of postglomerular albuminuria in diabetic nephropathy: amelioration by soluble TGF- $\beta$  type II receptor. *Diabetes*, 56, 380-388.
- RYAN, S.-L., BAIRD, A.-M., VAZ, G., URQUHART, A. J., SENGE, H., RICHARD, D. J., O'BYRNE, K. J. & DAVIES, A. M. 2016. Drug discovery approaches utilizing three-dimensional cell culture. *Assay drug development technologies*, 14, 19-28.
- SABOLIĆ, I., BRELJAK, D., ŠKARICA, M. & HERAK-KRAMBERGER, C. M. J. B. 2010. Role of metallothionein in cadmium traffic and toxicity in kidneys and other mammalian organs. 23, 897-926.
- SACHANA, M. 2019. Adverse Outcome Pathways and Their Role in Revealing Biomarkers. *Biomarkers in Toxicology*. Elsevier.
- SADER, H. S., RHOMBERG, P. R., FARRELL, D. J. & JONES, R. N. 2015. Differences in potency and categorical agreement between colistin and polymyxin B when testing 15,377 clinical strains collected worldwide. *Diagnostic microbiology infectious disease*, 83, 379-381.
- SAFTIG, P. & KLUMPERMAN, J. 2009. Lysosome biogenesis and lysosomal membrane proteins: trafficking meets function. *Nature reviews Molecular cell biology*, 10, 623-635.
- SANDRI, A. M., LANDERSDORFER, C. B., JACOB, J., BONIATTI, M. M., DALAROSA, M. G., FALCI, D. R., BEHLE, T. F., BORDINHÃO, R. C., WANG, J. & FORREST, A. 2013. Population pharmacokinetics of intravenous polymyxin B in critically ill patients: implications for selection of dosage regimens. *Clinical infectious diseases*, 57, 524-531.
- SANTAMARÍA, C., MYKIETIUK, A., TEMPORITI, E., STRYJEWSKI, M. E., HERRERA, F. & BONVEHI, P. 2009. Nephrotoxicity associated with the use of intravenous colistin. *Scandinavian journal of infectious diseases*, 41, 767-769.
- SCHNELLMANN, R. G. 2008. Toxic responses of the kidney. *Cassarett Doull's Toxicology*. New York: McGraw-Hill Medical Publishing Division.
- SCHUH, C. D., POLESEL, M., PLATONOVA, E., HAENNI, D., GASSAMA, A., TOKONAMI, N., GHAZI, S., BUGARSKI, M., DEVUYST, O. & ZIEGLER, U. 2018. Combined structural and functional imaging of the kidney reveals major axial differences in proximal tubule endocytosis. *Journal of the American Society of Nephrology*, 29, 2696-2712.

- SECKER, P. F., LUKS, L., SCHLICHENMAIER, N. & DIETRICH, D. R. 2018. RPTEC/TERT1 cells form highly differentiated tubules when cultured in a 3D matrix. *Alternatives to Animal Experimentation: ALTEX*, 35, 223-234.
- SEWELL, F., GELLATLY, N., BEAUMONT, M., BURDEN, N., CURRIE, R., DE HAAN, L., HUTCHINSON, T. H., JACOBS, M., MAHONY, C. & MALCOMBER, I. 2018. The future trajectory of adverse outcome pathways: a commentary. *Archives of toxicology*, 92, 1657-1661.
- SHAH, M., BATERINA JR, O. Y., TAUPIN, V. & FARQUHAR, M. G. 2013. ARH directs megalin to the endocytic recycling compartment to regulate its proteolysis and gene expression. *Journal of Cell Biology*, 202, 113-127.
- SHAHRBAF, F. G. & ASSADI, F. 2015. Drug-induced renal disorders. *Journal of renal injury prevention*, 4, 57.
- SHIDA, Y., NOHDA, S., GROSS, A. S., PALMER, J. L., MORIMOTO, K. & EGAWA, A. 2005. Pharmacokinetics of Adefovir after Oral Administration of Adefovir Dipivoxil 10 mg in Healthy Japanese Males and Japanese Patients with Chronic Hepatitis B. *Rinsho yakuri/Japanese Journal of Clinical Pharmacology Therapeutics*, 36, 289-296.
- SHIMOHATA, H., SAKAI, S., OGAWA, Y., HIRAYAMA, K. & KOBAYASHI, M. 2013. Osteomalacia due to Fanconi's syndrome and renal failure caused by long-term low-dose adefovir dipivoxil. *Clinical experimental nephrology*, 17, 147.
- SHRIVASTAVA, A. & GUPTA, V. B. 2011. Methods for the determination of limit of detection and limit of quantitation of the analytical methods. *Chronicles of young scientists*, 2, 21.
- SIMON, B., WILSON, M. & WICKLIFFE, J. 2014b. The RPTEC/TERT1 cell line models key renal cell responses to the environmental toxicants, benzo [a] pyrene and cadmium. *Toxicology reports*, 1, 231-242.
- SIMON, T. W., SIMONS JR, S. S., PRESTON, R. J., BOOBIS, A. R., COHEN, S. M., DOERRER, N. G., FENNER-CRISP, P. A., MCMULLIN, T. S., MCQUEEN, C. A. & ROWLANDS, J. C. 2014a. The use of mode of action information in risk assessment: quantitative key events/dose-response framework for modeling the dose-response for key events. *Critical reviews in toxicology*, 44, 17-43.
- SLATTERY, C., JANG, Y., KRUGER, W., HRYCIW, D., LEE, A. & PORONNIK, P. 2013.  $\gamma$ -Secretase inhibition promotes fibrotic effects of albumin in proximal tubular epithelial cells. *British journal of pharmacology*, 169, 1239-1251.
- SMITH, H. W. 1951. *The kidney: structure and function in health and disease*, Oxford University Press, USA.
- SORLÍ, L., LUQUE, S., GRAU, S., BERENQUER, N., SEGURA, C., MONTERO, M. M., ÁLVAREZ-LERMA, F., KNOBEL, H., BENITO, N. & HORCAJADA, J. P. 2013. Trough colistin plasma level is an independent risk factor for nephrotoxicity: a prospective observational cohort study. *BMC infectious diseases*, 13, 1-9.
- SORLÍ, L., LUQUE, S., SEGURA, C., CAMPILLO, N., MONTERO, M., ESTEVE, E., HERRERA, S., BENITO, N., ALVAREZ-LERMA, F. & GRAU, S. 2017. Impact of colistin plasma levels on the clinical outcome of patients with infections caused by extremely drug-resistant *Pseudomonas aeruginosa*. *BMC infectious diseases*, 17, 11.
- SPINU, N., BAL-PRICE, A., CRONIN, M. T., ENOCH, S. J., MADDEN, J. C. & WORTH, A. P. 2019. Development and analysis of an adverse outcome pathway network for human neurotoxicity. *Archives of toxicology*, 93, 2759-2772.



- STADNICKA-MICHALAK, J., KNÖBEL, M., ŽUPANIČ, A. & SCHIRMER, K. 2018. A validated algorithm for selecting non-toxic chemical concentrations. *ALTEX-Alternatives to animal experimentation*, 35, 37-50.
- STANKOV, M. V., LÜCKE, T., DAS, A. M., SCHMIDT, R. E. & BEHRENS, G. M. 2010. Mitochondrial DNA depletion and respiratory chain activity in primary human subcutaneous adipocytes treated with nucleoside analogue reverse transcriptase inhibitors. *Antimicrobial agents chemotherapy*, 54, 280-287.
- STEYGER, P. S., PETERS, S., REHLING, J., HORDICHOK, A. & DAI, C. 2003. Uptake of gentamicin by bullfrog saccular hair cells in vitro. *Journal of the Association for Research in Otolaryngology*, 4, 565-578.
- STOKNIENE, J., POWELL, L. C., AARSTAD, O. A., AACHMANN, F. L., RYE, P. D., HILL, K. E., THOMAS, D. W. & FERGUSON, E. L. J. P. 2020. Bi-Functional Alginate Oligosaccharide–Polymyxin Conjugates for Improved Treatment of Multidrug-Resistant Gram-Negative Bacterial Infections. 12, 1080.
- STORM, T., CHRISTENSEN, E. I., CHRISTENSEN, J. N., KJAERGAARD, T., ULDBJERG, N., LARSEN, A., HONORÉ, B. & MADSEN, M. 2016. Megalin is predominantly observed in vesicular structures in first and third trimester cytotrophoblasts of the human placenta. *Journal of Histochemistry Cytochemistry*, 64, 769-784.
- STRAY, K. M., BAM, R. A., BIRKUS, G., HAO, J., LEPIST, E.-I., YANT, S. R., RAY, A. S. & CIHLAR, T. 2013. Evaluation of the effect of cobicistat on the in vitro renal transport and cytotoxicity potential of tenofovir. *Antimicrobial agents chemotherapy*, 57, 4982-4989.
- SUZUKI, T., YAMAGUCHI, H., OGURA, J., KOBAYASHI, M., YAMADA, T. & ISEKI, K. 2013. Megalin contributes to kidney accumulation and nephrotoxicity of colistin. *Antimicrobial agents chemotherapy*, 57, 6319-6324.
- TALMON, G., CORNELL, L. & LAGER, D. Mitochondrial changes in cidofovir therapy for BK virus nephropathy. *Transplantation proceedings*, 2010. Elsevier, 1713-1715.
- TANEVA, E., CROOKER, K., PARK, S. H., SU, J. T., OTT, A., CHESHENKO, N., SZLEIFER, I., KISER, P. F., FRANK, B. & MESQUITA, P. M. 2016. Differential mechanisms of tenofovir and tenofovir disoproxil fumarate cellular transport and implications for topical preexposure prophylaxis. *Antimicrobial agents chemotherapy*, 60, 1667-1675.
- TANJI, N., TANJI, K., KAMBHAM, N., MARKOWITZ, G. S., BELL, A. & D'AGATI, V. D. 2001. Adefovir nephrotoxicity: possible role of mitochondrial DNA depletion. *Human pathology*, 32, 734-740.
- TAURIS, J., CHRISTENSEN, E. I., NYKJÆR, A., JACOBSEN, C., PETERSEN, C. M. & OVESEN, T. 2009. Cubilin and megalin co-localize in the neonatal inner ear. *Audiology Neurotology*, 14, 267-278.
- THAKAR, J., MOHANTY, S., WEST, A. P., JOSHI, S. R., UEDA, I., WILSON, J., MENG, H., BLEVINS, T. P., TSANG, S. & TRENTALANGE, M. J. 2015. Aging-dependent alterations in gene expression and a mitochondrial signature of responsiveness to human influenza vaccination. *Aging*, 7, 38.
- THOMAS, R. S., PAULES, R. S., SIMEONOV, A., FITZPATRICK, S. C., CROFTON, K. M., CASEY, W. M. & MENDRICK, D. L. 2018. The US Federal Tox21 Program: A strategic and operational plan for continued leadership. *ALTEX-Alternatives to animal experimentation*, 35, 163.

- 
- THOMAS, R. S., PHILBERT, M. A., AUERBACH, S. S., WETMORE, B. A., DEVITO, M. J., COTE, I., ROWLANDS, J. C., WHELAN, M. P., HAYS, S. M. & ANDERSEN, M. E. 2013. Incorporating new technologies into toxicity testing and risk assessment: moving from 21st century vision to a data-driven framework. *Toxicological sciences*, 136, 4-18.
- THOMASINA BARRON, E., O'BRIEN, A. & RYAN, M. 1990. Primary cultures of rat and rabbit renal proximal epithelium as models for nephrotoxicity investigations. *Toxicology letters*, 53, 161-165.
- THUL, P. J., ÅKESSON, L., WIKING, M., MAHDESSIAN, D., GELADAKI, A., BLAL, H. A., ALM, T., ASPLUND, A., BJÖRK, L. & BRECKELS, L. M. 2017. A subcellular map of the human proteome. *Science*, 356, eaal3321.
- TIONG, H. Y., HUANG, P., XIONG, S., LI, Y., VATHSALA, A. & ZINK, D. 2014. Drug-induced nephrotoxicity: clinical impact and preclinical in vitro models. *Molecular pharmaceutics*, 11, 1933-1948.
- TODARO, G. J., FRYLING, C. & DE LARCO, J. E. 1980. Transforming growth factors produced by certain human tumor cells: polypeptides that interact with epidermal growth factor receptors. *Proceedings of the National Academy of Sciences*, 77, 5258-5262.
- TRAN, T. B., VELKOV, T., NATION, R. L., FORREST, A., TSUJI, B. T., BERGEN, P. J. & LI, J. 2016. Pharmacokinetics/pharmacodynamics of colistin and polymyxin B: are we there yet? *International journal of antimicrobial agents*, 48, 592-597.
- TURK, B. & STOKA, V. 2007. Protease signalling in cell death: caspases versus cysteine cathepsins. *FEBS letters*, 581, 2761-2767.
- TURK, V., STOKA, V., VASILJEVA, O., RENKO, M., SUN, T., TURK, B. & TURK, D. 2012. Cysteine cathepsins: from structure, function and regulation to new frontiers. *Biochimica et Biophysica Acta - Proteins Proteomics*, 1824, 68-88.
- UHLÉN, M., BJÖRLING, E., AGATON, C., SZIGYARTO, C. A.-K., AMINI, B., ANDERSEN, E., ANDERSSON, A.-C., ANGELIDOU, P., ASPLUND, A. & ASPLUND, C. 2005. A human protein atlas for normal and cancer tissues based on antibody proteomics. *Molecular cellular proteomics*, 4, 1920-1932.
- UHLÉN, M., FAGERBERG, L., HALLSTRÖM, B. M., LINDSKOG, C., OKSVOLD, P., MARDINOGLU, A., SIVERTSSON, Å., KAMPF, C., SJÖSTEDT, E. & ASPLUND, A. 2015. Tissue-based map of the human proteome. *Science*, 347, 1260419.
- UHLÉN, M., OKSVOLD, P., FAGERBERG, L., LUNDBERG, E., JONASSON, K., FORSBERG, M., ZWAHLEN, M., KAMPF, C., WESTER, K. & HOBER, S. 2010. Towards a knowledge-based human protein atlas. *Nature biotechnology*, 28, 1248.
- UHLÉN, M., ZHANG, C., LEE, S., SJÖSTEDT, E., FAGERBERG, L., BIDKHORI, G., BENFEITAS, R., ARIF, M., LIU, Z. & EDFORS, F. 2017. A pathology atlas of the human cancer transcriptome. *Science*, 357, eaan2507.
- VAARA, M. 1992. Agents that increase the permeability of the outer membrane. *Microbiology Molecular Biology Reviews*, 56, 395-411.
- VAARA, M. 2010b. Polymyxins and their novel derivatives. *Current opinion in microbiology*, 13, 574-581.
- VAARA, M., SIIKANEN, O., APAJALAHTI, J., FOX, J., FRIMODT-MØLLER, N., HE, H., POUDYAL, A., LI, J., NATION, R. L. & VAARA, T. 2010a. A novel polymyxin derivative that lacks the fatty acid tail and carries only three positive charges has strong
-

- synergism with agents excluded by the intact outer membrane. *Antimicrobial agents chemotherapy*, 54, 3341-3346.
- VAIDYA, V. S., FERGUSON, M. A. & BONVENTRE, J. V. 2008. Biomarkers of acute kidney injury. *Annu. Rev. Pharmacol. Toxicol.*, 48, 463-493.
- VAN DER HOEVEN, N. 1997. How to measure no effect. Part III: statistical aspects of NOEC, EC<sub>x</sub> and NEC estimates. *Environmetrics: The official journal of the International Environmetrics Society*, 8, 255-261.
- VATTIMO, M. D. F. F., WATANABE, M., DA FONSECA, C. D., DE MOURA NEIVA, L. B., PESSOA, E. A. & BORGES, F. T. 2016. Polymyxin B nephrotoxicity: from organ to cell damage. *PloS one*, 11.
- VIDAL, F., DOMINGO, J. C., GUALLAR, J., SAUMOY, M., CORDOBILLA, B., DE LA ROSA, R. S., GIRALT, M., ALVAREZ, M. L., LÓPEZ-DUPLA, M., TORRES, F. J. A. A. & CHEMOTHERAPY 2006. In vitro cytotoxicity and mitochondrial toxicity of tenofovir alone and in combination with other antiretrovirals in human renal proximal tubule cells. 50, 3824-3832.
- VIGANO, M., LAMPERTICO, P. & COLOMBO, M. 2011. Drug safety evaluation of adefovir in HBV infection. *Expert opinion on drug safety*, 10, 809-818.
- VILLENEUVE, D. L., CRUMP, D., GARCIA-REYERO, N., HECKER, M., HUTCHINSON, T. H., LALONE, C. A., LANDESMANN, B., LETTIERI, T., MUNN, S. & NEPELSKA, M. 2014. Adverse outcome pathway (AOP) development I: strategies and principles. *Toxicological Sciences*, 142, 312-320.
- VINKEN, M. 2013. The adverse outcome pathway concept: a pragmatic tool in toxicology. *Toxicology*, 312, 158-165.
- VINKEN, M., KNAPEN, D., VERGAUWEN, L., HENGSTLER, J. G., ANGRISH, M. & WHELAN, M. 2017. Adverse outcome pathways: a concise introduction for toxicologists. *Archives of toxicology*, 91, 3697-3707.
- VINKEN, P., STARCKX, S., BARALE-THOMAS, E., LOOSZOVA, A., SONEE, M., GOEMINNE, N., VERSMISSEN, L., BUYENS, K. & LAMPO, A. 2012. Tissue Kim-1 and urinary clusterin as early indicators of cisplatin-induced acute kidney injury in rats. *Toxicologic pathology*, 40, 1049-1062.
- VRBOVA, M., DASTYCHOVA, E. & ROUSAR, T. 2016. Renal cell lines for study of nephrotoxicity in vitro. *Mil Med Sci Lett*, 85, 69-74.
- WALLIG, M. A., BOLON, B., HASCHEK, W. M. & ROUSSEAU, C. G. 2017. *Fundamentals of toxicologic pathology*, Academic Press.
- WANG, B. F., WANG, Y., WANG, B. Y., SUN, F. R., ZHANG, D. & CHEN, Y. S. 2015. Osteomalacia and Fanconi's syndrome caused by long-term low-dose adefovir dipivoxil. *Journal of clinical pharmacy therapeutics*, 40, 345-348.
- WANG, F., GÓMEZ-SINTES, R. & BOYA, P. 2018. Lysosomal membrane permeabilization and cell death. *Traffic*, 19, 918-931.
- WIEGERS, T. C., DAVIS, A. P., COHEN, K. B., HIRSCHMAN, L. & MATTINGLY, C. J. 2009. Text mining and manual curation of chemical-gene-disease networks for the comparative toxicogenomics database (CTD). *BMC bioinformatics*, 10, 326.
- WIESER, M., STADLER, G., JENNINGS, P., STREUBEL, B., PFALLER, W., AMBROS, P., RIEDL, C., KATINGER, H., GRILLARI, J. & GRILLARI-VOGLAUER, R. J. A. J. O. P.-R. P. 2008. hTERT alone immortalizes epithelial cells of renal proximal tubules without changing their functional characteristics. 295, F1365-F1375.

- WIGNALL, J. A., SHAPIRO, A. J., WRIGHT, F. A., WOODRUFF, T. J., CHIU, W. A., GUYTON, K. Z. & RUSYN, I. 2014. Standardizing benchmark dose calculations to improve science-based decisions in human health assessments. *Environmental health perspectives*, 122, 499-505.
- WILL, Y. & DYKENS, J. A. 2018. *Mitochondrial Dysfunction Caused by Drugs and Environmental Toxicants*, John Wiley & Sons.
- WILMES, A., ASCHAUER, L., LIMONCIEL, A., PFALLER, W. & JENNINGS, P. 2014. Evidence for a role of claudin 2 as a proximal tubular stress responsive paracellular water channel. *Toxicology applied pharmacology*, 279, 163-172.
- WILMES, A., BIELOW, C., RANNINGER, C., BELLWON, P., ASCHAUER, L., LIMONCIEL, A., CHASSAIGNE, H., KRISTL, T., AICHE, S. & HUBER, C. G. 2015. Mechanism of cisplatin proximal tubule toxicity revealed by integrating transcriptomics, proteomics, metabolomics and biokinetics. *Toxicology in Vitro*, 30, 117-127.
- WILMES, A., LIMONCIEL, A., ASCHAUER, L., MOENKS, K., BIELOW, C., LEONARD, M. O., HAMON, J., CARPI, D., RUZEK, S. & HANDLER, A. 2013. Application of integrated transcriptomic, proteomic and metabolomic profiling for the delineation of mechanisms of drug induced cell stress. *Journal of proteomics*, 79, 180-194.
- WOLFF, N. A., LEE, W.-K. & THÉVENOD, F. 2011. Role of Arf1 in endosomal trafficking of protein–metal complexes and cadmium–metallothionein-1 toxicity in kidney proximal tubule cells. *Toxicology letters*, 203, 210-218.
- WORTH, A., BARROSO, J., BREMER, S., BURTON, J., CASATI, S., COECKE, S., CORVI, R., DESPREZ, B., DUMONT, C. & GOULIARMOU, V. 2014. Alternative methods for regulatory toxicology—a state-of-the-art review. *Joint Res Counc Sci Policy Rep EUR*, 26797, 1-470.
- YANG, H. & SHU, Y. 2015. Cadmium transporters in the kidney and cadmium-induced nephrotoxicity. *International journal of molecular sciences*, 16, 1484-1494.
- YOON, I.-S., SON, J.-H., KIM, S.-B., CHOI, M.-K. & MAENG, H.-J. 2015. Effects of 1 $\alpha$ , 25-Dihydroxyvitamin D3 on Intestinal Absorption and Disposition of Adefovir Dipivoxil and Its Metabolite, Adefovir, in Rats. *Biological Pharmaceutical Bulletin*, 38, 1732-1737.
- YOON, M., CAMPBELL, J. L., ANDERSEN, M. E. & CLEWELL, H. J. 2012. Quantitative in vitro to in vivo extrapolation of cell-based toxicity assay results. *Critical reviews in toxicology*, 42, 633-652.
- YU, F., PERSSON, B., LÖFÅS, S. & KNOLL, W. 2004. Attomolar sensitivity in bioassays based on surface plasmon fluorescence spectroscopy. *Journal of the American Chemical Society*, 126, 8902-8903.
- YU, L., LI, H., ZHANG, C., ZHANG, Q., GUO, J., LI, J., YUAN, H., LI, L., CARMICHAEL, P. & PENG, S. 2020. Integrating in vitro testing and physiologically-based pharmacokinetic (PBPK) modelling for chemical liver toxicity assessment—A case study of troglitazone. *Environmental Toxicology Pharmacology*, 74, 103296.
- ZAVASCKI, A. P., GOLDANI, L. Z., CAO, G., SUPERTI, S. V., LUTZ, L., BARTH, A. L., RAMOS, F., BONIATTI, M. M., NATION, R. L. & LI, J. J. C. I. D. 2008. Pharmacokinetics of intravenous polymyxin B in critically ill patients. 47, 1298-1304.

- ZAVASCKI, A. P. & NATION, R. L. 2017. Nephrotoxicity of polymyxins: is there any difference between colistimethate and polymyxin B? *Antimicrobial agents chemotherapy*, 61, e02319-16.
- ZENG, M., MAO, Y., YAO, G., WANG, H., HOU, J., WANG, Y., JI, B. N., CHANG, C. N. P. & BARKER, K. F. 2006. A double-blind randomized trial of adefovir dipivoxil in Chinese subjects with HBeAg-positive chronic hepatitis B. *Hepatology*, 44, 108-116.
- ZENNARO, C., ARTERO, M., MASO, V. & CARRARO, M. 2014. Small molecule membrane transporters in the mammalian podocyte: a pathogenic and therapeutic target. *International journal of molecular sciences*, 15, 21366-21380.
- ZHANG, M., VAN RAVENZWAAY, B., FABIAN, E., RIETJENS, I. M. & LOUISSE, J. 2018b. Towards a generic physiologically based kinetic model to predict in vivo uterotrophic responses in rats by reverse dosimetry of in vitro estrogenicity data. *Archives of toxicology*, 92, 1075-1088.
- ZHANG, X., SCIALIS, R. J., FENG, B. & LEACH, K. 2013. Detection of statin cytotoxicity is increased in cells expressing the OATP1B1 transporter. *Toxicological sciences*, 134, 73-82.
- ZHANG, X., WANG, R., PIOTROWSKI, M., ZHANG, H. & LEACH, K. L. 2015. Intracellular concentrations determine the cytotoxicity of adefovir, cidofovir and tenofovir. *Toxicology in Vitro*, 29, 251-258.
- ZHAO, X., SUN, K., LAN, Z., SONG, W., CHENG, L., CHI, W., CHEN, J., HUO, Y., XU, L. & LIU, X. 2017. Tenofovir and adefovir down-regulate mitochondrial chaperone TRAP1 and succinate dehydrogenase subunit B to metabolically reprogram glucose metabolism and induce nephrotoxicity. *Scientific reports*, 7, 46344.
- ZHENG, X.-Y., WEI, R.-B., TANG, L., LI, P. & ZHENG, X.-D. 2012. Meta-analysis of combined therapy for adult hepatitis B virus-associated glomerulonephritis. *World journal of gastroenterology: WJG*, 18, 821.
- ZHUO, J. L. & LI, X. C. 2013. Proximal nephron. *Comprehensive Physiology*, 3, 1079-1123.
- ZOU, Z., CHUNG, B., NGUYEN, T., MENTONE, S., THOMSON, B. & BIEMESDERFER, D. 2004. Linking receptor-mediated endocytosis and cell signaling evidence for regulated intramembrane proteolysis of megalin in proximal tubule. *Journal of Biological Chemistry*, 279, 34302-34310.



## 8 Appendix

**Table 40**  
**Raw data LAMP-1/2 assay**

<b>Polymyxin B / NRK-52E / 24 h</b>					
Conc. [ $\mu$ M]	Experiment 1 [%]	Experiment 2 [%]	Experiment 3 [%]	Mean [%]	Stand. Dev. [%]
0	100	100	100	100	0
7.81	120.699	96.15575	153.0711	123.31	23.31
15.60	119.6294	142.8694	185.8536	149.45	27.43
31.25	114.9092	142.027	246.6801	167.87	56.81
62.50	182.4805	211.0384	266.9995	220.17	35.10
250.00	202.5814	226.8268	336.3092	255.24	58.17
500.00	217.8385	267.8733	580.3704	355.36	160.41
1000.00	189.3477	523.5794	592.1245	435.02	175.95

<b>Colistin / NRK-52E / 24 h</b>					
Conc. [ $\mu$ M]	Experiment 1 [%]	Experiment 2 [%]	Experiment 3 [%]	Mean [%]	Stand. Dev. [%]
0	100	100	100	100	0
7.81	105.96	102.29	94.74	101.00	4.67
15.60	106.22	106.39	108.59	107.07	1.08
31.25	108.56	106.58	105.32	106.82	1.33
62.50	124.46	118.27	118.71	120.48	2.82
250.00	154.79	123.07	211.86	163.24	36.74
500.00	179.38	151.18	242.51	191.02	38.18
1000.00	251.27	207.16	282.38	246.94	30.86

<b>Polymyxin B nonapeptide / NRK-52E / 24 h</b>					
Conc. [ $\mu$ M]	Experiment 1 [%]	Experiment 2 [%]	Experiment 3 [%]	Mean [%]	Stand. Dev. [%]
0	100	100	100	100	0
7.81	105.43	93.43	96.1	98.32	5.14
15.60	96.85	98.03	111.07	101.98	6.44
31.25	101.6	103.43	99.12	101.38	1.77
62.50	99.93	124.69	98.75	107.79	11.96
250.00	121.02	133.02	114.12	122.72	7.81
500.00	94.92	148.09	132.72	125.24	22.34
1000.00	126.1	152.74	188.36	155.73	25.51

---

*Appendix*

---

<b>Polymyxin B / RPTEC/TERT1 / 24 h</b>					
Conc. [ $\mu$ M]	Experiment 1 [%]	Experiment 2 [%]	Experiment 3 [%]	Mean [%]	Stand. Dev. [%]
0	100	100	100	100	0
7.81	101.6996	134.6512	124.3629	120.24	13.77
15.60	137.1429	150.8767	136.6493	141.56	6.59
31.25	138.1185	214.9114	159.6767	170.90	32.34
62.50	259.3306	584.5974	218.7361	354.22	163.74
250.00	281.4996	843.5814	362.3629	495.81	248.11
500.00	751.2188	1519.376	623.5669	964.72	395.65
1000.00	772.6115	1729.663	657.0115	1053.10	480.73

<b>Colistin / RPTEC/TERT1 / 24 h</b>					
Conc. [ $\mu$ M]	Experiment 1 [%]	Experiment 2 [%]	Experiment 3 [%]	Mean [%]	Stand. Dev. [%]
0	100	100	100	100	0
7.81	138.0294	96.22747	145.7859	126.68	21.77
15.60	152.7305	83.32288	202.0147	146.02	48.69
31.25	171.6029	209.6187	207.6659	196.30	17.48
62.50	234.6295	321.132	251.9739	269.25	37.37
250.00	336.6539	432.1527	355.7548	374.85	41.26
500.00	424.1752	441.1259	471.0949	445.47	19.40
1000.00	396.1911	437.6824	830.5048	554.79	195.69

<b>Polymyxin B nonapeptide / RPTEC/TERT1 / 24 h</b>					
Conc. [ $\mu$ M]	Experiment 1 [%]	Experiment 2 [%]	Experiment 3 [%]	Mean [%]	Stand. Dev. [%]
0	100	100	100	100	0
7.81	130.56	154.44	150.23	145.08	10.41
15.60	158.17	123.79	120.45	134.14	17.05
31.25	106.96	143.16	154.46	134.86	20.26
62.50	197.31	171.19	241.31	203.27	28.93
250.00	159.87	114.61	193.3	155.93	32.25
500.00	170.78	119.63	168.26	152.89	23.54
1000.00	243.09	182.25	187.42	204.25	27.54

---



**Table 41**  
**Raw data cathepsin assay**

<b>Polymyxin B / NRK-52E / 24 h</b>					
Conc. [ $\mu$ M]	Experiment 1 [%]	Experiment 2 [%]	Experiment 3 [%]	Mean [%]	Stand. Dev. [%]
0	100	100	100	100	0
7.81	82.97	93.50	90.28	88.91	4.41
15.60	64.67	76.52	84.81	75.33	8.26
31.25	48.70	74.79	75.83	66.44	12.55
62.50	59.16	67.69	33.26	53.37	14.64
250.00	31.46	49.61	24.74	35.27	10.50
500.00	32.65	38.65	13.53	28.28	10.71
1000.00	32.37	39.52	11.91	27.94	11.70

<b>Colistin / NRK-52E / 24 h</b>					
Conc. [ $\mu$ M]	Experiment 1 [%]	Experiment 2 [%]	Experiment 3 [%]	Mean [%]	Stand. Dev. [%]
0	100	100	100	100	0
7.81	115.39	88.83	83.90	96.04	13.83
15.60	110.11	83.93	86.08	93.37	11.87
31.25	104.45	67.26	69.76	80.49	16.97
62.50	98.37	39.01	64.09	67.16	24.33
250.00	96.74	37.02	56.78	63.51	24.84
500.00	82.00	46.73	49.35	59.36	16.04
1000.00	74.88	43.53	44.24	54.22	14.61

<b>Polymyxin B nonapeptide / NRK-52E / 24 h</b>					
Conc. [ $\mu$ M]	Experiment 1 [%]	Experiment 2 [%]	Experiment 3 [%]	Mean [%]	Stand. Dev. [%]
0	100	100	100	100	0
7.81	95.34	97.23	98.51	97.03	1.30
15.60	93.65	100.76	91.12	95.18	4.08
31.25	87.84	69.09	84.04	80.32	8.09
62.50	90.13	73.89	76.70	80.24	7.09
250.00	83.89	81.00	70.60	78.50	5.71
500.00	79.55	43.78	81.88	68.40	17.44
1000.00	70.46	37.29	81.75	63.17	18.87

*Appendix*

---

<b>Polymyxin B / RPTEC/TERT1 / 24 h</b>					
Conc. [ $\mu$ M]	Experiment 1 [%]	Experiment 2 [%]	Experiment 3 [%]	Mean [%]	Stand. Dev. [%]
0	100	100	100	100	0
7.81	96.83786	86.80987	97.64777	93.77	4.93
15.60	85.40186	80.70342	80.15585	82.09	2.35
31.25	67.50954	73.39803	58.2196	66.38	6.25
62.50	63.51284	61.49759	45.38321	56.80	8.11
250.00	48.58479	39.52644	47.89075	45.33	4.12
500.00	38.61866	24.09679	39.75847	34.16	7.13
1000.00	32.56665	24.67188	27.91441	28.38	3.24

**Table 42**  
**Raw data cytotoxicity AOP1**

<b>Polymyxin B / NRK-52E / 24 h</b>					
Conc. [ $\mu$ M]	Experiment 1 [%]	Experiment 2 [%]	Experiment 3 [%]	Mean [%]	Stand. Dev. [%]
0	100	100	100	100	0
7.81	96.20946	101.2908	94.77428	97.42	2.80
15.60	91.01471	98.12798	96.89226	95.34	3.10
31.25	94.20738	84.50402	97.85079	92.19	5.63
62.50	92.80848	85.86594	96.69768	91.79	4.48
125.00	93.92182	89.94665	91.07245	91.65	1.67
250.00	80.12465	75.65588	78.31246	78.03	1.84
500.00	56.55874	48.4963	57.12189	54.06	3.94
1000.00	23.21612	15.62412	30.97812	23.27	6.27
2000.00	0.781095	0.5375952	2.362663	1.23	0.81
<b>Colistin / NRK-52E / 24 h</b>					
Conc. [ $\mu$ M]	Experiment 1 [%]	Experiment 2 [%]	Experiment 3 [%]	Mean [%]	Stand. Dev. [%]
0	100	100	100	100	0
7.81	99.9154	106.2477	80.23142	95.46	11.08
15.60	97.66199	107.0786	94.50298	99.75	5.34
31.25	98.17638	105.0073	95.37501	99.52	4.05
62.50	98.00205	108.2595	98.37193	101.54	4.75
125.00	96.82562	107.1121	96.53476	100.16	4.92
250.00	93.08305	105.4681	91.45713	96.67	6.26
500.00	93.33035	92.82756	90.08087	92.08	1.43
1000.00	79.42406	72.8168	74.58723	75.61	2.79
2000.00	57.69582	54.46556	30.76035	47.64	12.01
<b>Polymyxin B nonapeptide / NRK-52E / 24 h</b>					
Conc. [ $\mu$ M]	Experiment 1 [%]	Experiment 2 [%]	Experiment 3 [%]	Mean [%]	Stand. Dev. [%]
0	100	100	100	100	0
7.81	96.24838	94.33091	97.35288	95.98	1.25
15.60	100.3661	97.60231	87.79912	95.26	5.39
31.25	91.11298	85.18277	89.83543	88.71	2.55
62.50	101.4156	88.97209	88.75589	93.05	5.92
125.00	99.7525	93.5285	92.4405	95.24	3.22
250.00	99.08726	93.9119	89.36948	94.12	3.97
500.00	98.73338	96.34101	92.6076	95.89	2.52
1000.00	95.77887	92.28139	93.09589	93.72	1.49
2000.00	92.39053	86.19843	76.73977	85.11	6.44

*Appendix*

<b>Polymyxin B / RPTEC/TERT1 / 24 h</b>					
Conc. [ $\mu$ M]	Experiment 1 [%]	Experiment 2 [%]	Experiment 3 [%]	Mean [%]	Stand. Dev. [%]
0	100	100	100	100	0
7.81	97.38998	103.2233	90.61765	97.08	5.15
15.60	82.20299	102.5386	95.82825	93.52	8.46
31.25	82.70555	96.70928	93.86275	91.09	6.04
62.50	39.1975	43.8261	38.95761	40.66	2.24
125.00	6.635727	8.382122	3.512132	6.18	2.01
250.00	1.785227	0.931605	0.8962226	1.20	0.41
500.00	0.317896	0.2888312	0.2696041	0.29	0.02
1000.00	0.124326	0.1088665	0.09576051	0.11	0.01
2000.00	0.07995707	0.08554432	0.08057243	0.08	0.00

<b>Colistin / RPTEC/TERT1 / 24 h</b>					
Conc. [ $\mu$ M]	Experiment 1 [%]	Experiment 2 [%]	Experiment 3 [%]	Mean [%]	Stand. Dev. [%]
0	100	100	100	100	0
7.81	95.24521	94.34537	96.87212	95.49	1.05
15.60	85.39441	102.7058	96.34161	94.81	7.15
31.25	89.07421	100.8318	93.18286	94.36	4.87
62.50	87.30845	86.7738	92.99959	89.03	2.82
125.00	57.13114	68.89393	68.23672	64.75	5.40
250.00	25.46572	14.20204	16.59388	18.75	4.85
500.00	3.791618	2.942552	4.972667	3.90	0.83
1000.00	2.057608	0.2950578	0.7197173	1.02	0.75
2000.00	0.5780392	0.1457759	0.2712694	0.33	0.18

<b>Polymyxin B nonapeptide / RPTEC/TERT1 / 24 h</b>					
Conc. [ $\mu$ M]	Experiment 1 [%]	Experiment 2 [%]	Experiment 3 [%]	Mean [%]	Stand. Dev. [%]
0	100	100	100	100	0
7.81	94.27635	95.5771	98.17969	96.01	1.62
15.60	91.0409	92.44712	92.75854	92.08	0.75
31.25	88.74993	99.28193	86.96297	91.66	5.44
62.50	86.19971	96.63611	94.92244	92.59	4.57
125.00	92.93916	100.8883	94.00822	95.95	3.52
250.00	88.59222	102.7872	92.59472	94.66	5.98
500.00	89.9554	102.9075	96.7616	96.54	5.29
1000.00	86.10595	87.50899	91.19511	88.27	2.15
2000.00	55.59627	52.00483	65.13201	57.58	5.54

**Table 43**  
**Raw data LC-MS/MS**

Experiment	Sample name	Peak area_PB	Peak area_Col (int. Std.)	PB/Col	PB [nM]	Cell number from sample	Total volumen of viable cells = $4/3\pi r^3$ [mm <sup>3</sup> ]	Intracellular concentration = (Total amount of drugs detected in the cell sample / Total volumen of viable cells) * 10 (dilution factor) [nM]
	NRK-52E+34uM 30.8-1.9.17+Col 2' (A1)	4826	261900	0.01842688	19.05	400000	1.03	185.12
	NRK-52E+34uM 30.8-1.9.17+Col 1h (A2)	5817	301300	0.01930634	23.01	470000	1.21	190.33
	NRK-52E+34uM 30.8-1.9.17+Col 3h (A3)	9221	494500	0.01864712	20.04	370000	0.95	210.56
	NRK-52E+34uM 30.8-1.9.17+Col 6h (A4)	10613	395800	0.02681405	56.85	255000	0.66	866.59
	NRK-52E+34uM 30.8-1.9.17+Col 24h (A'1)	15017	377800	0.03974854	115.14	515000	1.32	869.07
	NRK-52E+34uM 30.8-1.9.17+Col 24h Recov (A'2)	6365	335500	0.01897168	21.50	1015000	2.61	82.36
	NRK-52E+34uM 30.8-1.9.17+Col 2' (B1)	8617	478800	0.01799708	17.11	470000	1.21	141.53
	NRK-52E+34uM 30.8-1.9.17+Col 1h (B2)	10100	526900	0.01916872	22.39	410000	1.05	212.30
	NRK-52E+34uM 30.8-1.9.17+Col 3h (B3)	11045	475800	0.02321354	40.62	410000	1.05	385.13
	NRK-52E+34uM 30.8-1.9.17+Col 6h (B4)	11356	583700	0.0194552	23.68	335000	0.86	274.82
	NRK-52E+34uM 30.8-1.9.17+Col 24h (B'1)	20410	532900	0.03829987	108.61	705000	1.81	598.86
	NRK-52E+34uM 30.8-1.9.17+Col 24h Recov (B'2)	8718	506700	0.01720545	13.54	995000	2.56	52.92
	NRK-52E+34uM 30.8-1.9.17+Col 2' (C1)	11856	579100	0.02047315	28.27	470000	1.21	233.82
	NRK-52E+34uM 30.8-1.9.17+Col 1h (C2)	11450	588300	0.01946286	23.72	250000	0.64	368.79
	NRK-52E+34uM 30.8-1.9.17+Col 3h (C3)	11620	535700	0.02169125	33.76	310000	0.80	423.34
	NRK-52E+34uM 30.8-1.9.17+Col 6h (C4)	14850	562300	0.02640939	55.02	195000	0.50	1096.87
	NRK-52E+34uM 30.8-1.9.17+Col 24h (C'1)	24830	601400	0.041287	122.07	335000	0.86	1416.49
	NRK-52E+34uM 30.8-1.9.17+Col 24h Recov (C'2)	9200	493400	0.01864613	20.04	625000	1.61	124.62

1

Experiment	Sample name	Peak area_PB	Peak area_Col (int. Std.)	PB/Col	PB [nM]	Cell number from sample	Total volume of viable cells = $\frac{4}{3}\pi r^3$ [mm <sup>3</sup> ]	Intracellular concentration = (Total amount of drugs detected in the cell sample / Total volume of viable cells) * 10 (dilution factor) [nM]
	NRK-52E+34uM 6.9-8.9.17+Col 2' (A1)	13998	1064000	0.01315602	-4.70	270000	0.69	50.00
	NRK-52E+34uM 6.9-8.9.17+Col 1h (A2)	16320	946300	0.01724612	13.73	280000	0.72	190.58
	NRK-52E+34uM 6.9-8.9.17+Col 3h (A3)	20520	1010600	0.02030477	27.51	375000	0.96	285.19
	NRK-52E+34uM 6.9-8.9.17+Col 6h (A4)	22710	960000	0.02365625	42.61	355000	0.91	466.65
	NRK-52E+34uM 6.9-8.9.17+Col 24h (A'1)	41430	1089000	0.03804408	107.45	625000	1.61	668.34
	NRK-52E+34uM 6.9-8.9.17+Col 24h Recov (A'2)	15520	1019000	0.01523062	4.64	910000	2.34	50.00
	NRK-52E+34uM 6.9-8.9.17+Col 2' (B1)	15560	1121000	0.01388046	-1.44	365000	0.94	50.00
	NRK-52E+34uM 6.9-8.9.17+Col 1h (B2)	17040	1036000	0.01644788	10.13	310000	0.80	127.03
	NRK-52E+34uM 6.9-8.9.17+Col 3h (B3)	19160	1059000	0.01809254	17.54	425000	1.09	160.45
	NRK-52E+34uM 6.9-8.9.17+Col 6h (B4)	22730	965000	0.0235544	42.16	220000	0.57	744.89
	NRK-52E+34uM 6.9-8.9.17+Col 24h (B'1)	37380	1001000	0.03734266	104.29	635000	1.63	638.46
	NRK-52E+34uM 6.9-8.9.17+Col 24h Recov (B'2)	19380	957000	0.02025078	27.27	850000	2.19	124.71
	NRK-52E+34uM 6.9-8.9.17+Col 2' (C1)	16170	1098000	0.01472678	2.37	230000	0.59	40.12
	NRK-52E+34uM 6.9-8.9.17+Col 1h (C2)	19630	1179000	0.0166497	11.04	285000	0.73	150.58
	NRK-52E+34uM 6.9-8.9.17+Col 3h (C3)	19080	1187000	0.01607414	8.45	230000	0.59	142.75
	NRK-52E+34uM 6.9-8.9.17+Col 6h (C4)	24540	995000	0.02466332	47.15	215000	0.55	852.57
	NRK-52E+34uM 6.9-8.9.17+Col 24h (C'1)	39050	1129000	0.03458813	91.88	455000	1.17	784.99
	NRK-52E+34uM 6.9-8.9.17+Col 24h Recov (C'2)	19140	1107000	0.01728997	13.93	665000	1.71	81.40

Experiment	Sample name	Peak area_PB	Peak area_Col (int. Std.)	PB/Col	PB [nM]	Cell number from sample	Total volumen of viable cells = cell number * $4/3\pi r^3$ [mm <sup>3</sup> ]	Intracellular concentration = (Total amount of drugs detected in the cell sample / Total volumen of viable cells) * 10 (dilution factor) [nM]
	NRK-52E+34uM 13.9-15.9.17+Col 2' (A1)	10591	841500	0.01258586	-7.27	270000	0.69	50.00
	NRK-52E+34uM 13.9-15.9.17+Col 1h (A2)	12090	752400	0.01606858	8.42	235000	0.60	139.30
	NRK-52E+34uM 13.9-15.9.17+Col 3h (A3)	15930	766500	0.02078278	29.67	225000	0.58	512.54
	NRK-52E+34uM 13.9-15.9.17+Col 6h (A4)	17240	799200	0.02157157	33.22	270000	0.69	478.29
	NRK-52E+34uM 13.9-15.9.17+Col 24h (A'1)	29570	793500	0.03726528	103.94	580000	1.49	696.67
	NRK-52E+34uM 13.9-15.9.17+Col 24h Recov (A'2)	15730	776600	0.02025496	27.29	920000	2.37	115.30
	NRK-52E+34uM 13.9-15.9.17+Col 2' (B1)	12528	823500	0.01521311	4.57	250000	0.64	70.99
	NRK-52E+34uM 13.9-15.9.17+Col 1h (B2)	14680	747500	0.0196388	24.51	235000	0.60	405.45
	NRK-52E+34uM 13.9-15.9.17+Col 3h (B3)	14560	787600	0.01848654	19.32	260000	0.67	288.82
	NRK-52E+34uM 13.9-15.9.17+Col 6h (B4)	18320	744000	0.02462366	46.97	345000	0.89	529.30
	NRK-52E+34uM 13.9-15.9.17+Col 24h (B'1)	31180	735200	0.04241023	127.13	620000	1.59	797.10
	NRK-52E+34uM 13.9-15.9.17+Col 24h Recov (B'2)	13600	817600	0.01663405	10.97	695000	1.79	61.35
	NRK-52E+34uM 13.9-15.9.17+Col 2' (C1)	9821	809000	0.01213968	-9.28	200000	0.51	50.00
	NRK-52E+34uM 13.9-15.9.17+Col 1h (C2)	11225	824700	0.01361101	-2.65	275000	0.71	50.00
	NRK-52E+34uM 13.9-15.9.17+Col 3h (C3)	15250	799000	0.01908636	22.02	195000	0.50	438.98
	NRK-52E+34uM 13.9-15.9.17+Col 6h (C4)	17780	783200	0.02270174	38.31	210000	0.54	709.23
	NRK-52E+34uM 13.9-15.9.17+Col 24h (C'1)	30240	733100	0.04124949	121.90	n.a.	n.a.	n.a.
	NRK-52E+34uM 13.9-15.9.17+Col 24h Recov (C'2)	13510	746100	0.01810749	17.61	690000	1.77	99.21

Experiment	Sample name	Peak area_Col (int. Std.)	Peak area_PB (int. Std.)	Col/PB	Col [nM]	Cell number from sample	Total volumen of viable cells = cell number * $\frac{4}{3}\pi \cdot r^3$ [mm <sup>3</sup> ]	Intracellular concentration = (Total amount of drugs detected in the cell sample / Total volumen of viable cells) * 10 (dilution factor) [nM]
	NRK-52E+34uM Col. 20.9-21.9.17+PB 2' (A1)	5490	899600	0.00610271	3.43	255000	0.66	52.30
	NRK-52E+34uM Col. 20.9-21.9.17+PB 1h (A2)	7419	896700	0.00827367	11.68	320000	0.82	141.92
	NRK-52E+34uM Col. 20.9-21.9.17+PB 3h (A3)	9383	884100	0.01061305	20.57	240000	0.62	333.25
	NRK-52E+34uM Col. 20.9-21.9.17+PB 6h (A4)	9872	986100	0.01001116	18.29	240000	0.62	296.19
	NRK-52E+34uM Col. 20.9-21.9.17+PB 24h (A'1)	20900	927700	0.02252883	65.86	675000	1.74	379.31
	NRK-52E+34uM Col. 22.9.17+PB 24h Recov (A'2)	10118	1087300	0.00930562	15.60	1000000	2.57	60.66
	NRK-52E+34uM Col. 20.9-21.9.17+PB 2' (B1)	5602	895300	0.00625712	4.02	145000	0.37	107.72
	NRK-52E+34uM Col. 20.9-21.9.17+PB 1h (B2)	8444	980600	0.00861105	12.96	270000	0.69	186.66
	NRK-52E+34uM Col. 20.9-21.9.17+PB 3h (B3)	8916	814500	0.01094659	21.84	285000	0.73	297.92
	NRK-52E+34uM Col. 20.9-21.9.17+PB 6h (B4)	11624	839400	0.01384799	32.87	280000	0.72	456.34
	NRK-52E+34uM Col. 20.9-21.9.17+PB 24h (B'1)	17040	916500	0.01859247	50.90	595000	1.53	332.57
	NRK-52E+34uM Col. 22.9.17+PB 24h Recov (B'2)	9470	1283600	0.00737769	8.28	830000	2.14	50.00
	NRK-52E+34uM Col. 20.9-21.9.17+PB 2' (C1)	5412	857300	0.00631284	4.23	265000	0.68	62.05
	NRK-52E+34uM Col. 20.9-21.9.17+PB 1h (C2)	17206	740100	0.02324821	68.60	230000	0.59	1159.42
	NRK-52E+34uM Col. 20.9-21.9.17+PB 3h (C3)	11405	855400	0.01333294	30.91	175000	0.45	686.66
	NRK-52E+34uM Col. 20.9-21.9.17+PB 6h (C4)	12823	965600	0.01327983	30.71	260000	0.67	459.16
	NRK-52E+34uM Col. 20.9-21.9.17+PB 24h (C'1)	18740	922900	0.02030556	57.41	445000	1.14	501.55
	NRK-52E+34uM Col. 22.9.17+PB 24h Recov (C'2)	8800	1257000	0.0070008	6.84	700000	1.80	50.00

1



Experiment	Sample name	Peak area_Col	Peak area_PB (int. Std.)	Col/PB	Col [nM]	Cell number from sample	Total volumen of viable cells = cell number * $\frac{4}{3}\pi r^3$ [mm <sup>3</sup> ]	Intracellular concentration = (Total amount of drugs detected in the cell sample / Total volumen of viable cells) * 10 (dilution factor) [nM]
	NRK-52E+34uM Col. 27.9-29.9.17+PB 2' (A1)	17260	2161500	0.0079852	10.59	285000	0.73	144.39
	NRK-52E+34uM Col. 27.9-29.9.17+PB 1h (A2)	21850	2289000	0.00954565	16.52	450000	1.16	142.68
	NRK-52E+34uM Col. 27.9-29.9.17+PB 3h (A3)	23690	2246000	0.01054764	20.33	535000	1.38	147.69
	NRK-52E+34uM Col. 27.9-29.9.17+PB 6h (A4)	31420	2216000	0.0141787	34.13	500000	1.29	265.32
	NRK-52E+34uM Col. 27.9-29.9.17+PB 24h (A'1)	35790	1952000	0.01833504	49.92	960000	2.47	202.16
	NRK-52E+34uM Col. 27.9-29.9.17+PB 24h Recov (A'2)	16310	2310000	0.00706061	7.07	1090000	2.80	50.00
	NRK-52E+34uM Col. 27.9-29.9.17+PB 2' (B1)	15020	1940000	0.00774227	9.66	300000	0.77	125.21
	NRK-52E+34uM Col. 27.9-29.9.17+PB 1h (B2)	17960	2101000	0.00854831	12.73	450000	1.16	109.94
	NRK-52E+34uM Col. 27.9-29.9.17+PB 3h (B3)	23510	1889000	0.01244574	27.54	390000	1.00	274.51
	NRK-52E+34uM Col. 27.9-29.9.17+PB 6h (B4)	28010	2174000	0.01288408	29.21	565000	1.45	200.95
	NRK-52E+34uM Col. 27.9-29.9.17+PB 24h (B'1)	33220	1906000	0.01742917	46.48	765000	1.97	236.19
	NRK-52E+34uM Col. 27.9-29.9.17+PB 24h Recov (B'2)	14670	2086000	0.0070326	6.97	765000	1.97	50.00
	NRK-52E+34uM Col. 27.9-29.9.17+PB 2' (C1)	18150	2214400	0.00819635	11.39	365000	0.94	121.29
	NRK-52E+34uM Col. 27.9-29.9.17+PB 1h (C2)	21920	2198000	0.0099727	18.14	300000	0.77	235.06
	NRK-52E+34uM Col. 27.9-29.9.17+PB 3h (C3)	24870	2331000	0.01066924	20.79	360000	0.93	224.47
	NRK-52E+34uM Col. 27.9-29.9.17+PB 6h (C4)	35580	2235000	0.01591946	40.74	325000	0.84	487.33
	NRK-52E+34uM Col. 27.9-29.9.17+PB 24h (C'1)	36150	2228000	0.01622531	41.91	565000	1.45	288.32
	NRK-52E+34uM Col. 27.9-29.9.17+PB 24h Recov (C'2)	16400	2145000	0.00764569	9.30	600000	1.54	60.23

Experiment	Sample name	Peak area_Col	Peak area_PB (int. Std.)	Col/PB	Col [nM]	Cell number from sample	Total volumen of viable cells = cell number * $4/3\pi r^3$ [mm <sup>3</sup> ]	Intracellular concentration = (Total amount of drugs detected in the cell sample / Total volumen of viable cells) * 10 (dilution factor) [nM]
	NRK-52E+34uM Col. 4.-6.10.17+PB 2' (A1)	5844	990300	0.00590124	2.67	560000	1.44	50.00
	NRK-52E+34uM Col. 4.-6.10.17+PB 1h (A2)	8104	855900	0.0094684	16.22	460000	1.18	137.10
	NRK-52E+34uM Col. 4.-6.10.17+PB 3h (A3)	12830	866200	0.01481182	36.53	580000	1.49	244.86
	NRK-52E+34uM Col. 4.-6.10.17+PB 6h (A4)	15950	857700	0.01859625	50.92	540000	1.39	366.54
	NRK-52E+34uM Col. 4.-6.10.17+PB 24h (A'1)	26930	976800	0.02756962	85.02	710000	1.83	465.52
	NRK-52E+34uM Col. 4.-6.10.17+PB 24h Recov (A'2)	6280	871400	0.00720679	7.63	1220000	3.14	50.00
	NRK-52E+34uM Col. 4.-6.10.17+PB 2' (B1)	2527	754900	0.00334746	-7.04	390000	1.00	50.00
	NRK-52E+34uM Col. 4.-6.10.17+PB 1h (B2)	5158	693100	0.00744193	8.52	495000	1.27	66.92
	NRK-52E+34uM Col. 4.-6.10.17+PB 3h (B3)	10750	684600	0.0157026	39.92	375000	0.96	413.81
	NRK-52E+34uM Col. 4.-6.10.17+PB 6h (B4)	11440	683700	0.01673249	43.83	570000	1.47	298.94
	NRK-52E+34uM Col. 4.-6.10.17+PB 24h (B'1)	12450	727200	0.01712046	45.31	1100000	2.83	160.12
	NRK-52E+34uM Col. 4.-6.10.17+PB 24h Recov (B'2)	3973	679900	0.00584351	2.45	1415000	3.64	50.00
	NRK-52E+34uM Col. 4.-6.10.17+PB 2' (C1)	2649	750400	0.00353012	-6.35	320000	0.82	50.00
	NRK-52E+34uM Col. 4.-6.10.17+PB 1h (C2)	6914	699700	0.00988138	17.79	200000	0.51	345.84
	NRK-52E+34uM Col. 4.-6.10.17+PB 3h (C3)	4971	656000	0.00757774	9.04	165000	0.42	212.92
	NRK-52E+34uM Col. 4.-6.10.17+PB 6h (C4)	11440	642500	0.01780545	47.91	315000	0.81	591.26
	NRK-52E+34uM Col. 4.-6.10.17+PB 24h (C'1)	18820	678400	0.02774175	85.68	1090000	2.80	305.56
	NRK-52E+34uM Col. 4.-6.10.17+PB 24h Recov (C'2)	3565	667200	0.00534323	0.54	1100000	2.83	50.00

Experiment	Sample name	Peak area_PB	Peak area Col (int. Std.)	PB/Col	PB [nM]	Cell number from sample	Total volumen of viable cells = cell number * $4/3\pi r^3$ [mm <sup>3</sup> ]	Intracellular concentration = (Total amount of drugs detected in the cell sample / Total volumen of viable cells) * 10 (dilution factor) [nM]
	RPTEC/TERT1+34uM 30.8-1.9.17+Col 2' (A1)	7976	386800	0.020620476	28.93	560000	2.011	143.87
	RPTEC/TERT1+34uM 30.8-1.9.17+Col 1h (A2)	11490	388400	0.029582904	69.32	630000	2.263	306.39
	RPTEC/TERT1+34uM 30.8-1.9.17+Col 3h (A3)	20940	409900	0.051085631	166.23	530000	1.903	873.30
	RPTEC/TERT1+34uM 30.8-1.9.17+Col 6h (A4)	33510	414900	0.08076645	299.98	750000	2.694	1113.72
	RPTEC/TERT1+34uM 30.8-1.9.17+Col 24h (A'1)	97730	388800	0.251363169	1068.78	590000	2.119	5044.04
	RPTEC/TERT1+34uM 30.8-1.9.17+Col 24h Recov (A'2)	47420	353800	0.134030526	540.02	560000	2.011	2685.11
	RPTEC/TERT1+34uM 30.8-1.9.17+Col 2' (B1)	9800	521100	0.018806371	20.76	870000	3.124	66.44
	RPTEC/TERT1+34uM 30.8-1.9.17+Col 1h (B2)	14620	463100	0.031569855	78.28	535000	1.921	407.40
	RPTEC/TERT1+34uM 30.8-1.9.17+Col 3h (B3)	27610	473800	0.058273533	198.62	685000	2.460	807.37
	RPTEC/TERT1+34uM 30.8-1.9.17+Col 6h (B4)	55080	460800	0.11953125	474.68	640000	2.298	2065.19
	RPTEC/TERT1+34uM 30.8-1.9.17+Col 24h (B'1)	124580	452100	0.275558505	1177.82	685000	2.460	4787.73
	RPTEC/TERT1+34uM 30.8-1.9.17+Col 24h Recov (B'2)	97860	474500	0.206238145	865.43	770000	2.765	3129.54
	RPTEC/TERT1+34uM 30.8-1.9.17+Col 2' (C1)	10389	566500	0.018338923	18.65	465000	1.670	111.69
	RPTEC/TERT1+34uM 30.8-1.9.17+Col 1h (C2)	14790	558200	0.02649588	55.41	595000	2.137	259.31
	RPTEC/TERT1+34uM 30.8-1.9.17+Col 3h (C3)	22110	549900	0.04020731	117.20	690000	2.478	472.97
	RPTEC/TERT1+34uM 30.8-1.9.17+Col 6h (C4)	56110	533100	0.105252298	410.33	645000	2.316	1771.39
	RPTEC/TERT1+34uM 30.8-1.9.17+Col 24h (C'1)	145630	531400	0.27404968	1171.02	560000	2.011	5822.61
	RPTEC/TERT1+34uM 30.8-1.9.17+Col 24h Recov (C'2)	85170	506100	0.1682869	694.40	465000	1.670	4158.11

1

Experiment	Sample name	Peak area_PB (int. Std.)	Peak area_Col (int. Std.)	PB/Col	PB [nM]	Cell number from sample	Total volumen of viable cells = cell number * $4/3\pi r^3$ [mm <sup>3</sup> ]	Intracellular concentration = (Total amount of drugs detected in the cell sample / Total volumen of viable cells) * 10 (dilution factor) [nM]
	RPTEC/TERT1+34uM 6.9-8.9.17+Col 2' (A1)	15990	909000	0.0175908	15.28	610000	2.191	69.75
	RPTEC/TERT1+34uM 6.9-8.9.17+Col 1h (A2)	24370	859000	0.0283702	63.86	530000	1.903	335.49
	RPTEC/TERT1+34uM 6.9-8.9.17+Col 3h (A3)	46570	1026000	0.0453899	140.56	720000	2.586	543.58
	RPTEC/TERT1+34uM 6.9-8.9.17+Col 6h (A4)	105550	850000	0.1241765	495.61	640000	2.298	2156.27
	RPTEC/TERT1+34uM 6.9-8.9.17+Col 24h (A'1)	163060	947400	0.1721132	711.64	630000	2.263	3145.29
	RPTEC/TERT1+34uM 6.9-8.9.17+Col 24h Recov (A'2)	100580	890000	0.11130112	445.30	570000	2.047	2175.28
	RPTEC/TERT1+34uM 6.9-8.9.17+Col 2' (B1)	18040	1133000	0.0159223	7.76	740000	2.658	50.00
	RPTEC/TERT1+34uM 6.9-8.9.17+Col 1h (B2)	27470	988000	0.0278036	61.31	455000	1.634	375.17
	RPTEC/TERT1+34uM 6.9-8.9.17+Col 3h (B3)	54540	1014000	0.053787	178.40	585000	2.101	849.14
	RPTEC/TERT1+34uM 6.9-8.9.17+Col 6h (B4)	97990	922000	0.1062798	414.96	630000	2.263	1834.03
	RPTEC/TERT1+34uM 6.9-8.9.17+Col 24h (B'1)	181800	1092000	0.1664835	686.27	640000	2.298	2985.77
	RPTEC/TERT1+34uM 6.9-8.9.17+Col 24h Recov (B'2)	149760	1036000	0.144556	587.45	590000	2.119	2772.44
	RPTEC/TERT1+34uM 6.9-8.9.17+Col 2' (C1)	21370	1058000	0.0201985	27.03	615000	2.209	122.39
	RPTEC/TERT1+34uM 6.9-8.9.17+Col 1h (C2)	32160	1024000	0.0314063	77.54	650000	2.334	332.17
	RPTEC/TERT1+34uM 6.9-8.9.17+Col 3h (C3)	54170	1010000	0.0536337	177.71	465000	1.670	1064.14
	RPTEC/TERT1+34uM 6.9-8.9.17+Col 6h (C4)	93490	939000	0.0995634	384.69	700000	2.514	1530.23
	RPTEC/TERT1+34uM 6.9-8.9.17+Col 24h (C'1)	220700	977000	0.2258956	954.01	625000	2.245	4250.26
	RPTEC/TERT1+34uM 6.9-8.9.17+Col 24h Recov (C'2)	118860	1066000	0.11115009	438.49	470000	1.688	2597.78

Experiment	Sample name	Peak area_PB (int. Std.)	Peak area_Col (int. Std.)	PB/Col	PB [nM]	Cell number from sample	Total volumen of viable cells = cell number * $4/3\pi r^3$ [mm <sup>3</sup> ]	Intracellular concentration = (Total amount of drugs detected in the cell sample / Total volumen of viable cells) * 10 (dilution factor) [nM]
3	RPTEC/TERT1+34uM 13.9-15.9.17+Col 2' (A1)	12699	604600	0.021004	30.66	810000	2.909	105.40
	RPTEC/TERT1+34uM 13.9-15.9.17+Col 1h (A2)	17450	744900	0.023426	41.58	690000	2.478	167.78
	RPTEC/TERT1+34uM 13.9-15.9.17+Col 3h (A3)	33920	613900	0.0552533	185.01	675000	2.424	763.18
	RPTEC/TERT1+34uM 13.9-15.9.17+Col 6h (A4)	67310	714700	0.0941794	360.43	630000	2.263	1593.02
	RPTEC/TERT1+34uM 13.9-15.9.17+Col 24h Recov (A'2)	147900	665900	0.2221054	936.93	800000	2.873	3261.06
	RPTEC/TERT1+34uM 13.9-15.9.17+Col 2' (B1)	14670	782700	0.0187428	20.47	810000	2.909	70.38
	RPTEC/TERT1+34uM 13.9-15.9.17+Col 1h (B2)	19460	772600	0.0251877	49.52	745000	2.676	185.07
	RPTEC/TERT1+34uM 13.9-15.9.17+Col 3h (B3)	31670	639700	0.0495076	159.11	670000	2.406	661.27
	RPTEC/TERT1+34uM 13.9-15.9.17+Col 6h (B4)	75880	731000	0.103803	403.80	820000	2.945	1371.17
	RPTEC/TERT1+34uM 13.9-15.9.17+Col 24h Recov (B'2)	191800	687000	0.2791849	1194.16	550000	1.975	6045.63
	RPTEC/TERT1+34uM 13.9-15.9.17+Col 2' (C1)	13930	817300	0.0170439	12.82	660000	2.370	54.07
	RPTEC/TERT1+34uM 13.9-15.9.17+Col 1h (C2)	17650	802600	0.021991	35.11	675000	2.424	144.84
	RPTEC/TERT1+34uM 13.9-15.9.17+Col 3h (C3)	51670	813100	0.0635469	222.38	720000	2.586	860.02
	RPTEC/TERT1+34uM 13.9-15.9.17+Col 6h (C4)	65660	821000	0.0799756	296.42	670000	2.406	1231.89
RPTEC/TERT1+34uM 13.9-15.9.17+Col 24h Recov (C'2)	126500	742500	0.1703704	703.79	610000	2.191	3212.57	

Experiment	Sample name	Peak area_PB	Peak area_Col (int. Std.)	PB/Col	PB [nM]	Cell number from sample	Total volumen of viable cells = cell number * $\frac{4}{3}\pi r^3$ [mm <sup>3</sup> ]	Intracellular concentration = (Total amount of drugs detected in the cell sample / Total volumen of viable cells) * 10 (dilution factor) [nM]
	RPTEC/TERT1+34uM PB 11.-13.10.17+Col 2' (A1)	12800	997300	0.0128347	-6.15	405000	1.455	50.00
	RPTEC/TERT1+34uM PB 11.-13.10.17+Col 1h (A2)	17960	946400	0.0189772	21.53	1E+06	4.202	51.24
	RPTEC/TERT1+34uM PB 11.-13.10.17+Col 3h (A3)	35830	1022100	0.0350553	93.99	885000	3.178	295.70
	RPTEC/TERT1+34uM PB 11.-13.10.17+Col 6h (A4)	48080	1039000	0.0462753	144.55	625000	2.245	643.98
	RPTEC/TERT1+34uM PB 11.-13.10.17+Col 24h (A'1)	161700	1090000	0.1483486	604.55	815000	2.927	2065.44
	RPTEC/TERT1+34uM PB 11.-13.10.17+Col 24h Recov (A'2)	112810	1069700	0.1054595	411.26	995000	3.573	1150.90
	RPTEC/TERT1+34uM PB 11.-13.10.17+Col 2' (B1)	18770	972600	0.0192988	22.98	520000	1.868	123.04
	RPTEC/TERT1+34uM PB 11.-13.10.17+Col 1h (B2)	22700	1038900	0.02185	34.48	840000	3.017	114.28
	RPTEC/TERT1+34uM PB 11.-13.10.17+Col 3h (B3)	43410	1102000	0.039392	113.53	920000	3.304	343.60
	RPTEC/TERT1+34uM PB 11.-13.10.17+Col 6h (B4)	42240	1044900	0.0404249	118.18	605000	2.173	543.93
	RPTEC/TERT1+34uM PB 11.-13.10.17+Col 24h (B'1)	161000	1080300	0.1490327	607.63	995000	3.573	1700.42
	RPTEC/TERT1+34uM PB 11.-13.10.17+Col 24h Recov (B'2)	134100	1059000	0.1266289	506.66	1E+06	4.579	1106.50
	RPTEC/TERT1+34uM PB 11.-13.10.17+Col 2' (C1)	18770	1122000	0.0167291	11.40	1E+06	3.771	30.22
	RPTEC/TERT1+34uM PB 11.-13.10.17+Col 1h (C2)	24980	960200	0.0260154	53.25	1E+06	3.771	141.20
	RPTEC/TERT1+34uM PB 11.-13.10.17+Col 3h (C3)	36190	1140000	0.0317456	79.07	550000	1.975	400.30
	RPTEC/TERT1+34uM PB 11.-13.10.17+Col 6h (C4)	60030	1115400	0.0538193	178.55	615000	2.209	808.38
	RPTEC/TERT1+34uM PB 11.-13.10.17+Col 24h (C'1)	178700	1106000	0.1615732	664.14	795000	2.855	2326.13
	RPTEC/TERT1+34uM PB 11.-13.10.17+Col 24h Recov (C'2)	116100	1124000	0.1032918	401.50	925000	3.322	1208.59

4

Experiment	Sample name	Peak area_Col	Peak area_PB (int. Std.)	Col/PB	Col [nM]	Cell number from sample	Total volume of viable cells = cell number * $\frac{4}{3}\pi r^3$ [mm <sup>3</sup> ]	Intracellular concentration = (Total amount of drugs detected in the cell sample / Total volume of viable cells) * 10 (dilution factor) [nM]
	RPTEC/TERT1+34uM Col. 20.9-21.9.17+PB 2' (A1)	9170	767300	0.011951	25.66	650000	2.33	109.92
	RPTEC/TERT1+34uM Col. 20.9-21.9.17+PB 1h (A2)	12720	721200	0.01763727	47.27	640000	2.30	205.67
	RPTEC/TERT1+34uM Col. 20.9-21.9.17+PB 3h (A3)	26390	739000	0.03571042	115.97	830000	2.98	389.04
	RPTEC/TERT1+34uM Col. 20.9-21.9.17+PB 6h (A4)	36860	782700	0.04709339	159.23	745000	2.68	595.13
	RPTEC/TERT1+34uM Col. 20.9-21.9.17+PB 24h (A'1)	128800	841600	0.15304183	561.92	625000	2.24	2503.44
	RPTEC/TERT1+34uM Col. 22.9.17+PB 24h Recov (A'2)	111800	1248500	0.08954746	320.59	780000	2.80	1144.45
	RPTEC/TERT1+34uM Col. 20.9-21.9.17+PB 2' (B1)	6404	836000	0.00766029	9.35	645000	2.32	50.00
	RPTEC/TERT1+34uM Col. 20.9-21.9.17+PB 1h (B2)	12470	896100	0.01391586	33.13	785000	2.82	117.51
	RPTEC/TERT1+34uM Col. 20.9-21.9.17+PB 3h (B3)	31340	780200	0.04016919	132.91	735000	2.64	503.52
	RPTEC/TERT1+34uM Col. 20.9-21.9.17+PB 6h (B4)	37780	828200	0.045617	153.62	580000	2.08	737.49
	RPTEC/TERT1+34uM Col. 20.9-21.9.17+PB 24h (B'1)	126500	825700	0.15320334	562.54	700000	2.51	2237.66
	RPTEC/TERT1+34uM Col. 22.9.17+PB 24h Recov (B'2)	136900	1176900	0.11632254	422.36	730000	2.62	1611.01
	RPTEC/TERT1+34uM Col. 20.9-21.9.17+PB 2' (C1)	7730	772400	0.01000777	18.27	825000	2.96	61.68
	RPTEC/TERT1+34uM Col. 20.9-21.9.17+PB 1h (C2)	15030	832700	0.01804972	48.84	790000	2.84	172.14
	RPTEC/TERT1+34uM Col. 20.9-21.9.17+PB 3h (C3)	25380	835400	0.03038066	95.71	755000	2.71	352.97
	RPTEC/TERT1+34uM Col. 20.9-21.9.17+PB 6h (C4)	37020	875400	0.04228924	140.97	720000	2.59	545.17
	RPTEC/TERT1+34uM Col. 20.9-21.9.17+PB 24h (C'1)	102700	872900	0.1176538	427.42	790000	2.84	1506.49
	RPTEC/TERT1+34uM Col. 22.9.17+PB 24h Recov (C'2)	123500	1095300	0.1127545	408.80	740000	2.66	1538.21

1

Experiment	Sample name	Peak area_Col	Peak area_PB (int. Std.)	Col/PB	Col [nM]	Cell number from sample	Total volumen of viable cells = cell number * $\frac{4}{3}\pi r^3$ [mm <sup>3</sup> ]	Intracellular concentration = (Total amount of drugs detected in the cell sample / Total volumen of viable cells) * 10 (dilution factor) [nM]
	RPTEC/TERT1+34uM Col. 27.9-29.9.17+PB 2' (A1)	18370	1667000	0.0110198	22.12	530000	1.90	116.21
	RPTEC/TERT1+34uM Col. 27.9-29.9.17+PB 1h (A2)	31420	1815000	0.01731129	46.03	640000	2.30	200.28
	RPTEC/TERT1+34uM Col. 27.9-29.9.17+PB 3h (A3)	70190	2375000	0.02955368	92.56	625000	2.24	412.39
	RPTEC/TERT1+34uM Col. 27.9-29.9.17+PB 6h (A4)	103000	2065000	0.04987893	169.82	755000	2.71	626.29
	RPTEC/TERT1+34uM Col. 27.9-29.9.17+PB 24h (A'1)	193200	2078000	0.09297401	333.61	625000	2.24	1486.30
	RPTEC/TERT1+34uM Col. 27.9-29.9.17+PB 24h Recov (A2)	171700	2410000	0.07124481	251.03	795000	2.86	879.21
	RPTEC/TERT1+34uM Col. 27.9-29.9.17+PB 2' (B1)	14200	1678000	0.00846246	12.40	615000	2.21	56.14
	RPTEC/TERT1+34uM Col. 27.9-29.9.17+PB 1h (B2)	41570	2071000	0.02007243	56.53	735000	2.64	214.15
	RPTEC/TERT1+34uM Col. 27.9-29.9.17+PB 3h (B3)	58770	2085000	0.02818705	87.37	785000	2.82	309.91
	RPTEC/TERT1+34uM Col. 27.9-29.9.17+PB 6h (B4)	101700	2078000	0.04894129	166.25	515000	1.85	898.88
	RPTEC/TERT1+34uM Col. 27.9-29.9.17+PB 24h (B'1)	247000	2027000	0.12185496	443.39	595000	2.14	2074.94
	RPTEC/TERT1+34uM Col. 27.9-29.9.17+PB 24h Recov (B'2)	176600	2167000	0.08149515	289.99	685000	2.46	1178.76
	RPTEC/TERT1+34uM Col. 27.9-29.9.17+PB 2' (C1)	15240	1868000	0.00815846	11.24	545000	1.96	57.45
	RPTEC/TERT1+34uM Col. 27.9-29.9.17+PB 1h (C2)	28890	2077000	0.01390948	33.10	575000	2.07	160.30
	RPTEC/TERT1+34uM Col. 27.9-29.9.17+PB 3h (C3)	68800	2015000	0.03414392	110.01	675000	2.42	453.81
	RPTEC/TERT1+34uM Col. 27.9-29.9.17+PB 6h (C4)	61890	2232000	0.02772849	85.63	495000	1.78	481.67
	RPTEC/TERT1+34uM Col. 27.9-29.9.17+PB 24h (C'1)	236700	1968000	0.12027439	437.38	670000	2.41	1817.71
	RPTEC/TERT1+34uM Col. 27.9-29.9.17+PB 24h Recov (C'2)	159800	1995000	0.08010025	284.68	610000	2.19	1299.49



Experiment	Sample name	Peak area_Col	Peak area_PB (int. Std.)	Col/PB	Col [nM]	Cell number from sample	Total volume of viable cells = cell number * $\frac{4}{3}\pi r^3$ [mm <sup>3</sup> ]	Intracellular concentration = (Total amount of drugs detected in the cell sample / Total volume of viable cells) * 10 (dilution factor) [nM]
	RPTEC/TERT1+34uM Col. 4.-6.10.17+PB 2' (A1)	2829	888400	0.00318438	-7.66	700000	2.51	50.00
	RPTEC/TERT1+34uM Col. 4.-6.10.17+PB 1h (A2)	19320	846700	0.022818	66.96	875000	3.14	213.09
	RPTEC/TERT1+34uM Col. 4.-6.10.17+PB 3h (A3)	33000	903100	0.0365408	119.12	900000	3.23	368.54
	RPTEC/TERT1+34uM Col. 4.-6.10.17+PB 6h (A4)	54170	937900	0.05775669	199.76	650000	2.33	855.73
	RPTEC/TERT1+34uM Col. 4.-6.10.17+PB 24h (A'1)	132700	950000	0.13968421	511.15	700000	2.51	2033.26
	RPTEC/TERT1+34uM Col. 4.-6.10.17+PB 24h Recov (A'2)	46420	1012000	0.04586957	154.58	795000	2.86	541.40
	RPTEC/TERT1+34uM Col. 4.-6.10.17+PB 2' (B1)	6033	968400	0.00622986	3.91	810000	2.91	50.00
	RPTEC/TERT1+34uM Col. 4.-6.10.17+PB 1h (B2)	23490	1009000	0.02328048	68.72	1130000	4.06	169.34
	RPTEC/TERT1+34uM Col. 4.-6.10.17+PB 3h (B3)	48740	1017000	0.04792527	162.39	1170000	4.20	386.47
	RPTEC/TERT1+34uM Col. 4.-6.10.17+PB 6h (B4)	57770	898400	0.06430321	224.64	745000	2.68	839.60
3	RPTEC/TERT1+34uM Col. 4.-6.10.17+PB 24h (B'1)	138200	1037300	0.1332305	486.62	860000	3.09	1575.56
	RPTEC/TERT1+34uM Col. 4.-6.10.17+PB 24h Recov (B'2)	38550	971000	0.03970134	131.13	1025000	3.68	356.23
	RPTEC/TERT1+34uM Col. 4.-6.10.17+PB 2' (C1)	5407	925000	0.00584541	2.45	1050000	3.77	50.00
	RPTEC/TERT1+34uM Col. 4.-6.10.17+PB 1h (C2)	22540	901700	0.02499723	75.25	960000	3.45	218.25
	RPTEC/TERT1+34uM Col. 4.-6.10.17+PB 3h (C3)	37270	955000	0.03902618	128.57	580000	2.08	617.23
	RPTEC/TERT1+34uM Col. 4.-6.10.17+PB 6h (C4)	47070	932800	0.05046098	172.03	785000	2.82	610.20
	RPTEC/TERT1+34uM Col. 4.-6.10.17+PB 24h (C'1)	123100	983300	0.12519068	456.06	655000	2.35	1938.77
	RPTEC/TERT1+34uM Col. 4.-6.10.17+PB 24h Recov (C'2)	44180	951200	0.04644659	156.77	950000	3.41	459.50

Experiment	Sample name	Peak area_PB	Peak area_Col (int. Std.)	PB/Col	PB [nM]	Cell number from sample	Total volumen of viable cells = cell number * $\frac{4}{3}\pi r^3$ [mm <sup>3</sup> ]	Intracellular concentration = (Total amount of drugs detected in the cell sample / Total volumen of viable cells) * 10 (dilution factor) [nM]
	NRK-52E+62.5uM PB. 2min. A1	12600	1072000	0.01175373	-11.024	400000	1.029	50.00
	NRK-52E+62.5uM PB. 1h. A2	15810	1121000	0.01410348	-0.435	470000	1.209	50.00
	NRK-52E+62.5uM PB. 3h. A3	18660	1047000	0.01782235	16.324	370000	0.952	171.51
	NRK-52E+62.5uM PB. 6h. A4	22000	1097000	0.02005469	26.384	255000	0.656	402.22
	NRK-52E+62.5uM PB. 24h. A'1	31490	1136000	0.02772007	60.929	515000	1.325	459.91
	NRK-52E+62.5uM PB. 24h Recov. A'2	19670	1180000	0.01666949	11.129	1015000	2.611	42.62
	NRK-52E+62.5uM PB. 2min. B1	17010	1094000	0.01554845	6.077	470000	1.209	50.26
	NRK-52E+62.5uM PB. 1h. B2	19550	1106000	0.01767631	15.666	410000	1.055	148.54
	NRK-52E+62.5uM PB. 3h. B3	23270	1160000	0.02006034	26.410	410000	1.055	250.40
	NRK-52E+62.5uM PB. 6h. B4	21750	1027000	0.02117819	31.447	335000	0.862	364.92
	NRK-52E+62.5uM PB. 24h. B'1	41780	1208000	0.03458609	91.871	705000	1.814	506.57
	NRK-52E+62.5uM PB. 24h Recov. B'2	18430	1158000	0.01591537	7.730	995000	2.560	30.20
	NRK-52E+62.5uM PB. 2min. C1	0	8130	0	-63.993	470000	1.209	50.00
	NRK-52E+62.5uM PB. 1h. C2	20550	1070000	0.01920561	22.558	250000	0.643	350.76
	NRK-52E+62.5uM PB. 3h. C3	21640	1191000	0.01816961	17.889	310000	0.797	224.33
	NRK-52E+62.5uM PB. 6h. C4	23210	1136000	0.02043134	28.082	195000	0.502	559.81
	NRK-52E+62.5uM PB. 24h. C'1	44450	1160000	0.03831897	108.693	335000	0.862	1261.28
	NRK-52E+62.5uM PB. 24h Recov. C'2	14440	1174000	0.01229983	-8.563	625000	1.608	50.00

1

Experiment	Sample name	Peak area_PB	Peak area_Col (int. Std.)	PB/Col	PB [nM]	Cell number from sample	Total volumen of viable cells = cell number * $4/3\pi r^3$ [mm <sup>3</sup> ]	Intracellular concentration = (Total amount of drugs detected in the cell sample / Total volumen of viable cells) * 10 (dilution factor) [nM]
	NRK-52E+62.5uM PB. 1.4.18. 2 min. A1	16812	1163600	0.01444826	1.119	270000	0.695	16.11
	NRK-52E+62.5uM PB. 1.4.18. 1 h. A2	20456	1261800	0.01621176	9.066	280000	0.720	125.87
	NRK-52E+62.5uM PB. 1.4.18. 3 h. A3	23920	1257500	0.01902187	21.730	375000	0.965	225.26
	NRK-52E+62.5uM PB. 1.4.18. 6 h. A4	30780	1244000	0.02474277	47.511	355000	0.913	520.26
	NRK-52E+62.5uM PB. 12.4.18. 24 h. A1'	42990	1205000	0.03567635	96.784	625000	1.608	601.97
	NRK-52E+62.5uM PB. 13.4.18. 24 h Recov.. A2'	20230	1167000	0.01733505	14.128	910000	2.341	60.35
	NRK-52E+62.5uM PB. 1.4.18. 2 min. B1	18150	1256000	0.01445064	1.130	365000	0.939	12.03
	NRK-52E+62.5uM PB. 1.4.18. 1 h. B2	16380	1257000	0.01303103	-5.268	310000	0.797	50.00
	NRK-52E+62.5uM PB. 1.4.18. 3 h. B3	23970	1218000	0.0196798	24.695	425000	1.093	225.88
2	NRK-52E+62.5uM PB. 1.4.18. 6 h. B4	32450	1185000	0.02738397	59.414	220000	0.566	1049.83
	NRK-52E+62.5uM PB. 12.4.18. 24 h. B1'	47430	1250000	0.037944	107.003	635000	1.633	655.05
	NRK-52E+62.5uM PB. 13.4.18. 24 h Recov.. B2'	19990	1213000	0.0164798	10.274	850000	2.187	46.99
	NRK-52E+62.5uM PB. 1.4.18. 2 min. C1	17804	1250000	0.0142432	0.195	230000	0.592	3.29
	NRK-52E+62.5uM PB. 1.4.18. 1 h. C2	15920	1282000	0.0124181	-8.030	285000	0.733	50.00
	NRK-52E+62.5uM PB. 1.4.18. 3 h. C3	24650	1131400	0.02178717	34.192	230000	0.592	577.90
	NRK-52E+62.5uM PB. 1.4.18. 6 h. C4	31820	1297000	0.02453354	46.568	215000	0.553	841.99
	NRK-52E+62.5uM PB. 12.4.18. 24 h. C1'	45030	1138000	0.03956942	114.328	455000	1.170	976.78
	NRK-52E+62.5uM PB. 13.4.18. 24 h Recov.. C2'	25220	1285000	0.01962646	24.455	665000	1.711	142.95

Experiment	Sample name	Peak area_PB (int. Std.)	Peak area_Col (int. Std.)	PB/Col	PB [nM]	Cell number from sample	Total volumen of viable cells = cell number * $\frac{4}{3}\pi \cdot r^3$ [mm <sup>3</sup> ]	Intracellular concentration = (Total amount of drugs detected in the cell sample / Total volumen of viable cells) * 10 (dilution factor) [nM]
	NRK-52E+62.5uM PB. 18.4.18. 2min. A1	12403	896800	0.01383029	-1.666	270000	0.695	50.00
	NRK-52E+62.5uM PB. 18.4.18. 1h. A2	14410	927500	0.01553639	6.022	235000	0.605	99.62
	NRK-52E+62.5uM PB. 18.4.18. 3h. A3	18070	906000	0.01994481	25.889	225000	0.579	447.29
	NRK-52E+62.5uM PB. 18.4.18. 6h. A4	23350	881500	0.02648894	55.381	270000	0.695	797.35
	NRK-52E+62.5uM PB. 18.4.18. 24h. A1'	32350	916800	0.03528578	95.024	580000	1.492	636.88
	NRK-52E+62.5uM PB. 18.4.18. 24h Recov.. A2'	13350	967600	0.01379702	-1.816	920000	2.367	50.00
	NRK-52E+62.5uM PB. 18.4.18. 2min. B1	14860	915000	0.01624044	9.195	250000	0.643	142.98
	NRK-52E+62.5uM PB. 18.4.18. 1h. B2	15280	882000	0.01732426	14.080	235000	0.605	232.90
	NRK-52E+62.5uM PB. 18.4.18. 3h. B3	18270	961900	0.01899366	21.603	260000	0.669	322.99
	NRK-52E+62.5uM PB. 18.4.18. 6h. B4	23830	951700	0.0250394	48.848	345000	0.887	550.41
	NRK-52E+62.5uM PB. 18.4.18. 24h. B1'	32750	987600	0.0331612	85.449	620000	1.595	535.76
	NRK-52E+62.5uM PB. 18.4.18. 24h Recov.. B2'	16700	941200	0.01774331	15.968	695000	1.788	89.31
	NRK-52E+62.5uM PB. 18.4.18. 2min. C1	12140	891000	0.01362514	-2.591	200000	0.514	50.00
	NRK-52E+62.5uM PB. 18.4.18. 1h. C2	12680	843900	0.01502548	3.720	275000	0.707	52.59
	NRK-52E+62.5uM PB. 18.4.18. 3h. C3	17480	882400	0.01980961	25.280	195000	0.502	503.96
	NRK-52E+62.5uM PB. 18.4.18. 6h. C4	19890	841400	0.02363917	42.538	210000	0.540	787.43
	NRK-52E+62.5uM PB. 18.4.18. 24h. C1'	34470	926600	0.03720052	103.653	220000	0.566	1831.52
	NRK-52E+62.5uM PB. 18.4.18. 24h Recov.. C2'	13600	911200	0.01492537	3.269	690000	1.775	50.00

3

Experiment	Sample name	Peak area_PB	Peak area_Col (int. Std.)	PB/Col	PB [nM]	Cell number from sample	Total volumen of viable cells = cell number * $4/3\pi r^3$ [mm <sup>3</sup> ]	Intracellular concentration = (Total amount of drugs detected in the cell sample / Total volumen of viable cells) * 10 (dilution factor) [nM]
	RPTEC/TERT1+62.5uM PB. 2min. A1	14537	726100	0.02002066	26.231	560000	2.011	130.43
	RPTEC/TERT1+62.5uM PB. 1h. A2	16580	664100	0.02496612	48.518	630000	2.263	214.44
	RPTEC/TERT1+62.5uM PB. 3h. A3	20050	629800	0.0318355	79.475	530000	1.903	417.54
	RPTEC/TERT1+62.5uM PB. 6h. A4	31640	669000	0.04729447	149.141	750000	2.694	553.70
	RPTEC/TERT1+62.5uM PB. 24h. A'1	227500	629800	0.36122579	1563.884	590000	2.119	7380.62
	RPTEC/TERT1+62.5uM PB. 24h Recov.. A'2	96370	603900	0.1595794	655.157	560000	2.011	3257.60
	RPTEC/TERT1+62.5uM PB. 2min. B1	14761	685100	0.02154576	33.104	870000	3.124	105.95
	RPTEC/TERT1+62.5uM PB. 1h. B2	17430	608000	0.02866776	65.199	535000	1.921	339.34
	RPTEC/TERT1+62.5uM PB. 3h. B3	24600	614400	0.04003906	116.445	685000	2.460	473.34
	RPTEC/TERT1+62.5uM PB. 6h. B4	26890	626500	0.04292099	129.432	640000	2.298	563.12
1	RPTEC/TERT1+62.5uM PB. 24h. B'1	119090	647300	0.18397961	765.118	685000	2.460	3110.13
	RPTEC/TERT1+62.5uM PB. 24h Recov.. B'2	73490	574200	0.12798676	512.784	770000	2.765	1854.32
	RPTEC/TERT1+62.5uM PB. 2min. C1	14225	675000	0.02107407	30.978	465000	1.670	185.50
	RPTEC/TERT1+62.5uM PB. 1h. C2	14992	625100	0.02398336	44.089	595000	2.137	206.33
	RPTEC/TERT1+62.5uM PB. 3h. C3	26590	652700	0.04073847	119.597	690000	2.478	482.63
	RPTEC/TERT1+62.5uM PB. 6h. C4	32160	688300	0.04672381	146.570	645000	2.316	632.74
	RPTEC/TERT1+62.5uM PB. 24h. C'1	124090	599100	0.20712736	869.434	560000	2.011	4323.04
	RPTEC/TERT1+62.5uM PB. 24h Recov.. C'2	111580	518400	0.2152392	905.990	465000	1.670	5425.14

Experiment	Sample name	Peak area_PB	Peak area_Col (int. Std.)	PB/Col	PB [nM]	Cell number from sample	Total volumen of viable cells = cell number * $4/3\pi r^3$ [mm <sup>3</sup> ]	Intracellular concentration = (Total amount of drugs detected in the cell sample / Total volumen of viable cells) * 10 (dilution factor) [nM]
	RPTEC/TERT1+62.5uM PB. 28.2.18. 2 min. A1	12187	1096800	0.01111142	-13.919	610000	2.191	50.00
	RPTEC/TERT1+62.5uM PB. 28.2.18. 1h. A2	18890	1103700	0.01711516	13.137	530000	1.903	69.02
	RPTEC/TERT1+62.5uM PB. 28.2.18. 3h. A3	44090	1211000	0.03640793	100.081	720000	2.586	387.04
	RPTEC/TERT1+62.5uM PB. 28.2.18. 6h. A4	50350	1057000	0.04763482	150.675	640000	2.298	655.54
	RPTEC/TERT1+62.5uM PB. 1.3.18. 24h. A'1	114620	1216800	0.0941979	360.513	630000	2.263	1593.39
	RPTEC/TERT1+62.5uM PB. 2.3.18. 24h Recov.. A'2	112050	1283500	0.08730035	329.429	570000	2.047	1609.27
	RPTEC/TERT1+62.5uM PB. 28.2.18. 2 min. B1	16720	1316000	0.01270517	-6.737	740000	2.658	-25.35
	RPTEC/TERT1+62.5uM PB. 28.2.18. 1h. B2	19100	1281000	0.01491023	3.201	455000	1.634	19.59
	RPTEC/TERT1+62.5uM PB. 28.2.18. 3h. B3	40480	1246000	0.03248796	82.415	585000	2.101	392.28
	RPTEC/TERT1+62.5uM PB. 28.2.18. 6h. B4	51500	1319000	0.03904473	111.964	630000	2.263	494.85
	RPTEC/TERT1+62.5uM PB. 1.3.18. 24h. B'1	121920	1163100	0.10482332	408.397	640000	2.298	1776.82
	RPTEC/TERT1+62.5uM PB. 2.3.18. 24h Recov.. B'2	102080	1247000	0.08186047	304.914	590000	2.119	1439.02
	RPTEC/TERT1+62.5uM PB. 28.2.18. 2 min. C1	19850	1215000	0.01633745	9.632	615000	2.209	43.61
	RPTEC/TERT1+62.5uM PB. 28.2.18. 1h. C2	28270	1165000	0.02426609	45.363	650000	2.334	194.33
	RPTEC/TERT1+62.5uM PB. 28.2.18. 3h. C3	48330	1341000	0.03604027	98.424	465000	1.670	589.37
	RPTEC/TERT1+62.5uM PB. 28.2.18. 6h. C4	50180	1169000	0.04292558	129.453	700000	2.514	514.94
	RPTEC/TERT1+62.5uM PB. 1.3.18. 24h. C'1	105650	1107700	0.09537781	365.831	625000	2.245	1629.82
	RPTEC/TERT1+62.5uM PB. 2.3.18. 24h Recov.. C'2	213600	1166000	0.18319039	761.561	470000	1.688	4511.78

2

Experiment	Sample name	Peak area_PB	Peak area_Col (int. Std.)	PB/Col	PB [nM]	Cell number from sample	Total volumen of viable cells = cell number * $\frac{4}{3}\pi \cdot r^3$ [mm <sup>3</sup> ]	Intracellular concentration = (Total amount of drugs detected in the cell sample / Total volumen of viable cells) * 10 (dilution factor) [nM]
	RPTEC/TERT1+62.5uM PB. 7.3.18. 2min. A1	15630	954800	0.01636992	9.779	810000	2.909	33.62
	RPTEC/TERT1+62.5uM PB. 7.3.18. 1h. A2	24730	860900	0.02872575	65.461	690000	2.478	264.16
	RPTEC/TERT1+62.5uM PB. 7.3.18. 3h. A3	49610	902500	0.05496953	183.729	675000	2.424	757.91
	RPTEC/TERT1+62.5uM PB. 7.3.18. 6h. A4	55110	930800	0.05920713	202.826	630000	2.263	896.45
	RPTEC/TERT1+62.5uM PB. 8.3.18. 24h. A1'	125580	909800	0.13803034	558.046	640000	2.298	2427.90
	RPTEC/TERT1+62.5uM PB. 9.3.18. 24hRecov. A2'	90650	932100	0.09725351	374.284	800000	2.873	1302.72
	RPTEC/TERT1+62.5uM PB. 7.3.18. 2min. B1	15946	972300	0.01640029	9.916	810000	2.909	34.09
	RPTEC/TERT1+62.5uM PB. 7.3.18. 1h. B2	26100	978700	0.02666803	56.188	745000	2.676	210.00
	RPTEC/TERT1+62.5uM PB. 7.3.18. 3h. B3	42500	969600	0.04383251	133.540	670000	2.406	554.98
	RPTEC/TERT1+62.5uM PB. 7.3.18. 6h. B4	72960	1027600	0.07100039	255.973	820000	2.945	869.20
	RPTEC/TERT1+62.5uM PB. 8.3.18. 24h. B1'	149940	940500	0.15942584	654.465	830000	2.981	2195.58
	RPTEC/TERT1+62.5uM PB. 9.3.18. 24hRecov. B2'	106800	1081600	0.0987426	380.994	550000	1.975	1928.84
	RPTEC/TERT1+62.5uM PB. 7.3.18. 2min. C1	15789	1056300	0.01494746	3.368	660000	2.370	14.21
	RPTEC/TERT1+62.5uM PB. 7.3.18. 1h. C2	29580	965400	0.03064015	74.088	675000	2.424	305.62
	RPTEC/TERT1+62.5uM PB. 7.3.18. 3h. C3	50800	1003600	0.05061778	164.118	720000	2.586	634.69
	RPTEC/TERT1+62.5uM PB. 7.3.18. 6h. C4	41100	932800	0.04406089	134.569	670000	2.406	559.26
	RPTEC/TERT1+62.5uM PB. 8.3.18. 24h. C1'	131090	1011700	0.12957398	519.937	680000	2.442	2129.03
	RPTEC/TERT1+62.5uM PB. 9.3.18. 24hRecov. C2'	150280	1064200	0.14121406	572.393	610000	2.191	2612.79

3

Experiment	Sample name	Peak area_PB	Peak area_Col (Int. Std.)	PB/Col	PB [nM]	Cell number from sample	Total volume of viable cells = cell number * $4/3\pi r^3$ [mm <sup>3</sup> ]	Intracellular concentration = (Total amount of drugs detected in the cell sample / Total volume of viable cells) * 10 (dilution factor) [nM]
	NRK-52E+125uM PB. 14.3.18. 2 min. A1	17680	967200	0.018	18.385	400000	1.029	178.67
	NRK-52E+125uM PB. 14.3.18. 1h. A2	20550	765900	0.027	56.923	470000	1.209	470.81
	NRK-52E+125uM PB. 14.3.18. 3h. A3	25420	751200	0.034	88.505	370000	0.952	929.86
	NRK-52E+125uM PB. 14.3.18. 6h. A4	37030	851300	0.043	132.033	255000	0.656	2012.79
	NRK-52E+125uM PB. 15.3.18. 24h. A1'	98550	777800	0.127	507.001	515000	1.325	3826.98
	NRK-52E+125uM PB. 16.3.18. 24h Recov. A2'	32320	822200	0.039	113.155	1015000	2.611	433.37
	NRK-52E+125uM PB. 14.3.18. 2 min. B1	15247	836500	0.018	18.148	470000	1.209	150.11
	NRK-52E+125uM PB. 14.3.18. 1h. B2	19550	733300	0.027	56.153	410000	1.055	532.40
	NRK-52E+125uM PB. 14.3.18. 3h. B3	27730	763900	0.036	99.597	410000	1.055	944.31
	NRK-52E+125uM PB. 14.3.18. 6h. B4	34570	721200	0.048	152.023	335000	0.862	1764.09
1	NRK-52E+125uM PB. 15.3.18. 24h. B1'	96970	816800	0.119	471.020	705000	1.814	2597.20
	NRK-52E+125uM PB. 16.3.18. 24h Recov. B2'	33610	831600	0.040	118.144	995000	2.560	461.57
	NRK-52E+125uM PB. 14.3.18. 2 min. C1	16580	658700	0.025	49.440	470000	1.209	408.92
	NRK-52E+125uM PB. 14.3.18. 1h. C2	20700	832200	0.025	48.102	250000	0.643	747.96
	NRK-52E+125uM PB. 14.3.18. 3h. C3	32750	799900	0.041	120.517	310000	0.797	1511.26
	NRK-52E+125uM PB. 14.3.18. 6h. C4	36580	728100	0.050	162.417	195000	0.502	3237.81
	NRK-52E+125uM PB. 15.3.18. 24h. C1'	103610	766000	0.135	545.566	335000	0.862	6330.78
	NRK-52E+125uM PB. 16.3.18. 24h Recov. C2'	39280	847300	0.046	144.926	625000	1.608	901.41



Experiment	Sample name	Peak area_PB	Peak area_Col (int. Std.)	PB/Col	PB [nM]	Cell number from sample	Total volumen of viable cells = $4/3\pi r^3$ [mm <sup>3</sup> ]	Intracellular concentration = (Total amount of drugs detected in the cell sample / Total volumen of viable cells) * 10 (dilution factor) [nM]
	NRK-52E+125uM PB 21.3.18. 2min. A1	12954	768700	0.017	11.951	270000	0.695	172.06
	NRK-52E+125uM PB 21.3.18. 1h. A2	15303	728900	0.021	30.620	280000	0.720	425.11
	NRK-52E+125uM PB 21.3.18. 3h. A3	19800	769300	0.026	51.995	375000	0.965	538.99
	NRK-52E+125uM PB 21.3.18. 6h. A4	19500	784800	0.025	47.981	355000	0.913	525.41
	NRK-52E+125uM PB 22.3.18. 24h. A1'	44720	848600	0.053	173.495	625000	1.608	1079.10
	NRK-52E+125uM PB 23.3.18. 24h Recov. A2'	15040	954100	0.016	7.046	910000	2.341	50.00
	NRK-52E+125uM PB 21.3.18. 2min. B1	23590	848400	0.028	61.313	365000	0.939	653.00
	NRK-52E+125uM PB 21.3.18. 1h. B2	17840	850000	0.021	30.591	310000	0.797	383.61
	NRK-52E+125uM PB 21.3.18. 3h. B3	21780	829500	0.026	54.334	425000	1.093	496.98
2	NRK-52E+125uM PB 21.3.18. 6h. B4	19920	898800	0.022	35.885	220000	0.566	634.08
	NRK-52E+125uM PB 22.3.18. 24h. B1'	48710	962600	0.051	164.049	635000	1.633	1004.28
	NRK-52E+125uM PB 23.3.18. 24h Recov. B2'	27740	908200	0.031	73.654	850000	2.187	336.85
	NRK-52E+125uM PB 21.3.18. 2min. C1	19460	826100	0.024	42.165	230000	0.592	712.66
	NRK-52E+125uM PB 21.3.18. 1h. C2	19640	804000	0.024	46.092	285000	0.733	628.69
	NRK-52E+125uM PB 21.3.18. 3h. C3	19400	935300	0.021	29.482	230000	0.592	498.29
	NRK-52E+125uM PB 21.3.18. 6h. C4	24820	726200	0.034	90.031	215000	0.553	1627.83
	NRK-52E+125uM PB 22.3.18. 24h. C1'	49260	778100	0.063	221.307	455000	1.170	1890.77
	NRK-52E+125uM PB 23.3.18. 24h Recov. C2'	24610	913200	0.027	57.455	665000	1.711	335.86

Experiment	Sample name	Peak area_PB	Peak area_Col (int. Std.)	PB/Col	PB [nM]	Cell number from sample	Total volumen of viable cells = cell number * $\frac{4}{3}\pi r^3$ [mm <sup>3</sup> ]	Intracellular concentration = (Total amount of drugs detected in the cell sample / Total volumen of viable cells) * 10 (dilution factor) [nM]
	NRK-52E+125uM PB. 11.4.18. 2 min. A1	13470	1191800	0.011	-13.059	270000	0.695	50.00
	NRK-52E+125uM PB. 11.4.18. 1 h. A2	25390	1210000	0.021	30.570	235000	0.605	505.69
	NRK-52E+125uM PB. 11.4.18. 3 h. A3	28680	1178000	0.024	45.725	225000	0.579	790.00
	NRK-52E+125uM PB. 11.4.18. 6 h. A4	42670	1261000	0.034	88.500	270000	0.695	1274.19
	NRK-52E+125uM PB. 12.4.18. 24 h. A1'	87870	1251000	0.070	252.545	580000	1.492	1692.65
	NRK-52E+125uM PB. 13.4.18. 24 h Recov.. A2'	40310	1275000	0.032	78.484	920000	2.367	331.63
	NRK-52E+125uM PB. 11.4.18. 2 min. B1	22500	1384000	0.016	9.271	250000	0.643	144.16
	NRK-52E+125uM PB. 11.4.18. 1 h. B2	20370	1223000	0.017	11.067	235000	0.605	183.07
	NRK-52E+125uM PB. 11.4.18. 3 h. B3	36510	1245000	0.029	68.163	260000	0.669	1019.13
	NRK-52E+125uM PB. 11.4.18. 6 h. B4	40520	1327000	0.031	73.614	345000	0.887	829.47
	NRK-52E+125uM PB. 12.4.18. 24 h. B1'	84370	1270000	0.066	235.390	620000	1.595	1475.88
	NRK-52E+125uM PB. 13.4.18. 24 h Recov.. B2'	32710	1369000	0.024	43.683	695000	1.788	244.34
	NRK-52E+125uM PB. 11.4.18. 2 min. C1	14090	1187000	0.012	-10.499	200000	0.514	50.00
	NRK-52E+125uM PB. 11.4.18. 1 h. C2	29850	1306000	0.023	39.009	275000	0.707	551.42
	NRK-52E+125uM PB. 11.4.18. 3 h. C3	28800	1307000	0.022	35.310	195000	0.502	703.90
	NRK-52E+125uM PB. 11.4.18. 6 h. C4	44350	1230000	0.036	98.499	210000	0.540	1823.34
	NRK-52E+125uM PB. 12.4.18. 24 h. C1'	76190	1287000	0.059	202.793	220000	0.566	3583.31
	NRK-52E+125uM PB. 13.4.18. 24 h Recov.. C2'	39170	1286000	0.030	73.271	690000	1.775	412.80

3

Experiment	Sample name	Peak area_PB	Peak area_Col (int. Std.)	PB/Col	PB [nM]	Cell number from sample	Total volume of viable cells = cell number * $\frac{4}{3}\pi r^3$ [mm <sup>3</sup> ]	Intracellular concentration = (Total amount of drugs detected in the cell sample / Total volume of viable cells) * 10 (dilution factor) [nM]
	RPTEC/TERT1+125uM PB. 2min. A1	15430	694700	0.02221103	36.102	560000	2.011	179.51
	RPTEC/TERT1+125uM PB. 1h. A2	20190	589700	0.03423775	90.301	630000	2.263	399.11
	RPTEC/TERT1+125uM PB. 3h. A3	63460	636900	0.09963888	385.033	530000	1.903	2022.85
	RPTEC/TERT1+125uM PB. 6h. A4	102760	661300	0.1553909	636.282	750000	2.694	2362.27
	RPTEC/TERT1+125uM PB. 24h. A'1	105780	565400	0.18708879	779.129	590000	2.119	3677.04
	RPTEC/TERT1+125uM PB. 24h Recov.. A'2	47110	575400	0.08187348	304.973	560000	2.011	1516.40
	RPTEC/TERT1+125uM PB. 2min. B1	10383	644600	0.01610766	8.597	870000	3.124	50.00
	RPTEC/TERT1+125uM PB. 1h. B2	24260	604100	0.04015891	116.985	535000	1.921	608.86
	RPTEC/TERT1+125uM PB. 3h. B3	72960	634000	0.11507886	454.614	685000	2.460	1847.96
	RPTEC/TERT1+125uM PB. 6h. B4	85020	623300	0.13640302	550.712	640000	2.298	2395.99
1	RPTEC/TERT1+125uM PB. 24h. B'1	76570	644100	0.11887906	471.740	685000	2.460	1917.58
	RPTEC/TERT1+125uM PB. 24h Recov.. B'2	60730	594300	0.10218745	396.518	770000	2.765	1433.88
	RPTEC/TERT1+125uM PB. 2min. C1	13963	671800	0.02078446	29.673	465000	1.670	177.68
	RPTEC/TERT1+125uM PB. 1h. C2	21720	636800	0.03410804	89.716	595000	2.137	419.85
	RPTEC/TERT1+125uM PB. 3h. C3	35880	587600	0.06106195	211.185	690000	2.478	852.23
	RPTEC/TERT1+125uM PB. 6h. C4	38850	595200	0.06527218	230.159	645000	2.316	993.59
	RPTEC/TERT1+125uM PB. 24h. C'1	81220	656000	0.12381098	493.966	560000	2.011	2456.12
	RPTEC/TERT1+125uM PB. 24h Recov.. C'2	25800	598600	0.04310057	130.241	465000	1.670	779.90

Experiment	Sample name	Peak area_PB	Peak area_Col (int. Std.)	PB/Col	PB [nM]	Cell number from sample	Total volumen of viable cells = cell number * $4/3\pi r^3$ [mm <sup>3</sup> ]	Intracellular concentration = (Total amount of drugs detected in the cell sample / Total volumen of viable cells) * 10 (dilution factor) [nM]
	RPTEC/TERT1+125uM PB. 7.3.18. 2min. A1	29040	1126600	0.02577667	52.171	610000	2.191	238.14
	RPTEC/TERT1+125uM PB. 7.3.18. 1h. A2	49820	1097700	0.04538581	140.540	530000	1.903	738.35
	RPTEC/TERT1+125uM PB. 7.3.18. 3h. A3	90480	1001800	0.09031743	343.026	720000	2.586	1326.58
	RPTEC/TERT1+125uM PB. 7.3.18. 6h. A4	142050	838100	0.16949051	699.822	640000	2.298	3044.73
	RPTEC/TERT1+125uM PB. 8.3.18. 24h. A1'	112350	1052300	0.10676613	417.152	630000	2.263	1843.72
	RPTEC/TERT1+125uM PB. 9.3.18. 24hRecov. A2'	63570	1013900	0.06269849	218.560	570000	2.047	1067.67
	RPTEC/TERT1+125uM PB. 7.3.18. 2min. B1	34760	1140000	0.03049123	73.417	740000	2.658	276.25
	RPTEC/TERT1+125uM PB. 7.3.18. 1h. B2	41400	1059200	0.0390861	112.150	455000	1.634	686.32
	RPTEC/TERT1+125uM PB. 7.3.18. 3h. B3	172450	1063000	0.16222954	667.100	585000	2.101	3175.23
2	RPTEC/TERT1+125uM PB. 7.3.18. 6h. B4	182990	977800	0.18714461	779.381	630000	2.263	3444.69
	RPTEC/TERT1+125uM PB. 8.3.18. 24h. B1'	125070	1027600	0.12171078	484.501	640000	2.298	2107.93
	RPTEC/TERT1+125uM PB. 9.3.18. 24hRecov. B2'	95470	977800	0.09763755	376.014	590000	2.119	1774.57
	RPTEC/TERT1+125uM PB. 7.3.18. 2min. C1	45850	1129000	0.04061116	119.023	615000	2.209	538.88
	RPTEC/TERT1+125uM PB. 7.3.18. 1h. C2	40330	1028600	0.03920863	112.702	650000	2.334	482.79
	RPTEC/TERT1+125uM PB. 7.3.18. 3h. C3	112370	955400	0.111761566	466.046	465000	1.670	2790.72
	RPTEC/TERT1+125uM PB. 7.3.18. 6h. C4	215000	1009500	0.21297672	895.794	700000	2.514	3563.29
	RPTEC/TERT1+125uM PB. 8.3.18. 24h. C1'	98050	1004000	0.09765936	376.112	625000	2.245	1675.63
	RPTEC/TERT1+125uM PB. 9.3.18. 24hRecov. C2'	67900	966700	0.07023896	252.541	470000	1.688	1496.15

Experiment	Sample name	Peak area_PB	Peak area_Col (int. Std.)	PB/Col	PB [nM]	Cell number from sample	Total volumen of viable cells = cell number * $\frac{4}{3}\pi \cdot r^3$ [mm <sup>3</sup> ]	Intracellular concentration = (Total amount of drugs detected in the cell sample / Total volumen of viable cells) * 10 (dilution factor) [nM]
	RPTEC/TERT1+125uM PB. 14.3.18. 2 min. A1	18650	676900	0.02755208	60.172	810000	2.909	206.85
	RPTEC/TERT1+125uM PB. 14.3.18. 1h. A2	28850	731000	0.03946648	113.864	690000	2.478	459.49
	RPTEC/TERT1+125uM PB. 14.3.18. 3h. A3	47740	729100	0.06547799	231.086	675000	2.424	953.26
	RPTEC/TERT1+125uM PB. 14.3.18. 6h. A4	83490	776200	0.10756248	420.741	630000	2.263	1859.58
	RPTEC/TERT1+125uM PB. 15.3.18. 24h. A1'	148480	781100	0.1900909	792.658	640000	2.298	3448.63
	RPTEC/TERT1+125uM PB. 16.3.18. 24h Recov. A2'	81070	723600	0.11203704	440.906	800000	2.873	1534.60
	RPTEC/TERT1+125uM PB. 14.3.18. 2 min. B1	19650	930900	0.0211086	31.134	810000	2.909	107.03
	RPTEC/TERT1+125uM PB. 14.3.18. 1h. B2	23430	770500	0.03040883	73.046	745000	2.676	273.01
	RPTEC/TERT1+125uM PB. 14.3.18. 3h. B3	46970	793100	0.0592233	202.899	670000	2.406	843.23
	RPTEC/TERT1+125uM PB. 14.3.18. 6h. B4	103860	719300	0.14439038	586.707	820000	2.945	1992.27
	RPTEC/TERT1+125uM PB. 15.3.18. 24h. B1'	198110	804300	0.24631356	1046.028	830000	2.981	3509.18
	RPTEC/TERT1+125uM PB. 16.3.18. 24h Recov. B2'	70900	836600	0.08474779	317.926	550000	1.975	1609.55
	RPTEC/TERT1+125uM PB. 14.3.18. 2 min. C1	29480	918400	0.0320993	80.664	660000	2.370	340.31
	RPTEC/TERT1+125uM PB. 14.3.18. 1h. C2	25240	751800	0.03357276	87.304	675000	2.424	360.14
	RPTEC/TERT1+125uM PB. 14.3.18. 3h. C3	42540	835200	0.05093391	165.543	720000	2.586	640.20
	RPTEC/TERT1+125uM PB. 14.3.18. 6h. C4	72090	798300	0.0903044	342.967	670000	2.406	1425.34
	RPTEC/TERT1+125uM PB. 15.3.18. 24h. C1'	178060	855500	0.20813559	873.977	680000	2.442	3578.75
	RPTEC/TERT1+125uM PB. 16.3.18. 24h Recov. C2'	81500	905900	0.08996578	341.441	610000	2.191	1558.57

3

**Table 44**  
**Raw data cell volume**

<b>NRK-52E</b>			<b>Formula for sphere volume</b> <b><math>4/3*\pi*r^3</math></b>
<b>Cell number</b>	<b>Diameter [<math>\mu\text{m}</math>]</b>	<b>Radius [<math>\mu\text{m}</math>]</b>	<b>Volume sphere [<math>\mu\text{m}^3</math>]</b>
1	17.77	8.88	2936.1
2	20.63	10.31	4595.2
3	14.44	7.22	1575.9
4	15.99	8.00	2141.4
5	14.38	7.19	1556.3
6	18.88	9.44	3526.0
7	14.94	7.47	1746.7
8	16.44	8.22	2325.2
9	17.38	8.69	2747.9
10	19.55	9.78	3912.4
11	16.25	8.12	2245.1
12	14.72	7.36	1668.7
13	14.98	7.49	1758.3
14	17.52	8.76	2813.4
15	15.44	7.72	1926.5
16	15.33	7.67	1887.1
17	15.44	7.72	1926.5
18	17.44	8.72	2776.9
19	14.73	7.37	1674.8
20	16.50	8.25	2350.8
21	17.28	8.64	2699.8
22	17.35	8.67	2733.7
23	20.22	10.11	4326.0
24	18.28	9.14	3197.3
25	19.52	9.76	3893.2
26	16.55	8.27	2371.8
27	20.28	10.14	4367.8
28	18.31	9.15	3213.6
<b>Mean</b>	<b>17.02</b>	<b>8.51</b>	<b>2.674.8</b>
<b>Stad. Dev.</b>	<b>1.90</b>	<b>0.95</b>	<b>910.7</b>

<b>RPTEC/TERT1</b>			<b>Formula for sphere volume</b> $4/3*\pi*r^3$
<b>Cell number</b>	<b>Diameter [μm]</b>	<b>Radius [μm]</b>	<b>Volume sphere [μm<sup>3</sup>]</b>
1	19.11	9.56	3654.1
2	21.92	10.96	5516.2
3	16.36	8.18	2294.4
4	16.28	8.14	2258.0
5	19.28	9.64	3751.3
6	20.32	10.16	4392.4
7	15.99	8.00	2141.4
8	20.57	10.28	4553.9
9	19.00	9.50	3589.7
10	18.54	9.27	3334.1
11	15.90	7.95	2104.3
12	19.50	9.75	3884.8
13	19.22	9.61	3715.2
14	21.23	10.61	5007.3
15	18.39	9.19	3255.4
16	17.86	8.93	2980.4
17	19.12	9.56	3658.7
18	17.12	8.56	2629.1
19	17.53	8.76	2820.1
20	18.74	9.37	3444.3
21	21.39	10.70	5127.1
22	20.93	10.46	4800.0
23	20.82	10.41	4724.1
24	19.24	9.62	3728.6
25	22.87	11.43	6260.7
26	19.60	9.80	3943.7
27	18.17	9.09	3141.0
28	16.73	8.37	2452.7
<b>Mean</b>	<b>18.99</b>	<b>9.49</b>	<b>3.684.4</b>
<b>Stad. Dev.</b>	<b>1.85</b>	<b>0.93</b>	<b>1.070.0</b>

**Table 45**  
**Raw data aprotinin assay**

<b>NRK-52E</b>					
<b>4 h treatment</b>					
<b>with 100 µg/mL aprotinin</b>					
	Image Nr.	Area measured [µm <sup>2</sup> ]	Mean intensity	Nr. of nuclei	Mean intensity / nr. of nuclei [%]
Chamberslide 1	Image 1_1	28.4	3880.65	21	184.79
	Image 1_2	28.4	4630.65	33	140.32
	Image 1_3	28.4	3750.65	26	144.26
	Image 1_4	28.4	3645.65	13	280.43
				Mean	187.45
				Stand. Dev.	65.17
<b>RPTEC/TERT1</b>					
<b>4 h treatment</b>					
<b>with 100 µg/mL aprotinin</b>					
	Image Nr.	Area measured [µm <sup>2</sup> ]	Mean intensity	Nr. of nuclei	Mean intensity / nr. of nuclei [%]
Chamberslide 2	Image 2_1	28.4	4661.68	22	211.89
	Image 2_2	28.4	5166.68	27	191.36
	Image 2_3	28.4	4469.68	26	171.91
	Image 2_4	28.4	5428.68	20	271.43
				Mean	211.65
				Stand. Dev.	43.07
<b>RPTEC/TERT1</b>					
<b>4 h treatment</b>					
<b>with 100 µg/mL aprotinin</b>					
	Image Nr.	Area measured [µm <sup>2</sup> ]	Mean intensity	Nr. of nuclei	Mean intensity / nr. of nuclei [%]
Chamberslide 1	Image 1_1	28.4	5292.68	24	220.53
	Image 1_2	28.4	5538.68	17	325.80
	Image 1_3	28.4	6101.68	17	358.92
	Image 1_4	28.4	11258.68	23	489.51
				Mean	348.69
				Stand. Dev.	110.88
<b>RPTEC/TERT1</b>					
<b>4 h treatment</b>					
<b>with 100 µg/mL aprotinin</b>					
	Image Nr.	Area measured [µm <sup>2</sup> ]	Mean intensity	Nr. of nuclei	Mean intensity / nr. of nuclei [%]
Chamberslide 2	Image 2_1	28.4	8555.65	24	356.49
	Image 2_2	28.4	6465.65	22	293.89
	Image 2_3	28.4	6548.65	18	363.81
	Image 2_4	28.4	7926.65	21	377.46
				Mean	347.91
				Stand. Dev.	37.05



**Table 46**  
**Raw data mtDNA copy number assay**

<b>Adefovir / NRK-52E / 24 h</b>					
Conc. [ $\mu$ M]	Experiment 1 [%]	Experiment 2 [%]	Experiment 3 [%]	Mean [%]	Stand. Dev. [%]
0	100	100	100	100	0
15.60	124.39834	105.379251	100.1579779	109.98	10.42
62.50	104.917012	83.4495517	100.7898894	96.39	9.30
250	127.385892	129.01665	106.6350711	121.01	10.19
1000	119.834025	141.596698	122.5908373	128.01	9.67
2000	98.879668	144.684787	134.7748815	126.11	19.68
<b>ADV / NRK-52E / 24 h</b>					
Conc. [ $\mu$ M]	Experiment 1 [%]	Experiment 2 [%]	Experiment 3 [%]	Mean [%]	Stand. Dev. [%]
0	100	100	100	100	0
15.60	104.450438	121.847052	103.8805402	110.06	8.34
62.50	110.485502	118.616536	95.85314818	108.32	9.42
250	126.146325	106.406279	111.3753091	114.64	8.38
500	125.151719	108.778974	116.1498954	116.69	6.70
<b>Cidofovir / NRK-52E / 24 h</b>					
Conc. [ $\mu$ M]	Experiment 1 [%]	Experiment 2 [%]	Experiment 3 [%]	Mean [%]	Stand. Dev. [%]
0	100	100	100	100	0
15.60	87.7104619	126.935878	163.7658922	126.14	31.05
62.50	114.966182	129.176836	103.9894783	116.04	10.31
250	141.38725	207.987575	119.5966681	156.32	37.60
1000	183.465247	217.372975	154.4278825	185.09	25.72
2000	200.7627	306.567562	144.6295484	217.32	67.14

<b>Tenofovir / NRK-52E / 24 h</b>					
Conc. [ $\mu$ M]	Experiment 1 [%]	Experiment 2 [%]	Experiment 3 [%]	Mean [%]	Stand. Dev. [%]
0	100	100	100	100	0
15.60	128.616701	91.3419257	111.4976282	110.49	15.23
62.50	114.403423	116.360879	107.4090806	112.72	3.84
250	129.298051	130.796058	85.58843461	115.23	20.97
1000	155.236888	135.132676	110.3456065	133.57	18.36
2000	147.219141	159.181198	136.1192681	147.51	9.42
<b>TDF / NRK-52E / 24 h</b>					
Conc. [ $\mu$ M]	Experiment 1 [%]	Experiment 2 [%]	Experiment 3 [%]	Mean [%]	Stand. Dev. [%]
0	100	100	100	100	0
15.60	133.812831	129.169869	130.3021545	131.09	1.98
62.50	127.794312	125.883935	172.5433526	142.07	21.56
250	143.402778	168.00538	130.5570152	147.32	15.54
1000	145.734127	153.516526	161.1928534	153.48	6.31
<b>ddC / NRK-52E / 24 h</b>					
Conc. [ $\mu$ M]	Experiment 1 [%]	Experiment 2 [%]	Experiment 3 [%]	Mean [%]	Stand. Dev. [%]
0	100	100	100	100	0
15.60	92.2960894	84.2966194	148.5538763	108.38	28.59
62.50	70.7150838	63.0588877	128.8735457	87.55	29.39
250	52.3938547	128.176118	103.0499076	94.54	31.52
1000	44.1564246	46.9193021	106.4749375	65.85	28.75
2000	55.5111732	40.4252999	119.3867566	71.77	34.23

<b>Tenofovir / RPTEC/TERT1 / 24 h</b>						
Conc. [ $\mu$ M]	Experiment 1 [%]	Experiment 2 [%]	Experiment 3 [%]	Mean [%]	Stand. Dev. [%]	
0	100	100	100	100.00	0.00	
15.60	109.4573959	92.2424442	86.8745909	96.19	9.63	
62.50	75.91876209	87.0542699	62.5180024	75.16	10.03	
250	109.5133869	84.4313596	94.4683438	96.14	10.31	
1000	46.89504225	88.3636663	85.6635182	73.64	18.94	
2000	86.58760053	89.0965989	93.1123165	89.60	2.69	
<b>TDF / RPTEC/TERT1 / 24 h</b>						
Conc. [ $\mu$ M]	Experiment 1 [%]	Experiment 2 [%]	Experiment 3 [%]	Mean [%]	Stand. Dev. [%]	
0	100	100	100	100.00	0.00	
15.60	92.77863137	100.861508	89.2720084	94.30	4.85	
62.50	108.2732538	99.5742549	90.7256658	99.52	7.16	
250	103.4944648	107.062359	135.469241	115.34	14.31	
1000	100.8233857	93.3984473	108.838237	101.02	6.30	
<b>ddC / RPTEC/TERT1 / 24 h</b>						
Conc. [ $\mu$ M]	Experiment 1 [%]	Experiment 2 [%]	Experiment 3 [%]	Mean [%]	Stand. Dev. [%]	
0	100	100	100	100.00	0.00	
15.60	101.6618768	81.3212912	163.042751	115.34	34.74	
62.50	91.73226707	84.3619334	169.405232	115.17	38.47	
250	99.19613478	87.1115571	198.24045	128.18	49.78	
1000	93.12341205	83.9906339	174.001472	117.04	40.45	
2000	85.83031363	125.171433	165.130126	125.38	32.37	

<b>Adefovir / RPTEC/TERT1 / 24 h</b>						
Conc. [ $\mu$ M]	Experiment 1 [%]	Experiment 2 [%]	Experiment 3 [%]	Mean [%]	Stand. Dev. [%]	
0	100	100	100	100.00	0.00	
15.60	123.789348	116.688758	83.8834107	108.12	17.38	
62.50	119.471356	107.079166	87.4912993	104.68	13.17	
250	114.89906	103.693216	82.4332947	100.34	13.46	
1000	122.860357	117.598506	91.8242459	110.76	13.56	
2000	134.662176	106.416436	82.9466357	108.01	21.14	
<b>ADV / RPTEC/TERT1 / 24 h</b>						
Conc. [ $\mu$ M]	Experiment 1 [%]	Experiment 2 [%]	Experiment 3 [%]	Mean [%]	Stand. Dev. [%]	
0	100	100	100	100.00	0.00	
15.60	86.44024044	89.7824804	122.314237	99.51	16.18	
62.50	81.34380647	115.026566	103.108879	99.83	13.95	
250	90.13533945	88.0477726	113.589465	97.26	11.58	
500	106.8923553	101.925435	126.961716	111.93	10.82	
<b>Cidofovir / RPTEC/TERT1 / 24 h</b>						
Conc. [ $\mu$ M]	Experiment 1 [%]	Experiment 2 [%]	Experiment 3 [%]	Mean [%]	Stand. Dev. [%]	
0	100	100	100	100.00	0.00	
15.60	121.3205816	102.132989	86.5923934	103.35	14.20	
62.50	108.5349949	115.553042	72.7564349	98.95	18.74	
250	121.5669227	120.881474	68.939685	103.80	24.65	
1000	137.8882288	105.530419	80.4187476	107.95	23.52	
2000	161.285804	107.816918	93.0272762	120.71	29.32	

<b>Tenofovir / RPTEC/TERT1 / 14 d</b>						
Conc. [ $\mu$ M]	Experiment 1 [%]	Experiment 2 [%]	Experiment 3 [%]	Mean [%]	Stand. Dev. [%]	
0	100	100	100	100.00	0.00	
15.60	93.8049713	106.978491	103.912994	101.57	5.63	
62.50	102.791587	90.9627859	119.378636	104.38	11.65	
250	91.5742511	90.8569478	106.905731	96.45	7.40	
1000	91.5487572	84.1550017	100.939271	92.21	6.87	
2000	92.0586361	84.3188802	98.4104651	91.60	5.76	
<b>TDF / RPTEC/TERT1 / 14 d</b>						
Conc. [ $\mu$ M]	Experiment 1 [%]	Experiment 2 [%]	Experiment 3 [%]	Mean [%]	Stand. Dev. [%]	
0	100	100	100	100.00	0.00	
0.24	106.170704	87.6896928	99.0053177	97.62	7.61	
0.98	89.3137255	94.9374772	103.175332	95.81	5.69	
3.90	88.0709343	96.7666222	89.6323501	91.49	3.79	
15.60	80.2191465	100.182105	101.916676	94.11	9.84	
62.50	67.5	74.0237141	88.02173	76.52	8.56	
<b>ddC / RPTEC/TERT1 / 14 d</b>						
Conc. [ $\mu$ M]	Experiment 1 [%]	Experiment 2 [%]	Experiment 3 [%]	Mean [%]	Stand. Dev. [%]	
0	100	100	100	100.00	0.00	
0.06	112.651936	99.9214642	89.3257624	100.63	9.54	
0.24	118.662545	87.6767056	89.5650311	98.63	14.18	
0.98	104.502736	81.9811514	92.4362546	92.97	9.20	
3.90	96.4370745	72.0822236	86.9723591	85.16	10.02	
15.60	65.2186625	61.5720822	79.8050139	68.87	7.88	
<b>Adefovir / RPTEC/TERT1 / 14 d</b>						
Conc. [ $\mu$ M]	Experiment 1 [%]	Experiment 2 [%]	Experiment 3 [%]	Mean [%]	Stand. Dev. [%]	
0	100	100	100	100.00	0.00	
0.98	106.75357	105.253088	127.885445	113.30	10.33	
3.90	100.025728	86.8588883	109.489996	98.79	9.28	
15.60	117.164787	92.7698711	114.284033	108.07	10.88	
62.50	108.867544	68.7164339	126.120047	101.23	24.05	
250	92.0843875	62.3086735	101.981169	85.46	16.86	
<b>ADV / RPTEC/TERT1 / 14 d</b>						
Conc. [ $\mu$ M]	Experiment 1 [%]	Experiment 2 [%]	Experiment 3 [%]	Mean [%]	Stand. Dev. [%]	
0	100	100	100	100.00	0.00	
0.06	112.651936	99.9214642	89.3257624	100.63	9.54	
0.24	118.662545	87.6767056	89.5650311	98.63	14.18	
0.98	104.502736	81.9811514	92.4362546	92.97	9.20	
3.90	96.4370745	72.0822236	86.9723591	85.16	10.02	
15.60	65.2186625	61.5720822	79.8050139	68.87	7.88	
<b>Cidofovir / RPTEC/TERT1 / 14 d</b>						
Conc. [ $\mu$ M]	Experiment 1 [%]	Experiment 2 [%]	Experiment 3 [%]	Mean [%]	Stand. Dev. [%]	
0	100	100	100	100.00	0.00	
0.98	116.459198	124.022784	100.956561	113.81	9.60	
3.90	111.687414	101.403393	84.1152843	99.07	11.38	
15.60	120.447211	108.515293	88.6579154	105.87	13.11	
62.50	123.605348	119.730053	85.9331649	109.76	16.92	
125	142.646381	131.22962	95.8963104	123.26	19.90	

Table 47

## Raw data MitoTracker® assay

Cidofovir / NRK-52E / 24 h				
	Experiment 1		Experiment 2	
Conc. [ $\mu$ M]	Mean [%]	Stand. Dev. [%]	Mean [%]	Stand. Dev. [%]
1000	83.54592	3.174702	91.89178	0.487802
500	96.02651	0.164251	100.4328	1.143427
250	98.37721	2.615174	100.7243	0.079596
125	100.5929	1.573349	99.81658	2.667259
62.50	95.69229	0.032522	96.27717	1.332102
31.25	101.0868	1.543973	101.2636	2.342235
15.62	100.4407	1.279318	98.29438	1.789535
7.81	101.143	2.978637	101.6821	1.207263
3.91	98.03262	0.967298	96.55877	2.858812
1.95	96.20866	2.763519	96.89273	5.835911
0.98	97.96456	0.443218	99.35202	3.940263

Tenofovir / NRK-52E / 24 h				
	Experiment 1		Experiment 2	
Conc. [ $\mu$ M]	Mean [%]	Stand. Dev. [%]	Mean [%]	Stand. Dev. [%]
1000	93.28085	1.524389	101.2107	4.835252
500	96.62286	1.451723	99.66146	0.737834
250	101.3854	3.337713	99.37433	2.243958
125	101.4483	1.145064	100.9359	0.681258
62.50	100.843	0.636314	101.3902	4.69514
31.25	102.2721	1.998135	103.0439	0.620476
15.62	102.7095	0.56675	98.22971	3.175381
7.81	101.3593	2.834501	102.3794	0.502366
3.91	97.2387	1.14533	98.89481	2.482834
1.95	96.24313	0.610748	98.51427	1.753722
0.98	95.18274	1.96322	99.78864	3.171883

Appendix

---

<b>Cidofovir / RPTEC/TERT1 / 24 h</b>			
	Experiment 1		Experiment 2
Conc. [ $\mu$ M]	Mean [%]	Mean [%]	Stand. Dev. [%]
1000	101.8583	103.6899	0.9158
500	100.6584	101.9184	0.63
250	101.9852	104.5663	1.29055
125	103.1504	101.518	0.8162
62.50	90.82946	102.9101	6.04032
31.25	103.0254	101.0881	0.96865
15.62	103.2481	103.3276	0.03975
7.81	101.1667	99.08703	1.039835

---

<b>TDF / RPTEC/TERT1 / 24 h</b>			
	Experiment 1		Experiment 2
Conc. [ $\mu$ M]	Mean [%]	Mean [%]	Stand. Dev. [%]
1000	39.47183	24.00956	7.731135
500	64.3184	62.61079	0.853805
250	97.31955	104.3191	3.499775
125	106.7668	106.5568	0.105
62.50	93.4071	106.5752	6.58405
31.25	92.09883	94.72846	1.314815
15.62	95.15004	103.9511	4.40053
7.81	94.11481	100.002	2.943595

---

*Appendix*

**Adefovir / RPTEC/TERT1 / 14 d**

Conc. [ $\mu$ M]	Experiment 1 [%]	Experiment 2 [%]	Experiment 3 [%]	Mean [%]	Stand. Dev. [%]
0	100	100	100	100	0
1000	109.23	107.03	115.21	110.49	3.456279
333.3333	92.49	99.42	86.98	92.96333	5.089626
111.1111	82.32	88.97	84.16	85.15	2.803652
37.03704	91.52	84.22	101.26	92.33333	6.980283
12.34568	112.06	116.85	132.43	120.4467	8.696215
4.115226	107.44	108.89	99.22	105.1833	4.258062
1.371742	104	104.74	100.44	103.06	1.87709

**ddC / RPTEC/TERT1 / 14 d**

Conc. [ $\mu$ M]	Experiment 1 [%]	Experiment 2 [%]	Experiment 3 [%]	Mean [%]	Stand. Dev. [%]
0	100	100	100	100	0
1000	67.35	71.86	79.5	72.90333	5.01478
333.3333	85.96	82.99	76.77	81.90667	3.829206
111.1111	101.07	100.17	94.8	98.68	2.768068
37.03704	97.04	94.26	98.58	96.62667	1.787686
12.34568	111.49	113.65	108.54	111.2267	2.094442
4.115226	100.38	104	130.02	111.4667	13.20216
1.371742	101.65	98.78	102.26	100.8967	1.517286

**Cidofovir / RPTEC/TERT1 / 14 d**

Conc. [ $\mu$ M]	Experiment 1 [%]	Experiment 2 [%]	Experiment 3 [%]	Mean [%]	Stand. Dev. [%]
0	100	100	100	100	0
1000	26.94	48.13	102.1	59.05667	31.64175
333.3333	102.78	99.8	93.8	98.79333	3.734536
111.1111	97.84	96.88	96.22	96.98	0.665132
37.03704	87.3	84.17	89.36	86.94333	2.133766
12.34568	84.91	118.64	140.61	114.72	22.90775
4.115226	89.99	101	99.15	96.71333	4.813733
1.371742	91.84	103.33	102.17	99.11333	5.16478

*Appendix*

<b>Tenofovir / RPTEC/TERT1 / 14 d</b>					
Conc. [ $\mu$ M]	Experiment 1 [%]	Experiment 2 [%]	Experiment 3 [%]	Mean [%]	Stand. Dev. [%]
0	100	100	100	100	0
1000	132.05	128.86	132.93	131.28	1.748504
333.3333	105.19	101.77	127.67	111.5433	11.48843
111.1111	113.68	108.25	107.86	109.93	2.656426
37.03704	115.33	109.14	102.64	109.0367	5.181186
12.34568	153.12	133.32	145.78	144.0733	8.172904
4.115226	119.38	108.7	133.15	120.41	10.00821
1.371742	119.18	117.08	116.8	117.6867	1.062115

<b>TDF / RPTEC/TERT1 / 14 d</b>					
Conc. [ $\mu$ M]	Experiment 1 [%]	Experiment 2 [%]	Experiment 3 [%]	Mean [%]	Stand. Dev. [%]
0	100	100	100	100	0
500	19.66	19.57	19.43	19.55333	0.094634
166.6667	19.56	19.68	19.04	19.42667	0.277769
55.55556	92.38	89.44	92.12	91.31333	1.328893
18.51852	85.83	92.52	84.08	87.47667	3.637035
6.17284	113.47	107.96	109.83	110.42	2.287808
2.057613	105.97	100.99	97.32	101.4267	3.544821
0.685871	93.16	93.73	99.63	95.50667	2.924908

<b>ADV / RPTEC/TERT1 / 14 d</b>					
Conc. [ $\mu$ M]	Experiment 1 [%]	Experiment 2 [%]	Experiment 3 [%]	Mean [%]	Stand. Dev. [%]
0	100	100	100	100	0
330	18.44	18.38	18.51	18.44333	0.053125
110	59.73	18.27	18.66	32.22	19.45316
36.66667	85.33	73.98	80.07	79.79333	4.637746
12.22222	84.1	86.61	84.53	85.08	1.096023
4.074074	105.73	116.74	125.51	115.9933	8.092393
1.358025	102.38	107.97	105.18	105.1767	2.282109
0.452675	88.98	94.8	100.41	94.73	4.66654

**Table 48**  
**Raw data cytotoxicity AOP2**

<b>ddC / NRK-52E / 24 h</b>					
Conc. [ $\mu$ M]	Experiment 1 [%]	Experiment 2 [%]	Experiment 3 [%]	Mean [%]	Stand. Dev. [%]
0	100	100	100	100.00	0.00
7.81	94.75043	96.16096	103.3335	98.08	3.76
15.60	98.22424	92.73767	100.2881	97.08	3.19
31.25	97.72684	90.99935	99.70158	96.14	3.73
62.50	97.52947	91.70126	101.2646	96.83	3.94
125.00	86.86492	92.4856	104.4631	94.60	7.34
250.00	97.2243	93.52779	102.9585	97.90	3.88
500.00	95.48241	88.17017	98.91631	94.19	4.48
1000.00	87.61828	87.41005	102.7895	92.61	7.20
2000.00	92.31648	90.34374	92.54239	91.73	0.99
<b>Cidofovir / NRK-52E / 24 h</b>					
Conc. [ $\mu$ M]	Experiment 1 [%]	Experiment 2 [%]	Experiment 3 [%]	Mean [%]	Stand. Dev. [%]
0	100	100	100	100.00	0.00
7.81	92.73965	91.27991	88.8951	90.97	1.58
15.60	91.25865	92.039	92.38081	91.89	0.47
31.25	92.98126	91.21838	87.40096	90.53	2.33
62.50	93.45512	93.67527	84.40141	90.51	4.32
125.00	91.8374	92.88638	84.98068	89.90	3.51
250.00	87.94453	86.53314	80.70879	85.06	3.13
500.00	81.93463	81.31208	70.3909	77.88	5.30
1000.00	79.50275	75.59003	78.86527	77.99	1.71
2000.00	70.4445	58.34158	59.52951	62.77	5.45
<b>TDF / NRK-52E / 24 h</b>					
Conc. [ $\mu$ M]	Experiment 1 [%]	Experiment 2 [%]	Experiment 3 [%]	Mean [%]	Stand. Dev. [%]
0	100	100	100	100.00	0.00
7.81	87.99182	75.06825	96.39988	86.49	8.77
15.60	86.31231	66.07645	89.17549	80.52	10.28
31.25	86.30518	72.87305	85.47969	81.55	6.15
62.50	80.78753	60.54398	85.09743	75.48	10.70
125.00	71.75648	49.94577	82.04271	67.91	13.38
250.00	51.34572	34.61443	58.47152	48.14	10.00
500.00	31.27477	21.08099	30.0562	27.47	4.55
1000.00	20.36031	3.776839	16.76194	13.63	7.12
2000.00	9.453894	0.1274903	5.848485	5.14	3.84



*Appendix*

<b>Tenofovir / NRK-52E / 24 h</b>					
Conc. [ $\mu$ M]	Experiment 1 [%]	Experiment 2 [%]	Experiment 3 [%]	Mean [%]	Stand. Dev. [%]
0	100	100	100	100.00	0.00
7.81	86.36149	95.70152	102.7214	94.93	6.70
15.60	95.99515	92.36395	99.7086	96.02	3.00
31.25	89.11172	89.4609	93.61161	90.73	2.04
62.50	87.36269	93.56519	94.51208	91.81	3.17
125.00	86.80321	88.89719	95.01945	90.24	3.49
250.00	86.37344	92.95541	85.40839	88.25	3.35
500.00	93.22784	78.57595	85.14486	85.65	5.99
1000.00	84.27586	80.28934	80.70865	81.76	1.79
2000.00	77.11665	75.40871	86.68385	79.74	4.96

<b>Adefovir / NRK-52E / 24 h</b>					
Conc. [ $\mu$ M]	Experiment 1 [%]	Experiment 2 [%]	Experiment 3 [%]	Mean [%]	Stand. Dev. [%]
0	100	100	100	100.00	0.00
7.81	102.5177	101.2752	89.97881	97.92	5.64
15.60	95.73734	92.50294	93.11148	93.78	1.40
31.25	92.18857	89.83494	94.22026	92.08	1.79
62.50	91.66337	86.5738	81.93484	86.72	3.97
125.00	86.87448	82.2322	86.71175	85.27	2.15
250.00	88.475	86.11604	84.78229	86.46	1.53
500.00	87.1919	84.05711	78.35105	83.20	3.66
1000.00	80.1504	76.77206	72.52405	76.48	3.12
2000.00	75.91322	72.153	72.6339	73.57	1.67

<b>ADV / NRK-52E / 24 h</b>					
Conc. [ $\mu$ M]	Experiment 1 [%]	Experiment 2 [%]	Experiment 3 [%]	Mean [%]	Stand. Dev. [%]
0	100	100	100	100.00	0.00
7.81	83.17473	76.5793	72.91255	77.56	4.25
15.60	77.88047	75.34953	83.60262	78.94	3.45
31.25	65.77538	69.13766	75.52543	70.15	4.04
62.50	63.90684	63.62052	67.97382	65.17	1.99
125.00	47.90992	54.44749	52.27594	51.54	2.72
250.00	24.71059	27.61536	26.99333	26.44	1.25
500.00	11.38252	11.9136	12.93199	12.08	0.64
1000.00	7.950345	10.27194	8.783098	9.00	0.96
2000.00	0.05904046	0.06252085	0.0560479	0.06	0.00

*Appendix*

<b>ddC / RPTEC/TERT1 / 24 h</b>					
Conc. [ $\mu$ M]	Experiment 1 [%]	Experiment 2 [%]	Experiment 3 [%]	Mean [%]	Stand. Dev. [%]
0	100	100	100	100.00	0.00
7.81	82.37746	98.74775	100.1224	93.75	8.06
15.60	86.77511	95.33929	112.2086	98.11	10.57
31.25	89.62686	101.5564	114.0934	101.76	9.99
62.50	87.57668	95.99095	115.3053	99.62	11.61
125.00	87.26537	96.23816	110.5139	98.01	9.57
250.00	100.6577	98.16959	115.6198	104.82	7.71
500.00	81.2785	92.6836	111.2472	95.07	12.35
1000.00	83.54477	91.40234	104.3265	93.09	8.57
2000.00	90.93272	94.03428	115.4649	100.14	10.91

<b>Cidofovir / RPTEC/TERT1 / 24 h</b>					
Conc. [ $\mu$ M]	Experiment 1 [%]	Experiment 2 [%]	Experiment 3 [%]	Mean [%]	Stand. Dev. [%]
0	100	100	100	100.00	0.00
7.81	92.97028	95.13633	102.9771	97.03	4.30
15.60	91.34219	90.78519	103.1837	95.10	5.72
31.25	85.43504	91.85672	99.95493	92.42	5.94
62.50	94.07834	87.52689	102.9827	94.86	6.33
125.00	93.85494	88.09773	100.2847	94.08	4.98
250.00	105.483	91.3731	101.7755	99.54	5.97
500.00	95.4925	92.12895	98.6012	95.41	2.64
1000.00	98.7026	94.55498	97.60137	96.95	1.75
2000.00	102.7604	101.0178	97.37147	100.38	2.25

<b>TDF / RPTEC/TERT1 / 24 h</b>					
Conc. [ $\mu$ M]	Experiment 1 [%]	Experiment 2 [%]	Experiment 3 [%]	Mean [%]	Stand. Dev. [%]
0	100	100	100	100.00	0.00
7.81	90.60359	94.3723	92.24112	92.41	1.54
15.60	93.83479	89.6665	84.58886	89.36	3.78
31.25	99.89602	76.60994	88.0937	88.20	9.51
62.50	94.65726	77.50531	81.61942	84.59	7.31
125.00	91.3145	81.26001	76.62832	83.07	6.13
250.00	88.04074	68.37955	60.7035	72.37	11.51
500.00	76.60879	43.86367	27.90225	49.46	20.27
1000.00	20.17496	26.59499	29.42228	25.40	3.87
2000.00	45.9133	29.79557	31.14741	35.62	7.30

*Appendix*

<b>Tenofovir / RPTEC/TERT1 / 24 h</b>					
Conc. [ $\mu$ M]	Experiment 1 [%]	Experiment 2 [%]	Experiment 3 [%]	Mean [%]	Stand. Dev. [%]
0	100	100	100	100.00	0.00
7.81	93.98207	98.30043	95.19781	95.83	1.82
15.60	95.52563	88.94732	93.88176	92.78	2.80
31.25	95.08764	83.24094	98.21951	92.18	6.45
62.50	98.14007	85.87304	96.04078	93.35	5.36
125.00	95.33769	86.87209	94.79897	92.34	3.87
250.00	92.48784	90.53854	95.05936	92.70	1.85
500.00	94.02682	85.80109	89.02275	89.62	3.38
1000.00	94.53496	83.26069	81.85979	86.55	5.67
2000.00	91.07798	84.31526	87.78709	87.73	2.76

<b>Adefovir / RPTEC/TERT1 / 24 h</b>					
Conc. [ $\mu$ M]	Experiment 1 [%]	Experiment 2 [%]	Experiment 3 [%]	Mean [%]	Stand. Dev. [%]
0	100	100	100	100.00	0.00
7.81	96.9483	92.37007	92.1278574	93.82	2.22
15.60	97.19183	90.42714	92.9510234	93.52	2.79
31.25	109.3019	91.50895	86.3160038	95.71	9.84
62.50	95.60564	91.44407	100.525243	95.86	3.71
125.00	101.414	86.85015	97.9515161	95.41	6.21
250.00	98.32549	96.24939	91.2164625	95.26	2.98
500.00	99.65647	89.67072	89.5383578	92.96	4.74
1000.00	100.5163	84.13702	86.5480721	90.40	7.22
2000.00	97.07212	86.14017	66.153543	83.12	12.80

<b>ADV / RPTEC/TERT1 / 24 h</b>					
Conc. [ $\mu$ M]	Experiment 1 [%]	Experiment 2 [%]	Experiment 3 [%]	Mean [%]	Stand. Dev. [%]
0	100	100	100	100.00	0.00
7.81	98.44122	100.879291	98.2315617	99.18	1.20
15.60	92.79758	87.0658149	92.655595	90.84	2.67
31.25	94.24084	91.1533748	89.8799985	91.76	1.83
62.50	89.75991	92.9472743	84.6049726	89.10	3.44
125.00	73.11778	76.4115153	65.6889444	71.74	4.48
250.00	30.01679	52.3182694	43.9922004	42.11	9.20
500.00	27.99207	28.639085	30.8987177	29.18	1.25
1000.00	51.658	65.4670646	59.4356477	58.85	5.65
2000.00	33.54323	7.95500612	9.81537364	17.10	11.65

*Appendix*

<b>ddC / RPTEC/TERT1 / 14 d</b>					
Conc. [ $\mu$ M]	Experiment 1 [%]	Experiment 2 [%]	Experiment 3 [%]	Mean [%]	Stand. Dev. [%]
0	100	100	100	100.00	0.00
7.81	49.9640191	78.16879	55.71557	61.28	12.17
15.60	32.1718495	62.95671	51.53767	48.89	12.71
31.25	27.8939447	56.52841	51.62369	45.35	12.50
62.50	22.6803744	61.17651	45.28701	43.05	15.80
125.00	21.7524691	52.03608	46.86117	40.22	13.23
250.00	23.8192357	49.17593	47.21885	40.07	11.52
500.00	23.8983468	49.09142	47.01004	40.00	11.42
1000.00	30.4637713	48.19068	46.25776	41.64	7.94
2000.00	38.5084141	58.48341	48.97763	48.66	8.16
<b>Cidofovir / RPTEC/TERT1 / 14 d</b>					
Conc. [ $\mu$ M]	Experiment 1 [%]	Experiment 2 [%]	Experiment 3 [%]	Mean [%]	Stand. Dev. [%]
0	100	100	100	100.00	0.00
7.81	101.704468	71.9962547	80.84885	84.85	12.45
15.60	96.1707006	68.5016268	82.92477	82.53	11.30
31.25	86.8405788	70.6854022	72.30608	76.61	7.26
62.50	66.1652958	59.9852643	68.11559	64.76	3.47
125.00	41.5081141	51.4278271	48.45928	47.13	4.16
250.00	0.50304403	28.6183604	4.777582	11.30	12.37
500.00	0.08140752	12.4559604	0.0783292	4.21	5.83
1000.00	0.04202933	0.04250539	0.0484878	0.04	0.00
2000.00	0.12120989	0.00414136	0.02460043	0.05	0.05
<b>TDF / RPTEC/TERT1 / 14 d</b>					
Conc. [ $\mu$ M]	Experiment 1 [%]	Experiment 2 [%]	Experiment 3 [%]	Mean [%]	Stand. Dev. [%]
0	100	100	100	100.00	0.00
7.81	81.4806867	99.53757	86.55189	89.19	7.60
15.60	82.4615873	96.05444	92.01067	90.18	5.70
31.25	66.8681277	90.49705	94.28712	83.88	12.13
62.50	44.5800692	50.60534	64.8708	53.35	8.51
125.00	0.4806569	1.323795	0.9357875	0.91	0.34
250.00	0.01716013	0.01980695	0.03580973	0.02	0.01
500.00	0.01636279	0.01519895	0.01901335	0.02	0.00
1000.00	4.12713193	0.01806037	0.02307153	1.39	1.94
2000.00	0.70172787	0.01586786	0.02299638	0.25	0.32

*Appendix*

<b>Tenofovir / RPTEC/TERT1 / 14 d</b>					
Conc. [ $\mu$ M]	Experiment 1 [%]	Experiment 2 [%]	Experiment 3 [%]	Mean [%]	Stand. Dev. [%]
0	100	100	100	100.00	0.00
7.81	94.0058048	91.3618173	103.8489	96.41	5.37
15.60	100.249473	82.2712937	89.20362	90.57	7.40
31.25	104.559363	84.9553775	79.8831	89.80	10.64
62.50	93.6144982	96.313423	95.21451	95.05	1.11
125.00	94.0445262	94.8592921	86.93056	91.94	3.56
250.00	93.1767198	85.0307925	88.17625	88.79	3.35
500.00	84.8780569	92.3190914	85.98928	87.73	3.28
1000.00	79.4206604	91.2483432	88.35387	86.34	5.03
2000.00	92.1795422	94.349415	89.34495	91.96	2.05

<b>Adefovir / RPTEC/TERT1 / 14 d</b>					
Conc. [ $\mu$ M]	Experiment 1 [%]	Experiment 2 [%]	Experiment 3 [%]	Mean [%]	Stand. Dev. [%]
0	100	100	100	100.00	0.00
7.81	77.4619355	82.97009	91.6951984	84.04	5.86
15.60	67.9258081	102.0304	91.6807694	87.21	14.28
31.25	69.9246607	84.97353	88.8458315	81.25	8.16
62.50	71.9735813	92.76183	97.5056665	87.41	11.09
125.00	69.9026232	89.0323	95.3914902	84.78	10.83
250.00	52.3261679	88.88089	82.582046	74.60	15.96
500.00	20.0247968	60.22901	68.7855559	49.68	21.26
1000.00	6.0306127	56.267	75.6887133	46.00	29.35
2000.00	0.41200036	60.37529	48.3798542	36.39	25.91

<b>ADV / RPTEC/TERT1 / 14 d</b>					
Conc. [ $\mu$ M]	Experiment 1 [%]	Experiment 2 [%]	Experiment 3 [%]	Mean [%]	Stand. Dev. [%]
0	100	100	100	100.00	0.00
7.81	49.3472546	53.97181	76.5135	59.94	11.87
15.60	43.4953736	50.3378	73.91833	55.92	13.03
31.25	25.3135937	29.15414	64.32687	39.60	17.56
62.50	5.08191877	5.792503	26.6074	12.49	9.98
125.00	0.03665653	0.04010503	0.07327762	0.05	0.02
250.00	0.02251208	0.03514468	0.04380766	0.03	0.01
500.00	0.01214882	0.02877712	0.03470665	0.03	0.01
1000.00	0.00448141	0.02029878	0.03398434	0.02	0.01
2000.00	0.00280088	0.01980626	0.02333038	0.02	0.01



## **Acknowledgements**

Many thanks to Prof. Dr. Angela Mally for the confidence she has put in me and for the opportunity to work on my PhD thesis in this very interesting field, as well as for the chance to work in the international collaborative project and for the support and encouragement during my entire thesis. In the same vein, I would like to thank Prof. Dr. Leane Lehmann, who volunteered to participate as a first evaluator.

A big praise and a huge thank you to Heike Keim-Heussler, Nataly Bittner, Hannelore Popa-Henning, Dr. Elisabeth Limbeck, Tanja Röder and the rest of the working group for the help in the lab, the treatment of the cells for hours and days, the purifications, the measurements and many other steps that were necessary to bring the project to a successful end, as well as everything concerning the organization around the project. A huge thank you to Pia Reiser for her excellent work and many hours with the confocal microscope. Sincere thanks to Julian Scherer and Sabrina Frank for the data collected.

For the fantastic and interesting work, the supply of the PBPK & QIVIVE data a big thank you to the Risk-IT project partners of the University in Utrecht Dr. Nynke Kramer, Dr. Femke Taverne, Wu Jiaqing and the complete team of IRAS in Utrecht. Also, a personal thank you for the always welcoming and open-hearted nature during my stay in Utrecht which I have kept in great memory. Special thanks also to the project partners Dr. Stefano Di Fiore and Dr. Bernhard Ellinger from Fraunhofer Institute in Aachen & Hamburg for the provided data of the high-content images as well as the successful meetings, the constructive scientific exchange also outside the project and the encouraging words. I would also like to thank the project partners

Dr. Barbara Birk and Dr. Saskia Sperber from BASF Ludwigshafen for their excellent cooperation, the interesting scientific discussions during the entire project and the successful completion. Many thanks to the external advisors Dr. Phil Hewitt, Dr. Roland Frötschel, Dr. Susanne Brendler-Schwaab, Dr. Twan Ederveen, Dr. Peter Theunissen, who supported the project with expert advices and constructive ideas. Many thanks to Prof. Dr. Wolfgang Dekant for the donated rat kidney and also sincere thanks to Prof. Dr. Helga Stopper and her working group for the CaCo-2 cells and the help with technical questions concerning microscopy. Dr. Gracia Montag, I would like to thank you for your advice and being a friend. In memory of Roland Wartha also a thank you for the programming of the Risk-IT database.

Furthermore, I would like to thank all friends, colleagues and everyone I have forgotten, who always had an open ear for all problems and troubles and who were motivating to me even in tough situations. I want to thank Timo Grund, who was a great support for technical questions, literature research, search syntax and templates.

And finally, my deepest appreciation belongs to my family. I would like to thank my sister Claudia and my brother (in law) Holger for their countless help in every situation and for their trust in me. Victoria will have wonderful parents. It was only thanks to my mom and dad that I was able to get this far and there's no way I can pay you back, but my plan is to show you that I understand; you are appreciated... Tak bardzo was kocham.



## **Eidesstattliche Erklärung**

Ich versichere, dass ich die Arbeit ohne fremde Hilfe und ohne Benutzung anderer als der angegebenen Quellen angefertigt habe und dass die Arbeit in gleicher oder ähnlicher Form noch keiner anderen Prüfungsbehörde vorgelegen hat und von dieser als Teil einer Prüfungsleistung angenommen wurde. Alle Ausführungen, die wörtlich oder sinngemäß übernommen wurden, sind als solche gekennzeichnet.

Würzburg, den 4. Oktober 2021

---

Unterschrift